Aalborg Universitet

Stiffness Analysis of Nail-Plate Joints Subjected to Short-Term Loads

Nielsen, Jacob

Publication date:
1996

Document Version
Early version, also known as pre-print

[Link to publication from Aalborg University](#)

**STRUCTURAL DESIGN
PAPER NO. 2**

Ph.D.-Thesis defended publicly at Aalborg University on January 5, 1996

JACOB NIELSEN
STIFFNESS ANALYSIS OF NAIL-PLATE JOINTS SUBJECTED TO SHORT-TERM LOADS

The STRUCTURAL DESIGN papers are issued for early dissemination of research results from the Structural Design Group at the Department of Building Technology and Structural Engineering, University of Aalborg. These papers are generally submitted to scientific meetings, conferences or journals and should therefore not be widely distributed. Whenever possible reference should be given to the final publications (proceedings, journals, etc.) and not to the Structural Design papers.

STIFFNESS ANALYSIS OF NAIL-PLATE JOINTS SUBJECTED TO SHORT-TERM LOADS

by

Jacob Nielsen

Department of Building Technology and Structural Engineering

Aalborg University, Sohngaardsholmsvej 57, DK-9000 Aalborg, Denmark

Acknowledgements

Aalborg, October 1995

Jacob Nielsen

Contents

Appendices

Chapter 1

Introduction

In Denmark it has been an old tradition to use timber in all kinds of structures. In particular, timber has been widely used for the load-bearing structure in roofs, walls, and floors. Today timber is used for structures as roof trusses and floor joists almost only.

Timber structures are made with beams connected in joints with glue or a mechanical fastener. The types of the mechanical fasteners are: nails, staples, bolts, dowels, screws and nail-plates. Bolts and dowels are generally applied to joints in solid structures, and the other fastners are used in all kinds of light structures. Especially nail-plates are designed for trusses.

For many years, joints were made of boards with nails, but the increasing industrialism and the need for quick and usable assembly had the result that today nearly all trusses are prefabricated with nail-plates. The word "nail-plate" has been used for different types of plates. There are two main types of nail-plates: steel plates perforated with holes in which separate nails are used, and steel plates perforated by a stamping machine, so the nails are made from the plate, see figure 1.2 on page 7. This type is sometimes called "punched metal plate" and requires a hydraulic pressing tool to embed the nails into the wood. Only joints with a nail-plate of the latter type will be analysed in this thesis.

1.1 Motivation

The dimensions of the beams and nail-plates in the timber structures are controlled by different load-cases. The beams and joints must not fail when the truss is subjected to the maximum load (e.g. a snow or wind load), and the deformations in the serviceability state must not exceed certain values. The variation of the section forces and deformations of the trusses is determined by a model. Today, the design of trusses is determined using rather simple models which means that the material for the trusses is not optimally used.

1

In recent years, types of trusses have been used where the stiffness and strength are highly dependent on the joint properties, see figure 1.1, left. Furthermore, the design of all trusses in Denmark is almost always controlled by the deformations.
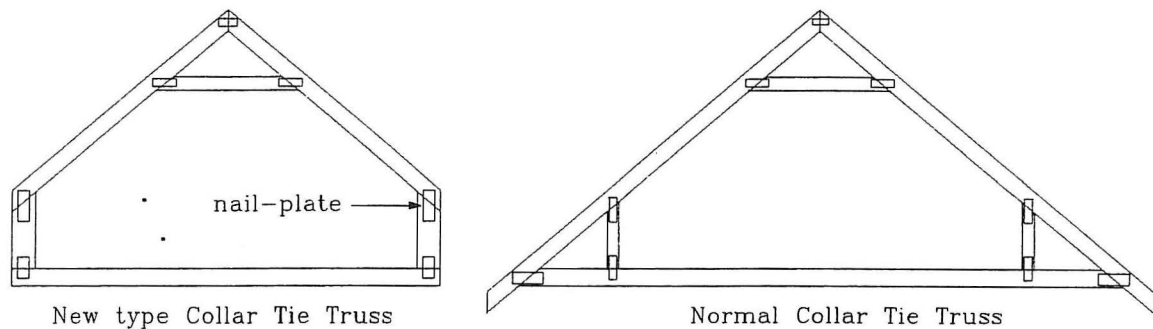
Figure 1.1: **Two types of collar tie trusses.**

The deformation of a truss is composed of the deformations of the beams, which are fairly well known, and the deformations of the joints, which are a rather neglected area.

The objective of this study is therefore to make better predictions of the deformations in the joints. Numerical methods for nail-plate joint modelling will be developed and tested. It is the idea that the models should serve as a research tool to achieve more knowledge about the joint behaviour so that more optimal designs can be determined. In the long term, the models may be introduced into pratical truss engineering resulting in less material consumption to be of benefit for the environment and the competitiveness of the factory. In addition to increased knowledge about their utilities and limitations, the use of new models will also demand new production methods as well as new attitudes among the design engineers, e.g. the notion that utilization of contact between the timber members is a "daring" phenomenon should be changed. Contact between the timber members will also be analysed in this thesis.

1.2   Modelling the Joint Behaviour

Many different types of models have been developed for the design of trusses and the most important are:

1 Plane beam elements with pinned or rigid moment joints.

2 Fictitious member model.

3 Spring model.

4 Foschi's model.

All the above models are plane frame models based on the finite element method, and the dissimililarities are found in the joint modelling alone. The wood members of the truss are modelled by linear elastic beam elements located in the system line. The output from the models is the section forces and deformations at the nodes.

In the first model, the joint can act as pinned or rigid, e.g. Suddart et al.(1981) and King et al.(1988) have modelled a parallel-chord wood truss with continuous chords with pinned web members. In order to account for the joint deformations, reduced modulus of eleasticity (MOE) values for the webs were used. The model has been implemented in the program Purdue Plane Structures Analyser II (PPSA II) described by Suddart et al.(1983).

The "fictitious members model" is a frequently used truss model. The joints can also here be pinned or fixed, but small "fictitious" bar elements are located between the "true" beam elements to achieve the semi-rigid properties. The properties of the fictitious elements are to be estimated. Riberholt(1982) proposed the stiffness of the fictitious element to be as stiff as the adjacent (true) elements and Beineke et al.(1979) concluded that the stiffness could be determined from the plate length.

In "the spring model" the joint stiffness is made by three mutually independent linear elastic springs each representing axial, shear and rotional stiffness of the joint. The stiffness of the rotary springs are in direct proportion to the contact area between the plate and wood and the axial and shear stiffness are increased with increasing plate area, Maraghechi et al.(1984).

Foschi(1979) has presented a model for nail-plate connections. The joint elements are treated as a special beam element. The joint element establishes a nonlinear connection between the nodes of the beams and the nodes of the nail-plate. The relative displacements between nail-plate and timber members are determined by rigid body considerations. The virtual work for the nails is based on the knowledge of four characteristic load-slip tests where the plate and the timber are located with the principal axes parallel or perpendicular to the load direction. Stiffness values in joints with other angels than tested are found using Hankinson's formula, see Foschi(1979) [15]. The load-slip description is nonlinear. Plate buckling, tension- and shear strength of the plate are also considered. Contact between the timber members is taken into account by geometric constraints (Lagrange multipliers). The constraints are used on selected points on the end of the timber members. The model has been implemented in the program SAT (Structural Analysis of Trusses).

Other and more complicated models have been used to model the joint properties. Hunt(1987) has used the finite element program ADINA to analyse a 90 degree portal knee joint. Timber and plate are modelled by two dimensional plane stress isoparametric 8 node elements with linear elastic orthotropic and isotropic material properties, respectively. The nails were modelled by 2 node Hermitian beam elements with fixed rotation. The stiffness of the nails was determined from single nail tests. Also analysis using a nonlinear nail model (3-D elasto-plastic rectangular beam elements with bilinear strain hardning) was made. The nail stiffness perpendicular to the grain was 70% of the nail stiffness parallel to the grain. Nail stiffness properties were determined by tests on single nail joints. No contact between the timber members was modelled. The model can estimate the distribution of the stresses in timber and plate and the size and direction of the forces in each nail.

1.2.1   Testing the Models

In order to know the reliability of the models, experimental tests have been made by many different researchers. The result of the experimental tests (load-slip curves) is compared to the result of the models. In the following, the conclusions of some of the works will be described in short. The model numbers refer to the item numbers on page 2.

Feldborg et al.(1981) has made a large test programme in which splices, heel joints and pitch trusses are tested in short- and long-term loading. Deflections of the tested trusses are compared to model 2. The stiffness of the fictitious member was determined by test on the mentioned joints. In general the model underestimates the deflections.

Lau(1986) has tested model 2 on heel joints with different plate sizes and plate locations. Also the properties of "shear joints" tested with different angles between the shear plane and the principal axes of the plate were compared to model 4. Good agreement of the experimental data with the predicted stiffness values (linear part of load-slip curve) of the shear tests was observed, but some differences exist. Model 4 has underestimated the deformations and the failure loads of all the heel joints. The failure loads were underestimated by about 50% and 60% of the observed values. It is assumed that the differences between the failure loads can be caused by friction between the timber members. A method for calibrating the stiffness of the fictitious members to be used for the heel joints was presented.

King et al.(1988) have tested parallel-chord wood trusses and compared deformations and section forces with four different joint analogs based on models 1 and 2. Analog 1 was made with continuous chords with pinned web members. Analog 2 was made as analog 1 but with a reduction factor for the MOE of the webs. Reduction factors were down to $\frac{1}{6}$ of the average modulus. Analog 3 uses fictitious members with properties based on contact area between plate and wood. Analog 4 uses fictitious members as well, but with properties based on plate embedment (the size of the gap between the wood and the plate) and the weight of the jointed timber members. It was concluded that the axial load is independent on the joint stiffness, but the bending moment is very sensitive to the joint stiffness. Analogs 3 and 4 predicted the deflections better than analogs 1 and 2.

Triche et al.(1988) have modelled several different truss types (parallel chord N- and V-trusses, pitched chord W-trusses) using model 4 and compared the deflections with experimental tests. Subroutines from SAT have been added to PPSA and a subroutine to calculate the nail forces from the node deformations has been made. The results are given as a ratio between the nail force and the maximum allowable nail force in each nail. The new program is called PPSAFT (PPSA Foschi-Triche), and it predicted the deformations very well. The midspan deflections were underestimated at the parallel chord trusses and overestimated at the pitch trusses.

Lum et al.(1988) have tested models 1 and 4 with experimental tests on parallel chord trusses. The same MOE was used in the two models, and therefore, any differences between the models can be attributed to the joint model alone. At load levels below

half the design load, model 1 was able to predict the midspan deflections within 13%, but model 4 was able to predict the deflection within 2% of the test results. The deformations predicted by model 1 were smaller than the deformations predicted by model 4, which again were smaller than the deformations found in the test.

Karacabeyli et al.(1990) have tested long span glulam pitched trusses and compared the deformations with models 1 and 4. In model 1, the chords are continuous and all the joints are pinned. It was found that both models 1 and 4 underestimated the bottom chord deflections by 20 and 10% at all load levels. Parameters of model 4 requiring special attention were the steel properties and location of the slot openings of the plate and the location of the gap control points. Model 4 underestimated the failure load of the truss by 20%, but it identified the true failure type (inner zone of the heel plate).

Kjær et al.(1992) and Mortensen et al.(1992) have tested the rotational stiffness of different knee joint designs and used the result to calibrate stiffness values used in model 3 and a finite element model with continum (timber and plate) and linear spring (nail) elements. The deformations from the models are compared to full-scale tests of modified collar tie trusses, as shown in figure 1.1, left. Good agreement between the deformations in the serviceability state was obtained.

1.2.2   Testing Nail-Plate Joints

The characteristics of a nail-plate joint depend on many different parameters as shown in table 1.1.

Joint part	Parameter
Timber	Type of wood
	Moisture content
	Density
	Late or early wood
	Part of the trunk
	Number and locations of knots
Nail-plate	Type of plate (Gang-Nail,HydroNail,etc.)
	Steel material
	Plate surface (galvanized,painted,oiled,etc.)
	Nail pattern
	Geometry of the nails
Joint characteristics	Geometry of the joint
	Size of the plate (number of nails)
	Contact between the timber members
	Friction between the timber members
	Grain and plate direction
	Craftsmanship
	Embedding procedure of the nail-plate
Loading	Load level, direction, duration
	Type of load (continuous,cyclic,random)

Table 1.1: **Parameters affecting deformation and strength of a joint.**

Many investigations on nail-plate joints have been made to analyse the influence of some of the parameters in table 1.1.

Aune(1970) has tested the influence of the angle of the grain with plate and load direction on the load-slip curves of the joints. The joints were tested in tension, bending and some in compression. A gap was made between the timber members to avoid contact in the bending tests.

Edlund(1971) has tested tensile and bending splices to analyse the effect of moisture content, specific gravity of the wood, load duration, contact between the timber members (gap sizes), gap between plate and timber, location of some nails in the gap between the timber members, eccentrically located nail-plates and combinations of moment, tension and shear on the stifness and strength. The work was followed up by tests on heel and peak joints together with tests on W-shaped pitch trusses with different inclination, Edlund(1973).

As mentioned before, all models estimate the deformations and the section forces at the nodes and with this knowledge, the deflections and section forces can be calculated at all points of the truss by means of different beam theories e.g. Bernoulli or Timoshenko. The section forces must be transmitted in the joints by the nails to the plate and/or by contact between the timber members. Many static models to handle this problem have been developed, see e.g. Noren(1981), Feldborg(1981) and others.

The works described above have formed some of the design foundation in Eurocode 5 [57].

1.3   Scope of the Project

A short formulation of the aim is given as:

> *Development and testing of models for determination of the stiffness properties of nail-plate joints.*

The aim is divided into the following specific objectives:

- Test and analysis of the basic properties of a selected nail-plate type and a selected type/quality of wood.
- Construct and test a complex numerical model to analyse arbitrary nail-plate joints.
- In the light of analysis on selected joints, develop and test a (simple) plane frame model and determine the effect of different parameters.

The scope of the study is limited to analyse short-term statically loaded joints, one type of nail-plate and one type of timber with constant moisture content. The experience

from the work can, however, be applied on other types of joints or joints with other types of nail-plates.

The analysed nail-plate is from Gang-Nail Systems, type GNA 20 S, see figure 1.2. This nail-plate differs from other plates by its thickness, which is only 1mm.
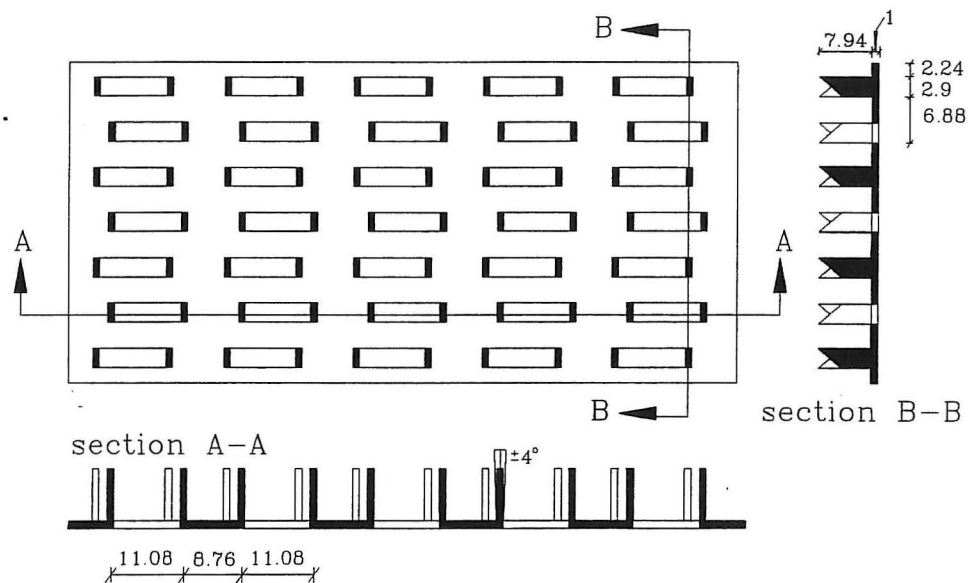
Figure 1.2: **Nail-plate GNA 20 S from Gang-Nail Systems. Dimensions in mm.**

The timber is Swedish spruce (Picea abies) of strength class K-24 according to the Danish Code of Practice for Structural Use of Timber (DS413, [56]). It is placed in a conditioning room at 65% RH and 21°C until the moisture content of the wood is about 13%.

Only deformations below the first peak load of the load-displacement curve will be predicted. The "softning" path is not treated. (Methods to handle the softning paths in timber joints are treated in Jensen(1994)). The influence of unloading on the load-displacements curves is analysed experimentally, but not implemented in any of the models.

The determination of failure loads and failure types of the joints is given a secondary treatment in this study. The nail-plates are located symmetrically in a joint.

The complex numerical model is made with the finite element package, ABAQUS ver. 5.2 from Habbit, Karlsson & Sorensen Inc. A numerical plane frame programme, AN-TRUSS (ANalysis of TRUSSes), is developed. The programme is based on further developments of the theory and techniques made by Foschi(1979).

1.4   Method

From the description in section 1.2 it appeared that the model during the development is often tested on large full-scale structures with many different nail-plate joints. However, this procedure will result in lack of knowledge of the validity of each joint model and different variations of joint parameters, perhaps due to financial circumstances.

The procedure for this study is shown in figure 1.3. The procedure is composed of seve-
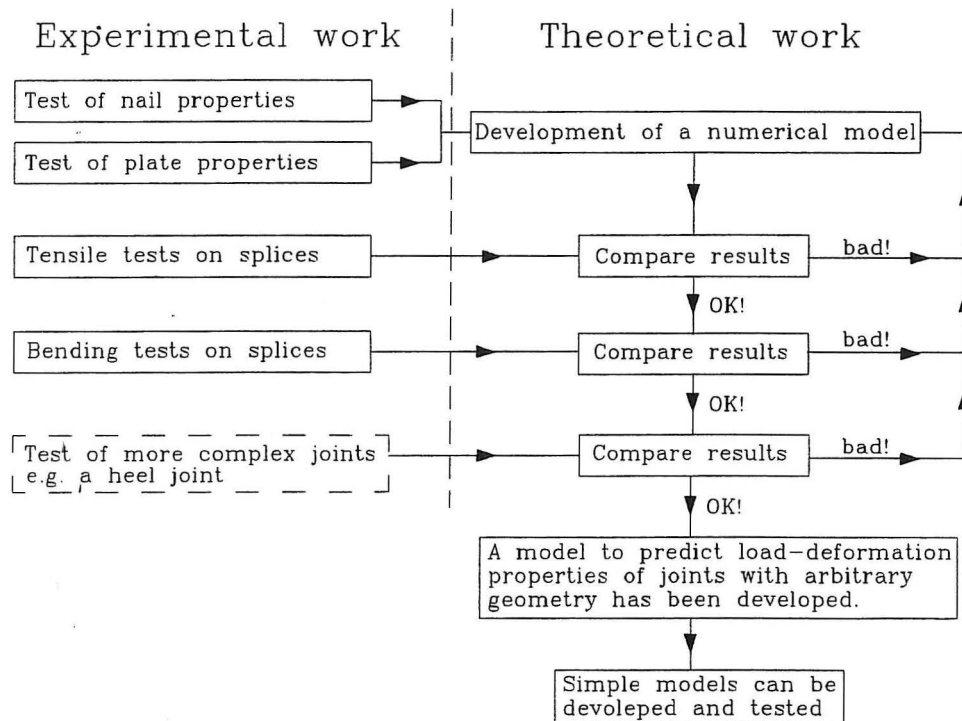
Figure 1.3: **Process diagram of the study.**

ral steps. First knowledge about the selected nail-plate and timber must be acquired. This is done by testing the plates and nails (nail-to-wood-behaviour) separately. Tests on the timber are only done in part. The compression and tension stiffness are tested in Jensen et al.(1993) and some bending test on beams are made in connection with this study. This "fundamental" knowledge is transferred to an ABAQUS model, which is still in progress. Second, in order to develop the ABAQUS model in "small steps", it is tested on a simple joint, the splice. In tension the splice gives an opportunity to test the "in grain" stiffness properties of the nails and the elastic-plastic properties of the plate. If there is divergence between the numerical result and the test result, the model is modified until an acceptable result is achieved. However, the need for the modification should be justified.

Afterwards, the splice is tested in pure bending to test the dependence on the nail stiffness in several directions, buckling effect in the plate and contact between the timber members. The same iterative procedure is used to obtain an acceptable result.

Afterwards, the numerical model is tested on a more complex joint - a heel joint. (No

experimental work has been made on this joint in this study.) Finally, a numerical model is developed to predict the deformation of arbitrary joints. Based on knowledge about the dependence and sensitivity of different parameters on the joint characteristics, a simple model will be developed.

1.5   Reader's Guide

In chapters 2 to 4 the ABAQUS model will be developed and in chapters 5 and 6 the AN-TRUSS model is developed. In the appendices, all the experimental tests are described.

In chapter, 2 a numerical model for the tensile splices is developed with ABAQUS. Properties of the nail and the plate used in the programme are determined in appendices A and B, respectively. Load-slip curves of the splices are compared to experimental test results described in appendix B. The distribution of the stresses in timber and plate and also the distribution of the nail forces are given.

In chapter 3 the ABAQUS model for the splice is further developed in bending. Plate sizes, plate location and the effect of the gap in the compression zone will be treated, and load-slip curves are compared to experimental bending test described in appendix D. The distribution of the stresses in timber and plate as well as the distribution of the nail forces is given.

In chapter 4, the ABAQUS model is used on a heel joint. The distribution of the stresses in timber and plate as well as the distribution of the nail forces is given.

In chapter 5, the AN-TRUSS model is described and the theory for the implemented elements and procedures is given.

In chapter 6, the AN-TRUSS model is used and the results are compared to the tests already made. Also, two examples of trusses are shown to highlight the difference between AN-TRUSS and a programme developed by Gang-Nail Systems based on fictitious elements.

Finally, the conclusions are given in chapter 7.

Chapter 2

Tensile Splices

In this chapter a plane ABAQUS-model of a spliced joint subjected to tension will be described. The properties of the elements used to model the plate and timber are given, however, the nail model is described in chapter 3. The ABAQUS-results are compared to the experimental results from the tensile test in appendix C, and finally the distribution of the stresses and the nail forces are shown.

To avoid confusion it must be emphasized that in this chapter the term "load-displacement curve" is used for the curve to describe the stiffness properties for a nail and the term "load-slip curve" is used when comparing the general joint properties. The gap is defined as the initial horizontal distance between the timber members. The slip is defined as the horizontal distance between the timber members minus the gap distance. The slip for a loaded splice with no gap is shown in figure 2.1.

2.1 Introduction

A tensile splice is shown in figure 2.1. Tensile splices are generally used in rafters and chords of trusses. The load is transmitted by the plate and nails alone.
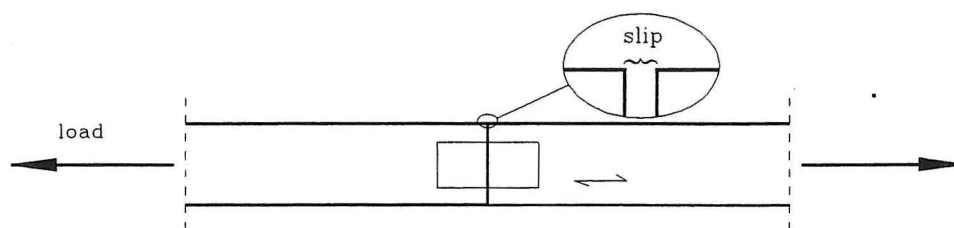

Figure 2.1: Tensile splice.

In the spring of 1993 analysis of tensile splices was made by Jensen et al.(1993). The load-slip curves of the joint and the deformation of the nail-plate were measured and compared to results from a ABAQUS model. Several plate sizes were tested, see

11

table 2.1 on page 14. The timber used was as described on page 7 with a cross-section of 170 × 45mm. The load procedure was controlled by the load and it was applied stepwise, see also appendix C.

Also, tests with few nails (one or two rows) have been performed to determine the stiffness of a single nail. The conclusions of the work are :

- If the load-displacement curve from tests with a few nails is used as a load-displacement curve for the springs in the numerical model, the load-slip curve from the model is too stiff compared to the load-slip curve from tests with tensile splices.

- If the average load-slip curves from the tensile splices with nail failure are used as load-displacement curves for the springs in the numerical model there is good agreement between the finite element predictions and the experimental results. This is valid even for the joints with plate failure.

- The minimum nail forces is 16% smaller than the maximum nail force in a nail-group.

- The plate can be considered as a rigid plate.

It has been assumed that the difference between the numerical results and the test results in the first item can be caused by a group effect in the nails.

Further experimental investigations of the nail behaviour have been made, see Nielsen et al.(1994). The objective of this work has been to analyse the influence of: number and location of the nails, unloading, grain direction and plate orientation on the nail stiffness. For further information, see Nielsen et al.(1994) or the summary of this paper in appendix A. The results from the paper will be used to determine the load-displacement curve of the nails in the present ABAQUS model.

The model described in section 2.2 is a simpler model than the model in Jensen et al.(1993) as the plate is modelled without holes and with a smaller number of elements.

2.2   The Model

A 2-dimentional model as shown in figure 2.2 is used to model the tensile splices.

Both plate and timber are modelled as disks without holes. The disks are connected by springs (nails). As the tensile splice is symmetric, see figure 2.1, only the right part of the joint is modelled. The tensile splice is also symmetric in the (1,3)-plane, but as the same model will be used to model the bending problem only the vertical symmetries are used.

In figure 2.2 the plate is hatched and the two disks are shown at different levels. In the numerical model the two disks are located at the same level and the springs have no extension in direction 3. The mesh of the plate elements coincides with the mesh of the timber elements.
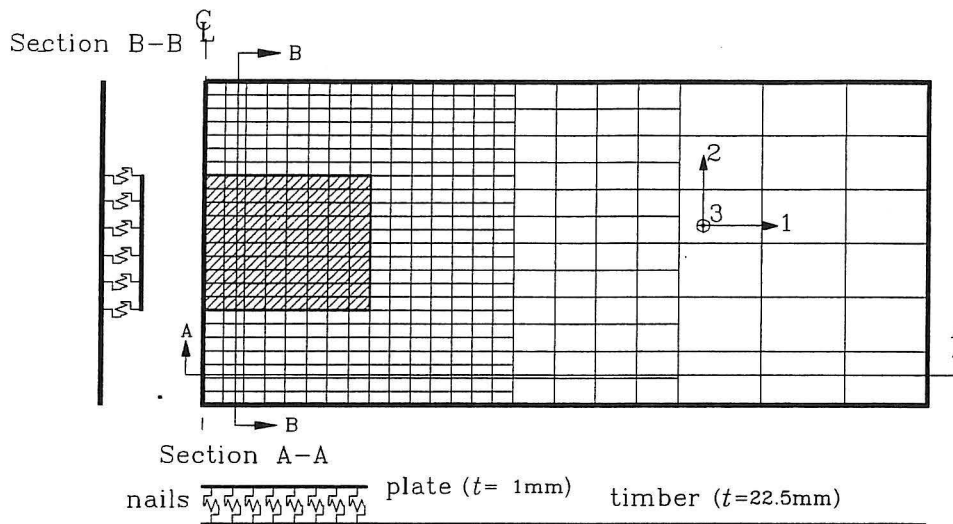
Figure 2.2: **The element mesh of timber and plate and location of springs.**

The timber and plate are modelled with 8-nodes biquadratic isoparametric plane stress elements. The plane stress assumption is good when the disks are thin or Possion's ratio, ν, is small. Each node has two degrees of freedom: displacements in direction 1 and 2, see figure 2.2. The thickness of the plate elements are 1mm and the thickness of the timber elements are $\frac{45\text{mm}}{2} = 22.5\text{mm}$.
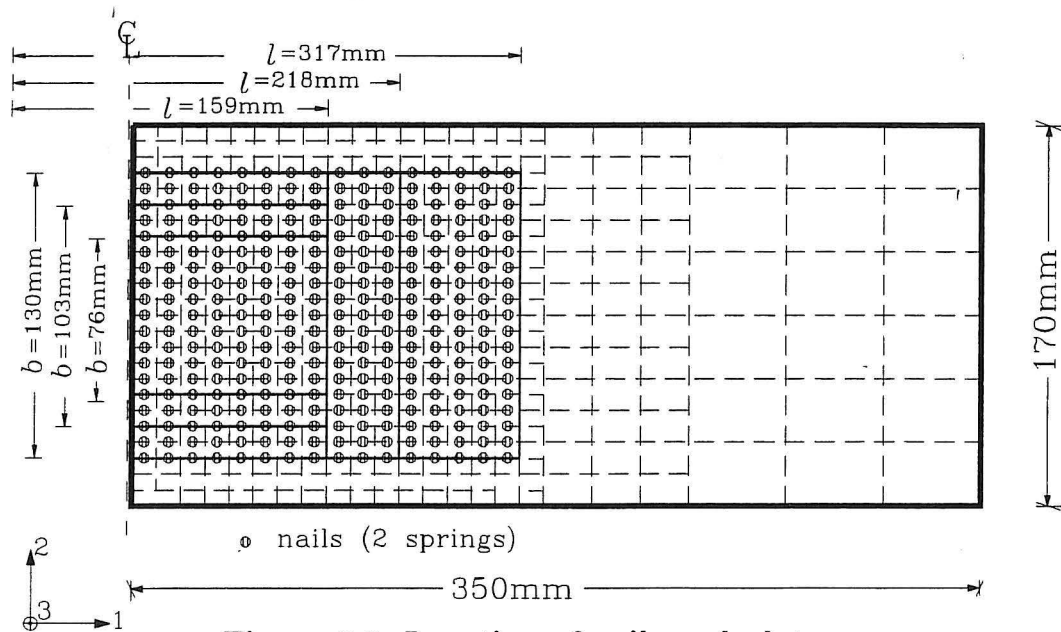
Figure 2.3: **Location of nails and plates.**

Five different plate sizes will be modelled and the number of plate elements and nails is dependent on the plate size, as shown in figure 2.3 and table 2.1.

The timber is modelled as an anisotropic linear elastic material with properties as shown in table 2.2.

The modulus of elasticity in direction 1, E_1, is found from test on the timber, see Jensen et al.(1993), and the modulus in direction 2, E_2, and the shear modulus,G, are characteristic values from DS 413 [56]. Possion's value, ν_{12}, is determined from Niēlsen

Plate size $b \times l$ mm	Number of plate elements	Number of nails on plate	Number of nails in model
76×159	10×8	11×16	11×8
103×159	14×8	15×16	15×8
130×159	18×8	19×16	19×8
130×218	18×11	19×22	19×11
130×317	18×16	19×32	19×16

Table 2.1: Number of plate elements and nails in the different plates.

	E_1 MPa	E_2 MPa	ν_{12} -	G MPa
Timber	12800	350	0.015	700

Table 2.2: Material data for timber.

et al.(1973). The numerical results are not sensitive to a variation of ν_{12} between $0,01$ and $0,02$, see Jensen et al.(1993).

The plate is modelled as an anisotropic linear elastic-plastic von Mises material with isotropic hardening. The anisotropic property is caused by the holes. The linear elastic stiffness properties are given in table 2.3 and they are determined by tensile test on nail-plates, see appendix B.

	E_1 MPa	E_2 MPa	ν_{12} -	G MPa
Plate	125000	85000	0.11	75000

Table 2.3: Material data for the plate.

It was found difficult to determine reliable stress-strain data of the plate, partly because the stress distribution in the plate is very complicated due to the holes. The nail stamping of the plate will give rise to prestresses in the material and the holes will cause stress concentrations. (An example of a stress distribution in a linear elastic nail-plate with holes is shown in Kloch et al.(1990) and Jensen et al.(1993)). The hardening poperties are given by parameters in table 2.4 which are determined by calibration of the model to the test results.

A nail is modelled by two non-linear springs placed in directions 1 and 2. (In ABAQUS the non-linear spring stiffness is given by multi-linear curves, see e.g. figure 2.14 on page 21). The load-displacement curves for the springs will be the same for directions 1 and 2 and they fit the load-displacement curves from the tests on nails, see also the discussion of the nail model on page 30. The "spring model" will behave too stiff for a nail displacement in other directions than 1 or 2. However, in tension the model is mainly dependent on the spring stiffness in direction 1, see also page 22.

The boundary constraints are shown in figure 2.4.

f_y [MPa]	ε_p
186	0.0
190	0.025
208	0.036
235	0.056
276	0.111
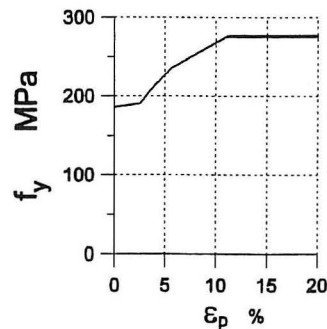
Table 2.4: The dependence of yield stress, f_y, on plastic strain, ε_p.
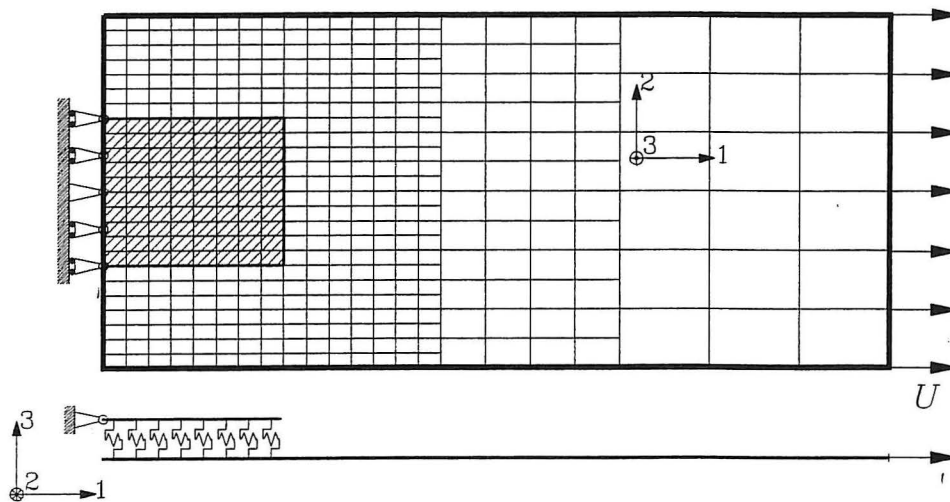
Figure 2.4: Boundary constraints on the model.

The left-hand edge of the plate (all nodes) is constrained in direction 1, and further-more, the midnode is constrained in direction 2 also. The model is "loaded" by a displacement, U, of the right-hand timber edge.

2.3   Results for the Tensile Splices

In this section the results for the tensile splices will be presented. The results from ABAQUS will be compared with the test results and the stress and nail force distribution will be shown.

2.3.1   Load-Slip Curves

In figures 2.5 to 2.9 the numerical results are compared to the experimental test results (Tensile test 1994) from appendix C. The solid lines are load-slip curves from ABAQUS

and the dashed lines are load-slip curves from tests. In the tests the specimens are unloaded once.
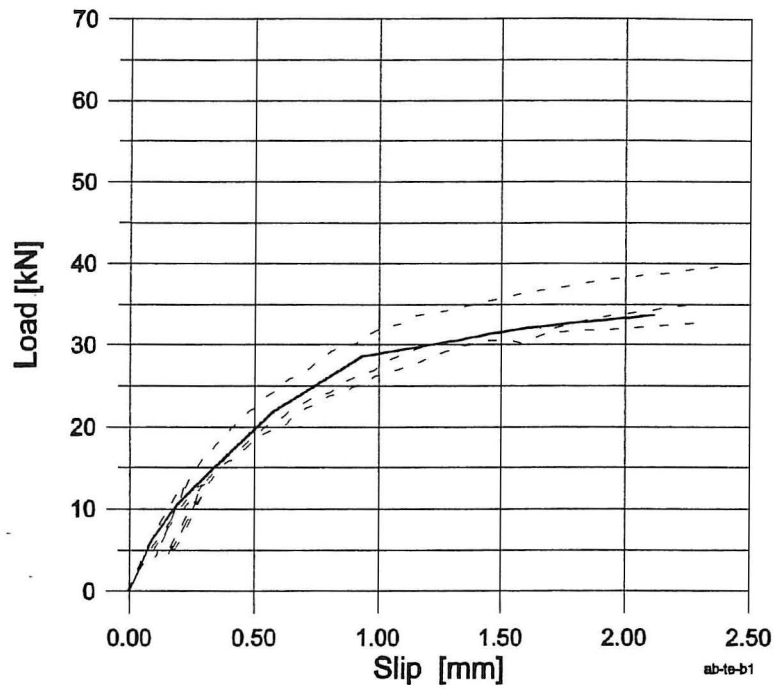
Figure 2.5: Load-slip curves from numerical and experimental tests of tensile splice with plate size 76X159mm.
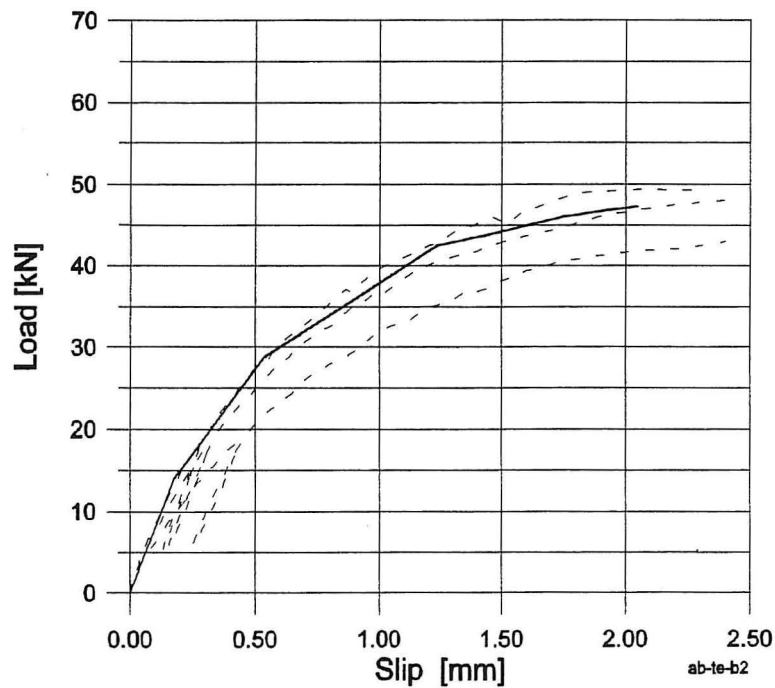
Figure 2.6: Load-slip curves from numerical and experimental tests of tensile splice with plate size 103X159mm.
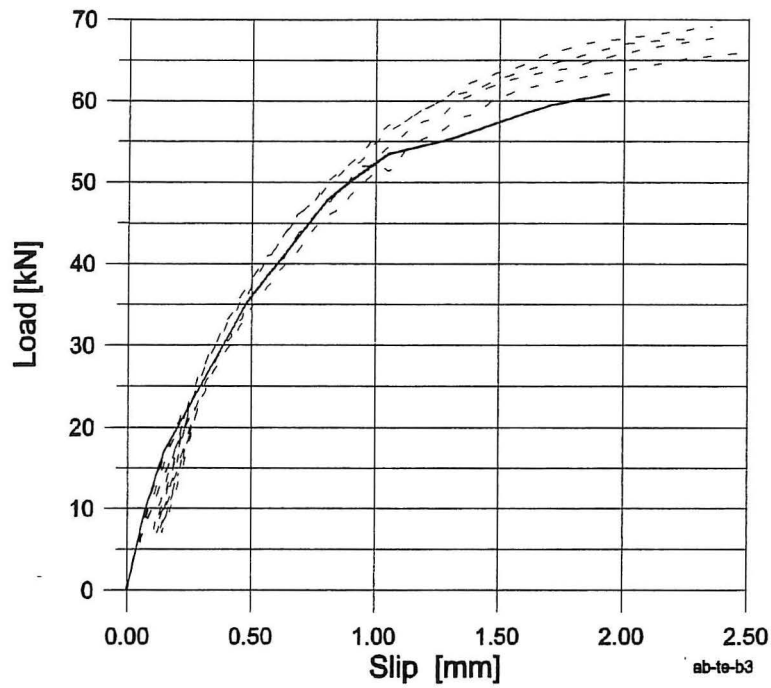
Figure 2.7: Load-slip curves from numerical and experimental tests of tensile splice with plate size 130x159mm.
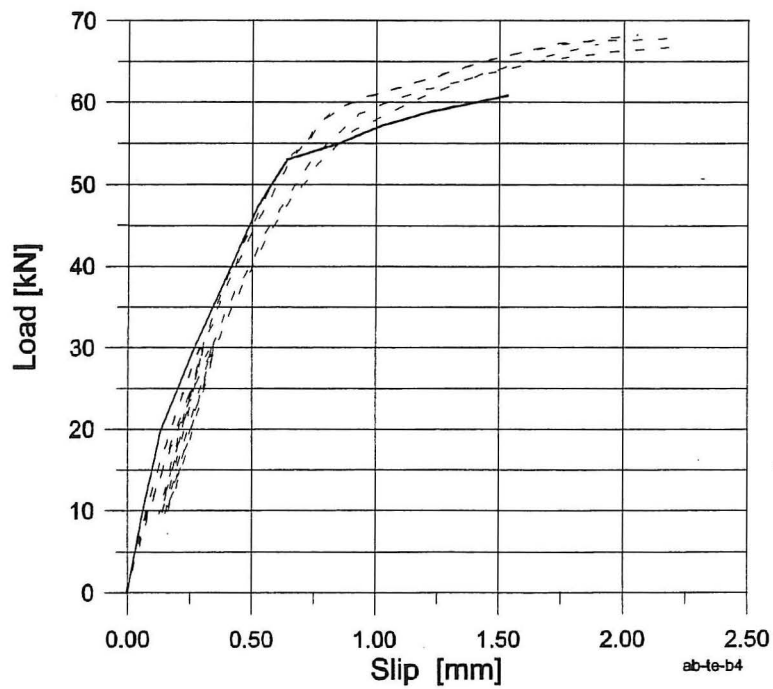
Figure 2.8: Load-slip curves from numerical and experimental tests of tensile splice with plate size 130x218mm.
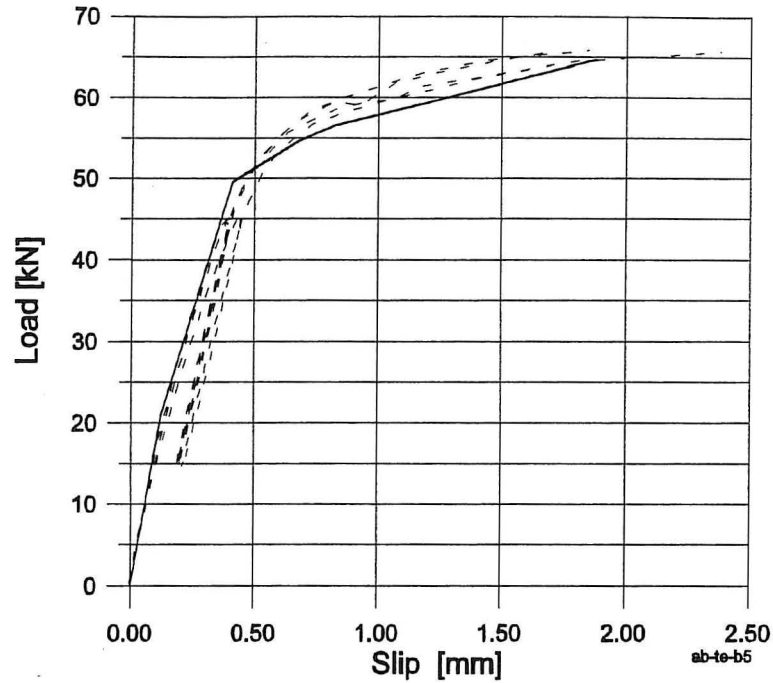
Figure 2.9: Load-slip curves from numerical and experimental tests of tensile splice with plate size 130x317mm.
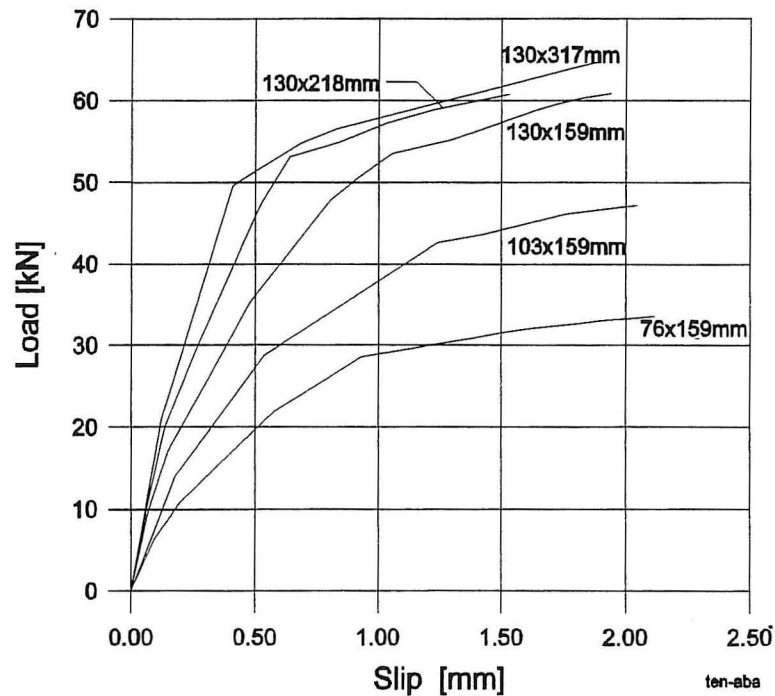
Figure 2.10: Load-slip curves from the five ABAQUS tensile tests.

In figures 2.5 to 2.9 it is seen that the numerical results correspond to the test results. In the tensile test with 130mm plate width, the plastic deformations are estimated on the safe side. The numerical model is loaded until a chosen deformation is obtained,

see U in figure 2.4. Therefore, the end of the solid curves do not indicate the failure load of the joint. In subsection 2.3.2 the failure type of the joint is discussed.

In figure 2.10 the five numerical load-slip curves are shown. The stiffness increases with increasing plate area, but the change in stiffness from a 130×218mm plate to a 130×317mm plate is modest. The deformations in these plates are mainly affected by the plate deformation. The effect is also seen on the failure load for these plate sizes, see e.g. the test results in table C.2 on page 141.

Since the numerical determined load-slip curve correspond to the test results, it is believed that ABAQUS can tell something about the joint behaviour when analysing deformations, stresses and strains. None of the following numerical results have been supported by experimental tests.

Numerical tests with different material properties show that the numerical model is very sensitive to a variation of the nail properties in the tensile direction. To show this effect, the horizontal displacements of different points on timber and plate are shown in figure 2.11. The location of the points is also shown. Point P on the plate is displaced

Figure 2.11: Load-displacement curves from different points on tensile splice with 103x159mm plate. Points A,B,C,D and E are located on the timber. Point P is located on the plate.

linearly until the plate becomes plastic in the area near the edge. The gradient of the linear part of curve P fits the modulus of the plate (E_1 in table 2.3), if the strain is assumed constant and the stress decreases linearly.

The displacements of the nodes between points B and C at the centre of the timber are almost identical, but the displacements increase as the distance to the horizontal

edges gets smaller. The difference between curves C and P denotes the displacements of the nails at this point. The deformed joint is shown in figure 2.16 on page 22. About 20% of the displacement at point C is caused by the deformation of the plate. This effect increases when the plate gets plastic. The total effect of the plate on the slip (measured at a point between points A and E) is, however, below 10%, as shown in figure 2.12. The effect from the timber is almost the same.
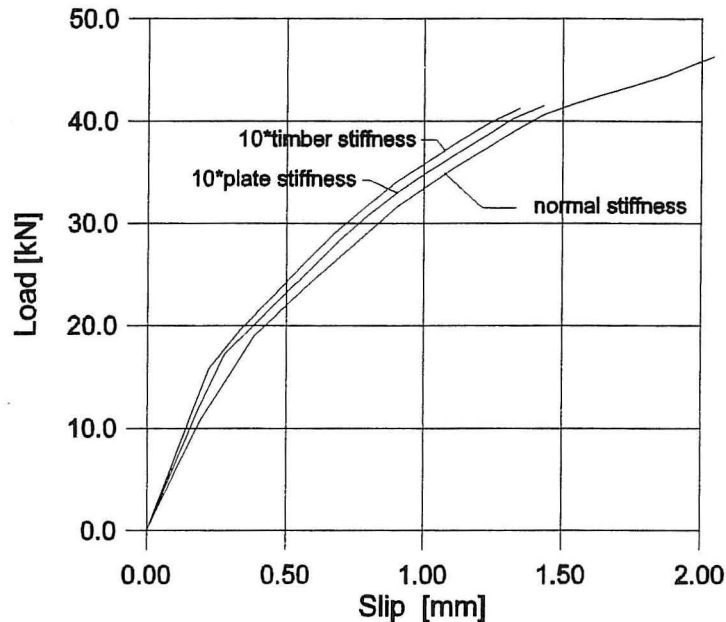
Figure 2.12: Load-slip curves for models with increased stiffness. Plate size 103x159mm.

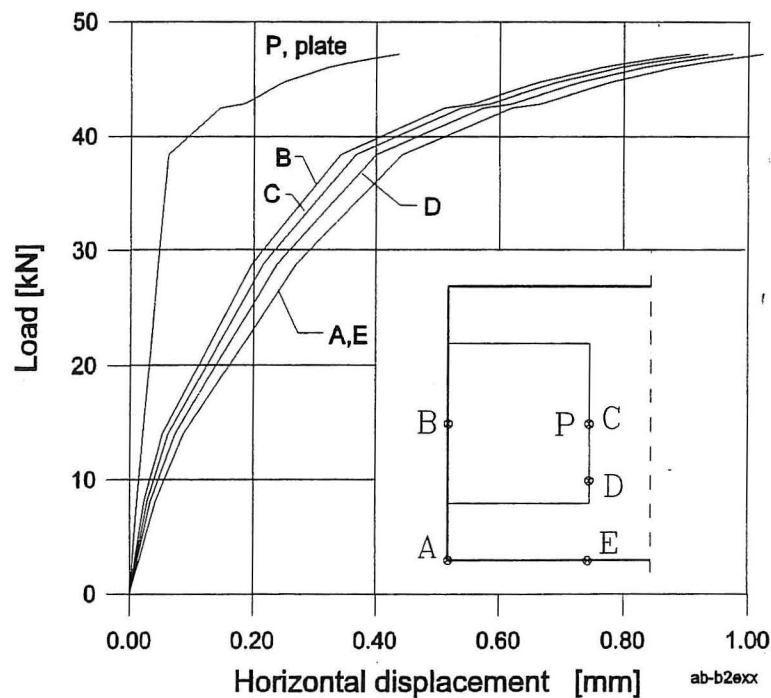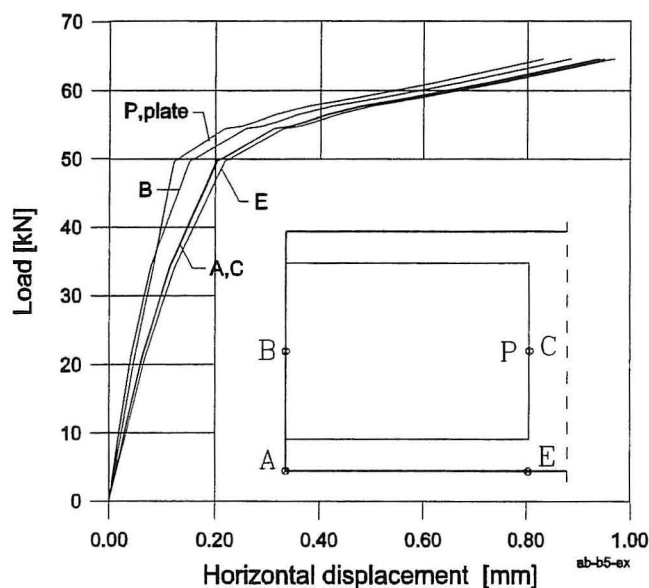Figure 2.13: Load-displacement curves from different points on tensile splice with 130x317mm plate. Points A,B,C and E are located on the timber. Point P is located on the plate.

In figure 2.13 and figure 2.20 on page 25 the deformations of a splice with plate size
130 × 317mm are shown. In figure 2.13 the displacements are increased from points B
to C. The displacements of point C are affected by more than 60% of the deformations
in the plate.

The difference between the displacement at point C and E is smaller caused by the
plate. The influence of the deformations from plate and nails can also be analysed in
figure 2.14. If the load of each curve is divided by the number of nails in a plate they
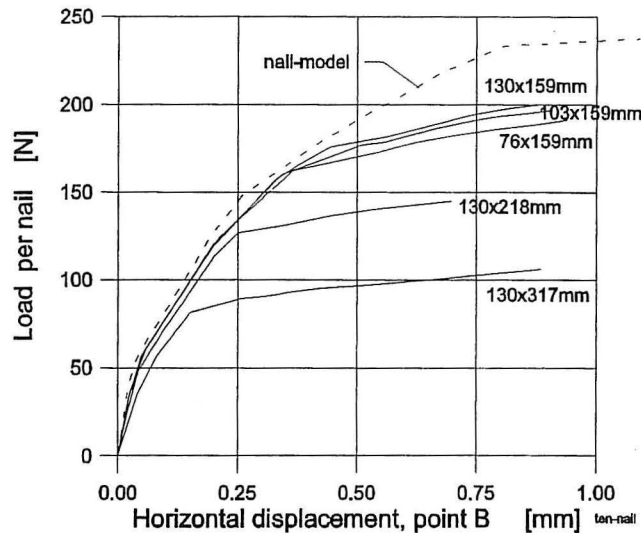
Figure 2.14: Load-displacement curves for the compared to the load-
displacement curve for the nail model.

can be compared to the load-displacement curves for the nail model used. The curve for
the nail model is fitted to the test results in figure A.8 on page 121, see also figure 3.5
on page 33 where the "I-beam curve" coincide with the nail model curve (not shown).
In figure 2.14 the five load-displacement curves from point B are compared with the
nail model. It is seen that the nail model is stiffer than the load-displacement curves
for the splices. The difference between the curves indicates the displacement caused by
the plate deformation near the edge. The effect is small for the three smallest plates,
but it has increased for the two largest plates. When the plate gets plastic the effect is
increased considerably. If the plate is assumed rigid the curves will coincide with the
nail model.

In figure 2.11 and figure 2.13 it is seen that there are significant deformations in the
joint area. This is important to notice, when test results and numerical results are
compared. In the determination of the nail stiffness the deformations of the plate must
influence as little as possible. For the analysed nail-plate the estimation of the nail
stiffness is best for a test with a plate length ≤ 159mm and a plate width equal to the
timber width. The displacements are measured on the edges. The nail stiffness is then
determined until the plate becomes plastic. Displacement measurings independent of
the plate deformation are given in Nielsen et al.(1994).

In figure 2.15 the load-slip curves from point B have been normalized. The load is
divided by the plate width, and the displacement is normalized by a plate length on
159mm (norm. disp. = displacement$\frac{l}{159mm}$). The curves in figure 2.15 almost coincide.
This means that a joint model, where the stiffness mainly depends on the plate area
should give resonable results, see also chapter 6.
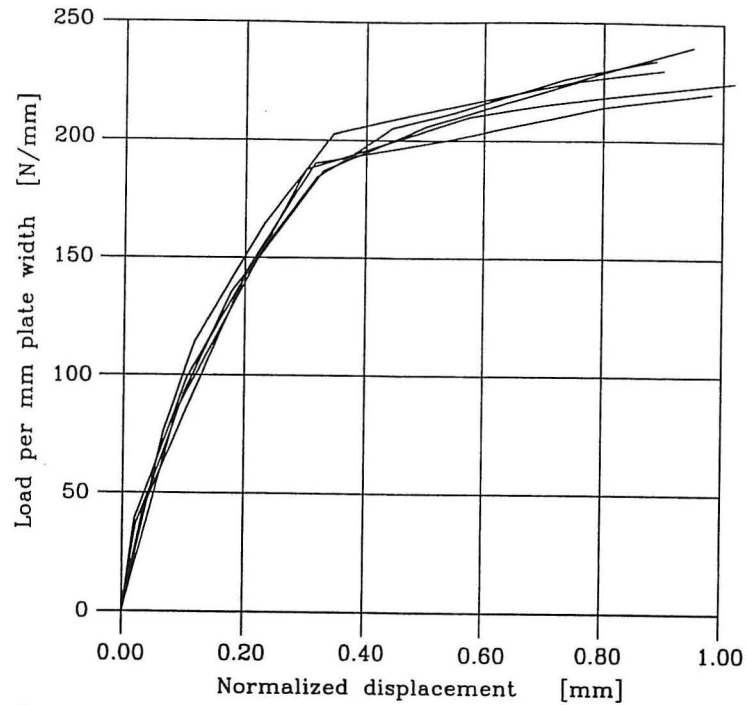
Figure 2.15: Normalized load-displacement curves.

2.3.1   Stress and Force Distribution

Numerical results will be presented for the plate sizes 103×159mm and 130×317mm. Scaled joint deformation will be shown and the stress distribution will be presented with contour curves. Nail forces will be shown in vector plots.

Tensile splice with plate size **103x159mm.**

In figure 2.16 the undeformed and deformed joint are shown.
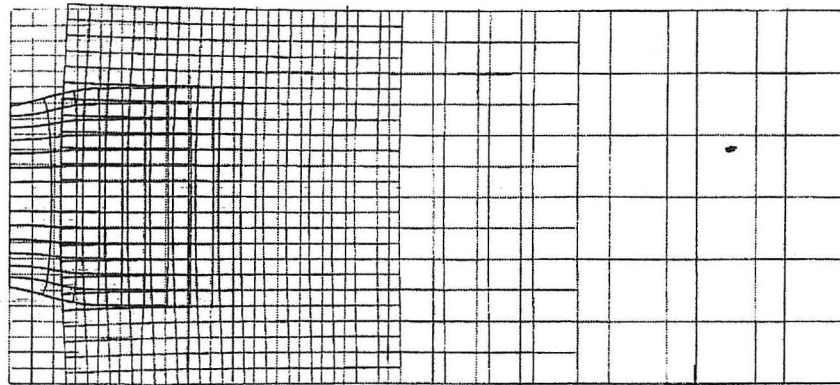
Figure 2.16: Undeformed joint (grey), deformed timber (green) timber
and deformed plate (red). Timber area originally covered
by the plate is shown in blue. Displacement magnification
factor: 25. Load: 47.2kN.

In figure 2.16 it is seen that a large part of the slip is caused by deformation of the nails and deformation of the plate near the edge. In figure 2.17, the stress distribution in the timber is shown. The maximum stress in the timber (9,42MPa) occurs at the
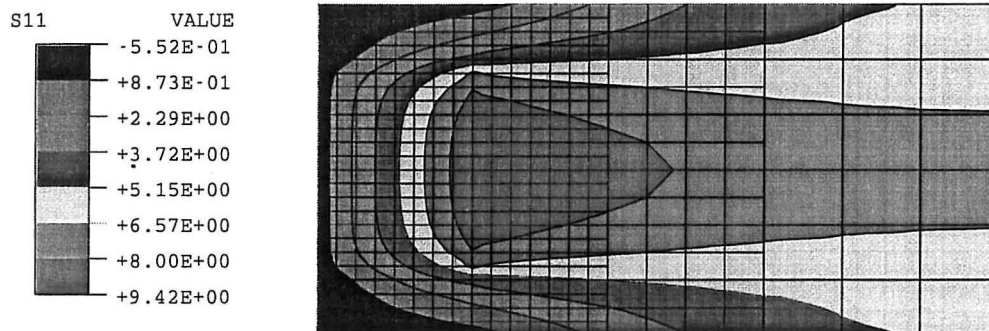
Figure 2.17: **Stresses in timber (MPa) parallel to the grain. The location of the plate is shown as a solid line. Load: 47.2kN.**

end of the plate, and it is 52% larger than the stress in the non-affected beam.

In figure 2.18 the nail forces on the upper half of the timber are shown. It is seen that
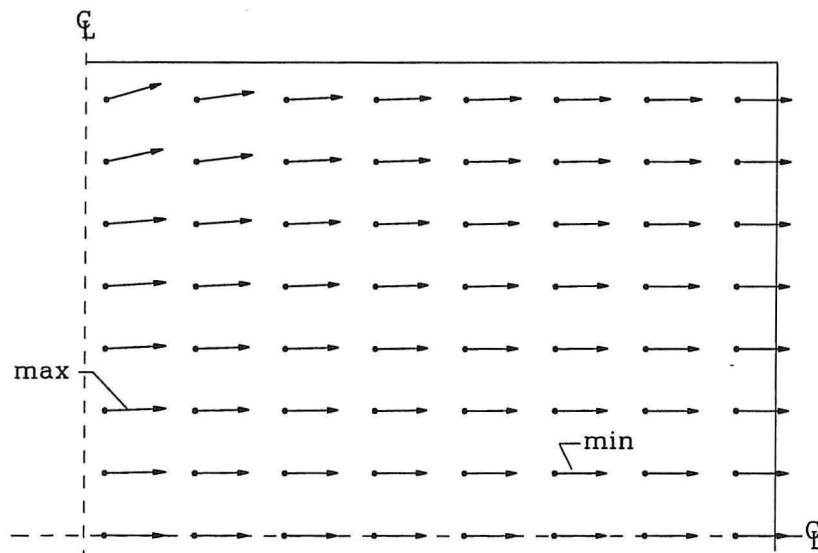
Figure 2.18: **Nail forces on the upper half of the plate. Load: 47.2kN.**

some nails are loaded in direction 2. This is caused by the deformation of plate and timber, see figure 2.16. The maximum force occurs in the first row and the forces are decreasing towards the right. The nail forces are distributed as shown in table 2.5. The minimum nail force is 15% smaller than the max. nail force.

From table 2.5 it is seen that the load capacity of the nails ($\sim$ 240N, see figure 2.14 on page 21 is not exhausted and the maximum von Mises stress in the plate is 232MPa, see figure 2.19, which is smaller than the maximum stress (276MPa), see table 2.4 on page 15. Tests on tensile splices with plate size 103 × 159mm failed at this load level at the nails, see table C.2 page 141. The numerical model has more load capacity and

Force interval [N]	No. of nails
$189.3 < p \leq 195.8$	75
$195.8 < p \leq 202.3$	24
$202.3 < p \leq 208.8$	6
$208.8 < p \leq 215.3$	4
$215.3 < p \leq 221.7$	11

Table 2.5: Nail force distribution in plate. Plate size 103×159mm.
Load: 47.2kN.

MISES	VALUE
	+5.91E+00
	+3.26E+01
	+5.94E+01
	+8.61E+01
	+1.12E+02
	+1.39E+02
	+1.66E+02
	+1.93E+02
	+2.20E+02
	+2.32E+02
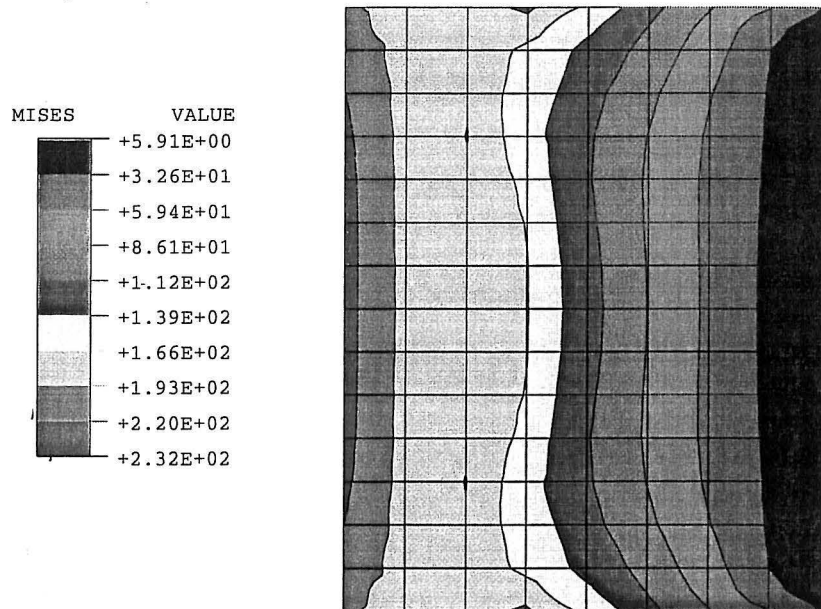
Figure 2.19: von Mises stresses in plate (MPa). Load: 47.2kN.

the failure type cannot be determined on the basis of the model at this load level. The failure in experimental tests was started by withdrawal of the nails at the back of the plate. This phenomenon depends on the geometry of the plate and the withdrawal resistance of the nails, which are not included in the numerical model.

Tensile splice with plate size 130x317mm.

In figure 2.20 the undeformed and deformed joint are shown.
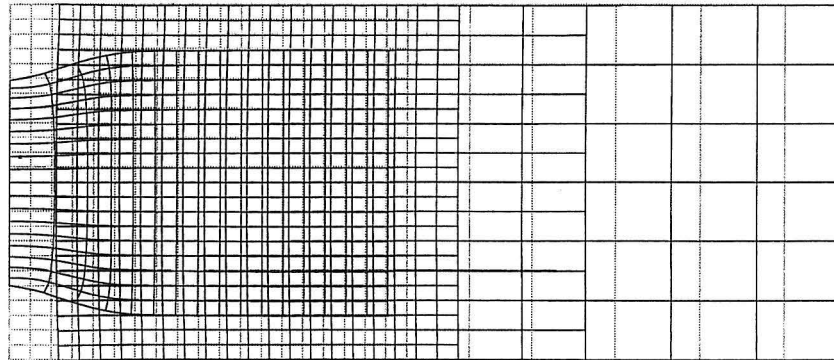
Figure 2.20: Undeformed joint (grey), deformed timber (green) and de-
formed plate (red). Timber area originally covered by the
plate is shown in blue. Displacement magnification factor:
25. Load: 64.7kN.

In figure 2.20 it is seen that a large part of the slip is caused by deformation of the left
area (close to the edge) of the plate. This part ($\sim$15mm) is in the plastic state, see the
plate stresses in figure 2.22.

In figure 2.21, the stress distribution in the timber in direction 1 is shown. The maxi-
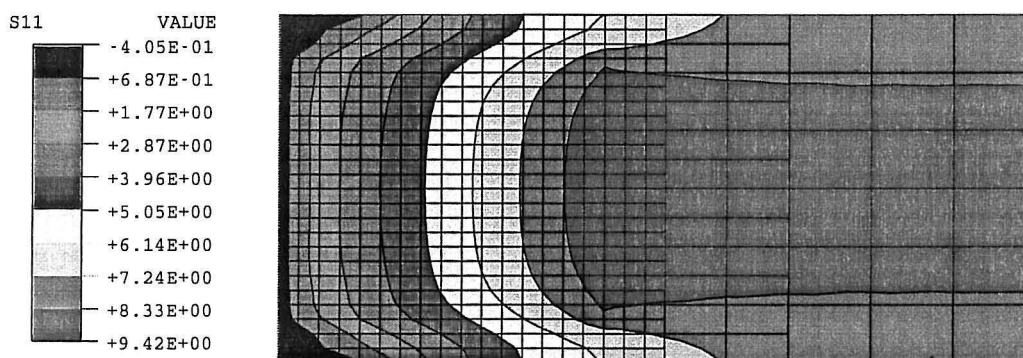
Figure 2.21: Stress in timber (MPa) parallel to the grain. The location
of the plate is shown as a solid line. Load: 64.7kN.

mum stress in the timber occurs in front of the plate and is 11% larger than the stress
in the non-affected beam.

In figure 2.23 the nail forces on the upper half of the timber are shown. The maximum
nail forces occur in the first nail rows, and from the fifth nail row the forces are almost
equal. The minimum nail force is 57% smaller than the maximum nail force, as seen
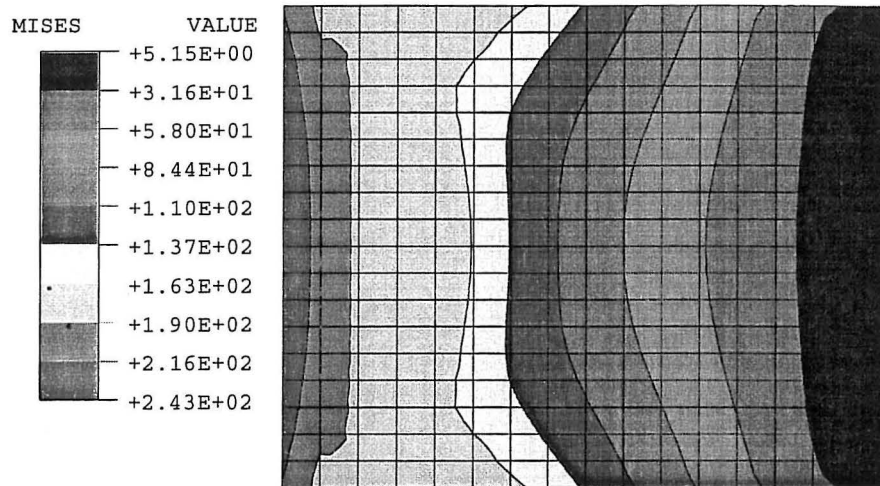
Figure 2.22: von Mises stresses in plate in MPa. Load: 64.7kN.
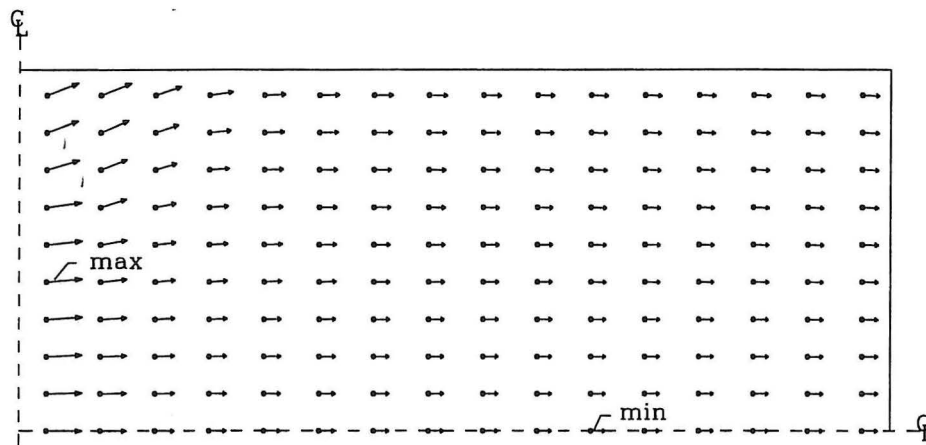
Figure 2.23: Nail forces on the upper half of the plate. Load: 64.7kN.

in table 2.6. The load capacity of the nails is not used, and the joint will fail in the plate due to the large stresses near the edge. This type of failure is also found by the tests.

2.4 Summary

A numerical model of the tensile splice has been made. Plate and timber are modelled as disks without holes. The timber is considered as a linear elastic material and the nail-plate is considered as a linear elastic, plastic von Mises material with isotropic strain hardning. The nails are modelled as nonlinear springs.

Load-slip curves from the numerical model correspond to the results from tests on five different plate sizes in tests with nail failure and in tests with plate failure as well. Since

Force interval [N]	No. nails
$84.6 < p \leq 109.9$	235
$109.9 < p \leq 135.2$	27
$135.2 < p \leq 160.5$	17
$160.5 < p \leq 185.8$	4
$185.8 < p \leq 211.2$	21

Table 2.6: Nail force distribution in plate. Load: 64.7kN.

the load-slip curves fit it is believed that the numerical model can estimate stresses and nail forces too.

The stiffness of a splice joint is sensitive to the stiffness of the nails and the stiffness of the plate area near the timber edge. The deformation of the plate can affect the slip of the joint by more than 60%.

From the discussion in appendix C it is concluded that the load procedure affects the stiffness and failure load of the joint. This is the reason for the divergences between the numerical model and the tests in the work done by Jensen et al.(1994).

The maximum stresses in the timber occur at the front edge of the plate. The maximum nail force, occurs in the middle of the first nail row. The variation of the nail forces is found to be 15% for a 103 × 159mm plate and to be 57% for a 130×317mm plate. The minimum nail force is found near the centre of the plate.

Chapter 3

Bending Splices

In this chapter, splice joints subjected to bending load, see figure 3.1, will be described. As described in the previous chapter, the load in the tensile splices was transmitted by the nails mainly in the grain direction. In the bending case the load will be transmitted by the nails through the plate and by contact between the timber members, if the gap here is so small that it can be closed. As the nails will be loaded in directions non-parallel to the grain direction, a more complex nail model must be used. The effect of plate size, plate location and contact between the timber members will be treated.

The numerical results are compared with the experimental bending tests described in appendix D. Some examples of the stress distribution in plate and timber are given and some plots of the force distribution in the nails are shown.
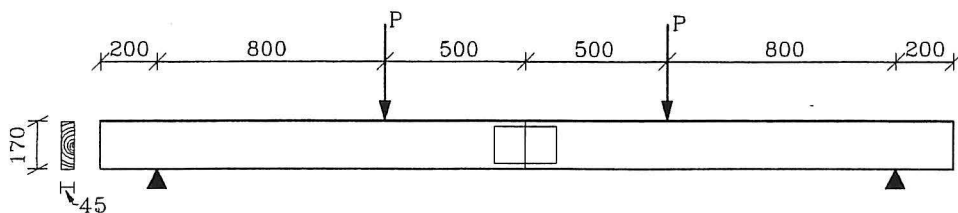
Figure 3.1: Bending load on the splices. Dimensions in mm.

3.1 The Model

A 2-D model, as shown in figure 3.2, is used to model a bending splice with an eccentrically located plate (the hatched area). As the bending splices are symmetric only, the right-hand part of the splice is modelled. The first 350mm of the model has the same grid and geometric dimensions as used for the tensile splice model, see figure 2.2 and figure 3.2. 23×6 "new" timber elements have been added to the tensile splice model.

In the experimental bending tests two "stiff" plates of the width 100mm are used to
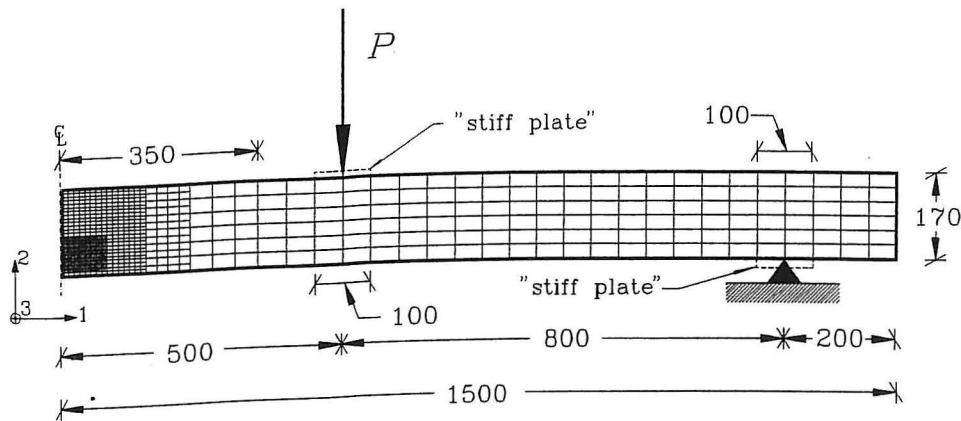
Figure 3.2: **ABAQUS model of a bending slice. Dimensions in mm.**

distribute the load and reaction, see appendix D. In the model, this constraint is made by forcing the nodes underneath the plates always to lie on a straight line, see figure 3.2. The plate edge at the centre line is constrained in direction 1, and the middle node of the stiff plate at the support is constrained in direction 2. The load is made by a vertical displacement of the middle node of the stiff plate above the beam.

The timber and plate elements have the same properties as mentioned in section 2.2.

Six different models are made to compare the numerical results with the experimental results. The plate size and location in each model and the corresponding test are given in table 3.1. The main difference between the models is the plate size and the location of the plate. The gap size can be changed in each model.

Model	Plate size mm	Plate location	Exp. bend test series no.
M0	-	-	BE0
M76C	76×159	centre	BE1
M76E	76×159	eccentric	BE2,BE4
M130C	130×317	centre	BE3
M103E	103×159	eccentric	BE5
M103C	103×159	centre	BE6,BE7,BE8

Table 3.1: **Plate size and location in the six ABAQUS bending models.**

3.1.1 Modelling the Nail

When modelling the nails, three different nail models can be used for ABAQUS, see figure 3.3.

Spring2 :   Two springs placed at right angles to each other acting in a fixed direction e.g. directions 1 and 2, see figure 3.3. The springs connects the two nodes
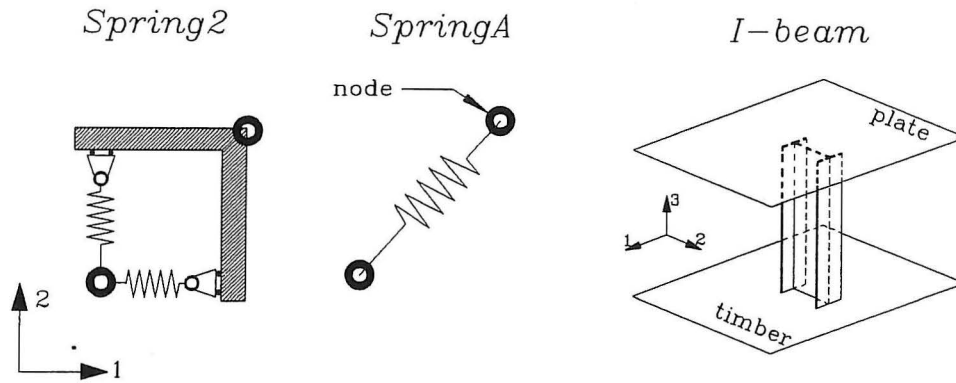
Figure 3.3: Three different nail models.

(shown as circles) each representing a point on the timber and the plate. This model has been used to model the tensile splices. The stiffness in the springs can be non-linear and different in each spring. The non-linear stiffness is given by multi-linear curves.

SpringA : One non-linear spring between two nodes whose line of action is the line joining the two nodes. As the rotation of the action line in this model will be large, the model will use a non-linear geometric solver, which will demand further iterations. The spring properties are "isotropic" since the stiffness is independent on the direction of the action line. The non-linear stiffness is given by multi-linear curves.

I-beam : An elastic-plastic I-beam is placed orthogonally on the (1,2)-plane between a node on the "timber plane" and a node on the "plate plane". Only displacements in the (1,2) plane are free. The stiffness and strength can depend on the load direction, and they are calibrated by the geometric dimensions on the beam, modulus of elasticity and the hardning parameters.

In appendix A it is found that initial stiffness is only slightly affected by orientation of the plate, grain and load. The failure load, however, is different since the ultimate load gets smaller when the angular difference between the grain and load direction is increased. These nail properties cannot be modelled with the *Spring2* and *SpringA* models. The *Spring2* model will act too stiffly in directions non-parallel to the principal axes, and *SpringA* will give the same stiffness and failure load in all directions. The *I-beam* model can model these properties, see figure 3.4.

In figure 3.4, five load-displacements curves with the *I-beam* model for different directions ($\gamma = 0^o, 20^o, 30^o, 45^o, 90^o$) of the displacement vector are shown. The numbers on the curves denote the angle between the displacement vector and the force vector, $(\gamma - \vartheta)$, at the load level. It is seen that the angle is increased with increasing load and the force vector searches against a stiffer area. $(\gamma - \vartheta)$ has a variation between 0° and 18°, which is of the same size as found by Jensen(1994). The load is parallel to the displacement in the directions of the principal system. $(\gamma = 0^o \wedge 90^o \Rightarrow \vartheta = \gamma)$

In figure 3.5, the load-displacement curve of the *I-beam* nail model is shown (solid line). The dashed curves are maximum and minimum load-displacement curves from tests with several nail rows loaded parallel to the grain, see figure A.8 on page 121.

The *Spring2* model was used for the nails in the tensile splice model, and the load-displacement curve for this model coincides with the *I-beam* curve in figure 3.5.

For $\gamma > 0^o$, the stiffness properties of the *I-beam* model are chosen so that the same load-displacements curves as shown in figure A.14 on page 125 are obtained. (Since no reliable test results have been made with $\gamma = 90^o$, the load-displacement curve for this angle is estimated).

In the following, the *I-beam* model will be used to model the nails. The difference between the load-displacement curves form a bending splice with the *I-beam* model and a bending splice with the *SpringA* model is analysed in section 3.2.1.

3.1.2 Modelling Contact

If the gap between the timber members is small, these will be in contact at the beam end above the plate, see figure 3.2. To model this effect, the nodes on the upper half of the beam are connected to a contact element (in ABAQUS: A slide line element). In the contact surfaces axial forces and friction forces can be transmitted. The friction between the timber members is dependent on the axial forces, a property which can be involved with the contact elements. However, friction is omitted in the models caused by a lack of informations on this subject. In the tested bending splices the influence of friction on the stiffness is small, whereas in heel joints the effect is considerable. According to Lau(1986), the friction effect can increase the strength of a heel joint and should not be ignored.

3.2 Results

In this section the results for the bending splices will be presented. The results from ABAQUS will be compared with the test results, and the stress and nail force distribution will be shown.

3.2.1 Load-Displacement Curves

In figure 3.6 to 3.11 the load-displacement curves from ABAQUS are compared to the load-displacement curves from tests described in appendix D. The load is given as half the total vertical load (P in figure 3.2 on page 30) and the vertical displacement is measured 40mm from the centre of the beam, see figure D.3 on page 151. The solid lines are load-vertical displacement curves from ABAQUS and the dashed lines are load-displacement curves from the tests. The test specimens are unloaded once. g is the gap size in mm. The end of the curves from ABAQUS do not denote failure load.
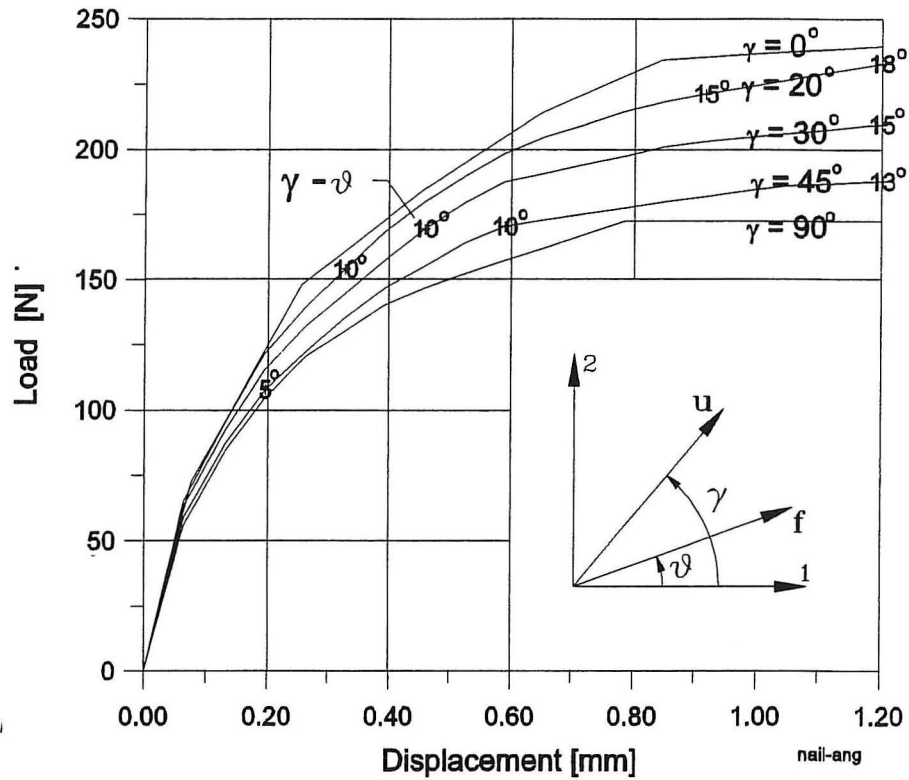
Figure 3.4: Load-displacement curves from the *I-beam* nail model. γ is the angle between the grain direction (1-axis) and the displacement vector *u*. ϑ is the angle between the force vector *f* and the grain direction (1-axis).
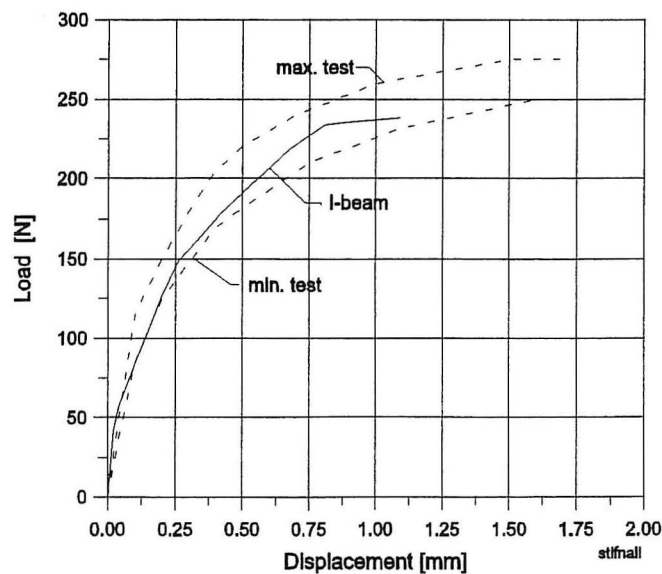
Figure 3.5: Load-displacement curves for the *I-beam* model. Dashed lines are load-displacement curves from nail tests with several nail rows loaded in the grain direction.
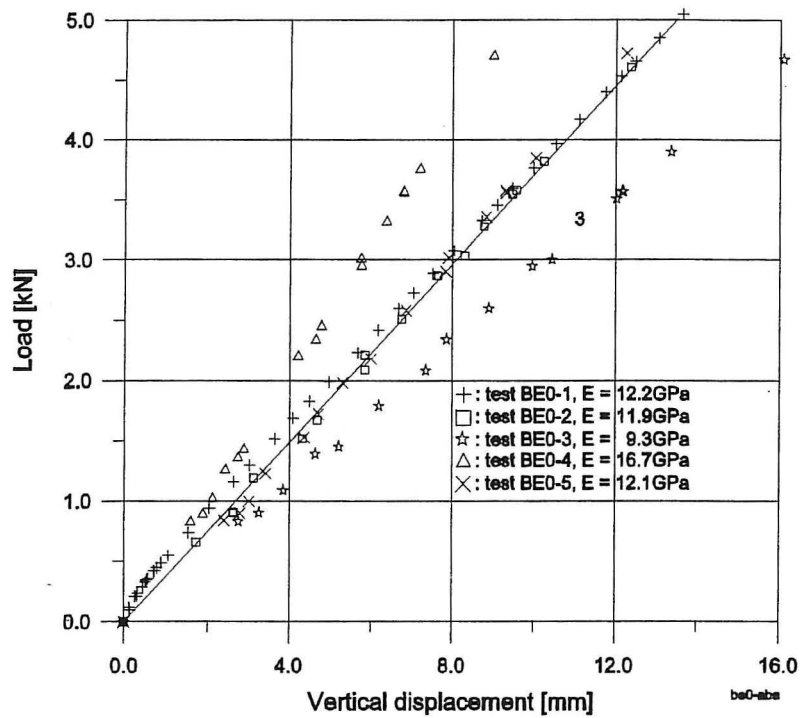
Figure 3.6: Load-displacement curves for a beam (with no plate). Series BE0.
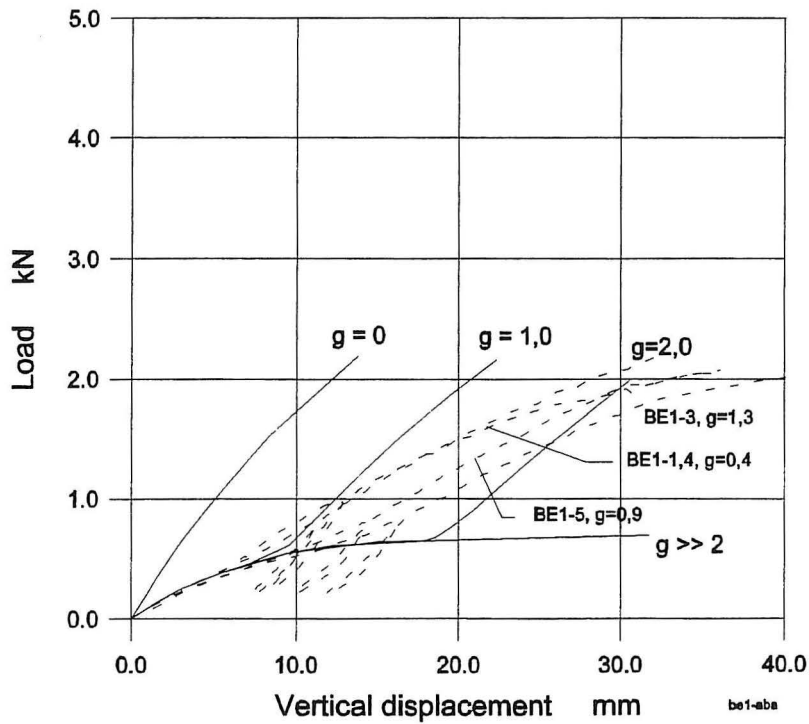
Figure 3.7: Load-displacement curves for bending splices with plate size 76x159mm centrically located. Series BE1.
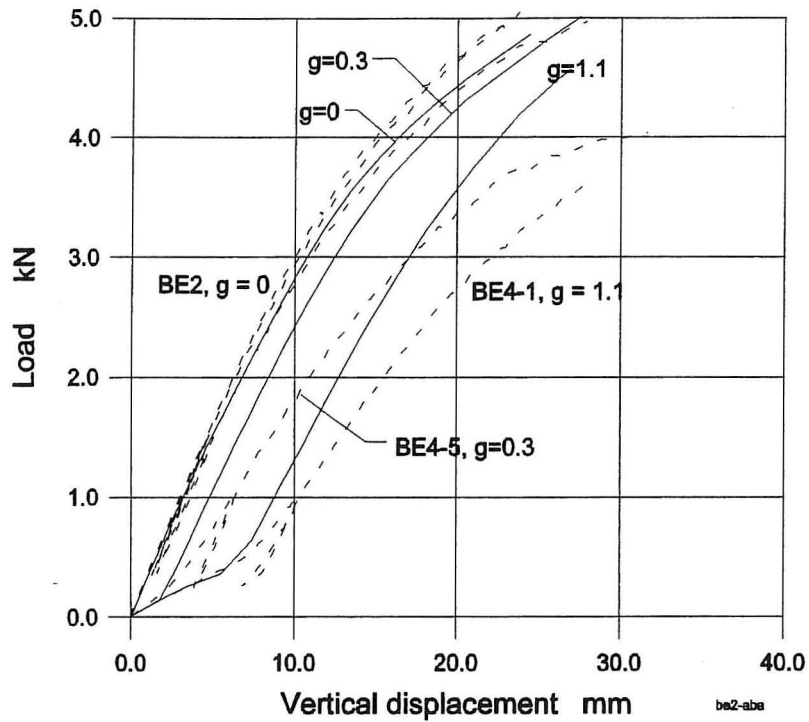
Figure 3.8: Load-displacement curves for bending splices with plate size 76x159mm eccentrically located. Series BE2, BE4.
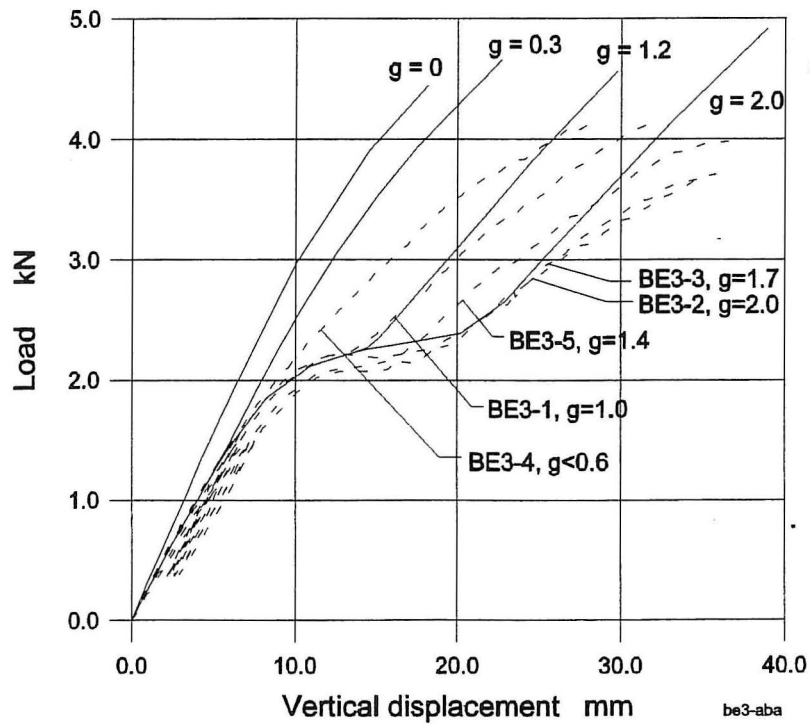
Figure 3.9: Load-displacement curves for bending splices with plate size 130x317mm centrically located. Series BE3.
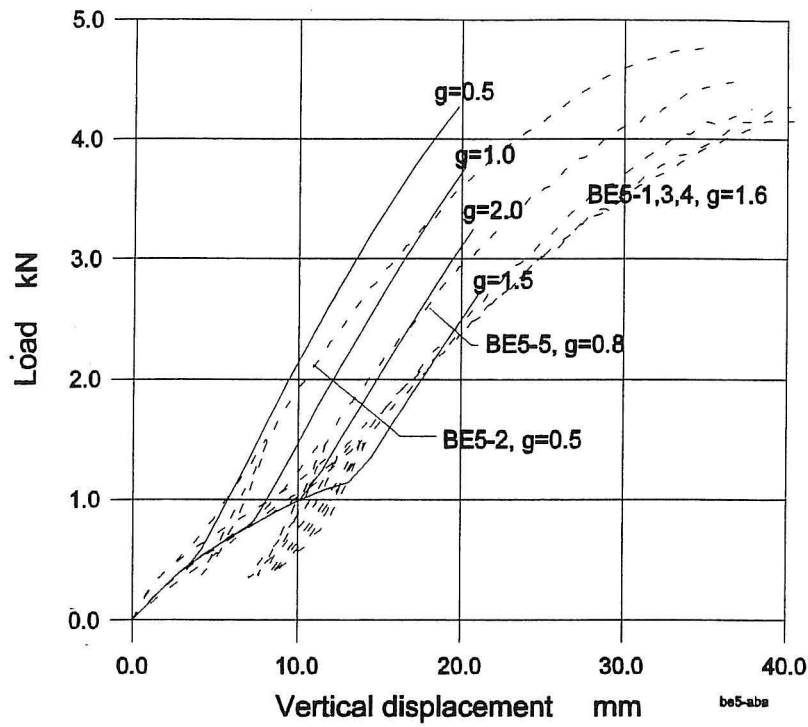
Figure 3.10: Load-displacement curves for bending splices with plate size 103x159mm eccentrically located. Series BE5.
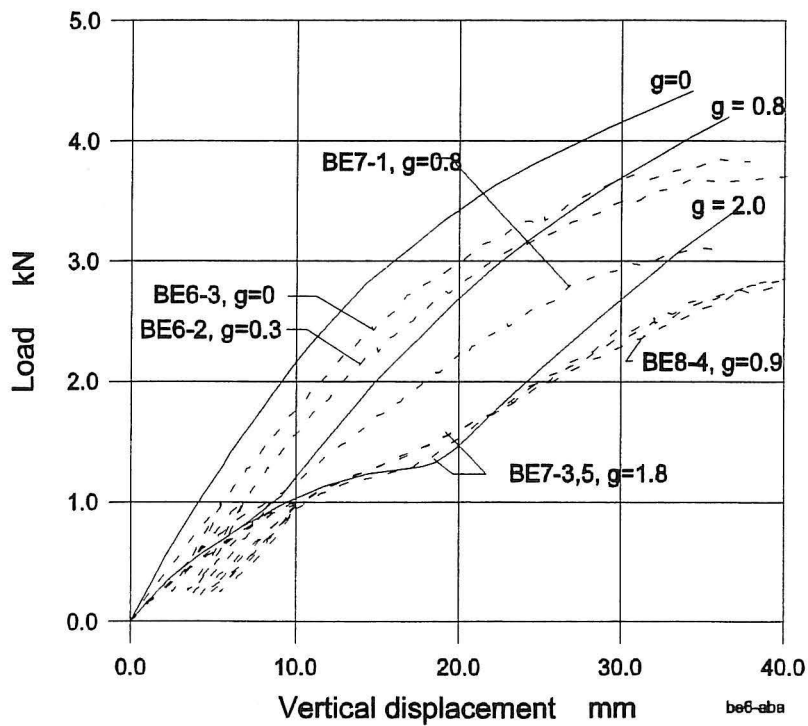
Figure 3.11: Load-displacement curves for bending splices with plate size 103 x159mm centrically located. Series BE6, BE7, BE8.

In figure 3.6 it is seen that the "timber model" (the model without a plate) fits the tests with $E \sim 12000$MPa. In general the load-displacement curves from ABAQUS fit the test results, but when contact occurs, the displacements are underestimated. In the bending tests, the fibres in the the contact zone are pressed into each other (called butt effect), which it is a well-known phenomenon from compression tests on timber. It will result in decreased stiffness in the compression zone whereas the stiffness in the ABAQUS model is unchanged. The butt effect is removed in test series BE2, and in figure 3.8 the numerical result fits the test result in contact. The butt efffect can be included in the model by decreasing the stiffness of the timber elements closest to the contact surface. The butt effect is largest in a splice, but in other joint types, e.g. a heel joint, the effect will vanish caused by the changed grain direction.

In test series BE3, buckling was observed before contact (is observed as the "horizontal" part of the load-displacements curves in figure 3.9). The load-displacement curves from ABAQUS fit the test results in buckling, but the vertical part is caused by plastic deformation in the plate.

The load level where contact occurs is also estimated well by the model. This is, since as no special attention has been given to achieve well-defined gaps and contact surfaces at the test specimens.

The stiffness of the bending splices is not sensitive to the modelling of the nail. In figure 3.12, two load-displacement curves with different nail models are shown. The splice has a 76×159mm eccentrically located plate and a gap size of 1.1mm. The numerical models with the *SpringA* nail model can then also be used to determine stiffness properties of a nail-plate joint.
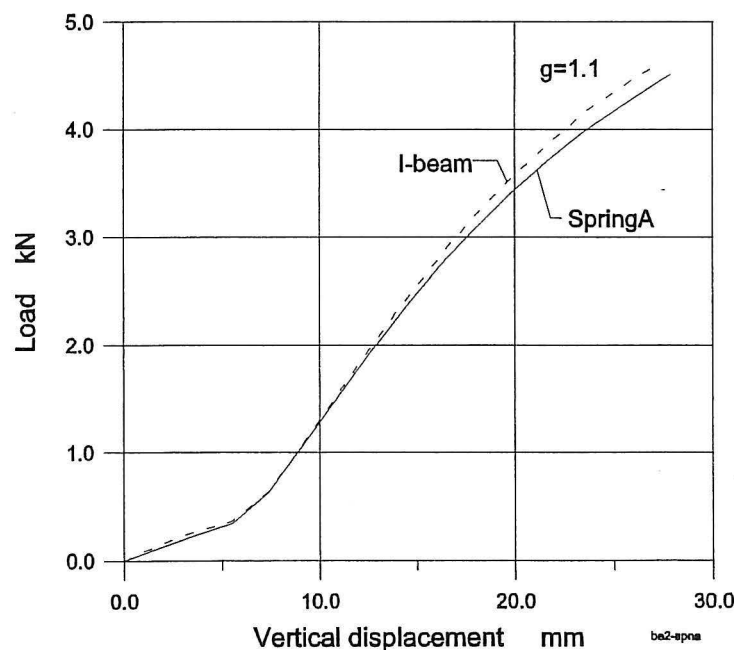
Figure 3.12: Load-displacement curves for bending splices with an *I-beam* and a *SpringA* nail model. Plate size 76×159mm, eccentrically located.

3.2.2   Stress and Force Distribution

In the following, the stress distributions in the timber and plate are given for splices with 76×159mm plates. First, results are given for a splice with a centrally located plate and without/with contact between the timber members. Second, results for a splice with an eccentrically located plate and contact between the timber members are shown.

Splice with Centrally Located Plate

In figure 3.13 the undeformed and the deformed model are shown.
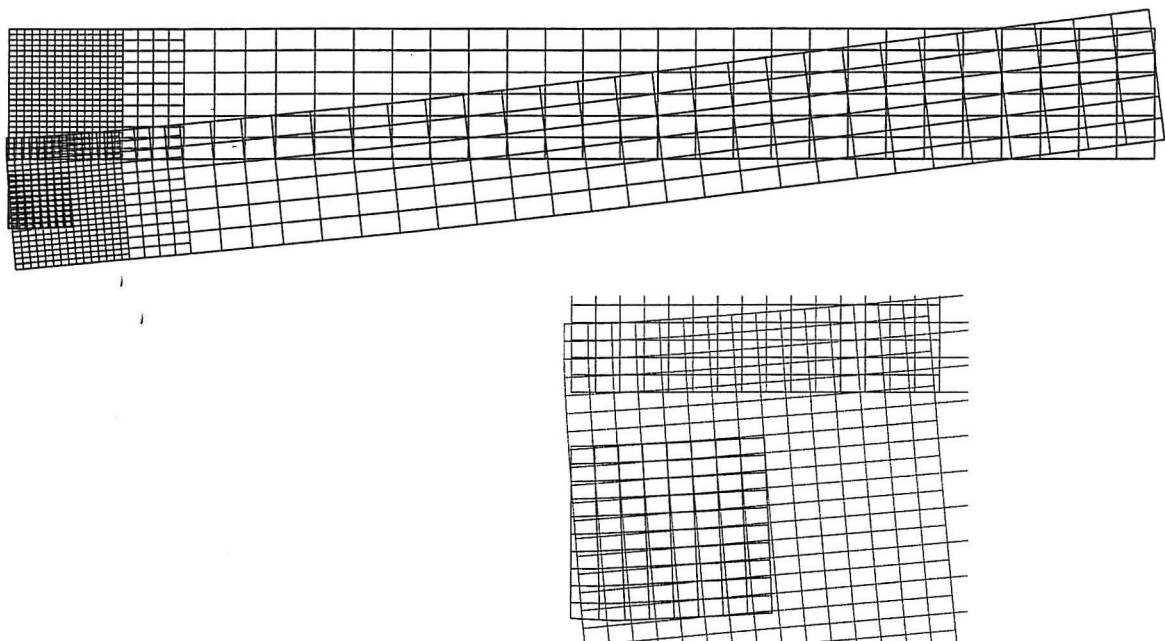
Figure 3.13: Undeformed (red) and deformed model (timber: green, plate: black) of a bending splice with a centrally located plate. Displacement magnification factor: 6.

In figure 3.14, the stresses in the left-hand part of the timber is shown. Contact between the timber members has not yet occurred.

The stress distribution in figure 3.14 is asymmetric, and the "Navier distribution" is established at a distance of 350mm from the timber edge (the right edge of figure 3.14). The stress on the lower edge calculated by Navier's formula is found as ~1.39MPa, which fits with the stress contour in figure 3.14. The maximum stresses occur at the plate corners, and they are 45% higher than the maximum stresses in an unjointed beam.
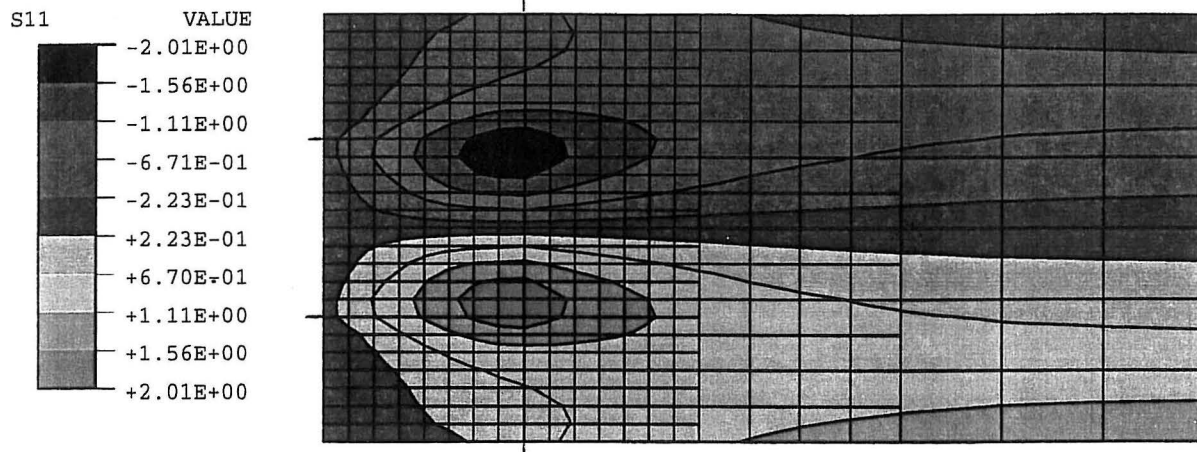
Figure 3.14: Stresses in timber parallel to the grain in MPa. Plate 76×159mm centrally located shown with a solid line. No contact. Load: 0.376kN.
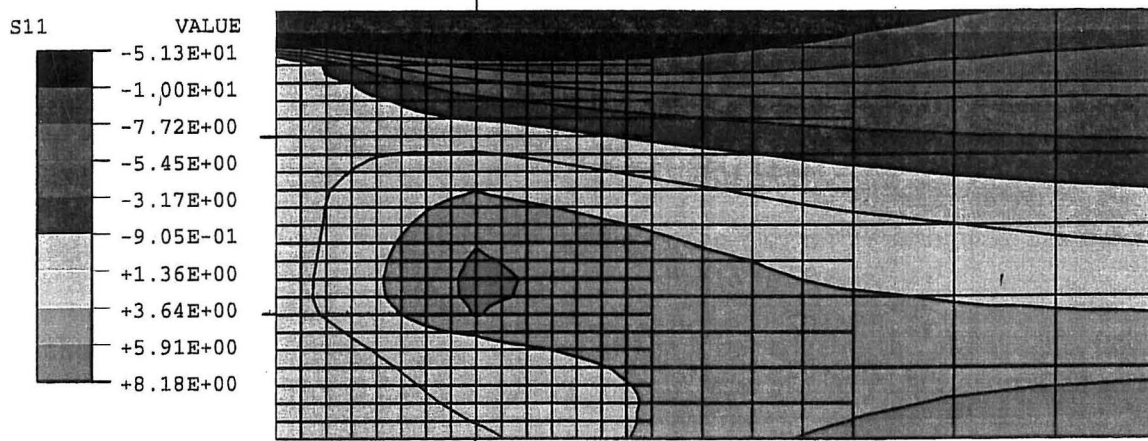
Figure 3.15: Stresses in timber parallel to the grain in MPa. Plate 76 ×159mm centrally located shown with a solid line. Contact between the timber members. Load: 2.376kN.

In figure 3.15, the stresses in the timber with contact between the timber members are shown. The compression zone extends to the contact area, which has a height of about 20mm. The maximum compression stress (51.3MPa) is rather high, but the timber did not fail in the tests. In the timber below the plate there are only tensile stresses and the "Navier distribution" is again recognized at the right-hand edge of figure 3.15.

The stress perpendicular to the grain is found between -0.59MPa and 3.06MPa, where the maximum stress appears at the lower part of the contact surface (not shown). The maximum shear stress is between 1.67MPa and 2.11MPa, where the maximum stress appears in the compression zone in the timber above the plate (not shown).

In figure 3.16, the von Mises stress distribution in the plate is shown. The distribution is symmectric. The stresses in the upper half of the plate are mainly affected by

MISES   VALUE
          +1.88E+00
          +2.39E+01
          +4.61E+01
          +6.82E+01
          +9.03E+01
          +1.12E+02
          +1.34E+02
          +1.56E+02
          +1.78E+02
          +2.00E+02
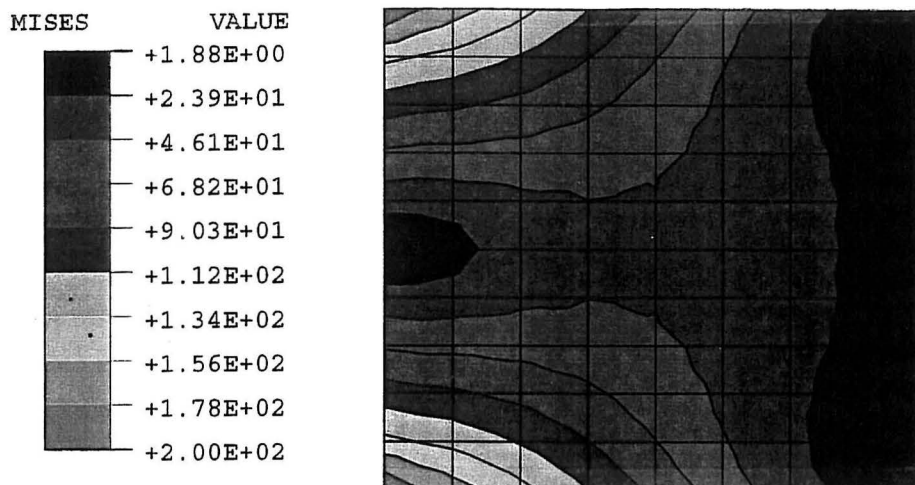
Figure 3.16: von Mises stresses in the plate in MPa. Plate 76x159mm
centrally located. No contact. Load: 0.376kN.

MISES   VALUE
          +4.42E+00
          +3.46E+01
          +6.49E+01
          +9.52E+01
          +1.25E+02
          +1.55E+02
          +1.86E+02
          +2.30E+02
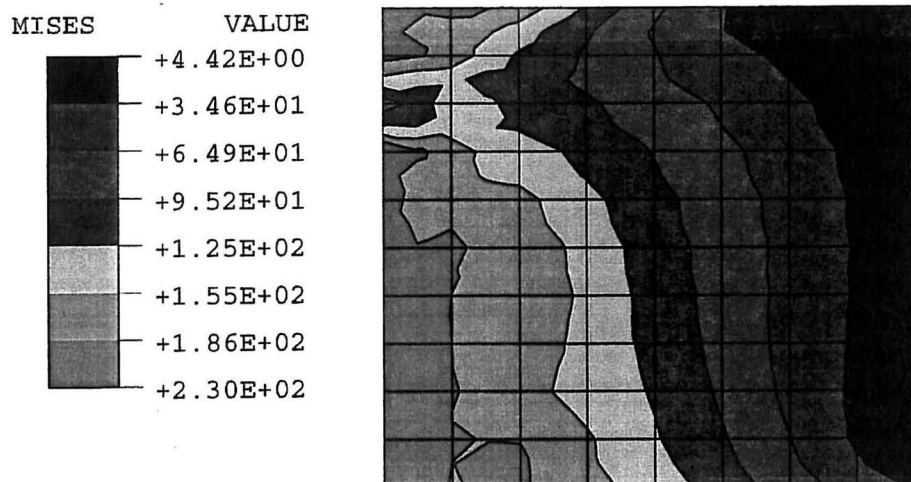
Figure 3.17: von Mises stresses in the plate in MPa. Plate 76x159mm
centrally located. Contact between the timber members.
Load: 2.376kN

compression stresses, and the stresses in the lower half are mainly affected by tensile
stresses. The maximum stresses, which are now already in plastic state, occur at the
plate edges above the gap. The plate areas in the middle and at the back are almost
unaffected by the load. In contact, the compression zone (the area in the upper left-
hand corner of figure 3.17) is getting smaller, and the tensile zone is enlarged and
moved against the contact zone. The main part of the compression is transmitted by
the contact surface of timber and the plate almost only transmits the tensile load.

The nail forces in the splice without contact are shown in figure 3.18, to the left. The
nail forces are increased with increasing distance from the centre of the nail group.
The maximum forces occur in the nails at the edge closest to the gap. The forces in
figure 3.18 to the left follow elliptical curves with a rotation centre near the middle of
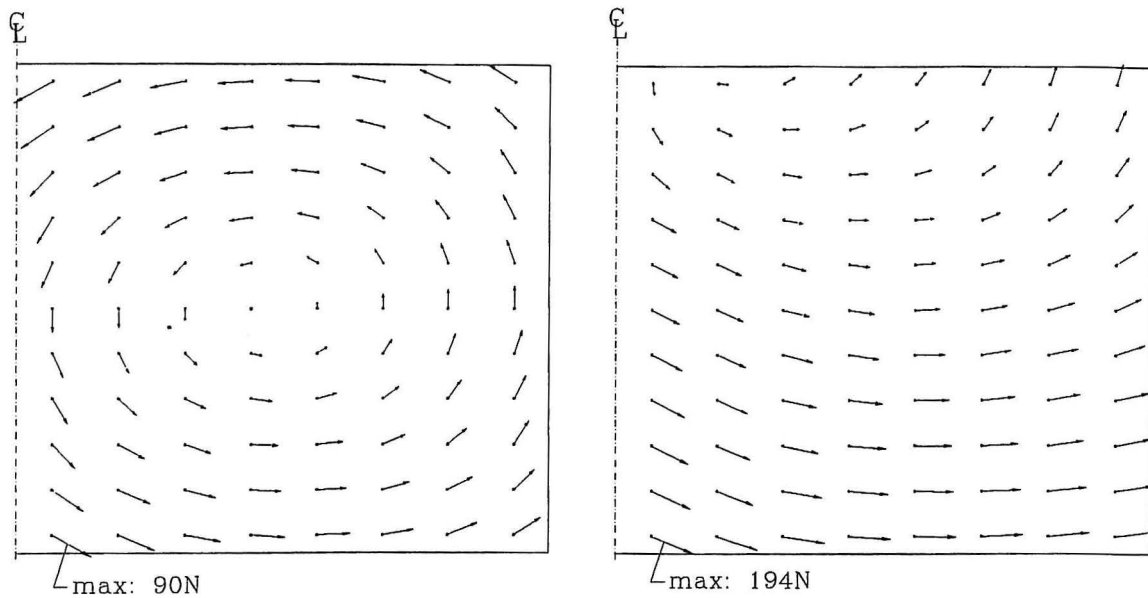
Figure 3.18: Nail forces on the plate. Plate size 76×159mm. In the left-hand figure a splice without contact (load: 0.376kN) and in the right-hand figure a splice with contact (load: 2.376kN).

caused by the orthotropic stiffness properties of the timber.

In figure 3.18 to the right the rotation centre of the nail forces is moved against the contact zone. The main direction is almost parallel to the grain.

In the tests, the joint failed by the tension at the lower edge of the plate. This failure type is also estimated by ABAQUS as the plate stresses are very high compared to the size of the nail forces, see figure 3.17 and figure 3.18 to the right.

Splice with Eccentrically Located Plate

In figure 3.19, the stresses in the timber are shown. The contact surface has a height of ~30mm and the maximum stress in the compression zone is 49.6MPa. The stress on the lower edge calculated by Navier's formula is found as ~16.4MPa, which fits the stress contour in figure 3.19. The stress distribution is unaffected by the joint of a distance of twice the height of the beam (2×170mm).
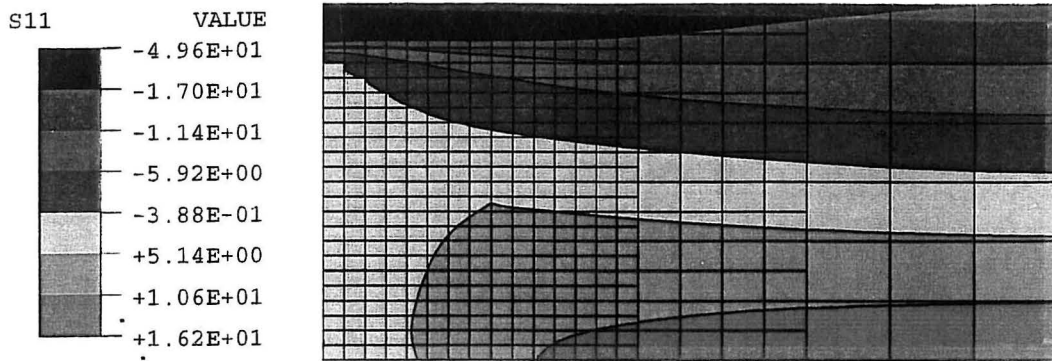
Figure 3.19: Stresses in timber parallel to the grain in MPa. Plate eccentrically located with size 76x159mm - shown as a solid line. Contact between the timber members. Load: 4.436kN.
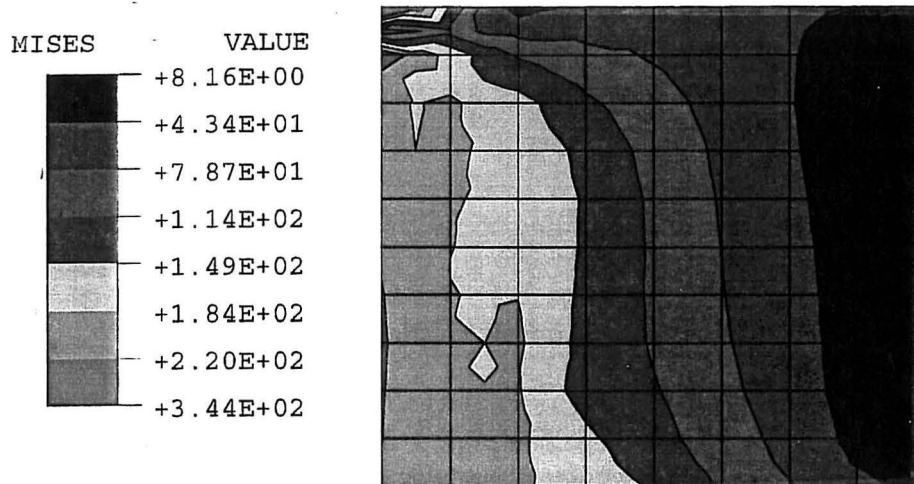
Figure 3.20: von Mises stresses in the plate in MPa. Plate eccentrically located with size 76x159mm. Contact between the timber members. Load: 4.436kN.

In figure 3.20, the von Mises stresses in the plate are shown. Near the gap the plate is in a plastic state which is mainly caused by the tensile force.

In figure 3.21, the nail forces on the timber are shown. The nails are mainly loaded in the grain direction.

The test specimens with this plate size and location failed by the plate, which is estimated by ABAQUS too.
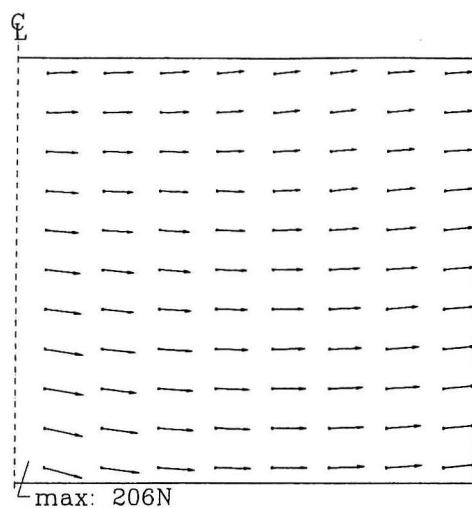
Figure 3.21: Nail forces on the plate. Plate eccentrically located size 76 x159mm. Contact, Load: 4.436kN.

3.3 Summary

An ABAQUS model for the splices in bending has been made. Timber and plates are modelled with the same properties as the tensile splices described in chapter 2, whereas the nails are modelled with small elastic-plastic I-beams to obtain the properties as found in appendix A. Also, a model with nails modelled as springs has been used.

The ABAQUS model can predict the load-displacement curve for several different sizes and locations of the plate. When contact between the timber members occurs, ABAQUS underestimates the displacements. This is caused by the butt effect in the contact zone of the tests specimens which is not included in the numerical model. It is, however, possible to model the effect, by decreasing the stiffness of the timber elements closest to the contact zone.

The joint stiffness is not very sensitive to the nail model used. There is almost no difference between load-displacement curves made from two different nail models.

At a distance of twice the beam height the timber stresses are unaffected by the joint. In contact, the timber transmits the compression stresses and the plate transfers the tensile stresses.

When the plate is eccentrically located, contact appears at a lower load level and the stiffness and strength are increased compared to a joint with a centrally located plate of same size.

Chapter 4

A Heel Joint

This chapter deals with a heel joint, see figure 4.1. This joint type is very common in the most trusses. A heel joint is modelled by ABAQUS and subjected to a load. Load-displacement curves will be shown and some plots of the stress and nail force distributions are given. The results will be used in section 6.3 on page 84, where an AN-TRUSS model of the heel joint is described.

No experimental tests have been made to verify the numerical results.

4.1   The Model

In figure 4.1 the analysed heel joint is shown.
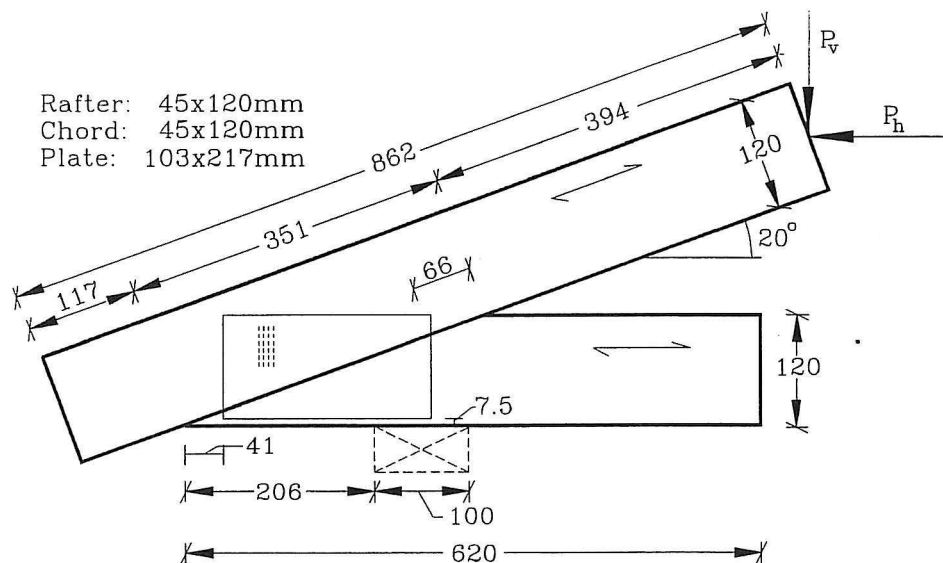
Figure 4.1: The analysed heel joint. Dimensions in mm.

The load is caused by a vertical displacement of the mid node at the top of the rafter, which will involve a horizontal load (P_h) and vertical load (P_v) at this point, see figure 4.1. There is no gap between the rafter and the chord, and during loading both contact and a gap will appear. No friction in the contact zone is assumed. The effect of friction in heel joints is described on page 32. The right-hand end of the chord is fixed and the vertical displacements at the sill are fixed too.

The timber and plate have the same properties as stated in chapter 2. The nails are modelled by the *SpringA* element, see section 3.1.1, because it is easier to assemble this element with the plate and timber elements when the meshes are not identical. However, in order to make the initial locations of the nodes of the *SpringA* elements identical, some of the timber elements on the rafter below the plate have a non-quadrilateral mesh, see figure 4.3. It is assumed that the stiffness of the joint with the *SpringA* elements is almost identical to the stiffness of a joint where the nails are modelled with *I-beams*. The mesh of the timber and plate is shown in figure 4.2.
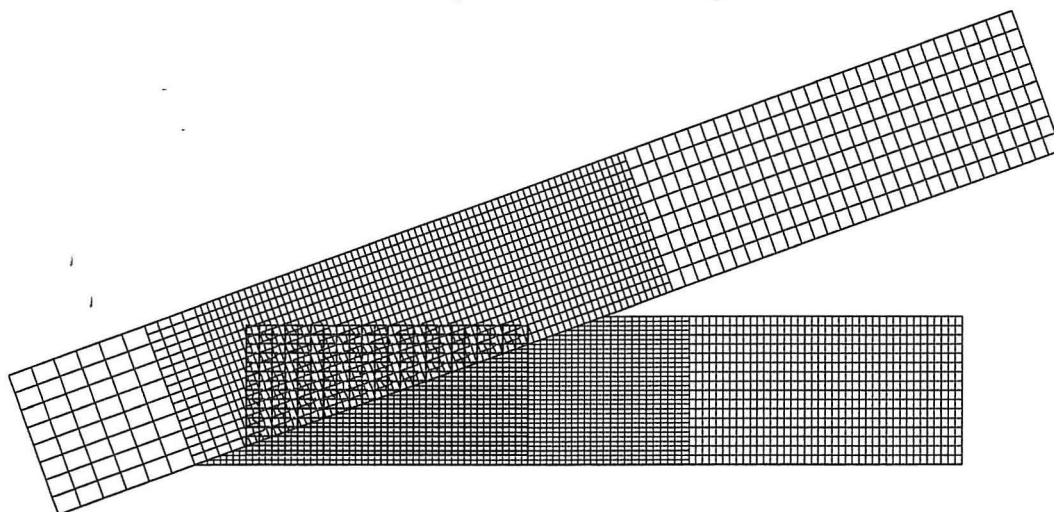
Figure 4.2: Mesh of the timber (red) and the plate (black).

4.1   Results

In this section, the numerical results from ABAQUS are presented. All plots in this section are given with a vertical displacement on 5mm at the end of the rafter, see also figure 4.4.

In figure 4.3, the deformed mesh of the rafter and chord is shown.

The chord is in contact with the whole width of the sill (observed as small discontinuities at bottom line of the chord). The rafter is in contact with the chord at the upper left-hand corner. In figure 4.3 it looks as if the outline of the rafter has passed the outline of the chord in the contact zone. This is caused by the displacement magnification factor.

In figure 4.4, the vertical and horizontal forces at the top of the rafter are plotted
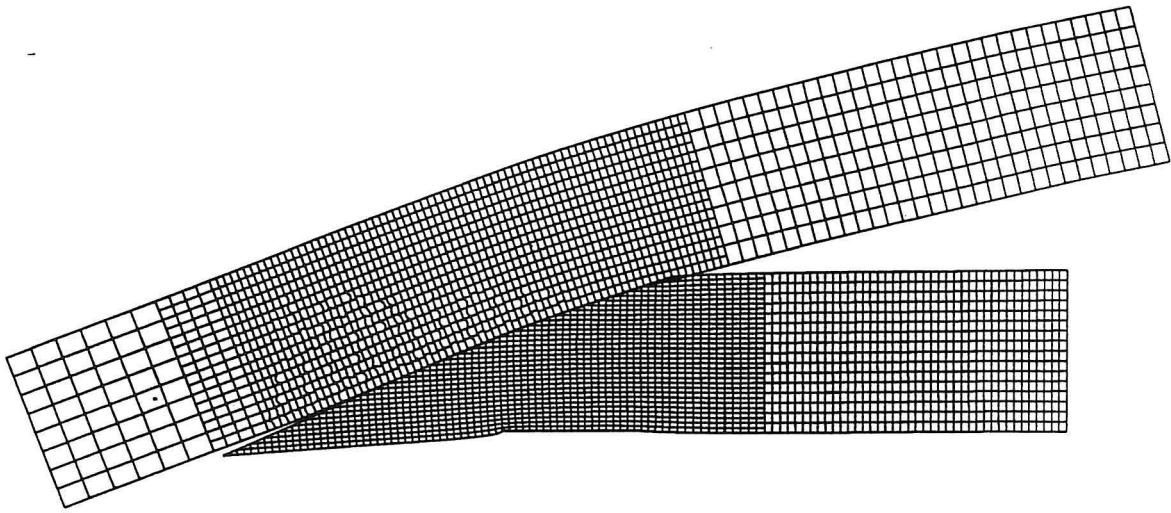
Figure 4.3: Deformed mesh of the timber. Displacement magnification factor: 10.

against the vertical displacement at the same point. Also the size of the total force in the contact zone and the reaction force at the sill are given. The positive directions of P_h and P_v are given in figure 4.1.
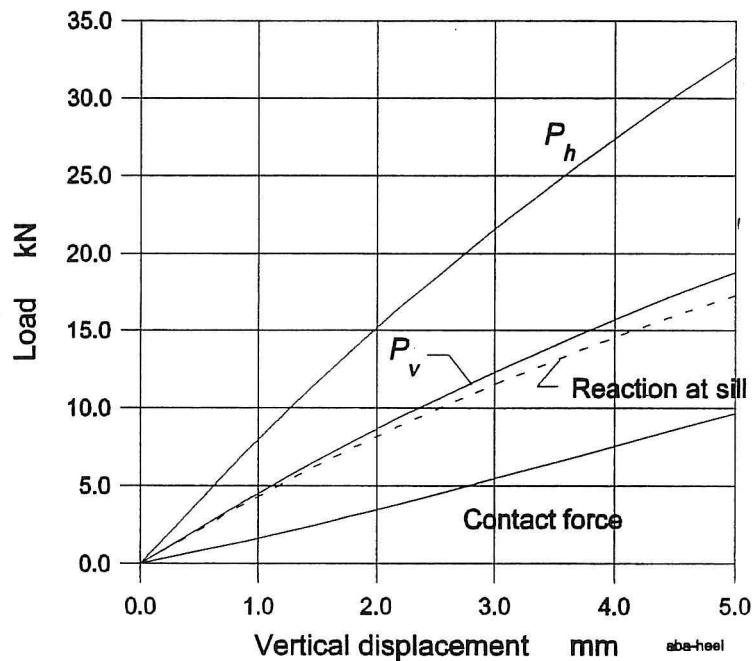
Figure 4.4: Load-displacements curves for the heel joint.

The curves of P_h and P_v are slightly non-linear, whereas the curve for the contact force is linear. Most of the vertical load is absorbed by the sill.

During loading the location of the total contact force is constant at a distance about 50mm from point a measured parallel to the rafter, see figure 4.5.

In figure 4.5, the variation of the section forces in the system line of the rafter is given. The outlines of the rafter, chord and plate are shown as dashed lines.
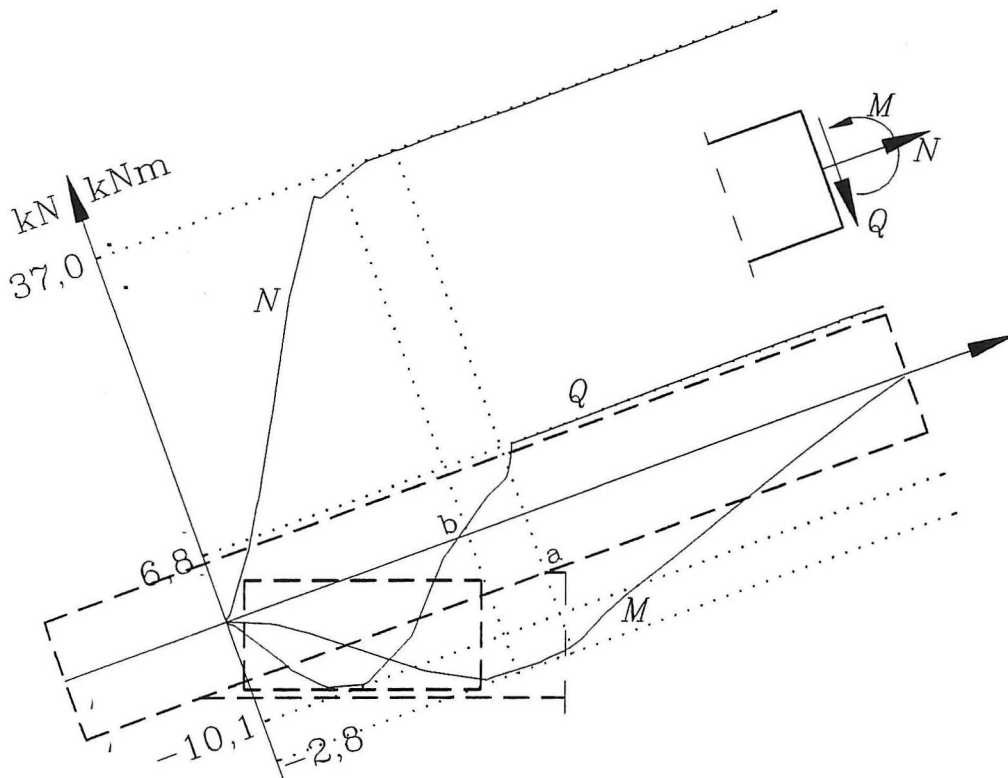
Figure 4.5: Variation of the section forces in the rafter.

The section forces are calculated by summing up the stresses on a section. The axial force, N is constant from the end of the rafter until the section by the plate, point b. Then the axial force is absorbed by the nails (observed by a decreasing value of N) and transmitted to the plate. At the left-hand end of the plate all the section forces are zero. The shear forces are also constant from the end of the rafter, but at the section by the chord (point a), they are decreased caused by the contact forces. The steep drop of Q at point a is caused by the large contact stresses in this area. Q becomes zero at a distance about 50-60mm from point a. In the same section, the moment, M, which has increased linearly from the end of the rafter, reaches the maximum value (2.8kNm). To the left of point b the contact forces and the nail forces generate a negative shear force, which at last is absorbed by the nails at the left-hand end of the plate, see also figure 4.6.

4.2.1   Stresses and Nail-Force Distribution

In figure 4.6, the nail forces on the plate are shown. The nail group on the rafter and the nail group on the chord are separated by the gap (the dashed line).

The nail forces are distributed as shown in table 4.1. The maximum nail force (219.2N) and minimum nail force (22.4N) are both located in the nail group on the rafter. The
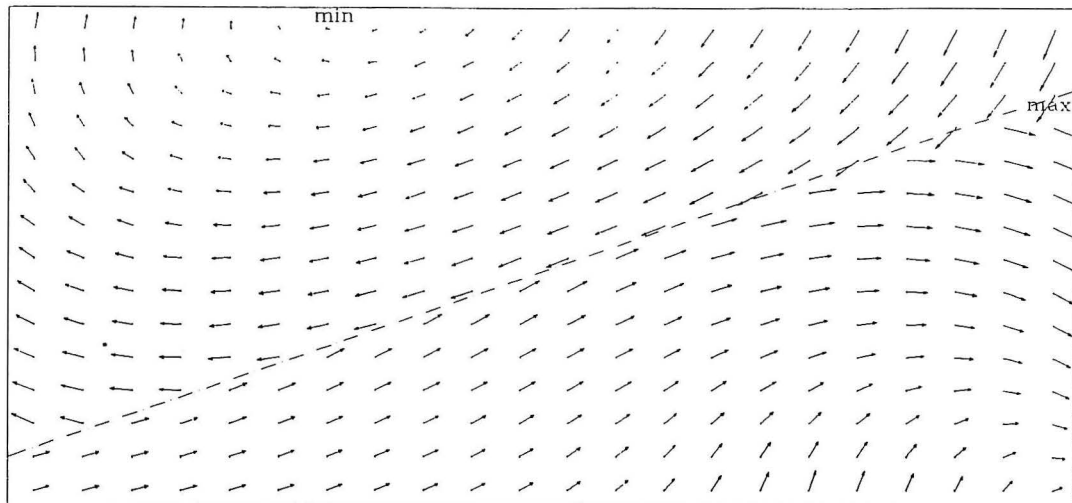
Figure 4.6: Nail forces on the plate.

value of the maximum nail force is close to the failure load of the nail.

In the upper right-hand corner of the plate it is seen that some of the compression force in the "contact area" is transmitted by the nails to the plate. The upper nail group has a "rotation centre" about a point near the minimum nail force. In the lower nail group the "rotation centre" is located at the lower right-hand corner.

Force interval [N]	No. of nails
$22.4 < p \le 61.8$	10
$61.8 < p \le 101.2$	41
$101.2 < p \le 140.5$	162
$140.5 < p \le 179.9$	93
$179.9 < p \le 219.2$	24
Total	330

Table 4.1: Distribution of the nail forces on the plate.

In figure 4.7 and figure 4.8 the stresses in the rafter are given. In the right-hand end of the rafter, only compression stresses are observed, see figure 4.7. At the upper side of the rafter tensile stresses are formed above the "contact area" caused by the moment. The maximum compression stress is rather high.

In the contact zone, the compression forces are absorbed and transmitted to the surrounding of the rafter, see figure 4.8. At the end of the plate, tensile stresses perpendicular to the grain are formed to absorb the tensile forces from the nails. However, the tension stresses are small and the risk of splitting in the timber should be negligible.

S11   VALUE
          -5.00E+01
          -2.50E+01
          -1.75E+01
          -1.00E+01
          -2.53E+00
          +4.95E+00
          +1.24E+01
          +1.99E+01
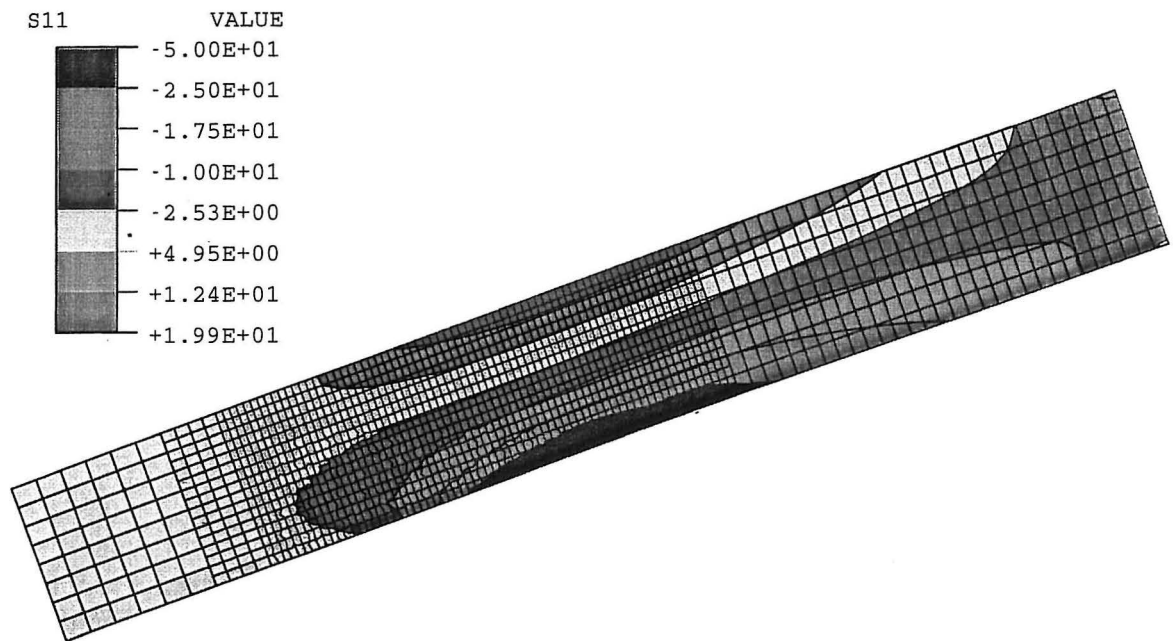
Figure 4.7: Stresses in the rafter parallel to the grain (MPa).

S22   VALUE
          -7.44E+00
          -1.00E+00
          -7.76E-01
          -5.52E-01
          -3.28E-01
          -1.04E-01
          +1.20E-01
          +9.37E-01
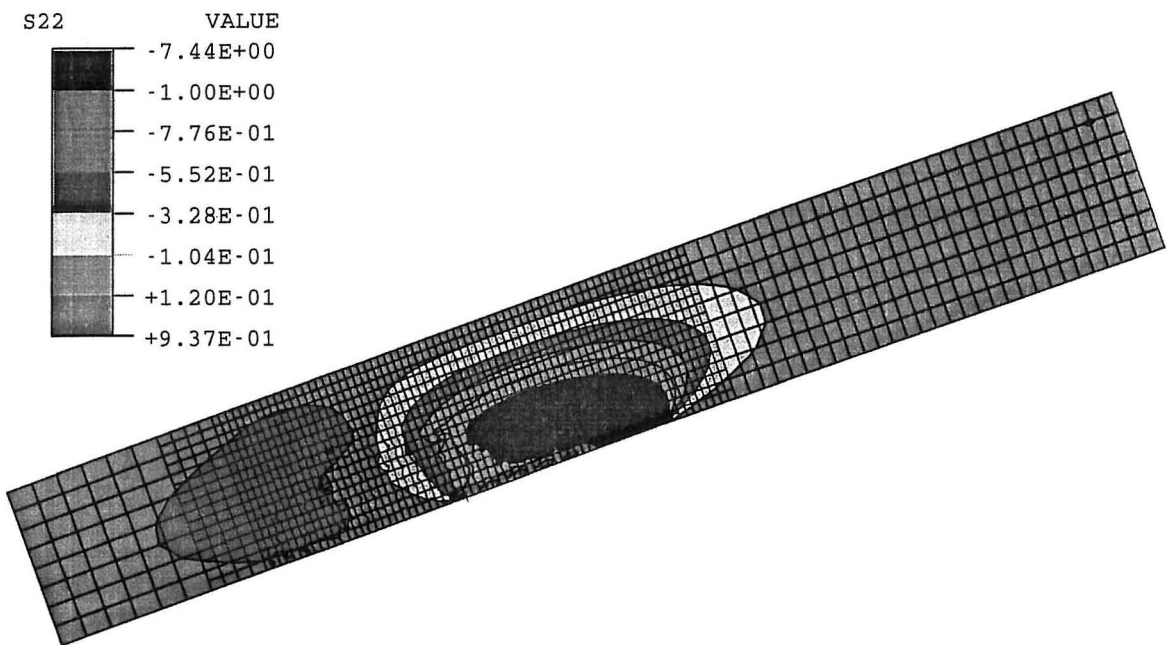
Figure 4.8: Stresses in the rafter perpendicular to the grain (MPa).

S11   VALUE
      ▬ -5.56E+01
      ▬ -6.00E+00
      ▬ -2.65E+00
      ▬ +6.85E-01
      ▬ +4.02E+00
      ▬ +7.37E+00
      ▬ +1.07E+01
      ▬ +1.40E+01
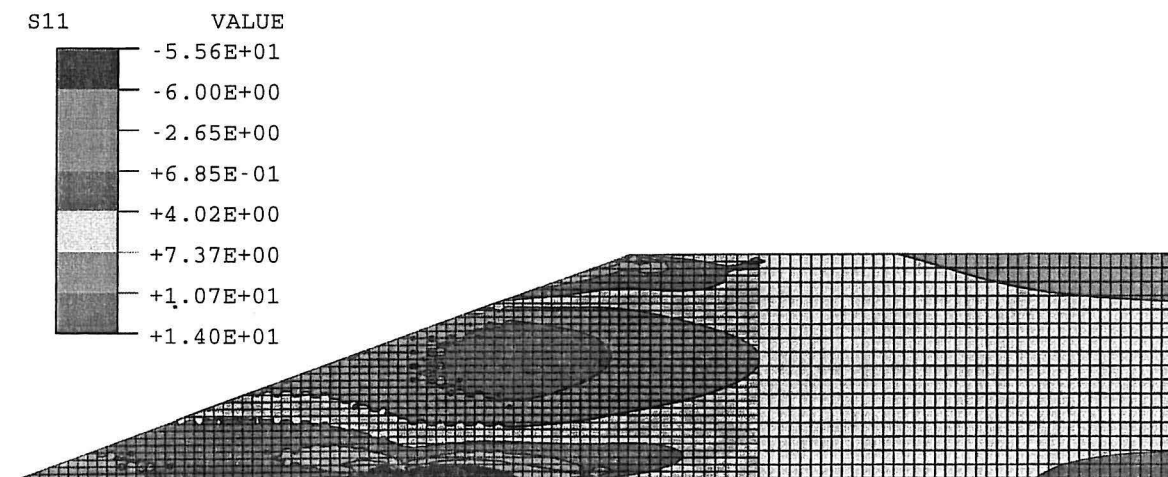
Figure 4.9: Stresses in the chord parallel to the grain (MPa).

S22   VALUE
      ▬ -1.92E+01
      ▬ -2.00E+00
      ▬ -1.54E+00
      ▬ -1.08E+00
      ▬ -6.20E-01
      ▬ -1.60E-01
      ▬ +3.00E-01
      ▬ +3.95E+00
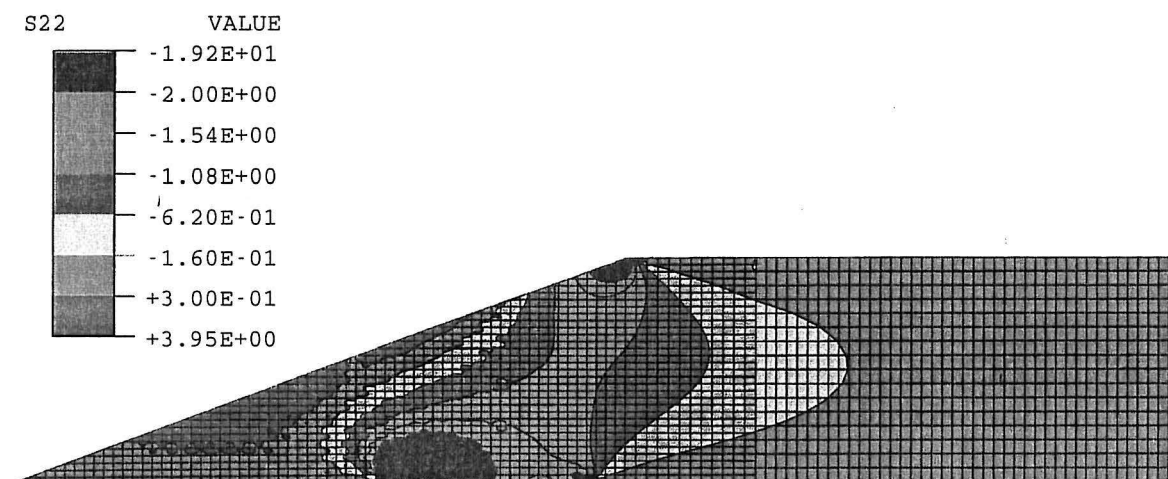
Figure 4.10: Stresses in the chord perpendicular to the grain (MPa).

In figure 4.9 and figure 4.10, the stresses in the chord are given. The maximum tensile stresses parallel to the grain appears below the plate. The tensile force is transmitted to the right end of the chord, see figure 4.9.

In figure 4.10, it is seen that the forces from contact are transmitted directly to the sill and result in high compression stresses in the area between the contact surface and the upper surface of the sill. At the left-hand end, some high tensile stresses perpendicular to the grain are observed. They may cause some cracks in the timber, but the risk of splitting should be prevented by the plate.
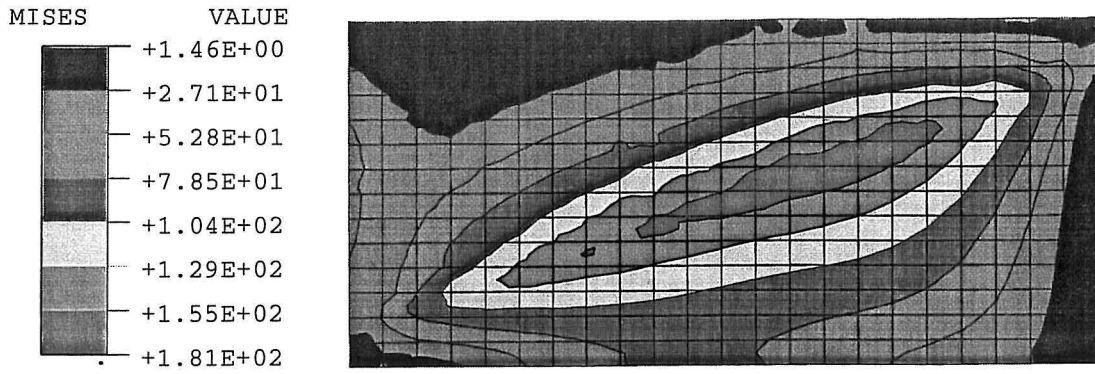
·Figure 4.11: von Mises stresses in the plate (MPa).
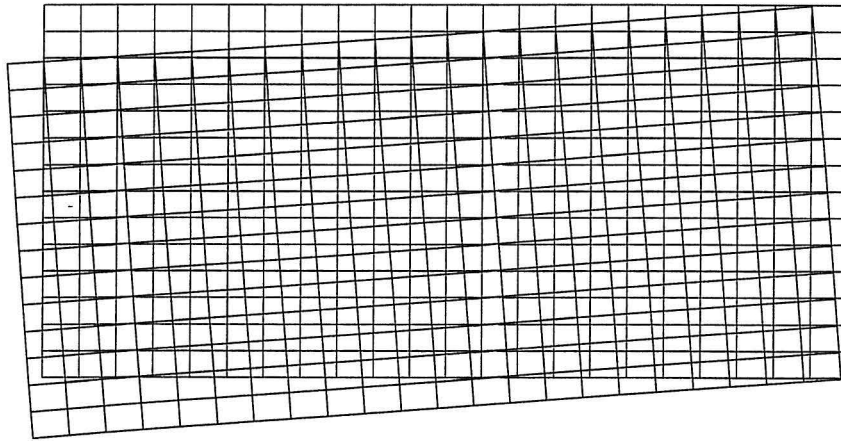
Figure 4.12: Undeformed (red) and deformed mesh (black) of the plate.
Displacement magnification factor: 10.

In figure 4.11, the von Mises stresses in the plate are given. The maximum stresses are observed above the gap (shown as solid line). The stresses are not in the plastic state.

In figure 4.12, the undeformed and the deformed mesh are shown. The plate makes a stiff body rotation around a point close to the lower right-hand corner.

4.2   Summary

A 20° heel joint is modelled by ABAQUS. The timber and plate have the same properties at stated in chapter 2. The nails are modelled with the *SpringA* model. The model has no gap and friction between the rafter and the chord.
The load-displacements curves are sligthly non-linear, whereas the contact force increases linearly. The location of the contact force is constant.
The maximum nail force is close to the failure value, and the maximum von Mises stress in the plate appears above the gap and is not in a plastic state.

Chapter 5

AN-TRUSS

In this chapter, the basic idea and the theory behind a developed plane frame programme is described. The programme is called AN-TRUSS, and it can be used for analysis of the stiffness properties of single nail-plate joints or of whole trusses. The programme is in general based on the "joint modelling idea" given by Foschi(1979), but some elements are developed further.

5.1   The AN-TRUSS Model

AN-TRUSS is a plane frame finite element programme. A model of an arbitrary nail-plate joint can be constructed by use of four different elements:

Beam element :   Used to model the timber members and located in the system line. The element is used as an auxiliary element also to absorb forces from e.g. a nail element or a contact element and transmit the forces to the system line of the timber members.

Nail element :   Used to model a single nail group of arbitrary geometric form. In general, the element is used to connect a beam and a plate element.

Plate element :   Used to model the plate. In general, the plate element connects two nail elements (nail groups).

Contact element :   Used to model the contact between two timber members. The contact elements match the beam element, but it is only "activated" if the deformed distance between two nodes is smaller than a certain value - the gap size.

Each element forms a coupling between two nodes each having three degrees of freedom (dof): two displacements, U, V and a rotation, α.

To get the basic idea (and the notation) of the AN-TRUSS model, consider the heel joint in figure 5.1.
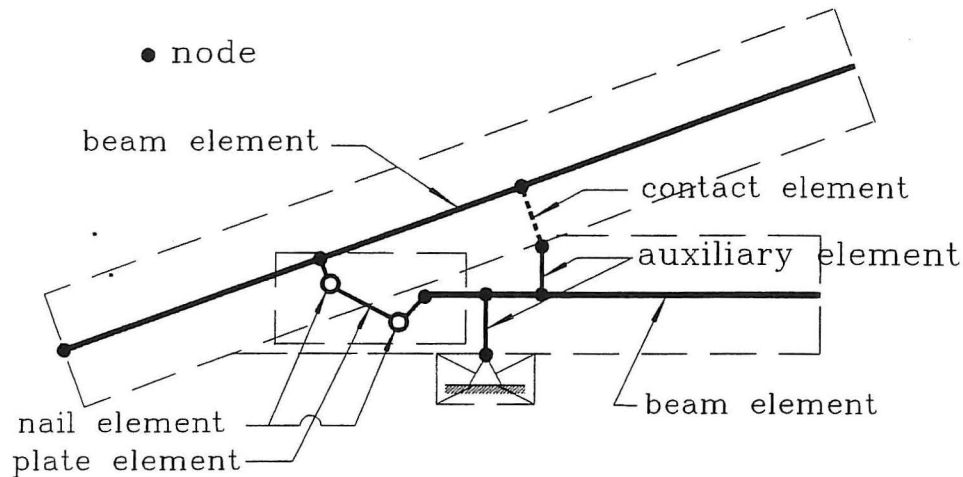
Figure 5.1: AN-TRUSS model of a heel joint.

The limitations of the rafter, the bottom chord, the plate and the sill are shown as thin dashed lines. The solid lines are beam or plate elements and the two circles are nail elements. The contact element is shown as a thick dashed line. The main beam elements of the rafter and the bottom chord are located in the system lines and small auxiliary beams elements are applied to absorb the forces from a contact element, nail element or a support. The stiffness of the small beams depends on the grain direction, but they are normally very stiff compared the other (main) elements. At the end of an element there is a node. The nodes of the plate element are located at the geometric centre of each nail group. A nail element (a circle) is located between the end of a beam element and a plate element each having a node. Thus, the nail element connects the 6 dof here.

The main differences between AN-TRUSS and the model developed by Foschi(1979) are found in the "joint elements". The stiffness of the nail element is not established by means of Hankinson's formula - a simple formula is used, see section 5.2.2 and section 6.2.1 on page 74. The plate element is based on Bernoulli beam theory and linear hardening, see section 5.2.3 and the contact element transmits the contact forces through beam elements, see section 5.2.4.

5.2   Elements

In this section, the theory used for the elements in AN-TRUSS is described. The theory for the elements will end up with the local finite element equation. The local system is given in (x, y) coordinates, and the global system is given in (x_g, y_g) coordinates. The local system is rotated an angle φ to the global system.

5.2.1 Beam Element

Consider the beam element in figure 5.2.
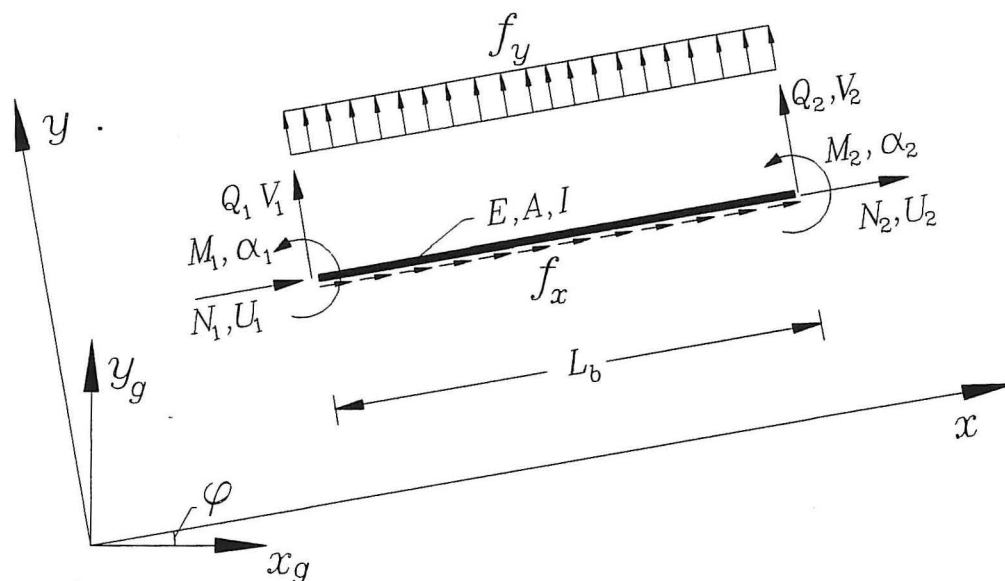
Figure 5.2: Forces and displacements in a beam element.

The beam element has three degrees of freedom (U, V, α) at either end of the beam. The element forces and the displacements of the beam, respectively, aré assembled in the vectors

$$\mathbf{f} = [N_1, Q_1, M_1, N_2, Q_2, M_2]^T \tag{5.1}$$

$$\mathbf{u} = [U_1, V_1, \alpha_1, U_2, V_2, \alpha_2]^T \tag{5.2}$$

The force vector of the uniformly distributed loads f_x and f_y is given by

$$\mathbf{f}^u = \left[-\frac{L_b}{2} f_x, -\frac{L_b}{2} f_y, -\frac{L_b^2}{12} f_y, -\frac{L_b}{2} f_x, -\frac{L_b}{2} f_y, \frac{L_b^2}{12} f_y \right]^T \tag{5.3}$$

The relation between the element forces and the displacements is given by

$$\mathbf{f} = \mathbf{f}^u + \mathbf{K}\,\mathbf{u} \tag{5.4}$$

$\mathbf{K}$ is the local element stiffness matrix. A stiffness matrix based on Timoshenko beam theory is given by (5.5).

$$
\mathbf{K} = \begin{bmatrix}
\frac{EA}{L_b} & & & & & \\
0 & 12\frac{EI}{(1+\Phi)L_b^3} & & & \text{sym.} & \\
0 & 6\frac{EI}{(1+\Phi)L_b^2} & \frac{4+\phi}{1+\Phi}\frac{EI}{L_b} & & & \\
-\frac{EA}{L_b} & 0 & 0 & \frac{EA}{L_b} & & \\
0 & -12\frac{EI}{(1+\Phi)L_b^3} & -6\frac{EI}{(1+\Phi)L_b^2} & 0 & 12\frac{EI}{(1+\Phi)L_b^3} & \\
0 & 6\frac{EI}{(1+\Phi)L_b^2} & \frac{2-\Phi}{1+\Phi}\frac{EI}{L_b} & 0 & -6\frac{EI}{(1+\Phi)L_b^2} & \frac{4+\phi}{1+\Phi}\frac{EI}{L_b}
\end{bmatrix}
\tag{5.5}
$$

where the properties of the beams are assumed linear elastic and given by Young's modulus E, the cross-sectional area of the beam A and the moment of inertia I. L_b is the length of the beam. Φ is a shear deformation parameter defined as

$$
\Phi = \frac{12\,E\,I}{(GA)_e L_b^2}
\tag{5.6}
$$

$(GA)_e$ is the effective shear stiffness given by $\frac{5}{6}G \cdot A$ where G is the shear modulus, see also Cowper(1966). The stiffness matrix based on Bernoulli theory is also given by (5.5) with $\Phi = 0$.

5.2.2   Nail Element

Consider the plate area (A-B-C-D) on a beam in figure 5.3.
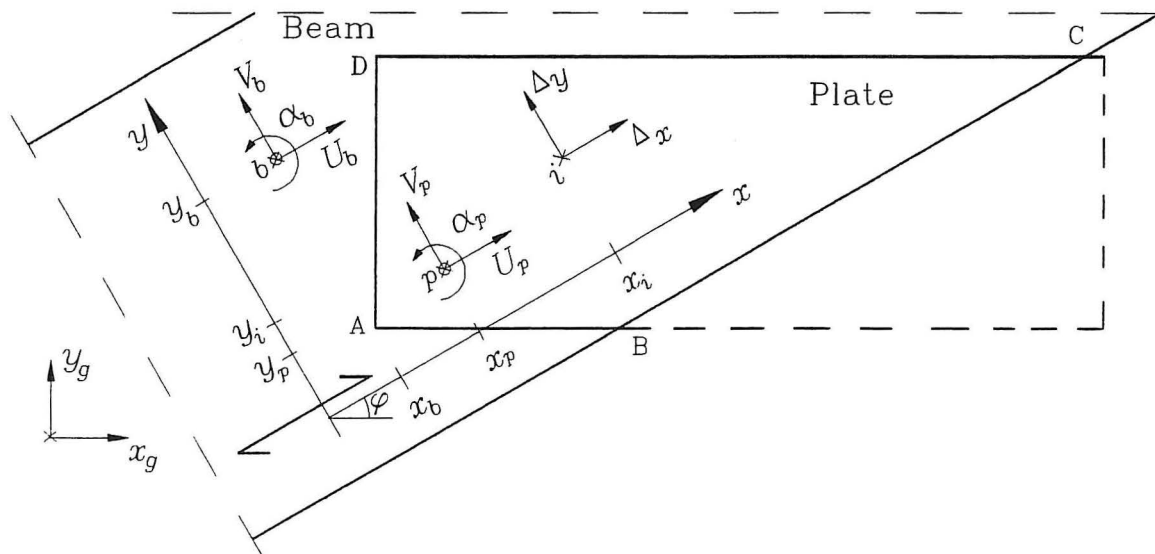
Figure 5.3: Global and local systems for a nail element.

The displacements of the beam are given by U_b, V_b, α_b in node b (x_b, y_b) and the displacements of the plate area (A-B-C-D) are given by U_p, V_p, α_p in node p (x_p, y_p). Node b

and p can be chosen artitrary. A local system (x, y) coincides with the grain direction of the beam, which is rotated an angle φ to the global system (x_g, y_g).

A nail at point i (x_i, y_i) is considered. It is assumed that the plate and beam perform like stiff bodies in the joint region, and the rotations α_b, α_p are small. The displacements of point i in the x and y-directions are given by

$$\Delta_x = \mathbf{q}_x^T \mathbf{u} \tag{5.7}$$
$$\Delta_y = \mathbf{q}_y^T \mathbf{u} \tag{5.8}$$

where

$$\mathbf{q}_x = \begin{bmatrix} 1 & 0 & -(y_i - y_p) & -1 & 0 & (y_i - y_b) \end{bmatrix}^T \tag{5.9}$$

$$\mathbf{q}_y = \begin{bmatrix} 0 & 1 & (x_i - x_p) & 0 & -1 & -(x_i - x_b) \end{bmatrix}^T \tag{5.10}$$

$$\mathbf{u} = \begin{bmatrix} U_p & V_p & \alpha_p & U_b & V_b & \alpha_b \end{bmatrix}^T \tag{5.11}$$

The force on the nail at point i, $p(\Delta)$, is found by (5.12), see also Foschi(1979).

$$p(\Delta) = (p_0 + k_1\,\Delta) \left(1 - \exp\left(\frac{-k_0\,\Delta}{p_0} \right) \right) \tag{5.12}$$

Δ is the absolute displacement of nail i found by (5.13), see also figure 5.5.

$$\Delta = \sqrt{\Delta_x^2 + \Delta_y^2} \tag{5.13}$$

The stiffness parameters p_0, k_1, k_0 in (5.12) are defined in figure 5.4 and they can depend on the angle between the grain direction and the principal axes of the plate, see section 6.2.1 on page 75.
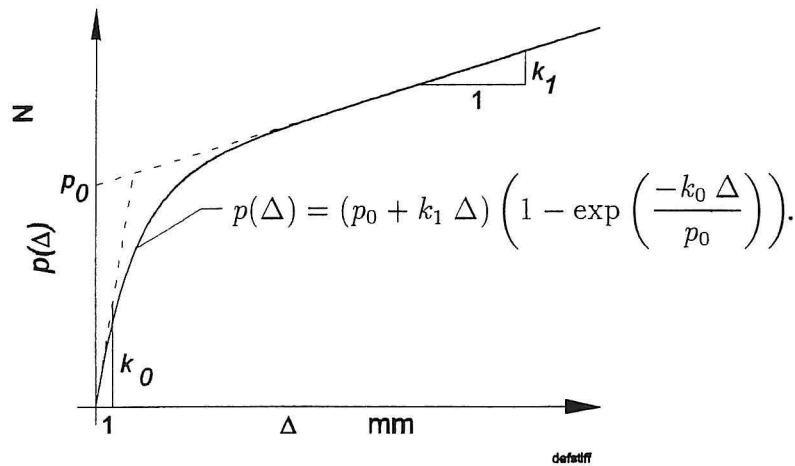
Figure 5.4: Definition of the stiffness parameteres used in the expression for the nail forces.
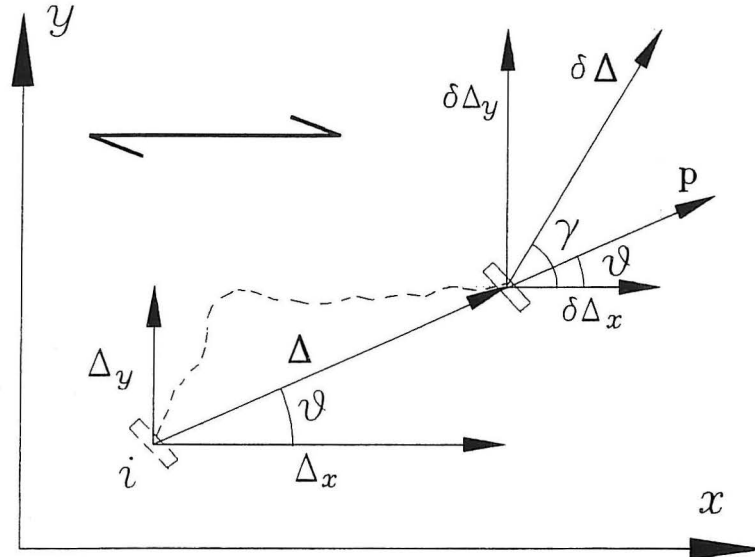
Figure 5.5: Force and virtual displacement of a nail.

A small variation in one of the displacement components of the displacement vector (5.11) causes a virtual displacement $\delta\mathbf{\Delta}$ in nail i, see figure 5.5. The virtual internal work done by nail i is then given by (5.14).

$$^i\delta W = \mathbf{p} \cdot \delta\mathbf{\Delta} = p(\Delta)\, \delta\Delta\, \cos(\gamma - \vartheta) \tag{5.14}$$

It is assumed that the nail force vector $\mathbf{p}$ is parallel to the displacement vector $\mathbf{\Delta}$. This is not true for nails in an orthotropic material, but the validity of the assumption is good as the angle between $\mathbf{p}$ and $\mathbf{\Delta}$ is small. This subject is discussed in Jensen(1994), see also the description on page 33.

The internal work from the n nails in the plate area $\mathcal{A}$ (A-B-C-D in figure 5.3) is given by

$$
\begin{aligned}
^i\delta W &= \sum_{i=1}^{n} \left(p(\Delta)\, \delta\Delta\, \cos(\gamma - \vartheta) \right) \tag{5.15} \\
&= \int_{\mathcal{A}} \Im\, p(\Delta)\, \delta\Delta\, \cos(\gamma - \vartheta) d\mathcal{A} \tag{5.16} \\
&= \int_{\mathcal{A}} \Im\, p(\Delta)\, \left(\cos(\vartheta)\, \delta\Delta_x + \sin(\vartheta)\, \delta\Delta_y \right)\, d\mathcal{A} \tag{5.17} \\
&= \int_{\mathcal{A}} \Im\, p(\Delta)\, \left(\frac{\Delta_x}{\Delta}\delta\Delta_x + \frac{\Delta_y}{\Delta}\, \delta\Delta_y \right) d\mathcal{A} \tag{5.18}
\end{aligned}
$$

where $\Im$ is the nail density $\left(\frac{\text{number of teeth}}{\text{area}} \right)$. Inserting (5.7) and (5.8) in (5.18), a variation in the displacement component u_j $(j = 1, 2, ..., 6)$ gives

$$
\begin{aligned}
^i\delta W_j &= \int_{\mathcal{A}} \Im\, \frac{p(\Delta)}{\Delta} \left(\mathbf{q}_x^T\, \mathbf{u}\, q_{x,j}\, \delta u_j + \mathbf{q}_y^T\, \mathbf{u}\, q_{y,j}\, \delta u_j \right) d\mathcal{A} \tag{5.19} \\
&= \left(\int_{\mathcal{A}} \Im\, \frac{p(\Delta)}{\Delta} \left(\mathbf{q}_x^T\, \mathbf{u}\, q_{x,j} + \mathbf{q}_y^T\, \mathbf{u}\, q_{y,j} \right) d\mathcal{A} \right) \delta u_j \tag{5.20}
\end{aligned}
$$

where $q_{x,j}$ and $q_{y,j}$ are components j of $\mathbf{q}_x$ and $\mathbf{q}_y$, respectively. The external virtual work for a variation in the displacement component u_j gives

$$^{e}\delta W_j = f_j\,\delta u_j \tag{5.21}$$

where f_j is the component j of the external force vector $\mathbf{f}$. As the principle of virtual work states $^{i}\delta W = {}^{e}\delta W$, it follows that

$$^{i}\delta W_j - {}^{e}\delta W_j = 0 \tag{5.22}$$

$$\left(\int_{\mathcal{A}} \Im\, \frac{p(\Delta)}{\Delta} \left(\mathbf{q}_x^T\,\mathbf{u}\,q_{x,j} + \mathbf{q}_y^T\,\mathbf{u}\,q_{y,j} \right) d\mathcal{A} - f_j \right) \delta u_j = 0 \tag{5.23}$$

As δu_j is arbitrary the finite element equation (5.26) is obtained.

$$\int_{\mathcal{A}} \Im\, \frac{p(\Delta)}{\Delta} \left(\mathbf{q}_x^T\,\mathbf{u}\,q_{x,j} + \mathbf{q}_y^T\,\mathbf{u}\,q_{y,j} \right) d\mathcal{A} - f_j = 0 \qquad j = 1, 2, ..6 \tag{5.24}$$

$$\left(\int_{\mathcal{A}} \Im\, \frac{p(\Delta)}{\Delta} \left(\mathbf{q}_x\,\mathbf{q}_x^T + \mathbf{q}_y\,\mathbf{q}_y^T \right) d\mathcal{A} \right) \mathbf{u} = \mathbf{f} \tag{5.25}$$

$$\mathbf{K}\,\mathbf{u} = \mathbf{f} \tag{5.26}$$

$\mathbf{K}$ is the local stiffness matrix given by

$$\mathbf{K} = \int_{\mathcal{A}} \Im\, \frac{p(\Delta)}{\Delta} \left(\mathbf{q}_x\,\mathbf{q}_x^T + \mathbf{q}_y\,\mathbf{q}_y^T \right) d\mathcal{A} \tag{5.27}$$

The integral in (5.27) is determined using a (2×2) Gauss quadrature. The procedure is the same as used for isoparametric elements, i.e. by means of shape functions, see e.g. Ottosen et al.(1990) or Cook et al.(1989).

5.2.3   Plate Element
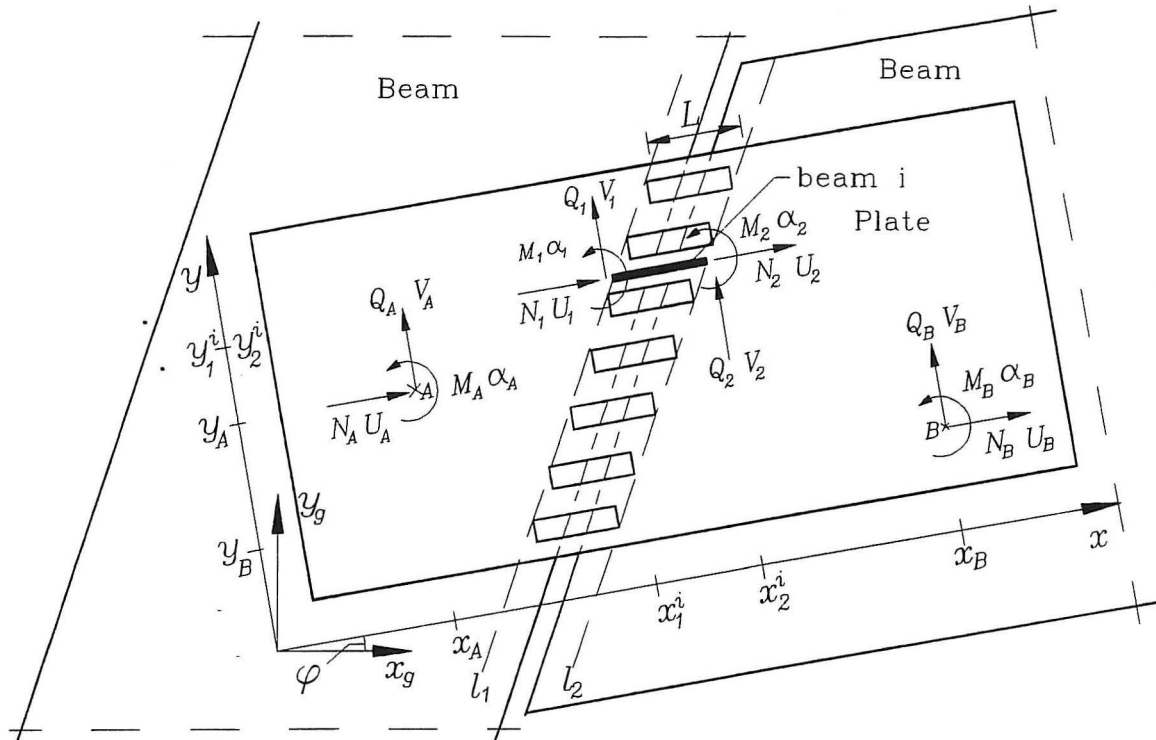
Figure 5.6: **Forces and displacements of the nodes (points A and B)**
and in beam i.

Consider a nail-plate as shown in figure 5.6. The two plate regions on the timber beams
are assumed to perform like stiff bodies. A number of small beams between line l_1 and
line l_2 connect the two stiff regions. The beams have the length L. The displacements
of the left-hand region are given by U_A, V_A, α_A at point A and the displacements of the
right-hand region given by U_B, V_B, α_B at point B. Point A and B are chosen arbitrary.
The nodes of the plate are located at points A and B. A local system (x, y) is rotated
an angle φ to the global system (x_g, y_g) so it coincides with the principal axes of the
plate.

The element forces and the displacements of beam i, respectively, are given by

$$\mathbf{f}^i = [N_1, Q_1, M_1, N_2, Q_2, M_2]^T \qquad (5.28)$$
$$\mathbf{u}^i = [U_1, V_1, \alpha_1, U_2, V_2, \alpha_2]^T \qquad (5.29)$$

The element forces and the displacements at points A and B, respectively, are given by

$$\mathbf{f} = [N_A, Q_A, M_A, N_B, Q_B, M_B]^T \qquad (5.30)$$
$$\mathbf{u} = [U_A, V_A, \alpha_A, U_B, V_B, \alpha_B]^T \qquad (5.31)$$

If small rotations are assumed, the displacements of beam i are

$$\mathbf{u}^i = \mathbf{D}^i \mathbf{u} \qquad (5.32)$$

where

$$\mathbf{D}^i = \begin{bmatrix} 1 & 0 & y_A - y_1^i & & & \\ 0 & 1 & x_1^i - x_A & & \mathbf{0} & \\ 0 & 0 & 1 & & & \\ & & & 1 & 0 & y_B - y_2^i \\ & \mathbf{0} & & 0 & 1 & x_2^i - x_B \\ & & & 0 & 0 & 1 \end{bmatrix} \qquad (5.33)$$

$\mathbf{D}^i$ is an orthogonal matrix ($\mathbf{D}^{iT} = \mathbf{D}^{i-1}$). The forces at points A and B are also expressed by $\mathbf{D}^i$ given as a summation of the forces in the n beams.

$$\mathbf{f} = \sum_i^n \left(\mathbf{D}^{iT} \, \mathbf{f}^i \right) \qquad (5.34)$$

The relation between the element forces of a small beam and the displacements is given by

$$\mathbf{f}^i = \mathbf{K}^b \, \mathbf{u}^i \qquad (5.35)$$

where $\mathbf{K}^i$ is the stiffness matrix of the beam.

$$\mathbf{K}^i = \begin{bmatrix} \frac{EA}{L} & & & & & \\ 0 & 12\frac{EI}{L^3} & & & \text{sym.} & \\ 0 & 6\frac{EI}{L^2} & 4\frac{EI}{L} & & & \\ -\frac{EA}{L} & 0 & 0 & \frac{EA}{L} & & \\ 0 & -12\frac{EI}{L^3} & -6\frac{EI}{L^2} & 0 & 12\frac{EI}{L^3} & \\ 0 & 6\frac{EI}{L^2} & 2\frac{EI}{L} & 0 & -6\frac{EI}{L^2} & 4\frac{EI}{L} \end{bmatrix} \qquad (5.36)$$

The properties of the small Bernoulli beams are assumed linear elastic and given by Young's modulus E, the cross-sectional area of the beam A and the moment of inertia I. L is the length of the beam, see figure 5.6.

By inserting (5.35) and (5.32) in (5.34) the local finite element equation for the plate element is given by (5.39).

$$\mathbf{f} = \sum_i^n \left(\mathbf{D}^{iT} \, \mathbf{K}^i \, \mathbf{u}^i \right) \qquad (5.37)$$

$$\mathbf{f} = \sum_i^n \left(\mathbf{D}^{iT} \, \mathbf{K}^i \, \mathbf{D}^i \right) \mathbf{u} \qquad (5.38)$$

$$\mathbf{f} = \mathbf{K} \, \mathbf{u} \qquad (5.39)$$

$\mathbf{K}$ is the local element stiffness matrix given by

$$\mathbf{K} = \sum_i^n \left(\mathbf{D}^{iT} \, \mathbf{K}^i \, \mathbf{D}^i \right) \qquad (5.40)$$

(5.36) is valid only for linear elastic beams. Plastic problems can be described by bi-linear load-displacement curves, see figure 5.8. For a given strain combination, the beams will act in the plastic state and a smaller value of E will be used. In figure 5.7, the plastic state is defined by three different yield surfaces.
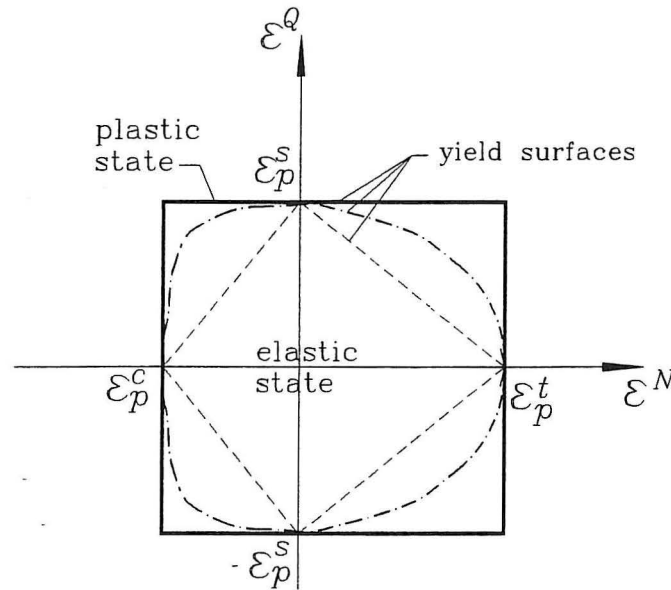
Figure 5.7: Yield surfaces to define the plastic state.

For a strain set $(\varepsilon^N, \varepsilon^Q)$ within the yield surface the beam is elastic, for a strain set $(\varepsilon^N, \varepsilon^Q)$ on the yield surface the beam is plastic. The strain conditions used are given by (5.41), (5.42) and (5.43)

$$\text{tension} : \varepsilon_p^t \;\leq\; \frac{U_2 - U_1}{L} \tag{5.41}$$

$$\text{compression} : \varepsilon_p^c \;\geq\; \frac{U_2 - U_1}{L} \tag{5.42}$$

$$\text{shear} \quad : \varepsilon_p^s \;\leq\; \frac{|\, V_1 - V_2 + \frac{L}{2}(\alpha_1 + \alpha_2)\,|}{L} \tag{5.43}$$

which match the outer yield surface in figure 5.7. This surface may be on the "un-safe side". In the following, the yield surface defined by (5.41), (5.42) and (5.43) will be used and no experimental tests have been made to evaluate the yield surface in detail.

In figure 5.7 and figure 5.8 a, it is seen that the plastic state for the axial force N is defined by two strains, ε_p^t and ε_p^c. Young's modulus is the same in tension and compression in the elastic state, but different from the value in the plastic state. The tangent stiffness in plastic tension is given by E_p^t, and the tangent stiffness in plastic compression is given by E_p^c. ε_p^c and E_p^c are used to model the buckling effect in the plate, and they are generally smaller than the "tension parameters" ε_p^t and E_p^t.

In figure 5.7 and figure 5.8 b, it is seen that the plastic state for the shear force is defined by one strain, ε_p^s. Young's modulus in the elastic and plastic state is assumed to be independent of the shear direction. The tangent stiffness in plastic shear is given
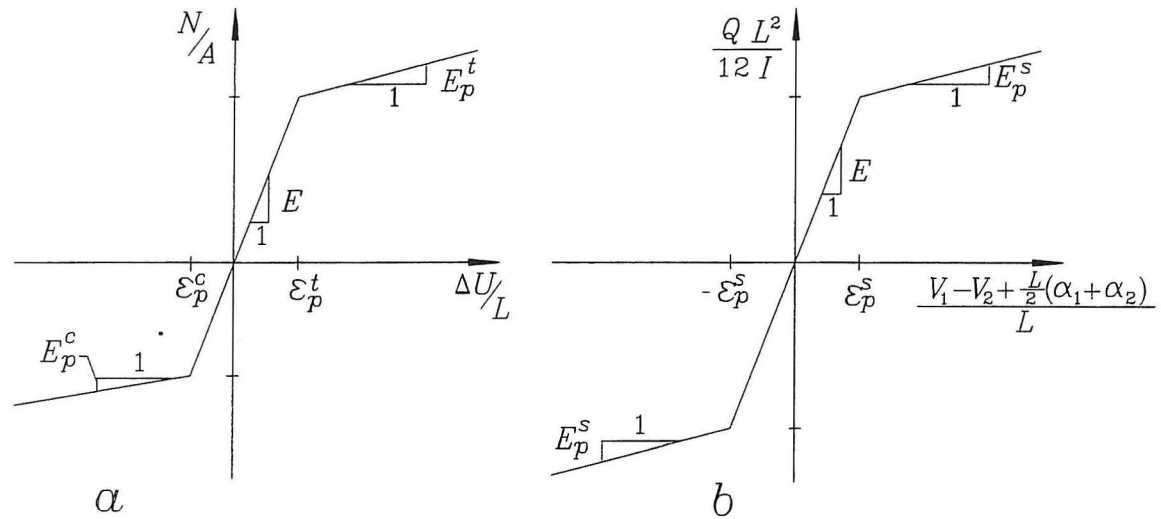
Figure 5.8: **Bi-linear load-displacement curves.**

by E_p^s. The shear force is generally dependent on the rotations also, but they are assumed small and, therefore, the contributions are negligible.

The values of ε_p^t, ε_p^c, ε_p^s, E, E_p^t, E_p^c and E_p^s can be determined from test specimens loaded in tension, shear, bending or a combination thereof.

If (5.41) is satisfied, the beam will be plastic in tension and only the "tensile components" of the stiffness matrix $(K_{11}, K_{13}, K_{31}, K_{33})$ will be changed, see (5.44). The same components will be changed if the compression condition (5.42) is satisfied, but with E_p^c as Young's modulus.

The tangent stiffness matrix for a beam in both plastic tension and plastic shear is then given by (5.44).

$$
\mathbf{K}^p = \begin{bmatrix}
\frac{E_p^t A}{L} & & & & & \\
0 & 12\frac{E_p^s I}{L^3} & & & \text{sym.} & \\
0 & 6\frac{E_p^s I}{L^2} & 4\frac{E_p^s I}{L} & & & \\
-\frac{E_p^t A}{L} & 0 & 0 & \frac{E_p^t A}{L} & & \\
0 & -12\frac{E_p^s I}{L^3} & -6\frac{E_p^s I}{L^2} & 0 & 12\frac{E_p^s I}{L^3} & \\
0 & 6\frac{E_p^s I}{L^2} & 2\frac{E_p^s I}{L} & 0 & -6\frac{E_p^s I}{L^2} & 4\frac{E_p^s I}{L}
\end{bmatrix} . \tag{5.44}
$$

The element forces corresponding to the tangent stiffness matrix (5.44) are then given by (5.45) to (5.50).

$$N_1 = \frac{(E - E_p^t)A}{L}\varepsilon_p^t L + \frac{E_p^t A}{L}(U_1 - U_2) \tag{5.45}$$

$$V_1 = 12\frac{(E - E_p^s)I}{L^3}\varepsilon_p^s L + 12\frac{E_p^s I}{L^3}(V_1 - V_2) + 6\frac{E_p^s I}{L^2}(\alpha_1 + \alpha_2) \tag{5.46}$$

$$M_1 = 6\frac{(E - E_p^s)I}{L^2}\varepsilon_p^s L + 6\frac{E_p^s I}{L^2}(V_1 - V_2) + \frac{E_p^s I}{L}(4\alpha_1 + 2\alpha_2) \tag{5.47}$$

$$N_2 = -N_1 \tag{5.48}$$

$$V_2 = -V_1 \tag{5.49}$$

$$M_2 = 6\frac{(E - E_p^s)I}{L^2}\varepsilon_p^s L + 6\frac{E_p^s I}{L^2}(V_1 - V_2) + \frac{E_p^s I}{L}(2\alpha_1 + 4\alpha_2) \tag{5.50}$$

The equations fulfil the equilibrium condition.

In AN-TRUSS it is further assumed that $E_p^s = E_p^t$.

5.2.4 Contact Element
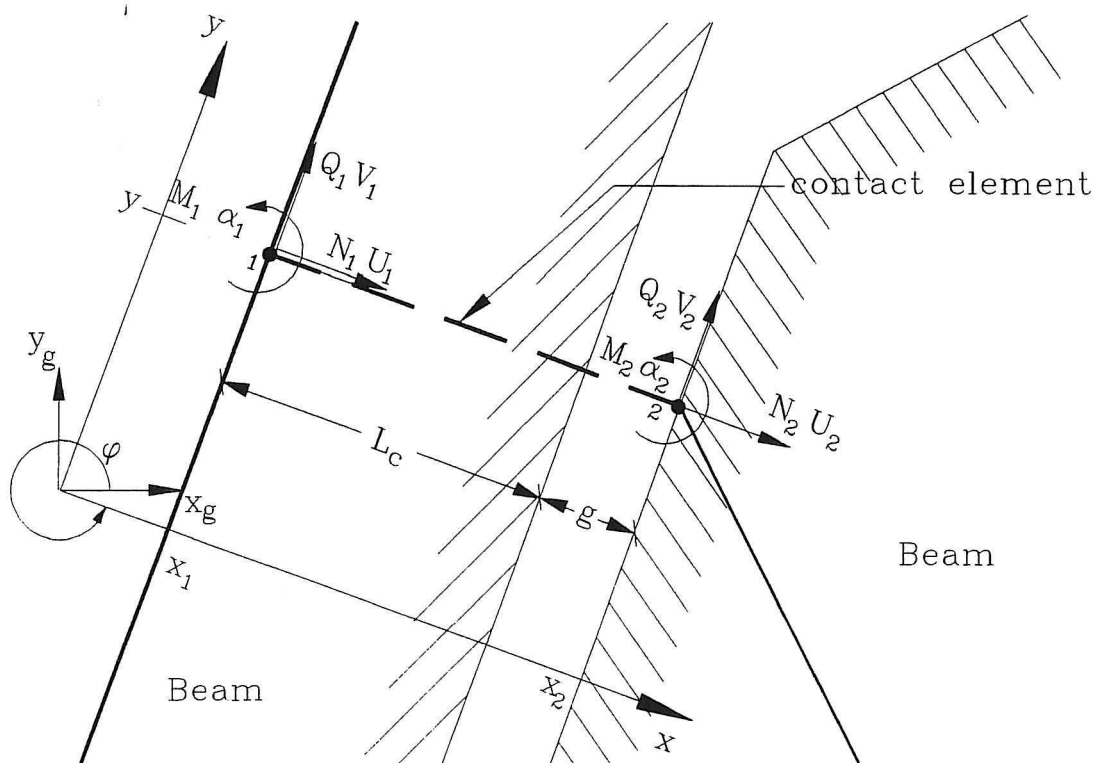
Figure 5.9: **Forces and displacements in a contact element.**

Consider the two parallel beam edges in figure 5.9. There is an initial gap of size g between the beams, which are represented by two nodes, 1 and 2. The displacements

and forces at the nodes are shown in a local xy-system. The local system is rotated an angle φ so that the y-axis is parallel to the beam edges. When the beams are deformed, the slip between the beams measured in the x-direction is given by

$$g + U_2 - U_1 \tag{5.51}$$

It is assumed that the one of the nodes (here node 2) is located in the contact area of the beams. Contact between the timber members is obtained when

$$U_2 - U_1 \le -g \tag{5.52}$$

In contact, the relation between the element forces and the displacements are given by

$$\mathbf{f} = \mathbf{K} \left(\mathbf{u} - \frac{1}{2}\mathbf{g} \right) \tag{5.53}$$

where

$$
\begin{aligned}
\mathbf{f} &= [N_1, Q_1, M_1, N_2, Q_2, M_2]^T & (5.54) \\
\mathbf{u} &= [U_1, V_1, \alpha_1, U_2, V_2, \alpha_2]^T & (5.55) \\
\mathbf{g} &= [g, 0, 0, -g, 0, 0]^T & (5.56)
\end{aligned}
$$

$\mathbf{K}$ is the local element stiffness matrix given by

$$
\mathbf{K} =
\begin{bmatrix}
\frac{EA_c}{L_c} & & & & & \\
0 & k_f & & & \text{sym.} & \\
0 & 0 & 0 & & & \\
-\frac{EA_c}{L_c} & 0 & 0 & \frac{EA_c}{L_c} & & \\
0 & -k_f & 0 & 0 & k_f & \\
0 & 0 & 0 & 0 & 0 & 0
\end{bmatrix}
\tag{5.57}
$$

where A_c is the estimated cross-section of the contact area. E is Young's modulus of the timber which depends on the grain direction. If there is no friction between the beams in the contact area, $k_f = 0$, otherwise, if there is friction, k_f is a parameter which depends on the size of the axial forces in the contact zone and has a value to be estimated. In the following, $k_f = 0$ and only axial forces occour in the contact element.

5.3 Assembly and Solve of the FE-Equation

The relations between the local and the global systems are given by

$$
\begin{aligned}
\mathbf{f} &= \mathbf{T}\,\mathbf{f}_g & (5.58) \\
\mathbf{u} &= \mathbf{T}\,\mathbf{u}_g & (5.59)
\end{aligned}
$$

where $\mathbf{T}$ is the transformation matrix given by (5.60).

$$\mathbf{T} = \begin{bmatrix} \cos(\varphi) & \sin(\varphi) & 0 & & & \\ -\sin(\varphi) & \cos(\varphi) & 0 & & \mathbf{0} & \\ 0 & 0 & 1 & & & \\ & & & \cos(\varphi) & \sin(\varphi) & 0 \\ & \mathbf{0} & & -\sin(\varphi) & \cos(\varphi) & 0 \\ & & & 0 & 0 & 1 \end{bmatrix} \qquad (5.60)$$

$\mathbf{T}$ is an orthogonal matrix $(\mathbf{T}^{-1} = \mathbf{T}^T)$. The local element equation is transformed to the global system by

$$\begin{aligned} \mathbf{f} &= \mathbf{K}\,\mathbf{u} \\ \mathbf{T}\,\mathbf{f}_g &= \mathbf{K}\,\mathbf{T}\,\mathbf{u}_g \\ \mathbf{f}_g &= \mathbf{K}_g\,\mathbf{u}_g \end{aligned} \qquad (5.61)$$

where

$$\mathbf{K}_g = \mathbf{T}^T\,\mathbf{K}\,\mathbf{T} \qquad (5.62)$$

(5.61) is solved by a Full Newton-Raphson iteration method, see e.g Krenk(1993), where $\mathbf{K}_g^{-1}$ is found using a profile solver as described in Hededal et al.(1993).

5.4   Summary

The theory for the four different elements used by AN-TRUSS is described. A linear elastic beam element is used to model the timber members and small auxiliary elements to absorb forces from the nail elements, contact elements or supports. A non-linear nail element models the stiffness of the nails in a nail group of arbitrary form. A plate element models the deformations in the plate area above the gap. The element is based on linear elastic Bernoulli beams with linear hardning. A contact element is activated if the deformed distance between two nodes is smaller than the gap size. The element is located in the contact zone between the timber members.

In table 5.1, the parameters to be estimated for the different elements are given.

Element	Parameter to estimate
Beam	E, G
Nail	k_0, k_1, p_0, (angle dependence)
Plate	$E, L, A, I, \varepsilon_p^s, \varepsilon_p^t, \varepsilon_p^c, E_p^s, E_p^t, E_p^c$
Contact	E, G, A_c, k_f, g, location of the element

Table 5.1: Parameters to estimate in AN-TRUSS.

In chapter 6, the parameters will be estimated and their influence on the stiffness analysed.

Chapter 6

Examples

In this chapter, different timber joints are modelled by AN-TRUSS and compared to the ABAQUS results. Simple tensile splices will be analysed, then splices in bending and later a heel joint. Finally, a collar tie truss and a pitched W-truss will be modelled by AN-TRUSS and compared to results from the programme ECOTRUSS, which is developed by Gang-Nail Systems and based on the "fictitious member" model.

6.1 Tensile Splices

6.1.1 Modelling

The tensile splices described in chapter 2 are modelled as shown in figure 6.1.
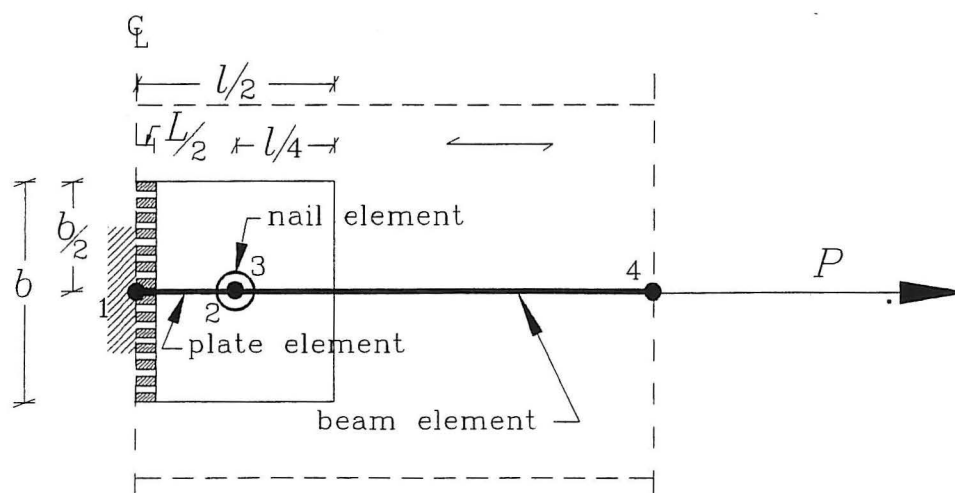
Figure 6.1: **AN-TRUSS model of a tensile splice.**

The model consists of a plate element between nodes 1 and 2, a beam element (timber) between nodes 3 and 4, and a nail element to connect nodes 2 and 3, which are both

located at the centre of the nail group. Node 1 is fully constrained and node 4 is loaded
in the grain direction of the beam element.

The material properties E, G of the beam element are chosen to be the same as used
in ABAQUS, see table 2.2 on page 14.

The size of the nail area is $\frac{b \cdot l}{2}$, see figure 6.1. The load-displacement curve of the
nails loaded parallel to the grain direction is determined by fitting the curve to the
load-displacement curves from the tensile splices modelled by ABAQUS, see figure 6.2.
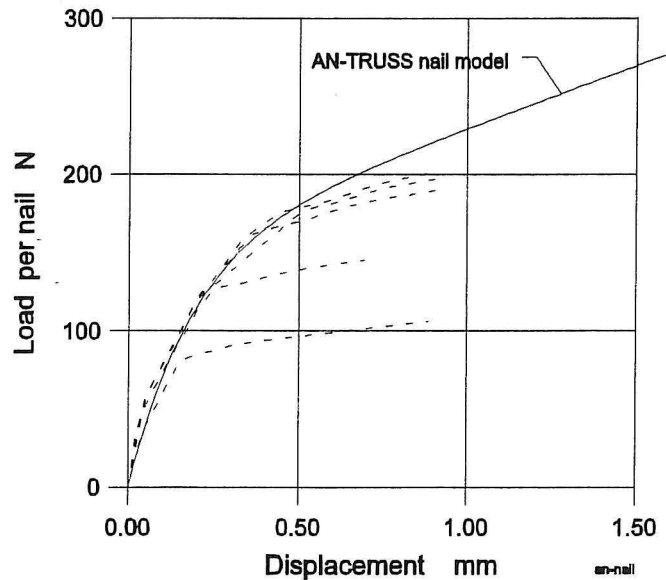
Figure 6.2: **Load-displacement curves from tensile splices modelled
by ABAQUS (dashed) and fitted load-displacement curve
used for the nail model by AN-TRUSS (solid).**

The dashed curves in figure 6.2 are the load-slip curves divided by the number of nails
at one side of the joint, see figure 2.14 on page 21. The reason for using the modified
load-slip curves is that they contain the linear deformations of the plate too.

The fitted parameters to the load-displacement curve of a nail (the solid line in fi-
gure 6.2) are found to be:
(see also figure 5.4 on page 57)

$$p = (p_0 + k_1 \, \Delta) \left(1 - \exp \left(\frac{-k_0 \, \Delta}{p_0} \right) \right) \qquad (6.1)$$

$$p_0 = 150\text{N}$$
$$k_0 = 900\text{N/mm}$$
$$k_1 = 80\text{N/mm}$$

The parameters have almost the same values as found by Lau(1987) who has tested a
GNA 20 nail-plate (no S! - which means a plate of lower quality steel than the GNA
20 S nail-plate) impressed into Canadian spruce and pine with $11 - 12\%$ RH.

In a real situation where the nail parameters are to be determined it must be recommended to use load-slip curves from tensile splices with different plate sizes and the slip measured at the timber below the centre of the plate. However, this measuring point is complicated to catch and a point at the edge of the plate may be used. The deformation of the nail will then be overestimated a bit, especially in tests with large plates, see the discussion on page 21.

The plate element consists of a number of small elastic-plastic beams located at the middle of the plate, see figure 6.1. The following stiffness parameters of the beams are to be determined:

E: MOE of the beams in the elastic state.

E_p^t: MOE of the beams in the plastic tension state.

ε_p^t : Strain to define the plastic state, when the plate is loaded in tension.

ε_p^s : Strain to define the plastic state, when the plate is loaded in shear. (Tensile tests are not dependent on this strain)

L : Length of the beams. (to be estimated)

In order to determine the stiffness parameters above, tensile and shear tests on the plates are made. The tensile tests loaded in the principal axes of the plate are used to determine the yielding load of the plate. (The measured tensile deformations cannot be used to determine ε_p^t directly, see discussion on page 137 in appendix B).

The shear tests are used to determine E and ε_p^s, but also E_p^t as it is assumed that $E_p^t = E_p^s$. However, the determination of the parameters is dependent on L which has to be estimated, as the constraints of the shear tests are not ideal. The shear tests are described in appendix B on page 132. For $L = 15$mm, the parameters of the plate element are found as:

$$E = 160000\text{MPa}$$
$$E_p^t = 3000\text{MPa}$$
$$\varepsilon_p^s = 0.01$$

In figure 6.3 the load-displacement curve from an AN-TRUSS plate element with the stiffness parameters above is compared with the results from three shear tests.

The MOE found for the plate in appendix B is an average modulus for the plate stiffness, as both areas with and without holes occur in the plate. Therefore, it is not directly a value for E used in the plate element. If the tested plate area is assumed to act like a beam with different cross-sections an estimate for E can be determined by the MOE ($E_1 = 125000$MPa) found for the test specimens loaded in direction 1, see figure B.2 on page 130 and table B.1 on page 133. An estimate for E is given by (6.2).

$$E = E_1 \frac{l_2}{l_m} 5 \left(\frac{l_1 \cdot A_2}{l_2 \cdot A_1} + 1 \right) = 176000\text{MPa} \tag{6.2}$$

where l_1 is the length of one section with the area A_1 with holes, and l_2 is the length of one section with the area A_2 without holes. The number 5 is caused by the measuring
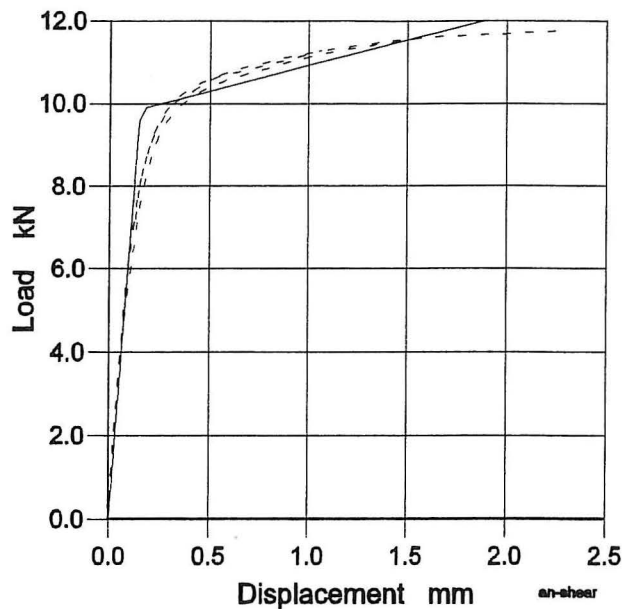
Figure 6.3: **Load-displacement curves from shear tests (dashed) and AN-TRUSS (solid).**

length $l_m \sim 5(l_1 + l_2)$. In a plate with quadrilateral holes and a tensile load, stress concentrations will occour to cause decreasing stiffness. Then the estimate of E in (6.2) is too high and a reduced value must be used. If the reduction is about 10%, the value $E = 160000$MPa is obtained (again). In the following, this value will be used.

E is assumed to be the MOE in all load combinations, and therefore ε_p^t can be estimated by (6.3), as the yield load of the plate in tension is determined as ~ 15.5kN, see figure B.8 on page 136. The plate width is 76mm which corresponds to 11 beams of 3.98mm width. (Plate thickness= 1.0mm).

$$\varepsilon_p^t = \frac{15500\text{N}}{11 \cdot 3.98\text{mm}^2 \cdot 160000\text{MPa}} = 0.0022 \tag{6.3}$$

The length L can also be used as a measure for the extension of the plastic zone of the plate. The size of the plastic zone is dependent on the length of the plate (number of nails). L is then not "just" a distance between two nail rows - it is a parameter to be estimated, see the following.

6.1.2 Results

In figure 6.4, the load-slip curves from AN-TRUSS are compared to the load-slip curves from ABAQUS. The slip from the AN-TRUSS model is defined as twice the displacement of node 3, see figure 6.1. The length of the plastic zone in the plate is estimated to L =20mm. The load-slip curves fit well but the plastic slips of splices with plate
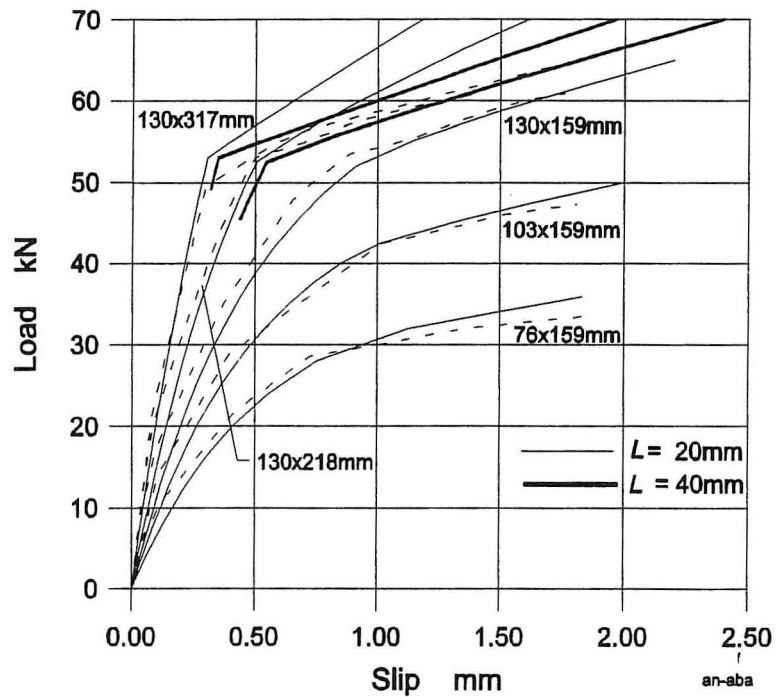
Figure 6.4: **Load-slip curves from AN-TRUSS(solid) compared to load-slip curves from ABAQUS (dashed).**

length >159mm are underestimated caused by a larger extension of the plastic zone for these plates. For L =40mm, the displacements are better estimated for plate lengths >159mm, see the thick solid lines in figure 6.4.

The size of the plastic zones found, fits the size of the plastic zones estimated by ABAQUS, see figure 2.19 on page 24 and figure 2.22 on page 26.

6.2 Bending Splices

In this example, the bending splices described in chapter 3 and appendix D are modelled by different AN-TRUSS models. The models are tested at several levels: First an unjointed beam (series BE0), second a beam with a centrally located nail-plate and finally a joint with an eccentrically located plate. The joints are analysed with and without contact between the timber members. The results are compared to results from ABAQUS. The sensitivity of changes in different properties is analysed too.

6.2.1 Modelling
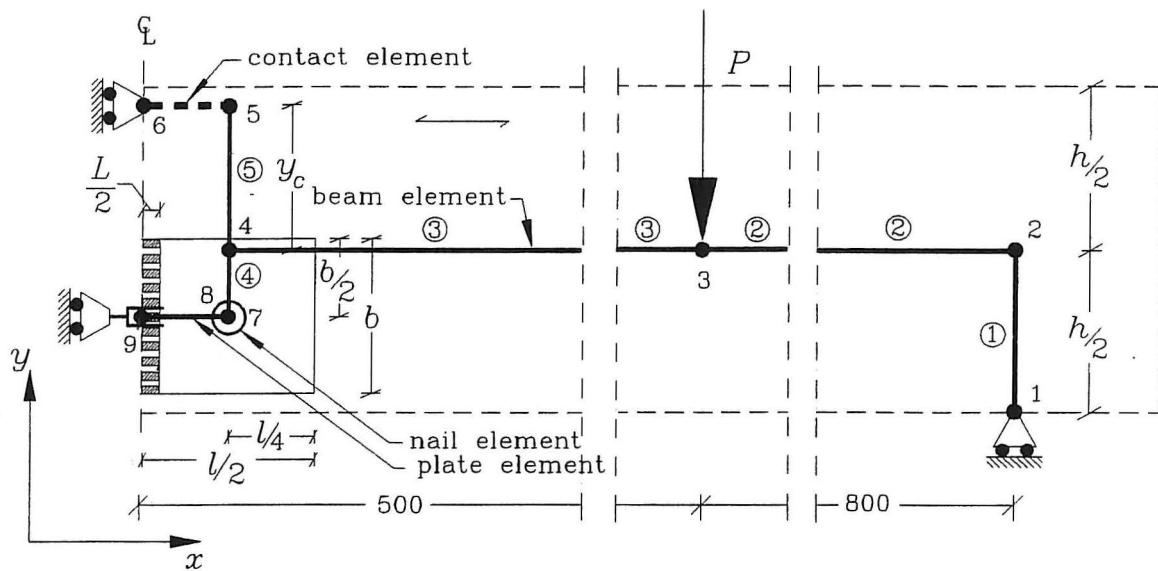
Figure 6.5: **AN-TRUSS model of a splice subjected to 4 point bending. Dimensions in mm. l and b are the dimensions of the nail-plate.**

An AN-TRUSS model of a bending splice with eccentrically located nail-plate and contact between the timber members is shown in figure 6.5. Since the splice is symmetric, only the right-hand part is modelled. Nodes 1 to 7 belong to the timber and nodes 8 and 9 belong to the plate. Nodes 6 and 1 are fixed in horizontal and vertical direction, respectively. Furthermore, the horizontal displacement and the rotation of node 9 are fixed. Node 3 has a load P in vertical direction. Five beam elements (numbers shown in circles), a contact element (between nodes 5 and 6), a plate element (between nodes node 8 and 9) and a nail element (between node 7 and 8) are connected between the nodes.

The properties of the plate element are the same as used in section 6.1. The extension of the plastic zone of the plate is increased to $L =$50mm, see discussion on page 80. The last two unknown plate parameters ε_p^c and E_p^c are estimated by fitting the AN-TRUSS results to the results from series BE3, where the buckling effect was distinct.

The properties of the beam and contact elements are shown in table 6.1.

Element no.	E MPa	G MPa	h mm	t mm
1	350	700	150	45
2,3	12800	700	170	45
4,5	100000	10000	200	45
Contact	12800	700	40	45

Table 6.1: Properties of the beam and contact elements.

In table 6.1, h and t are the height and thickness of the beams, respectively. The system line of beam element 1 is perpendicular to the grain direction (i.e E =350MPa). The vertical reaction force at node 1 is transmitted to the timber by a 100mm bearing plate and, therefore, the height of element 1 is estimated to 150mm caused by the pressure distribution.

Beam elements 4 and 5 have also a system line perpendicular to the grain, but these elements transmit the forces from the contact and nail element to the system line of the beam (elements 2 and 3). The load transmission is done by the timber in the joint area and when deformations are rather small, the stiffness properties of elements 4 and 5 are taken rather high.

The contact element is located in the line of the force resultant, which is determined by a linear distribution of the stresses perpendicular to the section height of the element. The distance from the system line of the beam to the contact element y_c is calculated by (6.4), where the height of the contact area is estimated as 40mm, see also appendix D.

$$y_c = \frac{h}{2} - \frac{1}{3}h_c = 85\text{mm} - \frac{1}{3}40\text{mm} \sim 72\text{mm} \tag{6.4}$$

The stiffness of the nails is determined by

$$p = (p_0 + k_1 \Delta)\left(1 - \exp\left(\frac{-k_0 \Delta}{p_0}\right)\right) \tag{6.5}$$

$$p_0 = \frac{p_0(\vartheta = 0°) + p_0(\vartheta = 90°)}{2} + \frac{p_0(\vartheta = 0°) - p_0(\vartheta = 90°)}{2}\cos(2\vartheta) \tag{6.6}$$

where ϑ is the angle between the nail force vector and the grain. (6.6) is made to ensure that the stiffness decreases with increasing ϑ, as shown in figure 3.4 on page 33. The constants are found to be:

$$p_0(\vartheta = 0°) = 150\text{N}$$
$$p_0(\vartheta = 90°) = 110\text{N}$$
$$k_0 = 900\text{N/mm}$$
$$k_1 = 80\text{N/mm}$$

The model of a beam without a joint is made with elements 1, 2 and 3 only. Node 4 is then located at the centre line with constraints as node 9 in figure 6.5.

When the joint has a centrally located nail-plate, element 4 and node 7 are removed from the model. The nail element is then located between nodes 4 and 8, see figure 6.5.

6.2.2   Results

In figure 6.6 to figure 6.11, results from AN-TRUSS are compared to results from ABAQUS. Load-displacement curves shown with solid curves are from AN-TRUSS and the dashed curves are from ABAQUS.
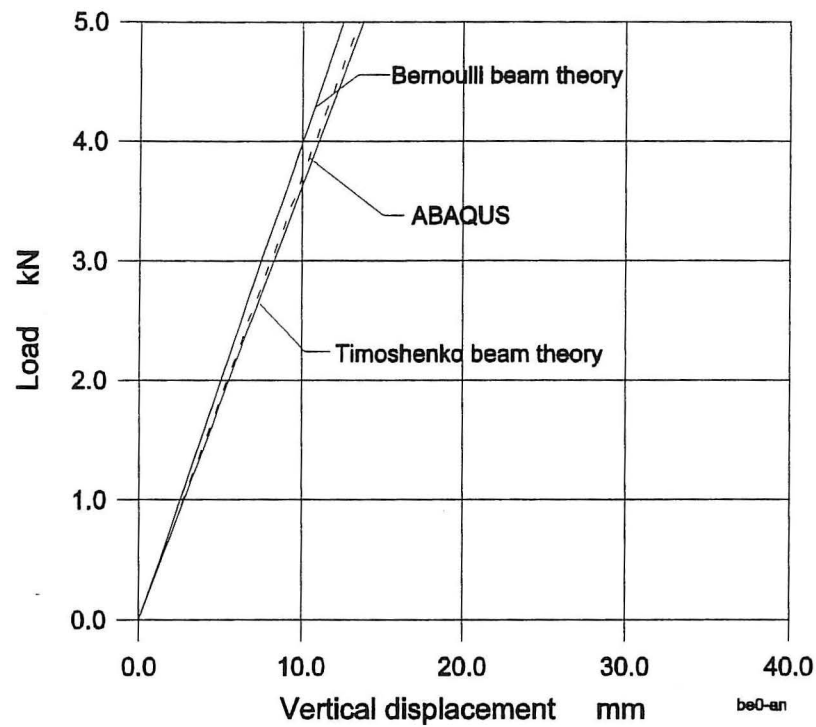
Figure 6.6: Load-displacement curves of an unjointed beam. Series BE0.
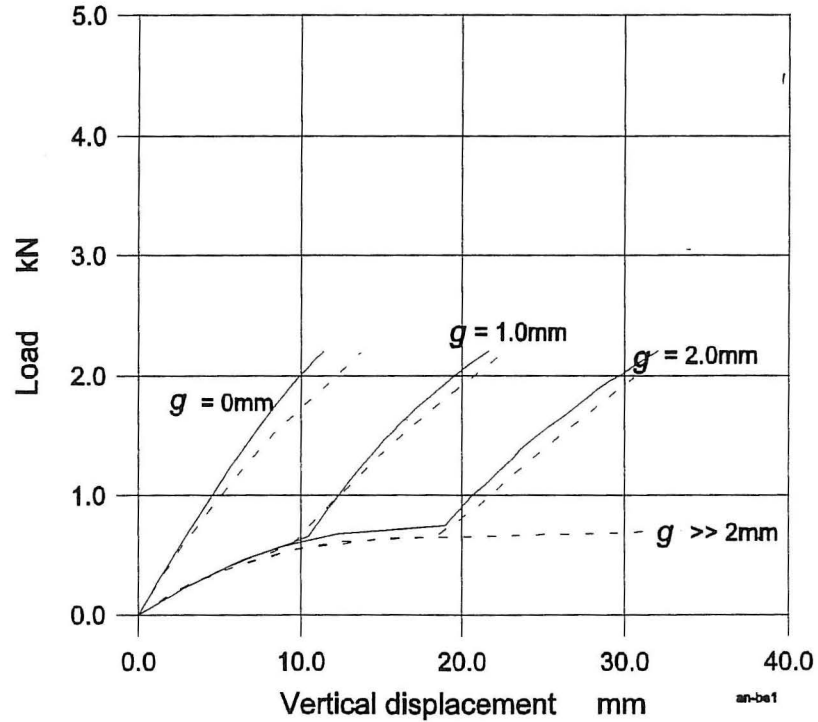
Figure 6.7: Load-displacement curves of a splice with centrally located 76x159mm plate and different gap sizes. Series BE1.
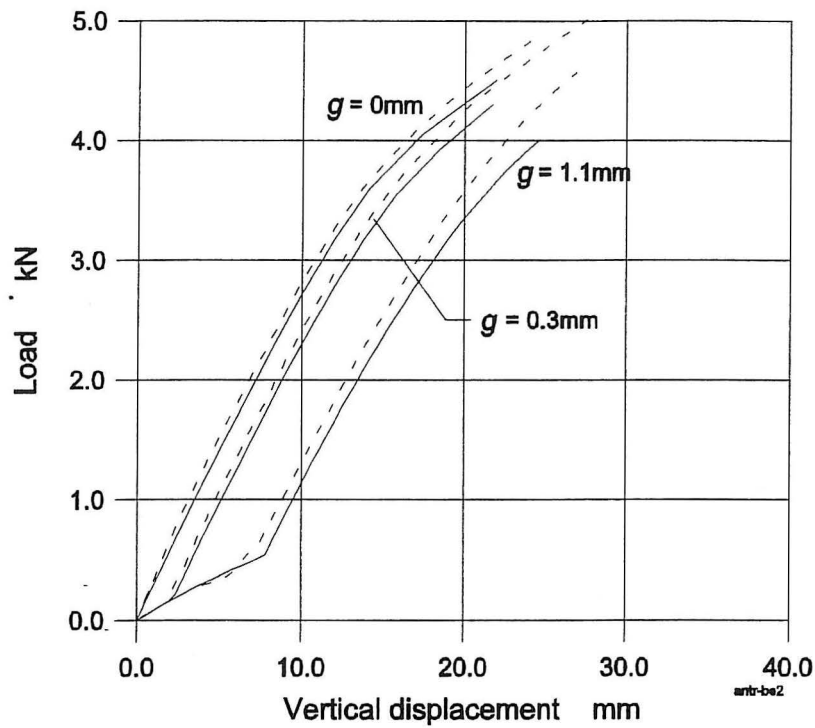
Figure 6.8: Load-displacement curves of a splice with eccentrically located 76x159mm plate and different gap sizes. Series BE2 and BE4.
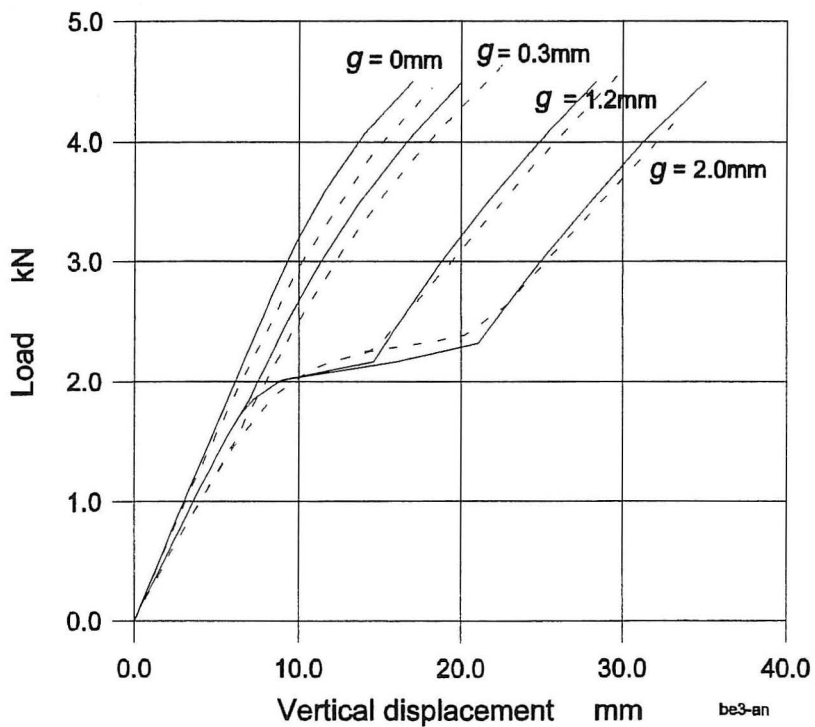
Figure 6.9: Load-displacement curves of a splice with centrally located 130x317mm plate different different gap sizes. Series BE3.
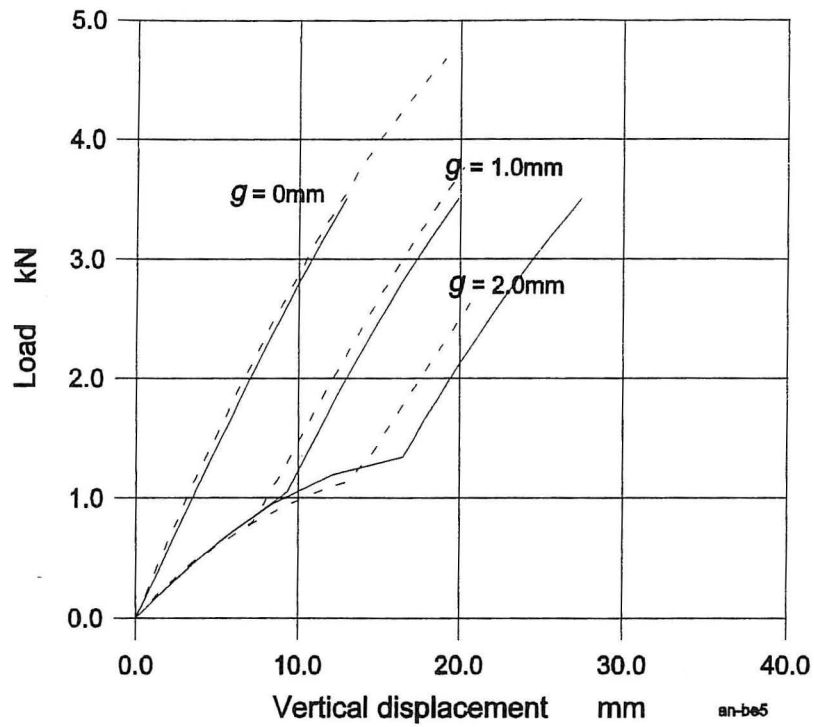
Figure 6.10: Load-displacement curves of a splice with eccentrically located 103×159mm plate and different gap sizes. Series BE5.
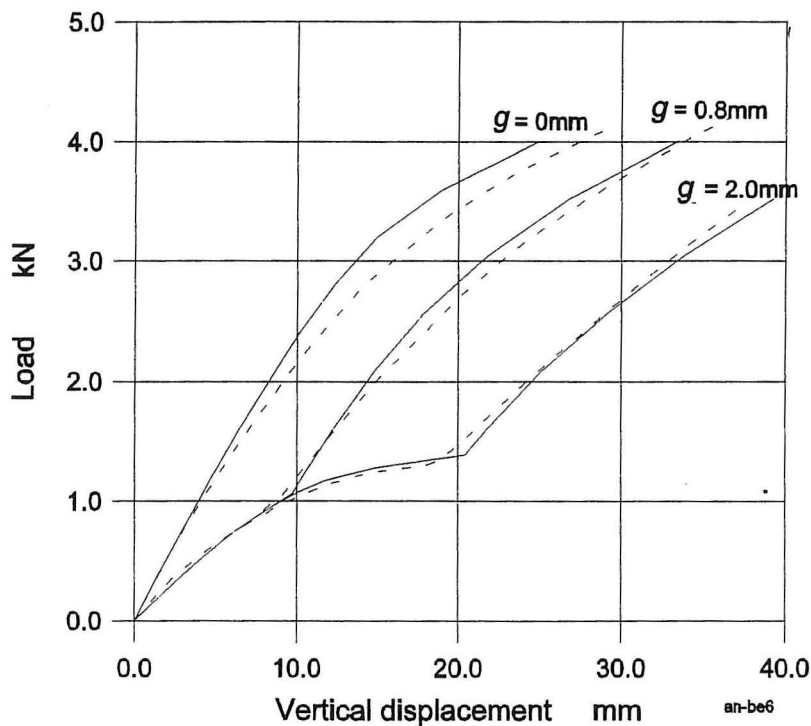
Figure 6.11: Load-displacement curves of a splice with centrally located 103x159mm plate and different gap sizes. Series BE6, BE7 and BE8.

6.2.3   Discussion

In figure 6.6 it is seen that the stiffness of the Timoshenko beam fits the ABAQUS result (and also the experimental tests) better than the stiffness of the Bernoulli beam. In the following Timoshenko beams are used only.

The last two plate parameters are determined to be

$$\varepsilon_p^c = 0.0009$$
$$E_p^c = 500\text{MPa}$$

The AN-TRUSS results for series BE3 are shown in figure 6.9. It was found that the sensitivity of the joint stiffness is small for a change in E_p^c. A decreasing value of ε_p^c will decrease the "yield load" of the joint without contact between the timber members. It will not affect the joint stiffness in contact.

During loading the following tendency is observed at all the bending joints tested with AN-TRUSS: The outermost beams in the compression zone of the plate become plastic before the outermost beams in the tension zone. This is caused by $\varepsilon_p^c < \varepsilon_p^t$. After that, the plastic zones extend towards the middle of the plate. If contact occurs, the compression zone gets smaller whereas the tension zone becomes still larger.

In figure 6.7 to figure 6.11 the following are observed:

- In general, the AN-TRUSS model estimates the displacements well according to the displacements determined by ABAQUS, but when the plate become plastic and there is still no contact between the timber members, the model underestimates the displacement a bit.
- The displacements are underestimated a bit in splices with centrally located plates and contact.
- The displacements are overestimated a bit in splices with eccentrically located plates and contact.

The differences between the load-displacement curves can be caused by several factors. The difference mentioned in the first item is most distinct in figure 6.7 and the main factor is found to be the length of the plastic zone, L. In figure 6.12, curves are shown with different values of L. An increased value of L of 40% will decrease the load at 15mm vertical displacement with 8%. The stiffness in contact is almost unaffected. In other tests, an increased value of L will cause an overestimation of the displacements. In bending, the nail-plate is subjected to shear and bending moment, in addition to tension and compression. The shear stiffness of the plate is very sensitive to a change in L, see (5.36) on page 61, where L is not "only" a plastic length, as stated in the previous section. AN-TRUSS estimates the displacements well with $L =50$mm, but the value of L is different from the value used at the tensile tests in the previous section. The theory described in section 5.2.3 on page 60 was based on one value of L, which is found to give bad results. A solution might be to split L into two independent parameters: a length, L^t to be applied to the tensile and compressive stiffness members
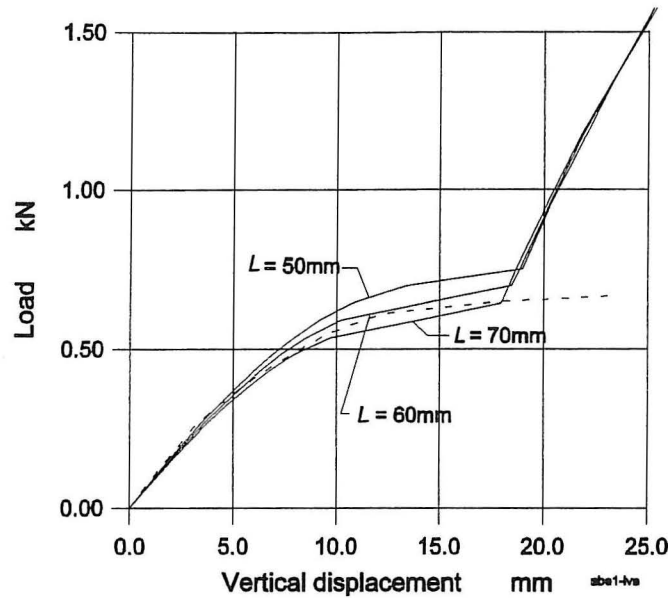
Figure 6.12: Load-displacement curves (solid) from the AN-TRUSS model with different values of L. Series BE1
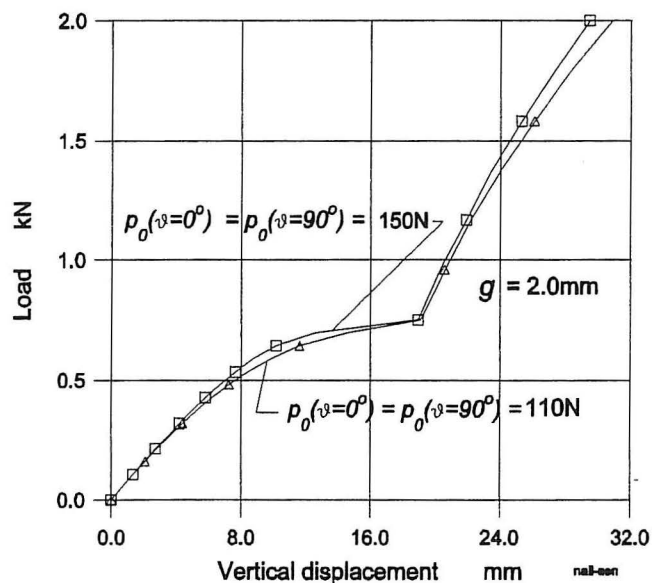
Figure 6.13: Load-displacement curves of a splice with centrally located 76x159mm plate and different values of p_0. Series BE1.

of (5.36) and a length L^s to be applied to the shear and bending members of (5.36). This has not been analysed in this thesis.

In figure 6.13, different stiffness values for the nails are used. The load-displacement curve found with the nail stiffness expressed with $p_0(\vartheta = 0°)$ =150N and $p_0(\vartheta = 90°)$ =110N is located between the curves in figure 6.13 (not shown). In figure 6.13, it is seen that the AN-TRUSS model is not very sensitive on p_0.

The two last-mentioned items on page 80 can be caused by the location and the size of the contact area. Tests with the model show, however, that the load-displacement curves are not affected by stiffness change in the contact element within ±25%. The joint stiffness is, on the other hand, sensitive to the location of the contact element given by the parameter y_c, see figure 6.14.
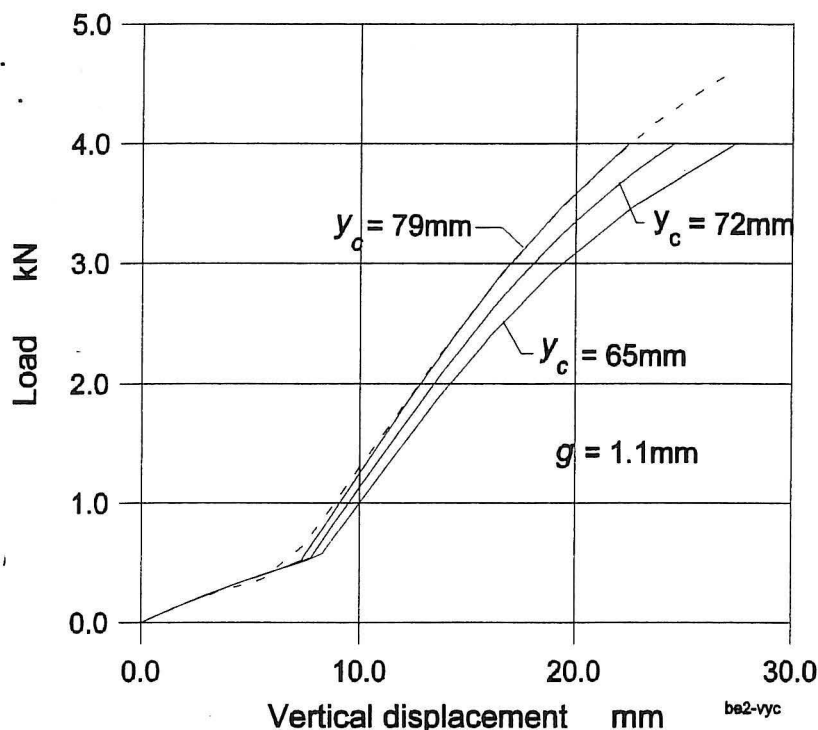
Figure 6.14: **Load-displacement curves from the AN-TRUSS model with different locations of the contact element. Series BE2.**

An decreased value of y_c will reduce the stiffness of the joint. The displacement value when contact occours will decrease because the contact element is activated by a smaller value of the rotation in node 4, see figure 6.5 on page 74.

As only one value of y_c is sought, y_c=72mm will give satisfactory results.

In chapter 3, it was found that ABAQUS underestimates the displacements in bending splices with contact between the timber members. The difference is caused by the butt effect. If a reduced stiffness value (E =2000MPa) is used for the contact element, AN-TRUSS can also estimate the displacements in contact, see figure 6.15.
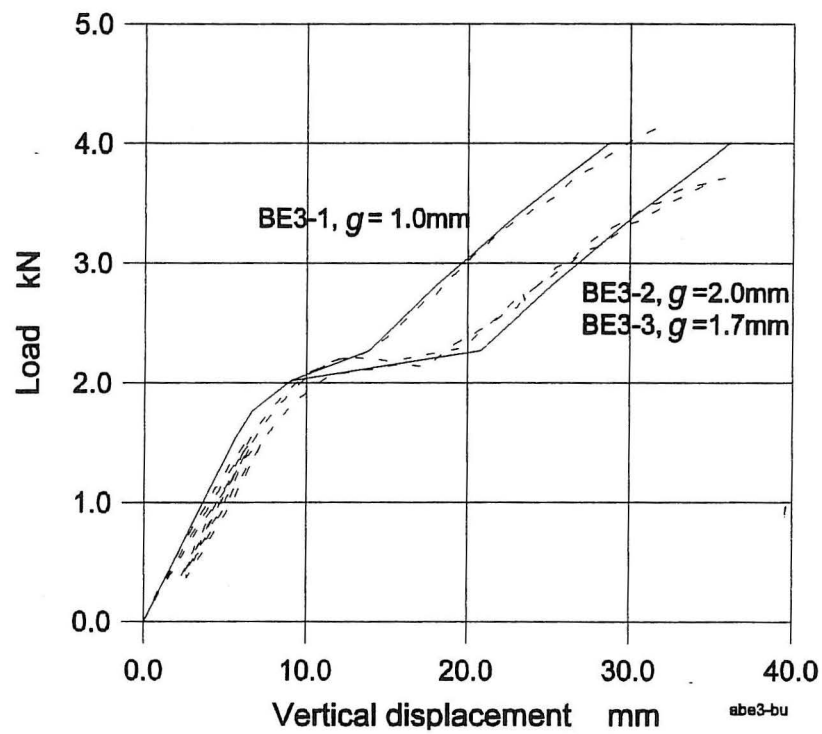
Figure 6.15: Load-displacement curves from AN-TRUSS with stiffness reduction of the contact element. Dashed curves are determined from bending tests on beams. Series 3.

6.3   A Heel Joint

The heel joint described in chapter 4 is modelled by an AN-TRUSS model. The results are compared to results from ABAQUS. The sensitivity of a change in different properties is also analysed.

6.3.1   Modelling

In figure 6.16, the AN-TRUSS model of the heel joint is shown.
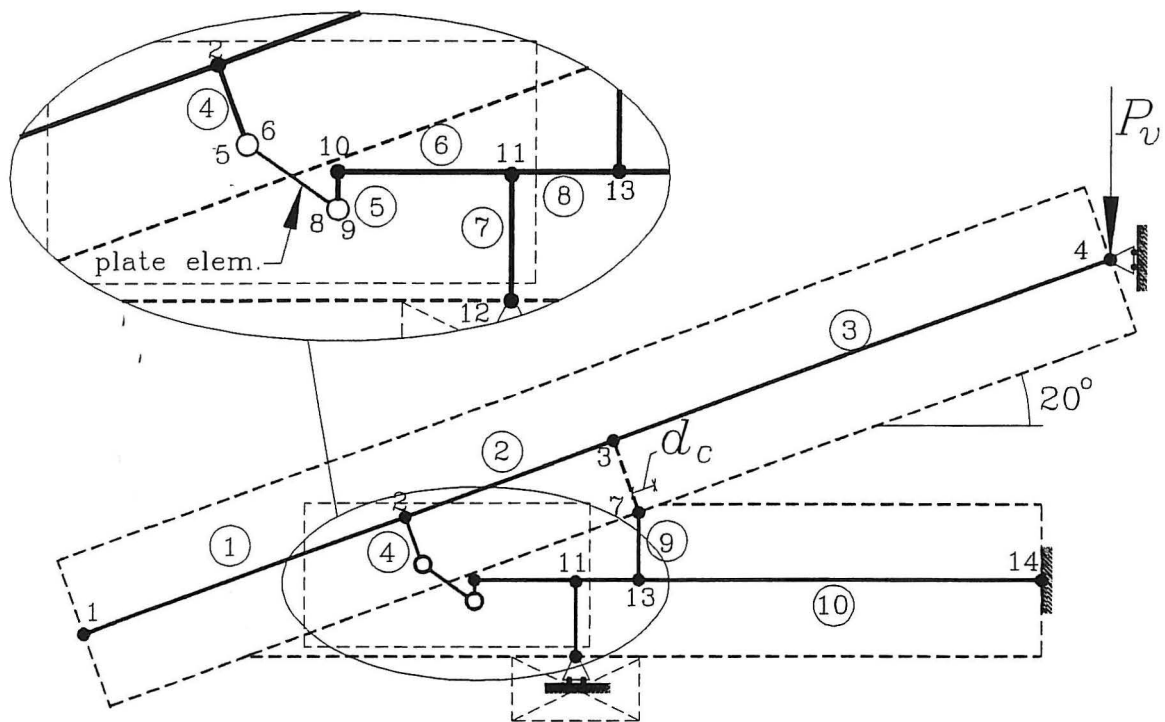
Figure 6.16: AN-TRUSS model of the heel joint.

The outlines of rafter, chord, plate and sill are shown as thin dashed lines. The model consists of 14 nodes, 10 beam elements, 2 nail elements, a plate element, and a contact element. The dimensions of the heel joint are shown in figure 4.1 on page 45. Node 4 is loaded with a vertical load P_v. Node 14 is fully constrained and nodes 4 and 12 are fixed in horizontal and vertical direction, respectively. Nodes 5 and 6 are located in the centre of the nail group on the rafter, and nodes 8 and 9 are located in the centre of the nail group on the chord. There is no gap between the rafter and the chord. The contact element is located at the distance d_c measured from the top end of the gap parallel to the rafter. d_c is fixed at 50mm, which is the same value as found by ABAQUS, see page 47.

The properties of the beam and contact element are given in table 6.2

Element	E MPa	G MPa	h_b mm	t mm	I mm^4	A m^2
1,2,3,6,8,10	12800	700	120	45	6480000	5400
4,5	100000	10000	-	-	30000000	5400
7	350	700			30000000	5400
9	350	700	-	-	30000000	5400
Contact	350	700	120	45	-	5400

Table 6.2: Properties of the beam and contact elements.

The properties of the nail elements are the same as in section 6.2.

The theory for the plate element assumes that the plate area above the gap can be modelled as a row of beams with identical cross-sections and stiffness, see section 5.2.3 on page 60. This assumption is only valid when the gap ("the beam row") coincides with the principal system of the plate, see figure 6.17. When the angle between the gap and the x-axis of the plate is $\leq 90°$, the plate areas (the beams) connecting the two nail groups are different with non-geometric form. The direction of the beams is perpendicular to the gap and thus not coinciding with the x-axis. The number of beams per length is reduced and the height of the cross-sections is increased. The height h and length L of the beams when the angle between the x-axis and the gap is 20°, are estimated as 8mm and 10mm, respectively. Other parameters of the plate are the same as in section 6.2.
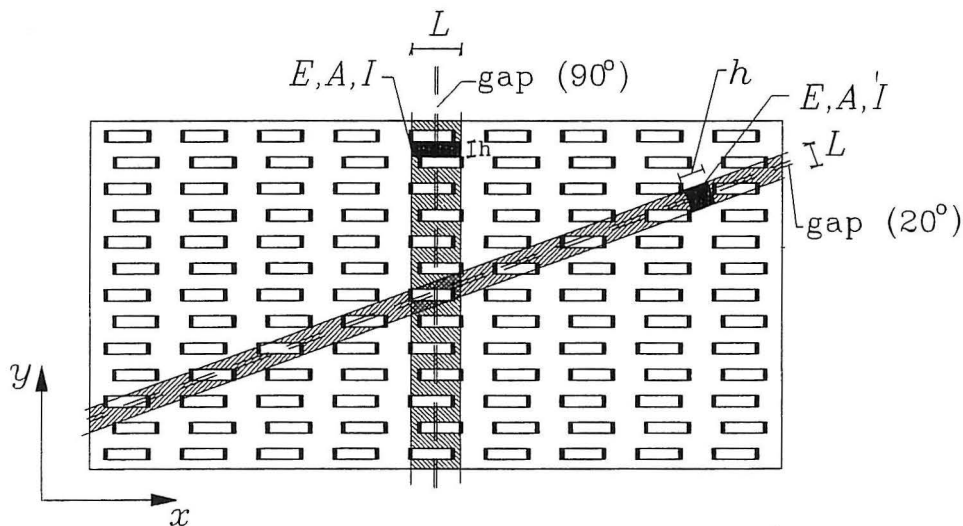
Figure 6.17: Plate areas above a gap (hatched) with 90° and 20° to the x-axis, which is modelled by small beams with the parameters E, A and I.

6.3.2   Results

In figure 6.18, load-displacement curves from AN-TRUSS (solid) are compared to results from ABAQUS (dashed).
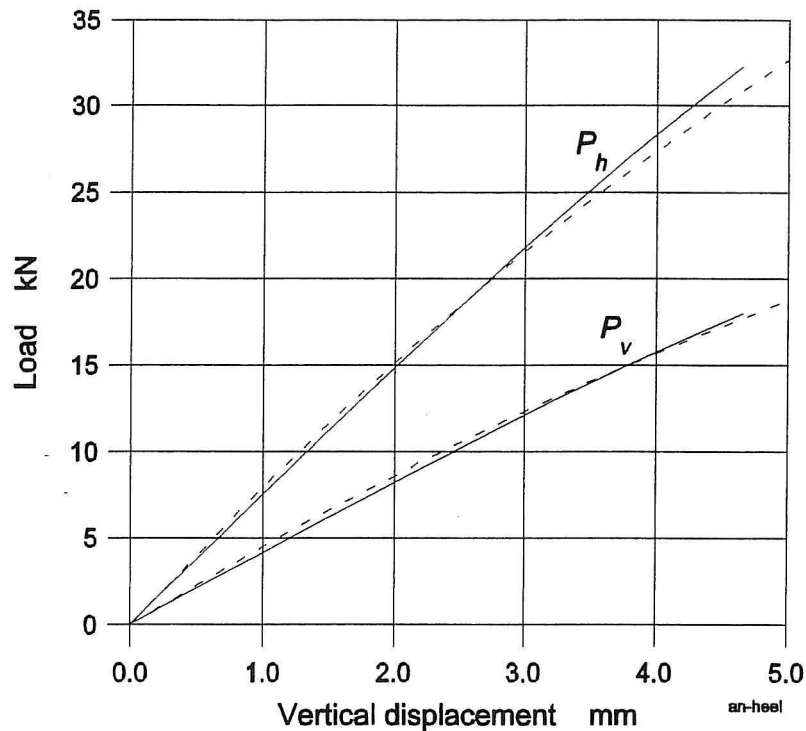
Figure 6.18: **Load-displacement curves from AN-TRUSS and ABAQUS.**

P_h and P_v are the horizontal reaction and vertical load in node 4, respectively. AN-TRUSS estimates the displacements very well. The plate element has not become plastic during loading.

Some of the parameters in the AN-TRUSS model are estimated, i.e d_c, A_c, L, h. In table 6.3, the effect of a variation in the paratemers is shown with P_v =18kN.

d_c	A_c	L	h	N_c	R_{sill}	M_{node3}	V_4	P_h
mm	mm^2	mm	mm	kN	kN	kNm	mm	kN
0	5400	10	8	7.96	16.36	2.49	4.49	31.03
50	5400	10	8	8.10	17.41	2.65	4.65	32.29
70	5400	10	8	8.29	17.50	2.71	4.71	32.73
50	3000	10	8	6.48	17.74	2.53	4.80	32.08
50	7000	10	8	8.74	17.28	2.64	4.60	32.10
50	5400	15	8	8.20	17.35	2.63	4.75	32.20
50	5400	10	6	8.07	17.37	2.62	4.70	32.23

Table 6.3: **Effect of the variation in d_c, A_c, L and h.**

In table 6.3, A_c is the area of the contact element, h is the height of the beams in the plate, N_c is the axial force in the contact element, R_{sill} is the vertical reaction at the

sill, M_{node3} is the section moment at node 3, V_4 is the vertical displacement of node 4 (positive in the same direction as P_v, see figure 6.16) and P_h is the horizontal reaction at node 4.

In table 6.3, it is seen that a variation in the location af the contact element between 0 and 70mm will change V_4 by less than 4%. Caused by the extended arm of the moment, M_{node3} increases with increased d_c.

A variation in the size of the contact area between 3000mm^2 and 7000mm^2 will change V_4 by less than 4%. An increased vaule of L will increase V_4 by less than 3% and a decreased value of h will decrease V_4 by less than 2%.

In general, a variation in any of the parameters has a low effect on the stiffness.

6.4   Collar Tie Truss

In this section, a collar tie truss is modelled by AN-TRUSS. The results are compared
with results from the programme ECOTRUSS ver.7.2 developed by Gang-Nail Systems.
ECOTRUSS is based on the fictitious member model. The results are given by the
section forces and the deflections at selected points.   Two different load cases are
analysed.

6.4.1   Modelling

The dimensions of the timber members and plates are given in appendix E.   In fi-
gure 6.19 the AN-TRUSS model of the collar tie truss is shown.
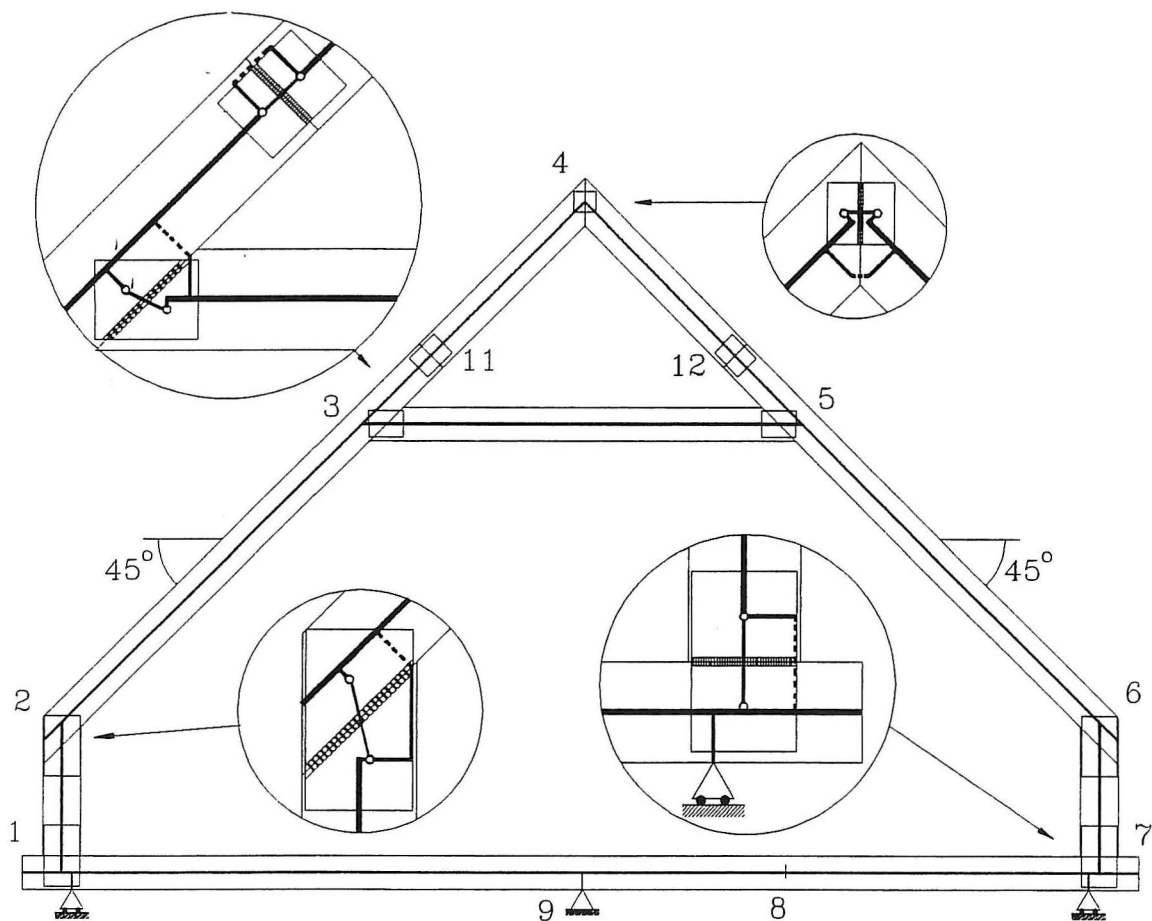
Figure 6.19: AN-TRUSS model of the collar tie truss.

The truss is supported in vertical direction at points 1, 9 and 7 and in horizontal
direction at point 9. The truss is symmetric and the roof pitch is 45°. The bottom
chord and the collar tie are made from timber of strength class K-18 according to DS
413 [56]. Other timber members are made of strength class K-24. The plate and nail
properties are the same as in the previous sections in this chapter, however, h and L

of the beams in each plate are estimated dependent on the angle between the gap and principal axes of the plate, see table 6.4.

angle	h mm	L mm	Used in joint at point no.
90°	4	20	1,7,11,12
45°	10	10	2,3,5,6
0°	9	13	4

Table 6.4: Plate properties dependent on the angle between the gap and the principal axis of the plate.

In each joint there are a contact element (dashed line), two nail elements (circles) and a plate element (line between the circles). The contact elements are located in the contact zones, however, the location of the contact zone depends on the truss load, and therefore, some contact elements can be located at the "other end" of the gap line.

In the ECOTRUSS model the joints in point 11, 12 and 4 are modelled as pinned and other joints are rigid.

The truss is subjected to two different load cases:

Load case 1 : a load case with an unsymmetric snow load, see figure 6.20 on page 90.

Load case 2 : a load case with the weight of the structure, 0.5(snow load), 1.3(the wind load) and 0.5(the load on the tie in use), see figure 6.21 on page 91.

Load cases 1 and 2 belong to the load duration classes medium-term and short-term, respectively. In each load case, different values of the timber stiffness must be used, see table 6.5 and DS-413 [56]. The values in table 6.5 are design values, and service class 2 is assumed. E_{90} is the modulus of elasticity perpendicular to the grain.

Strength class	K-18			K-24		
	E MPa	E_{90} MPa	G MPa	E MPa	E_{90} MPa	G MPa
Load duration class						
Medium-term (snow)	6300	210	420	7300	240	480
Short-term (wind)	7200	240	480	8400	280	560

Table 6.5: Properties of the timber dependent on the strength class and load duration.

In tables 6.6 to 6.9, the section forces and the displacements, calculated by the two models, are given at selected points shown in figure 6.20 and figure 6.21. The difference Δ between the results is calculated. A positive value of Δ signifies that the value calculated by AN-TRUSS is numerically larger than the value calculated by ECOTRUSS. The maximum values are shown as bold letters.

6.4.2   Results

Load case 1
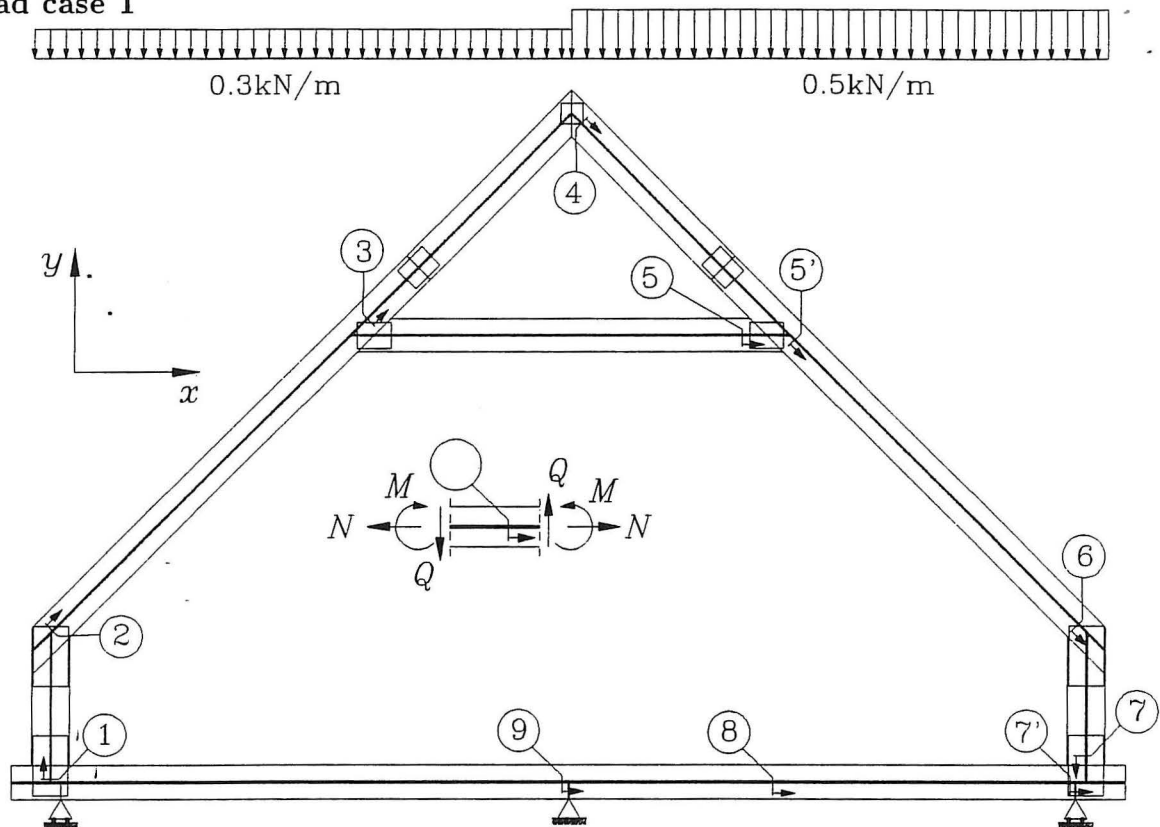
Figure 6.20: Loads on the collar tie truss in load case 1 and the location of the points at which the section forces are given.

	ECOTRUSS			AN-TRUSS			Difference		
Point	N	Q	M	N	Q	M	Δ_N	Δ_Q	Δ_M
	N	N	Nm	N	N	Nm	N	N	Nm
1	-1069	**-618**	180	-1069	-583	155	0	-35	-25
2	-1170	296	-362	-1145	330	-374	-25	34	12
3	-432	179	-77	-547	98	7	115	-81	(-84)
4	-95	158	0	-169	280	-43	74	172	43
5	-439	88	217	-265	46	95	-179	-42	-122
5'	-799	75	89	-752	-71	154	-47	-4	65
6	-1407	-533	**-468**	-1396	-573	-491	-11	40	23
7	**-1427**	**618**	76	-1427	583	55	0	-35	-21
7'	618	-87	-162	583	-74	-141	-35	-13	-21
8	618	-87	-9	583	-74	-10	-35	-13	1
9	618	115	95	583	102	80	-35	-13	-15

Table 6.6: Section forces at selected points. Load case 1.

Load case 2
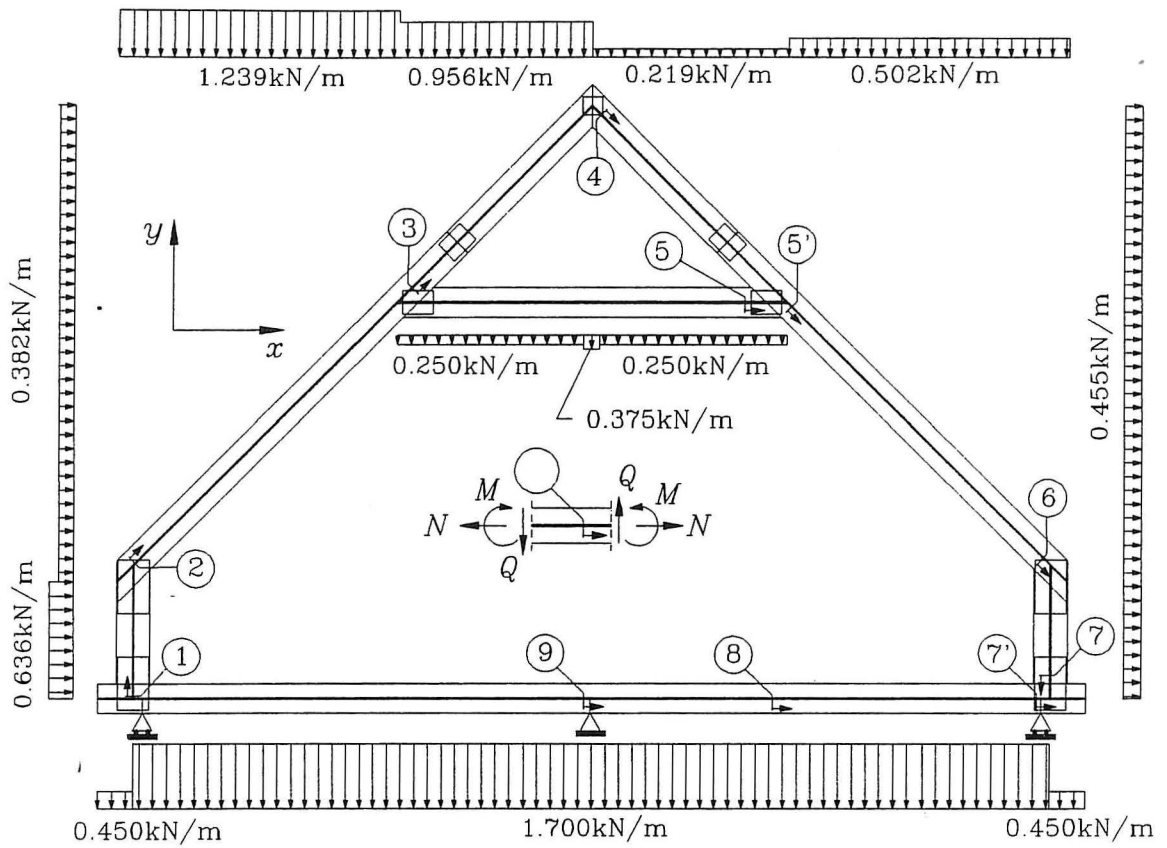
Figure 6.21: Loads on the collar tie truss in load case 2 and the location of the points at which the section forces are given.

Point	ECOTRUSS			AN-TRUSS			Difference		
	N	Q	M	N	Q	M	Δ_N	Δ_Q	Δ_M
	N	N	Nm	N	N	Nm	N	N	Nm
1	-2565	192	-169	-2557	309	-276	-8	117	107
2	-2006	1429	-255	-1887	1537	-339	-119	108	84
3	-449	798	-342	-243	287	444	-206	-511	(786)
4	-423	-75	0	-896	-253	-75	473	178	75
5	-1312	-1243	-1194	-975	-768	-553	-337	-475	-641
5'	-2845	189	-1134	-2698	92	-1040	-147	-97	-94
6	**-4009**	-132	-744	-3931	32	-880	-78	-100	136
7	-2841	**3376**	2034	-2841	3212	1760	0	-164	-274
7'	3376	-2826	**-2226**	3212	-2760	-1951	-164	-66	-275
8	3376	149	120	3212	215	275	-164	66	155
9	-192	-2941	-1287	309	-3067	-1549	117	126	262

Table 6.7: Section forces at selected points. Load case 2.

In table 6.8 and table 6.9 the displacements in the x and y-directions are given at selected points.

	ECOTRUSS		AN-TRUSS		Difference	
Point	disp_x	disp_y	disp_x	disp_y	Δdisp_x	Δdisp_y
	mm	mm	mm	mm	mm·100	mm·100
2	**-1.25**	-0.11	-1.03	-0.21	-22	10
3	-0.82	-0.59	-0.69	-0.61	-13	2
4	-0.29	-1.13	-0.26	-1.07	-3	-6
5	-0.84	**-1.66**	-0.74	-1.54	-10	-12
6	0.67	-0.09	0.55	-0.18	-12	9
8	0.01	0.15	0.02	0.11	1	-4

Table 6.8: **Displacements of selected points calculated with ECO-TRUSS and AN-TRUSS. Load case 1.**

	ECOTRUSS		AN-TRUSS		Difference	
Point	disp_x	disp_y	disp_x	disp_y	Δdisp_x	Δdisp_y
	mm	mm	mm	mm	mm·100	mm·100
2	5.45	0.28	5.34	0.32	-11	4
3	**12.23**	**-6.57**	11.99	-6.39	-24	-18
4	6.67	-1.02	6.94	-1.17	27	15
5	12.18	4.51	11.88	3.82	-30	-69
6	7.09	-0.41	6.78	-1.11	-31	70
8	0.06	0.47	0.17	-0.63	11	(110)

Table 6.9: **Displacements of selected points calculated with ECO-TRUSS and AN-TRUSS. Load case 2.**

6.4.3   Discussion

Load case 1

During loading there is no contact between the timber members (g=0.1mm) and the plates are in the elastic state. The load transmitted by the nails is very small ($< 15N$).

In table 6.6, it is seen that the max. moment calculated by AN-TRUSS is 5% larger than the max. moment from the ECOTRUSS model. It seems strange that the moment in AN-TRUSS is largest, when the joints at points 2, 3, 5 and 6 are made rigid by the ECOTRUSS model, but the timber member between points 5 and 6 is longer in the AN-TRUSS model caused by the way of modelling. The large differences in the section forces at points 3, 4 and 5 are caused by the different modelling of the joints at points 4, 11 and 12, see figure 6.19 on page 88.

In table 6.8, it is seen that the maximum displacements from AN-TRUSS are estimated to be 18% and 7% smaller in the x- and y-directions, respectively.

If the gap sizes are reduced to ($g=0$) in all joints, the moment at points 2 and 6 will decrease 2% and deflections will decrease very little.

Load case 2

During loading, buckling will occur in the plates at point 7 and at the splice on the left-hand rafter. The buckling zone at point 7 will be very large. If the gap sizes are larger than 0.52mm there is no contact between the timber members. The maximum nail force is 42N found in the right-hand nail group at point 5 (on the rafter).

In table 6.7, the max. moment in both models is found at point 7'. The moment calculated by AN-TRUSS is 12% smaller than the moment calculated by ECOTRUSS. However, the moments in other joints calculated by AN-TRUSS are larger. At points 3, 4 and 5, large differences in the section forces are observed, caused by the joint modelling used here.

In general, the displacements from AN-TRUSS are smaller than the displacements from ECOTRUSS, see table 6.9. The max. displacement is found at point 3. The "critical displacements" are evaluated to be found at points 2 or 6. The max. displacement here is calculated to be 4% smaller by AN-TRUSS.

If the gap sizes at points 3 and 7 are made very small ($g=0$) contact will occurs (with the contact elements located as shown in figure 6.19). The section forces and the displacements will change as shown in table 6.10.

	M		$disp_x$	
Point	no contact	with contact	no contact	with contact
	Nm	Nm	mm	mm
1	-276	-230		
2	-339	-331	5.34	4.08
3	444	494	11.99	11.52
6	-888	-774	6.78	6.43
7	1760	1766		

Table 6.10: **The influence of contact at points 3 and 7 on the moment and the vertical displacement calculated by AN-TRUSS. Load case 2.**

With contact at points 3 and 7, the max. nail force will be almost unchanged and at point 7, the buckling zone will be a bit smaller. In table 6.10, it is seen that the moment in the joints with contact will increase (by 10% in point 3). The displacement in the "critical" point 6 is reduced by 5%.

A model with rigid joints at points 1, 2, 6 and 7 (ECOTRUSS) will give satisfactory results on the safe side compared to the results found by AN-TRUSS.

6.5   W-Truss

In this section, a pitched W-truss is modelled by AN-TRUSS. The results are compared
with results from the programme ECOTRUSS ver.7.2 developed by Gang-Nail Systems.
The results are given by the section forces and the deflections at selected points. A
load case with unsymmetrical snow load is analysed.

6.5.1   Modelling

The dimensions of the timber members and plates are given in appendix E. In fi-
gure 6.22, the AN-TRUSS model of the W-truss is shown.
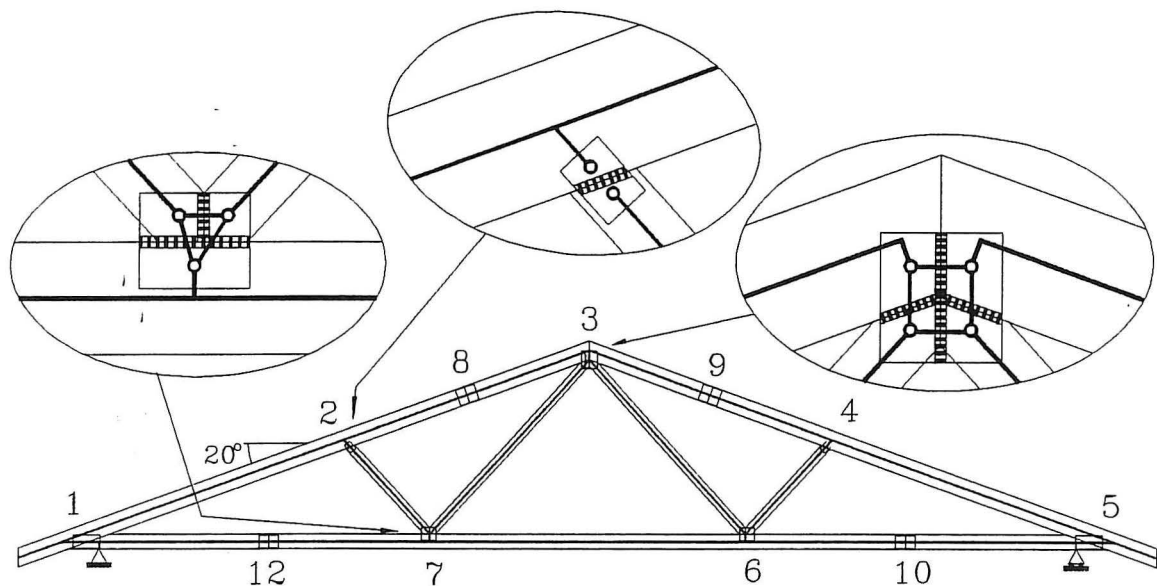
Figure 6.22: AN-TRUSS model of the W-truss.

The truss is supported in vertical direction at points 1 and 5 and in horizontal direction
at point 1. The truss is symmetric and the roof pitch is 20°. All the timber members
are made of strength class K-18 according DS 413 [56].

The heel joints at points 1 and 5 are modelled as shown in figure 6.16 on page 84 and
the splice joints at points 8, 9, 10 and 12 are modelled as shown in figure 6.19 on page
88. As bending stiffness of the webs are small compared to the stiffness of the rafter
and chord, the "web-joints" have no contact elements. The joints at points 6 and 7
consist of three nail elements and three plate elements. The joint at point 3 consists
of four nail elements and four plate elements.

In ECOTRUSS, the heel joint is modelled as shown in figure 6.23 and the joint at point
3 and the "web-joints" are modelled as pinned. Other joints are modelled as rigid.

The truss is subjected to a load case with the weight of the structure, 1.3(unsymmetrical
snow load), 1.0(load on the footbridge). The load case belongs to the load duration
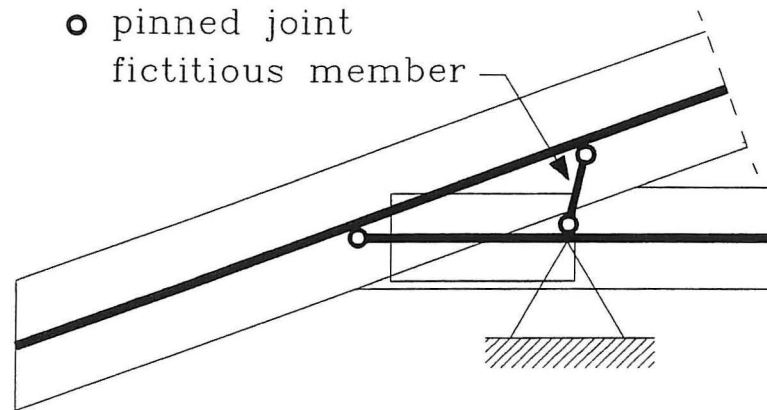
Figure 6.23: ECOTRUSS model of the heel joint.

classes medium-term. The stiffness values of the timber are as shown in table 6.5 on page 89. The properties of the nail and plate elements are the same as stated in previous sections.

In tables 6.11 to 6.12 the section forces and the displacements, calculated by the two models, given at selected points are shown in figure 6.24. The difference Δ between the results is calculated. A positive value of Δ signifies that the value calculated by AN-TRUSS is numerically larger than the value calculated by ECOTRUSS. The maximum values are shown as bold letters.

6.5.2   Results
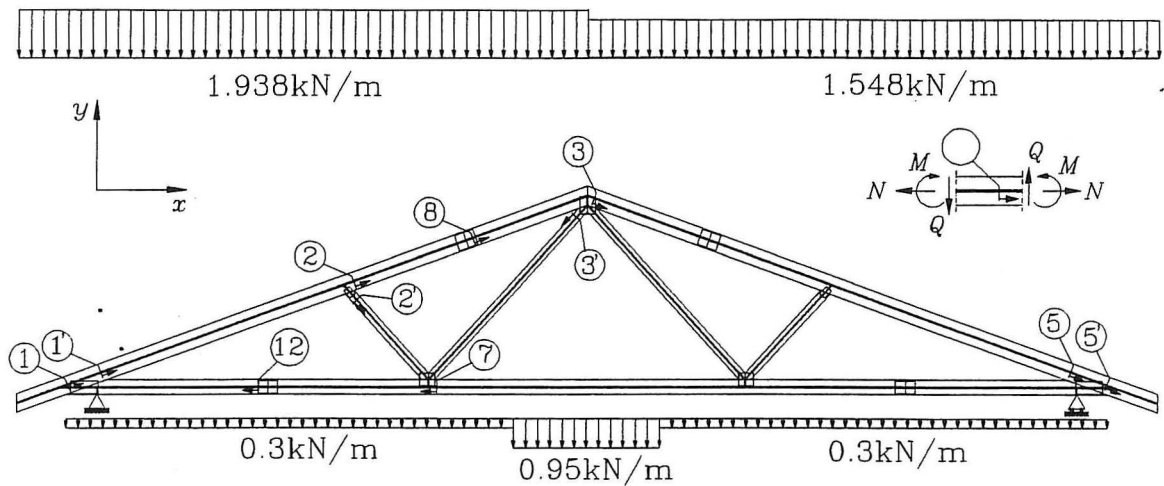
Figure 6.24: Loads on the W-truss and the location of the points at which the section forces are given.

Point	ECOTRUSS			AN-TRUSS			Difference		
	N	Q	M	N	Q	M	Δ_N	Δ_Q	Δ_M
	N	N	Nm	N	N	Nm	N	N	Nm
1	-13381	**-3687**	-121	-17543	-528	-1460	4162	-3159	1339
1'	**-17646**	2357	**-1507**	-17445	2516	-1563	-211	159	56
2	-15212	1942	-278	-15298	1475	-62	86	-467	-216
2'	-3312	0	0	-2679	-196	36	-633	196	36
3	-13483	1374	0	-13605	1733	-604	122	359	604
3'	4610	0	0	4192	-66	27	-418	66	27
5	-16430	-1992	-1357	-16239	-2137	-1408	190	145	51
5'	-12650	3388	-96	-16326	861	-1256	3665	-2527	1160
7	10680	-769	147	11073	759	122	395	-10	-25
8	-14551	-128	-819	-14615	-374	533	64	246	-286
12	15776	138	-76	15523	135	-69	-253	-3	-7

Table 6.11: Section forces at selected points on the W-truss.

In table 6.12, the displacements in the x and y-directions are given at selected points.

	ECOTRUSS		AN-TRUSS		Difference	
Point	$disp_x$	$disp_y$	$disp_x$	$disp_y$	$\Delta disp_x$	$\Delta disp_y$
	mm	mm	mm	mm	mm·100	mm·100
2	**2.23**	-11.01	2.65	-13.25	42	224
3	1.52	-11.25	1.37	-12.65	-15	140
4	0.99	-10.60	0.54	-12.69	-45	209
6	2.04	-11.32	2.05	-13.19	1	187
7	1.23	**-11.62**	1.21	-13.54	-2	192

Table 6.12: **Displacements of selected points calculated with ECO-TRUSS and AN-TRUSS.**

6.5.3 Discussion

During loading there is contact between the timber members at the heel joints and at the splices in the rafter (g=0.0mm). The plates at the splices in the rafter are in plastic compression. The max. nail force occurs in the above left-hand nail group in the pitch joint ($< 126N$).

In table 6.11, it is seen that the max. moment calculated by AN-TRUSS is 4% larger than the max. moment from the ECOTRUSS model. The large differences in the section forces at the heel joint and the pitch joint are caused by the different modelling. In the ECOTRUSS model, the webs are loaded more by axial forces than the webs in the AN-TRUSS model. The "missing" axial forces in the AN-TRUSS model are transmitted by the rafters. The section moments in the webs are very small, and the pinned model at the ends of the webs is a good approximation.

In table 6.12, it is seen that the maximum displacements from AN-TRUSS are estimated to be 17% larger than the displacements in the ECOTRUSS model.

Changes in gap sizes between 0.0 and 0.1mm have no significant effect on the results. If a contact element is inserted into the pitch joint, the section forces are almost unchanged and the maximum displacements from AN-TRUSS are estimated to be 12% larger than the displacements in the ECOTRUSS model.

The displacements from AN-TRUSS are estimated to be 12% larger than the displacements from the ECOTRUSS model, when the beams in AN-TRUSS are based on the same beam theory as ECOTRUSS (Bernoulli beam theory, $G \rightarrow \infty$).

6.6   Conclusions

Three different nail-plate joints have been modelled by AN-TRUSS and compared to results from ABAQUS. The results from ABAQUS can be used instead of the experimental results, because they give the mean results of the experimental results with one curve. Good agreement between the two models has been obtained, however, the AN-TRUSS results have not been made using the same value of the plate parameter L. The influence of L is largest in the plastic state and smallest in the elastic state. To describe the elastic and plastic stiffness of a joint in tension, compression, shear and bending, the theory of the plate element is based on one value of L only. This theory describes the plate in the plastic state very bad. An improvement of the plate element may be to operate with two independent values of L, which can be used for the tensile/compression members and the shear/bending members in the stiffness matrix, respectively. This subject has not been analysed.

Further tests on the plate with different angles between the load and the principal axes of the plate must be made to obtain a better calibration of the plate parameters h and L dependent on the angle between the gap line and the principal axes of the plate. The tests may be loaded in tension and shear.

The sensivity of the model (and therefore a nail-plate joint) to changes in different parameters, i.e. stiffness of the nails, location and stiffness of the contact element etc. has been analysed. The sensivity is low compared to the general variation of the results from tests on nail-plate joints.

AN-TRUSS models of two different trusses have been compared to results from the programme ECOTRUSS, which is based on the fictitious element model. The AN-TRUSS model of a collar tie truss estimated the maximum moment in the failure state (load case 3) to be 12% smaller than the maximum moment from ECOTRUSS. However, the same model estimated the maximum moment to be 5% larger with a load case in the serviceability state. In general, the estimated truss deformations from AN-TRUSS are smaller than the deformations determined by ECOTRUSS. The maximum displacements are estimated to be between 7% and 18% smaller with AN-TRUSS in proportion to the displacements from ECOTRUSS.

The AN-TRUSS model of the W-truss estimated a 4% larger maximum moment than ECOTRUSS, but the corresponding deformations are found up to 17% larger. The ECOTRUSS model of the collar tie truss and the W-truss is on the safe and the unsafe side, respectively, compared to the AN-TRUSS model.

The effect of contact between the timber members on deformations of the truss is small. The nail forces in the failure state are found to be small, but some plates become plastic. This is because the thickness of the tested plate is only 1mm. The forces on the each plates and nail groups are in contrast to ECOTRUSS given directly by AN-TRUSS. A comparison of the loads on plate and nail group from the two models has not been made.

Chapter 7

Conclusion

The aim of the work has been given as:

> *Development and testing of models for determination of the stiffness properties of nail-plate joints.*

The process diagram shown in figure 1.3 on page 8 has been followed closely. Two models for stiffness analysis of nail-plate joints have been developed. First, a complex model, where the timber is modelled by linear-elastic orthotropic continuum elements, the plate is modelled by linear-elastic plastic orthotropic continuum elements and the nails are modelled by elastic-plastic I-beams or nonlinear springs. This model has been called "the ABAQUS model".

Secondly, a frame model has been developed, where the timber and contact between the timber members are modelled by linear-elastic Timoshenko beams, the plate is modelled by a number of linear elastic-plastic Bernoulli beams, and the nails are modelled by a special non-linear nail element. The model has been called "the AN-TRUSS model". AN-TRUSS differs from other programmes in that the model is made directly by the knowledge of the physical location of the timber members and the nail-plates. The model is then sensitive to the plate location and the geometry of the connected timber members. The load on each nail group and plate is given directly too.

Results from both models have been compared to experimental test results. Tensile splices with different plate sizes, bending splices with different gap sizes, different plate sizes and locations have been used to test/calibrate the models.

Both models can predict the deformations very well compared to the test results. However, some phenomena demand special attention. Results from tests show, that the stiffness of splices subjected to bending moment decreases caused by a butt effect of the fibres in the contact zone. The AN-TRUSS model can predict deformations in those splices for a reduced stiffness of the contact element. The phenomenon is evaluated to be most distinct at the splices and the influence on other types of joints, i.e. a heel joint should be low.

99

When the plate becomes plastic, AN-TRUSS can predict the deformations, but different values of a single plate parameter must be used. It is impractical, and a proposal of improvement of the plate element is given. The proposal has not been tested.

Two different trusses have been modelled by AN-TRUSS and the results have been compared to results from the programme ECOTRUSS. At a collar tie truss the AN-TRUSS model predicts both larger and smaller maximum moment than predicted by ECOTRUSS. It depends on the load case. The deformations of the truss is predicted smaller - up to 18%. Comparisons of results from a W-truss show, however, that AN-TRUSS predicts larger moment (5%) and larger deformations (17%) at a load case in the ultimate limit state. At some joints there is large differences between the section forces given by the two models. This is caused by the different joint modelling. The sensivity of contact between the timber members on the stiffness of the trusses is found low with the AN-TRUSS model.

The AN-TRUSS model may be used on other types of mechanical joints i.e. other types of nail-plates or joints with steel plates/fiberboards with nails.

From truss factories and nail-plate manufacturers it is learnt that the truss programmes are still being developed, but the attention is concentrated on the joint modelling alone. The preprocessor, that is the way the truss is keyed in, created and changed, is also of great importance, as it will be most unfortunate if the profit of an optimized truss production is lost on comprehensive and time-consuming design processes.

In the present form, AN-TRUSS is a very powerful tool for the research on joints by estimation and optimization of the stiffness and strength of joints. With a few additions (see the list below), the model can be used in practical truss engineering.

In this thesis, the following items are contributions to the area of timber engineering:

- Comprehensive tests on nail-plates and nail-plate joints (more than 270 tests).
- Use of finite elements on nail-plate joints with and without contact between the timber members.
- Evaluation of the sensitivity of such parameters as nail stiffness, plate stiffness, and location/stiffness of contact between the timber members on the stiffness behaviour of several nail-plate joints and trusses.
- A developed plane frame programme which uses:
  - bilinear elastic-plastic Bernoulli beams to model the deformations in the plate
  - beam elements to model contact between the timber members.
  - small auxiliary elements to transmit the loads from supports, nail groups and contact.

List of topics for further research in the area of truss design:

- Further calibration of the AN-TRUSS model to estimate the failure load and failure type of arbitrary joints. This item will involve further analysis of the plate stiffness dependent on the angle between the principal axes of the plate and the gap direction. Also, ultimate values of the nail force and the plate deformations must be estimated. The influence of long-term load on the nail stiffness must be determined.

- Stiffness analysis of other types of nail-plates. The tested nail-plate (GNA 20 S) has a special relation between the properties of the plate and nails i.e. between stiffness and strength (the splice failed at the plate with rather few number of nails). Other types of plates have other relations between the nails and the plate.

- Tests on full-scale trusses to compare the deformations, failure types and failure locations with AN-TRUSS.

References

In the list of references books, theses and papers read in connection with the study are given. There is not referred to all the references in the thesis, but they are included for completeness.

[1] Aasheim E.(1991): *Design of Trusses*. International Timber Engineering Conference, London, 1991. (pp 1.89-1.96)

[2] Aasheim E.(1993): *Test of Nail Plates subjected to Moment*. International Council for Building Research Studies and Documentation Working Commission W18 - Timber Structures, (CIB-W18/26). Athens, Georgia USA 1993. (6 p.)

[3] Andersen H. & Larsen H.J. & E. Theilgaard & Thoft-Christensen P. (1977): *Beskrivelse af trækprøvemaskine til træ. (Rapp. nr. 7705)*(in Danish)(Description of tensile machine for timber.) Aalborg Universitet 1977. (7 p.)

[4] Aune P. (1970): *Investigations on Strength and Stiffness of Jqints made with Hydro-Nail Truss Plates*. Norges Tekniske Vitenskapsakademi 1970. (62 p.)

[5] Bulleit W.M. & Yates J.L. (1990): *Probabilistic Analysis of Wood Trusses*. Journal of Structual Engineering. Vol. 117 No. 10, pp. 3008-3025, 1990.

[6] Beineke L.A. & Suddarth S.K. (1979): *Modeling Joints made with Light-Gage Metal Connector Plates*. Forest Products Journal, 19(8) 1979, (pp. 39-45).

[7] Bulleit W.M. & Yates J.L. (1990): *Probabilistic Analysis of Wood Trusses*. Journal of Structual Engineering. Vol. 117 No. 10, pp. 3008-3025, 1990.

[8] Cook R.D. & Malkus D.S. & Plesha M.E. (1989): *Concepts and Applications of Finite Element Analysis*. Third edition, John Wiley & Sons 1989 (630 p.).

[9] Cowper G. R.(1966): *The Shear Coefficient in Timoshenko's Beam Theory*. Journal of Applied Mechanics, june 1966 (pp. 335-340).

[10] Edlund G. (1971): *R40:1971 Längdskarvning av träbalkar med spikplåtförband.*(in Swedish)(Splices with nail-plates.) Byggforskningen, 236 p., 1971.

[11] Edlund G. (1973): *R52:1973 Spikplåtar som förbindare i träfackverk.*(in Swedish) (Nail-plates as connector in trusses.) Byggforskningen 326 p., 1973.

[12] Erki M. A. (1991): *Modelling the Load-Slip behaviour of Timber Joints with Mechanical Fasteners.* Can. J. Civ. Eng. Vol 18, 1991 , (pp. 607-616)

[13] Feldborg Th. & Johansen M. (1981): *Wood Trussed Rafter Design.* SBI-rapport 118, Statens Byggeforskningsinstitut 1981, (166 p.)

[14] Foschi R.O. (1977): *Analysis of Wood Diaphragms and Trusses. Part II: Truss-Plate Connections.* Can. J. Eng. Vol. 4, pp. 353-362, 1977.

[15] Foschi R.O. (1979): *Truss Plate Modelling in the Analysis of Trusses.* Metal-Plate Wood-Truss Conference 1979, pp. 88-97, 1979.

[16] Gebremedhin K.G. & Crovella P.L.(1990): *Analysis of Light Frame Wood Truss Joint using an Elastic Foundation Model.* International Timber Engineering Conference, Tokyo, October 1990, (pp. 709-715).

[17] Gupta P. & Gebremedhin K.G.(1988): *Experimental Investigations to Determine the Strength of Tension Splice Joints.* International Conference in Timber Engineering, Vol. 1 1988, (pp. 257-265).

[18] Gupta P. & Gebremedhin K.G.(1990): *Reliability Analysis of Semirigidly Connected Metal Plate Wood Trusses.* International Timber Engineering Conference, Tokyo, October 1990, (pp. 287-294).

[19] Gramatikov K. & Gevrilovic P.(1990): *Experimental and Theoretical Investigations of Wooden Truss-Frame Structures under Cyclic Loads.* International Timber Engineering Conference, Tokyo, October 1990, (pp. 848-854).

[20] Hansen F.T. & Mortensen L.N. & Hansen L.P (1990): *Fuldskalaforsøg med trempelspær udsat for statisk og dynamisk last. Delrapport nr. 1: Forsøg og resultater.*(in Danish)(Full Scale Test on Collar Tie Trusses subjeted to Static and Dynamic Load, Part Report no. 1: Test and Results), Aalborg University 1990.

[21] Hededal O. & Krenk S.(1993): *A Profile Solver in C for Finite Element Equations.* Engineering Mechanics Paper no. 13, Aalborg University, 1993, (9 p.).

[22] Hiroto I.(1990): *The Moisture Content of the Wood in Combination with Matal Plate.* International Timber Engineering Conference, Tokyo October 1990 (pp. 681-685).

[23] Hunt R.D. (1987): *Mechanics of Laterally Loaded Nail Joints in Timber.* Ph.D-thesis, University of Auckland, School of Engineering, 1987, (214 p.).

[24] Hunt R.D. & Bryant A.H. (1988): *Moment Resisting Nail-Plate Joints. Recent Developments at Auckland University.* International Conference on Timber Engineering 1988, pp. 251-256, 1988.

[25] Hunt R.D. & Bryant A.H. (1989): *Strength of Timber Members in Joint Regions.* Pacific timber Engineering Conference, pp. 77-81, 1989.

[26] Hunt R.D. & Bryant A.H. (1990) : *Laterally Loaded Nail Joints in Wood.* Journal of Structural Engineering. Vol 116 No. 1. Jan 1990, pp. 111-124.

[27] Jensen H. & Rasmussen H. (1993) : *Undersøgelse af tandplader i stødsamlinger.*(in Danish)(Analysis of nail-plates in tension splices.) University of Aalborg, 1993, (90+56 p.)

[28] Jensen J.L. (1994) : *Dowel-Type Fastener Connections in Timber Structures subjected to Short-Term Loading.* (SBI 237) Danish Building Research Institute, 1994, (182 p.)

[29] Karacabeyli E. & Varoglu E. & Lum C. & Olson L.(1990): *Sturctural Performance of Metal Plated Gulam Trusses.* International Timber Engineering Conference, Tokyo, October 1990, (pp. 693-700)

[30] King C. G. & Whea D. L. (1988): *Deflection and Member Behavior of Metal-Plate-Connected Parallel-Chord Wood Trusses.* International Conference on Timber Engineering Vol. 1 1988, (pp. 482-497).

[31] Kjær K. & Sørensen S. (1992): *Rammehjørner i trempelspær.* (in Danish)(Knee Joints in Collar Tie Trusses.) B.Sc-Thesis, Aalborg University, 1992.

[32] Kloch S. & Hansen L.P (1990): *Fuldskalaforsøg med trempelspær udsat for statisk og dynamisk last. Delrapport nr. 2: Detailforsøg med tandplader.*(in Danish)(Full Scale Test on Collar Tie Trusses subjeted to Static and Dynamic Load, Part Report no. 2: Tests on Nail-Plates.), Aalborg University 1990.

[33] Kloch S. & Hansen F.T.: (1991): *Fuldskalaforsøg med trempelspær udsat for statisk og dynamisk last. Delrapport nr. 3: Detailforsøg med rammehjørner.*(in Danish)(Full Scale Test on Collar Tie Trusses subjeted to Static and Dynamic Load, Part Report no. 3: Tests on Knee Joints.), Aalborg University 1991.

[34] Krenk S. (1993): *Non-linear Analysis with Finite Elements,* Aalborg University 1993.

[35] Lau P.W.C. (1986): *Factores Affecting the Behavior and Modelling af Toothed Metal-Plate Joints.* Can. J. Civ. Eng. Vol. 14, pp. 183-195, 1987.

[36] Ljørring J. & Adelhøj J. (1989): *Tandpladeipresning + tilhørende bilag.*(in Danish)(Fastening of Punched Metal Plate Fasteners.), Teknologisk Institut 1989 (26 p.).

[37] Lum C. & Varoglu E. (1988): *Testing and Analysis of Parallel Chor Trusses.* International Conference On Timber Engineering. 1988 Vol. 1 (pp. 460-466).

[38] Maraghechi K. & Itani R.Y. (1984): *Influence of Truss Plate Connectores on the Analysis of Light Frame Structures.* Wood and Fiber Science, 16(3) 1984, pp. 306-322.

[39] Mortensen N.Lambert & Klock S. (1992): *Strength and stiffness of knee joints in timber frames.* Aalborg University 1992.

[40] Nielsen J. & Rathkjen A. (1994): *Laterally loaded Nail-plates.* University of Aalborg, 1994 (41 p.)

[41] Nielsen M.P & Hansen L.Pilegaard & Rathkjen A. (1973): *TRÆ 1.*(in Danish)(Timber 1), Danmarks Ingeniørakademi Bygningsafd. Aalborg, 1973 (174 p.)

[42] Norén B. (1973): *R60:1973 Traforband med spikplåtar. En undersökning av spik-gruppers förskjutning och vridning.*(in Swedish)(Jointing of timber using nail-plates. A study of the displacement and rotation of nail groups) Byggforskningen 1973 (76 p.)

[43] Norén B. (1981): *Design of Joints with Nail Plates* (second edition) International Council for Building Research Studies and Documentation Working Commission W18 -·Timber Structures, (CIB-W18/14). Warsaw, Poland 1981. (39 p.)

[44] Olsson K̇.G., & Petersson H. (1985): *Finite element-modellering av spikförband.*(in Swedish)(Finite element modelling of nail joints.) Lund Sweden 1985. (20 p.)

[45] Ottesen N.S. & Petersson H. (1990): *Introduction to Finite Element Method.* Lund Sweden 1990. (392 p.)

[46] Pagano N.J. & Halpin J.C.(1968): *Influence of End Constraints in the Testing of Anisotropic Bodies.* Journal of Composite Materials, Vol. 2, No. 1 (pp. 18-31), Jan 1968.

[47] Pellicane P.J. & Bodig J. & Mutuku R.N. (1989): *Modelling the Moment-rotation Behavior of Bolted Joints Subjected to Rotational Loading.* Pacific Timber Engineering Conference, Vol 2 pp. 43-47, 1989.

[48] Poutanen T.T. (1988a): *Analysis of Trusses with Connector Plate Joints.* Pacific Timber Engineering Conference 1988, pp. 155-159, 1988.

[49] Poutanen T.T. (1988b): *Eccentricity in a Nail-Plate Joint.* International Conference on Timber Engineering, pp. 266-273, 1988.

[50] Riberholt H. (1982): *Guidelines for Static Models of Trussed Rafters.* International Council for Building Research Studies and Documentation Working Commission W18 - Timber Structures, (CIB-W18/15). Karlsruhe, Federal Republic of Germany 1983. (31 p.)

[51] Suddarth S. K. (1972): *A Computerized Wood Engineering System: Purdue Plane Structures Analyser.* U.S.D.A. Forest service. Research Paper FPL 168,1972 (50 p.).

[52] Suddarth S. K. & Percival D.H. & Comus Q.B.(1981): *Testing and Analysis of 4×2 Parallel-Chord Metal-Plate Connected Trusses.* Research Report 81-1, Building Research Council, University of Illinois, 1981

[53] Suddarth S. K. & R. W. Wolfe (1983): *Purdue Plane Structures Analyser II - A Computerized Wood Engineering System.* General Technical Report FPL-40 U.S.D.A. Forest service, Forest Product Laboratory, General Technical Report FPL-40, Madison Wiscinsin, 1983.

[54] Triche M.H. & Suddarth S.K. (1988): *Advanced Design of Metal Plate Connector Joints.* Forest Products Journal Vol. 38, No. 9, pp. 7-12, 1988.

European and National Codes, Standards and Approvals

[55] Boligministeriet - Byggestyrelsen (1990): *MK-GODKENDELSE, MK 5.60/1034* Byggedata 2 p. 1990.

[56] Dansk Ingeniørforening (1992): *Trækonstruktioner DS 413* (in Danish)(Danish Code of Pratice for the Structural Use of Timber.) Dansk Ingeniørforening 4. udg. 84 p. 1982.

[57] Danish Standard Association (1994): *Eurocode no. 5: Design of timber structures, ENV 1995-1-1.* 222 p. 1994.

[58] Johansen B.L. (1990): *TRÆ 31. Træspær* (in Danish)(Timber 31, Trusses) Træbrancens Oplysningsråd 2. udg 1990,

Summary

This thesis deals with methods for modelling the stiffness of nail-plate joints.

Nail-plates are widely used to connect the timber members in prefabricated trusses. The nail-plate consists of a metal plate which is perforated by stamping so that nails with a length of 7-20mm occur perpendicular to the plate. After stamping there is oblong holes in the plate. The joint is made by embedding of the nails into the connected timber members. The advantages by this type of joint are that it is a cheap and easy to made and also a very stiff joint.

The dimensions of a truss are controlled by the load, which can occour and the deformations of the truss in use. The load carrying capacity and the deformations are determined by different models. However, the frequently used models are rather simple which means that the dimensions are too large in some cases and too small in other cases.

The aim of this thesis has been to analyse/develop models to estimate the stiffness of a nail-plate joint.

In chapter 1, the subject is introduced and the aim is accentuated and limited. The method and the process for the solution of the problem are given.

Chapter 2 deals with a tensile splice modelled by the programme ABAQUS ver. 5.2, which is based on finite element method. Timber and plate are modelled as two continuum disks connected with a small I-beam, which models the nails. The elements become properties which are determined by a large number of tests on timber, plate and nails. The results from the model are compared to results from tests on tensile splices with different plate sizes. Good agreement is obtained. The influence of the plate and nails on the joint stiffness is evaluated. The stress distribution in the timber and plate, as well as the distribution of the nail forces are given. .

In chapter 3, the ABAQUS model is extented to a bending splice. With this type of load there are nail forces in different directions, and therefore, different nail models are discussed. A nail model, which uses linear elastic plastic I-beams is selected. The results are compared to bending tests on splices with different plate size and location. The bending splices also have different gap sizes between the timber members, so the influence of contact can be determined. Good agreement between the results is obtained, however, the deformations are underestimeted in splices with contact between the timber members, caused by a butt of the fibres in the contact zone. The stress

distribution in the timber and plate, as well as the distribution of the nail forces are given for splices both with and without contact.

In chapter 4, an ABAQUS model of a 20° heel joint is made. The variation of the section forces in the rafter is given as well as the distribution of the nail forces and the stresses in plate and timber. No tests have been made to evaluate this model.

In chapter 5, the theory behind a developed, and more simple frame model is described. The model is called "the AN-TRUSS model". The timber members are modelled by beam elements. Plate and nails are modelled by special non-linear plate and nail elements and contact between the timber members is modelled by a contact element. The advantages by this model compared to the already used models are that the elements are located in the model based on knowledge of the geometry of the joint. The model is then dependent on plate size, location and contact between the timber members. The forces on each nail group and plate are given directly. In the model there are some parameters, which must be determined/calibrated. This is done in chapter 6.

In chapter 6, the AN-TRUSS model of the same three different nail-plate joints used to calibrate the ABAQUS model is described. First, an example of the tensile splice is used to calibration of the nail element and some parameters in the plate element. Good agreement is obtained between the results from the AN-TRUSS model and ABAQUS model and therefore also the test results. Second, an AN-TRUSS model of a bending splice with contact between the timber members and eccentrically and centrally located plates is built. The last plate parameters are calibrated and also here there is good agreement between the results. The sensivity of the joint to changes in nail stiffness, location and stiffness of the contact element as well as changes in some parameters of the plate element is analysed. A calibration of the contact element is made, so the model can estimate the deformations in splices with the butt effect too. An AN-TRUSS model of the heel joint gives results which agree with results from the ABAQUS model. The sensitivity of changes in different parameters is analysed. Finally, AN-TRUSS models of a collar tie truss and a pitched W-truss are described. The section forces and the deformations in selected points are compared to results from the programme ECOTRUSS, which is based on fictitious elements. In the example with the collar tie truss the moment is 5% larger and the deformations smaller than the results from ECOTRUSS in general. In the example of the W-truss, the maximum moment is 4% larger and the deformations up to 17% larger than the results from ECOTRUSS.

In chapter 7, it is concluded, that the AN-TRUSS is a powerful tool to estimate and optimise the design of trusses and nail-plate joints.

In the appendices, the more than 270 tests on nails, plates, tensile splices and bending splices are described.

Resumé på Dansk

Denne afhandling omhandler metoder til beskrivelse af tandpladesamlingers stivhed.

Tandplader bruges i vid udstrækning til samling af trædelene i præfabrikerede spær. Selve tandpladen består af en 1-2 mm tyk metalplade, hvori der udstanses tænder med en længde på ca. 7-20 mm. Tænderne udføres således af det samme plademateriale og er sammenhængende med pladen. Efter udstansningen er der aflange huller i pladen. Ved udførelsen af en samling presses tænderne ind i tilstødende trædele ved hjælp af en hydraulisk presse. Fordelen ved denne samling er, at den er nem og billig at udføre, samt at der opnås en meget stiv samling.

Ved dimensionering skal spæret kunne bære de laster, som kan opstå, og spæret må ikke få for store deformationer i brugstilstanden. Bæreevnen og deformationerne af spæret bestemmes ved hjælp af forskellige modeller. De hyppigt anvendte modeller er dog meget simple, hvilket kan medføre, at spærene i nogle tilfælde er overdimensioneret og i andre tilfælde underdimensioneret.

Formålet med denne afhandling har været at undersøge/udvikle modeller til bestemmelse af tandpladesamlingers stivhed.

I kapitel 1 introduceres emnet, og formålet med opgaven fremhæves og afgrænses. Metoden og fremgangsmåden for løsningen af problemet er angivet.

I kapitel 2 er en stødsamling modelleret ved hjælp af programpakken ABAQUS ver 5.2, som er baseret på finite element metoden. Stødsamlingen udsættes for træk. Træ og plade er modelleret som kontinuerte legemer sammensat med små I-bjælker, der modellerer tænderne. Elementerne får tildelt egenskaber, som er bestemt ved talrige forsøg på træ, plade og tænder. Resultaterne fra modellen sammenlignes med forsøgsresultater på flere forskellige pladestørrelser. Der er opnået god overenesstemmelse. Pladens og tændernes indflydelse på samlingens stivhed vurderes. Spændingsfordelingen i træ og plade er, ligesom fordelingen af sømkræfter, vist for enkelte samlinger.

I kapitel 3 udbygges den eksisterende ABAQUS model, således at stødsamlingen bliver udsat for ren bøjning. Herved opstår sømbelastninger i flere retninger, hvorfor tre modeller af sømmene diskuteres. Der vælges en model, hvor sømmene modelleres vha. lineær-elastiske plastiske I-bjælker. Resultaterne sammenlignes med bøjningsforsøg på bjælker med forskellige størrelse og placering af tandpladerne. Bjælkerne er også udført med forskellig spaltestørrelser, således at betydningen af kontakt mellem trædelene kan

vurderes. Der er opnået god overensstemmelse mellem resultaterne, dog er deformatio-
nerne ved kontakttryk mellem trædelene undervurderet af ABAQUS modellen, idet der
i forsøgsemnerne optræder stukning af fibrene i kontaktzonen. Spændingsfordelingen
i træ og plade er, ligesom fordelingen af sømkræfter, vist for enkelte samlinger både
med og uden kontakt.

I kapitel 4 opbygges en ABAQUS model af en 20° hæl samling. Fordelingen af snitkræf-
ter ned gennem spærhovedet er angivet, ligesom fordelingen af sømkræfter og spændin-
ger i træ og plade. Der er foreligger ingen forsøg til evaluering af denne samlingsmodel.

I kapitel 5 beskrives teorien bag en anden simplere model baseret på bjælketeori og
udviklet gennem projektet. Modellen kaldes "AN-TRUSS modellen". Trædelene er
modelleret med enkelte bjælke elementer, plade og tænder er modelleret ved speci-
elle ikke lineære plade- og sømelementer, og kontakt mellem trædelene er modelleret
med kontaktelementer. Fordelen ved denne model, i forhold til konventionelle modeller
baseret på bjælketeori, er, at de enkelte elementerne placeres ud fra kendskab til samlin-
gens geometriske udformning. Modellen er således følsom over for placering/størrelse
af plade og kontakt mellem trædelene. Belastingerne på de enkelte sømgrupper og
plader er givet direkte. I modellen optræder en del parametre som skal bestemmes/
kalibreres. Dette er beskrevet i kapitel 6.

I kapitel 6 beskrives AN-TRUSS modeller af de samme tre samlinger, som er anvendt
ved udvikling/test af ABAQUS modellen. Først udføres et eksempel med en trækbe-
lastet stødsamling, der anvendes til kalibrering af sømelementet og enkelte parametre i
pladeelementet. Der opnås god overensstemmelse med ABAQUS modellen og dermed
forsøgsresultaterne. Dernæst opbygges en model af en bøjningsbelastet stødsamling,
hvori kontakt mellem trædelene, og både centrisk og excentrisk placering af pladen
kan forekomme. De sidste pladeparametre kalibreres. Der er også her opnået god
overensstemmelse mellem AN-TRUSS og ABAQUS. Samlingens følsomheden over for
en ændring i søm elementets stivhed, placering og stivhed af kontakt elementet, samt
enkelte parametre i pladeelementet er undersøgt. En kalibrering af kontaktelementet
er udført, således at modellen også kan bestemme deformationer i stødsamlinger med
stukning i kontaktzonen. En AN-TRUSS model af hælsamlingen er også lavet med
god overensstemmelse med ABAQUS modellen. Følsomheden over for en ændring i
flere parametre er vurderet. Til sidst er AN-TRUSS modeller af et hanebånds - og
W-gitterspær beskrevet. Snitkræfter og deformationer i udvalgte punkter er sammen-
lignet med resultater fra programmet ECOTRUSS, som er baseret på en model med
fiktive elementer. I eksemplet med hanebåndsspæret er max. momentet 5% større og
deformationerne generelt mindre end resultaterne fra ECOTRUSS. I eksemplet med
gitterspæret er max. momentet 4% større og flytningerne op til 17% større end resul-
taterne fra ECOTRUSS.

I kapitel 7 konkluderes, at AN-TRUSS er et godt værktøj til vurdering og optimering
af spær og samlings design.

I appendiks beskrives de mere end 270 forsøg på tænder, plade, stødsamlinger i træk
og stødsamlinger i bøjning.

Appendix A

Test on Nails

In this appendix the experimental analysis of the "nail to wood" behaviour is described. The objectives of the tests are:

- to analyse the load-displacement curves of the dependence of nails on
  - number and location of the nails,
  - unloading,
  - grain direction and plate orientation,

- to analyse a newly developed measuring system.

A complete description of the tests is given in Nielsen et al.(1994), and a few sections have been omitted in this appendix. In Nielsen et al.(1994) the following is described further:

- test equipment,

- test results, (failure types, failure load, load-displacement curves of each test),

- analysis of the influence of:
  - number of nails in a row,
  - bending direction of the nails,
  - plate being locked or unlocked,
  - number of rows (1 or 2).

A description of the conceptions: row, bending direction and locked/unlocked plate is given.

A.1   Test Material

Timber
The timber specimens are shaped as shown in figure A.1 and figure A.2.

113
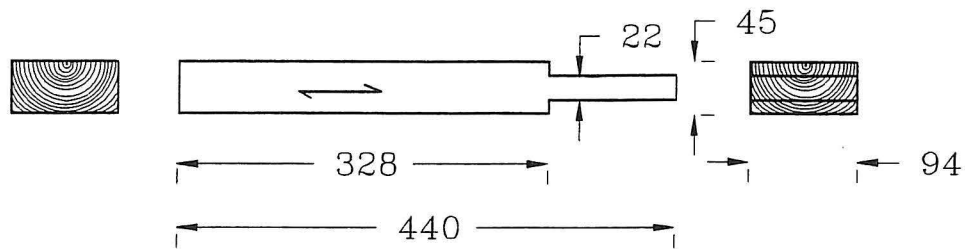
Figure A.1: **Measurement of timber specimens used in the series 1 to 22. Dimensions in mm.**

The timber dimensions 45×94mm in figure A.1 are made by planing. The recesses at the end of the specimens are due to the jaw distance in the tensile machine. The timber specimens for the series are randomly selected. In series 1-22, the tests have annual rings as shown in figure A.1.

In series 23 to 34 the timber specimens are shaped as shown in figure A.2. The timber dimensions 45×90mm are made by planing. The holes are made to fix the load equipment to the test specimens, see figure A.4.
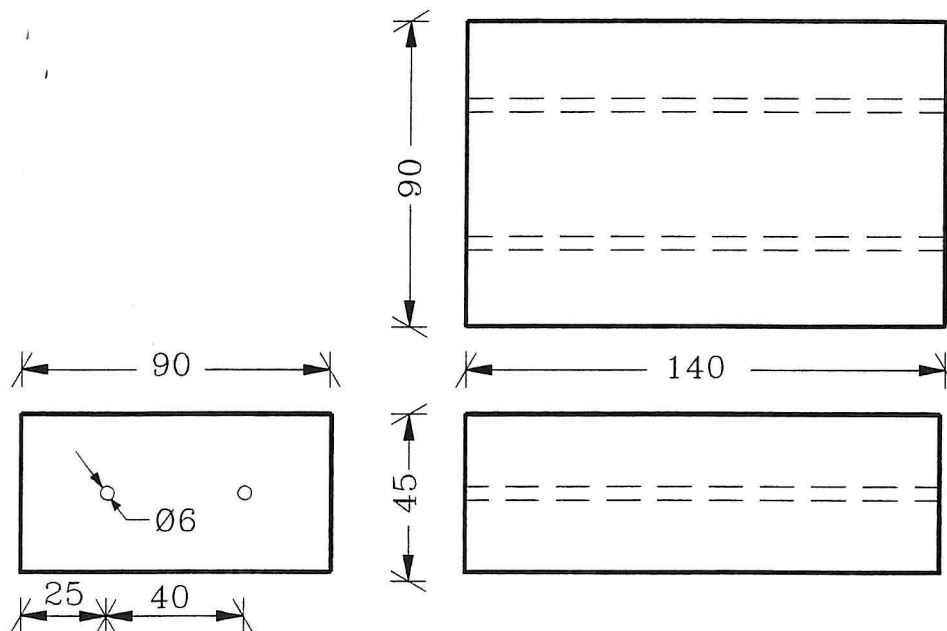
Figure A.2: **Measurement of timber specimens used in the series 23 to 34. Dimensions in mm.**

Nail-Plate
The galvanized nail-plate is shown in figure 1.2 on page 7. The plate thickness is 1mm and the nail density is about 1,47nails/cm^2. The tooth length is 7,9mm and the width is 2,9mm. The steel has the properties: 350MPa$< f_p <$470MPa, $f_u >$410MPa, where f_p is the limit stress of proportionality and f_u is the ultimate stress, Gang-Nail(1989).

Test Specimens

A test specimen consists of two nail-plates embedded in a timber specimen. The test specimens in series 1 to 22 are shown in figure A.3. The nail-plate size is 76×159mm.
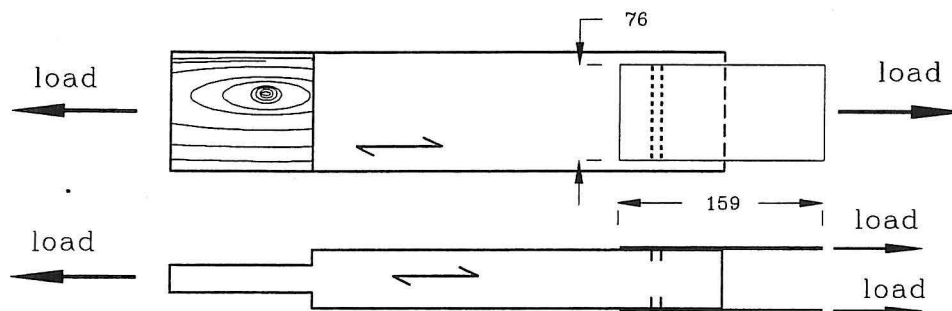

Figure A.3: Test specimen in series 1 to 22. Dimensions in mm.

The unwanted teeth are cut off. The centre line of the plate and the timber specimens coincide and in the 22 tests the load is parallel to the grain. Different locations of the plates are used. The number of teeth (nails) and nail-rows also differ in the series. A row is here defined as a number of nails in a line perpendicular to the load direction, see also the test programme in table A.1 and table A.2, on page 118.

As the timber specimens form an angle between their grain direction and the load direction, the test specimens in series 23 to 34 are made as shown in figure A.4.
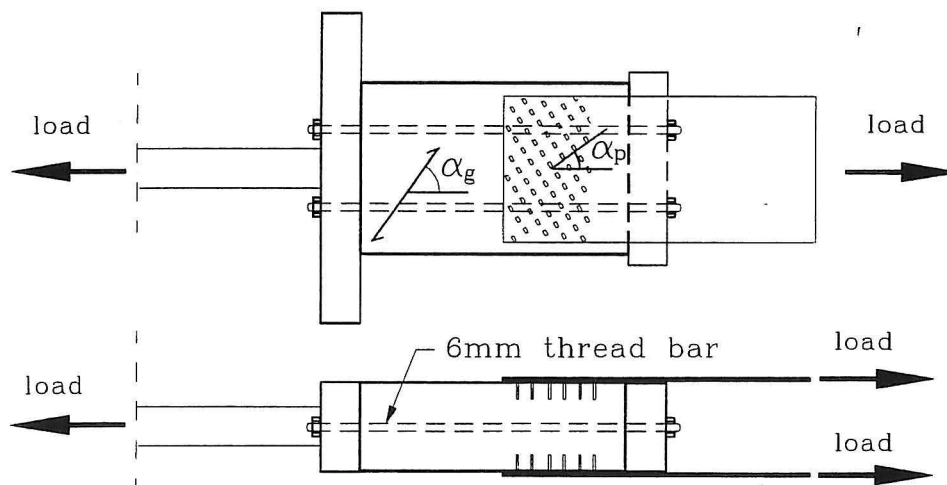
Figure A.4: Test specimen in series 23 to 34.

In series 20 to 34 the test specimens are made with different angles between grain, plate and load direction. α_g and α_p denote the angle between the load and the grain and the angle between the load and the principal axes of the plate, respectively. The choice of α_p is made so the the nails "make rows" perpendicular to the load direction. The tests are then made with $\alpha_p = 0°$, 34°, 54° and 90°. Corresponding values of α_p and α_g are shown in table A.3 on page 119. Because of the low tensile strength perpendicular to

the grain the load will be transmitted through two threaded bars as shown in figure A.4. The timber will then be loaded in compression.

A.2   Test Equipment

The tensile machine is a Mohr & Federhaff universal testing machine. The influence of the load velocity is tested in series 1, 2 and 3, see table A.1. In the other series the load velocity per.nail is held constant about 37N/min. At one end the timber specimens are placed beween the jaws of the tensile machine. At the other end the load is transmitted from the jaws to the nail-plate through a "T-fitting". The "T-fitting" transmits the load by friction. All test specimens are centrally loaded. In order to know the unloading properties of the load-displacement curves all the test specimens will be unloaded and reloaded once in a test.

One of the displacement systems uses HBM displacement transducers of type W2TK, The other system uses strain gauges on small cantilever beams (pins). In all tests, 5 displacement measurings (3 transduceres and 2 pins) are performed.

A storage programme from HBM, was used to store the data from the force and the five displacement measurings through an HBM data acquisition system (HMB UGR 60). The recording frequency was 0,1Hz.

A.3   Test Programme

The test programme is divided into 3 main programmes. In the main programmes, the following items will be analysed: (Numbers in brackets refer to the series number.)

- **Main programme 1 :** (Series no. 1 - 9)
  Dependence of the load-displacement curves on:

  - load velocity (1,2,3),
  - the bending direction (1,4)(5,9), The bending resistance perpendicular to the major axes of the plate is dependent on the nail bending direction, see figure A.5. The nails are divided into two types:
    * Type W:
      The nail is bending with the original stamping direction.
    * Type A:
      The nail is bending against the original stamping direction.
  - the plate being locked or unlocked to the timber (1,5)(4,9)(11,14). The back of the nail-plate will be fixed to the timber with a lock-fitting. During loading the back of an unlocked nail-plate will rise, see figure A.6. This will cause a different nail stiffness dependent on the location of the nails in
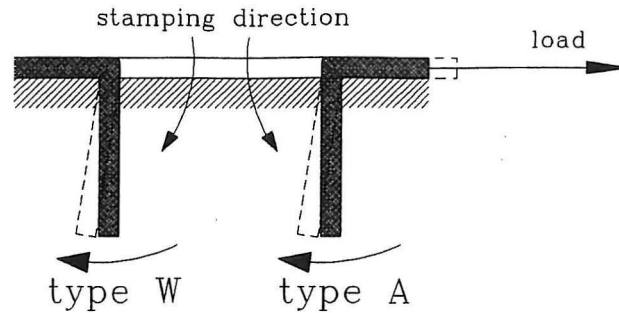
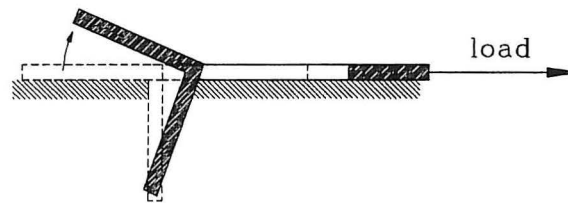Figure A.5: Bending direction/types of nail.

Figure A.6: Deformation of a unlocked plate with "W-type" nail.

plates with several nail-rows. The nail-plate under the lock-fitting can slide undisturbed parallel the load. The lock-fitting is fastened to the timber by star-screws.

- the number of nails in a row (1,7,8).
- the number of rows (1 or 2 rows), (1,4,6)

- **Main programme 2 :** (Series no. 10-18)

  - group effect of the nails (1, 6, 8, 5 and 4 rows in the series 1, 10, 11, 12 and 13).
  - edge distance (1,15,16) (13,17) (11,18).

- **Main programme 3 :** (Series no. 20-34)

  - angles between plate/load and grain/load. All the tests have an edge distance of 20mm and the nail-plates are not locked. The nails constitute minimum 5 rows on each plate.

The unloading properties in all the tests will also be analysed.
There are generally 6 identical tests in a series. However, in main programme 3 only 4 identical tests are made in a series.
The test programme is shown in tables A.1, A.2 and A.3.

MAIN PROGRAMME 1							
SERIES	TIMBER		NAILS/PLATE				LOAD
	edge dist. mm	α_g	α_p	No. row	No. teeth	Bending direc.	Lock	Load velocity $\frac{kN}{min}$ $(\frac{kN}{min \cdot nail})$
S1	40	0	0	1	2 x 11	W	Yes	0.8 (0.037)
S2	40	0	0	1	2 x 11	W	Yes	0.4 (0.018)
S3	40	0	0	1	2 x 11	W	Yes	1.2 (0.055)
S4	35	0	0	1	2 x 11	A	Yes	0.8 (0.037)
S5	40	0	0	1	2 x 11	W	No	0.8 (0.037)
S6	40	0	0	2	4 x 11	W/A	Yes	1.6 (0.037)
S7	40	0	0	1	2 x 7	W	Yes	0.5 (0.037)
S8	40	0	0	1	2 x 5	W	Yes	0.4 (0.037)
S9	35	0	0	1	2 x 11	A	No	0.8 (0.037)

Table A.1: Test series in main programme 1.

MAIN PROGRAMME 2							
SERIES	TIMBER		NAILS/PLATE				LOAD
	edge dist. mm	α_g	α_p	No. row	No. teeth	Bending direc.	Lock	Load velocity $\frac{kN}{min}$ $(\frac{kN}{min \cdot nail})$
S10	20	0	0	6	12 x 11	W/A	Yes	4.9 (0.037)
S11	20	0	0	8	16 x 11	W/A	Yes	6.5 (0.037)
S12	20	0	0	5	10 x 11	W/A	Yes	4.1 (0.037)
S13	20	0	0	4	8 x 11	W/A	Yes	3.3 (0.037)
S14	5	0	0	6	12 x 11	W/A	No	4.9 (0.037)
S15	5	0	0	1	2 x 11	W	Yes	0.8 (0.037)
S16	10	0	0	1	2 x 11	W	Yes	0.8 (0.037)
S17	5	0	0	4	8 x 11	W/A	Yes	3.3 (0.037)
S18	5	0	0	8	16 x 11	W/A	No	6.5 (0.037)

Table A.2: Test series in main programme 2.

MAIN PROGRAMME 3				
SERIES	TIMBER	NAILS/PLATE		LOAD
		α_p	No. teeth	Load velocity $\frac{kN}{min}$ ($\frac{kN}{min \cdot nail}$)
S20	$\alpha_g = 0°$	34°	2 x 56	4.1 (0.037)
S21		54°	2 x 54	4.0 (0.037)
S22		90°	2 x 48	3.6 (0.037)
S23	$\alpha_g = 34°$	0°	2 x 66	4.9 (0.037)
S24		34°	2 x 53	3.9 (0.037)
S25		54°	2 x 54	4.0 (0.037)
S26		90°	2 x 48	3.6 (0.037)
S27	$\alpha_g = 54°$	0°	2 x 66	4.9 (0.037)
S28		34°	2 x 56	4.1 (0.037)
S29		54°	2 x 54	4.0 (0.037)
S30		90°	2 x 48	3.6 (0.037)
S31	$\alpha_g = 90°$	0°	2 x 66	4.9 (0.037)
S32		34°	2 x 56	4.1 (0.037)
S33		54°	2 x 54	4.0 (0.037)
S34		90°	2 x 48	3.6 (0.037)

Table A.3: Test series in main programme 3.

A.4 Test Procedure

The test procedure is as follows:

- The T-fitting is placed on the nail-plates of the test specimen.
- The lock-fitting is placed if desired.
- The measuring systems are placed.
- The test specimen is placed and centred in the tensile machine.
- A small tensile force (1kN) is applied to the test specimen, so that the obliquity between the nail-plates is reduced.
- The bolts in the T-fitting are then tightened to 35Nm.
- The pins and transducers are adjusted. The pins are given a small prestress.
- The test specimen is unloaded and the transduceres are reset.
- The loading is then started.
- At a given load stage the test specimen is unloaded.
- At a given load stage the test specimen is reloaded until failure.
- Near failure the pin system is decoupled while the test is running.
- After failure, the measuring systems are dismounted, the timber specimen is weighed and the moisture content is determined.

A.5   Analysing Main Programmes 1 and 2

Comparisons of the series are made to find the influence of physical parameters on the load-displacement curve. This is done by comparing the individual ranges of variation of the load-displacement curves in each series. In figure A.7 the two thin solid lines are the maximum and the minimum load-displacement curves of series 1, $(S1)$, respectively. Other load-displacement curves of series 1 are then located between the maximum and the minimum line (not shown). The thick solid lines are then the max. and min. load-displacement curves of series 3 and the thick dashed lines are the max. and min. load-displacement curves of series 2.

A few load-displacement curves in some tests are discarded caused by knotty timber or extremely high density.

Load Velocity
Comparisons of the series 1, 2 and 3 show the influence of the load velocity. In figure A.7
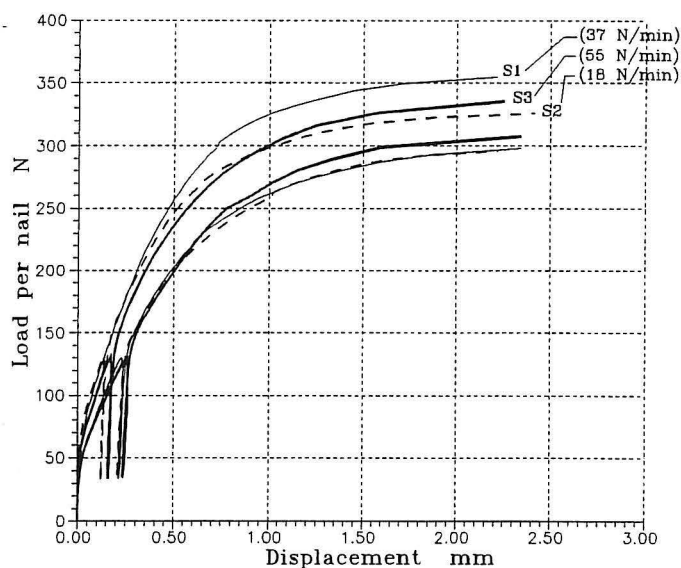
Figure A.7: **Variation of load-displacement curves of series 1, 2 and 3.**

it is seen that the tested load velocity has no significant effect on the load-displacement curves.

Series no.	load velocity $\frac{N}{mm \cdot nail}$	Mean max. load per nail N
2	18	311
1	37	316
3	55	325

Table A.4: **Comparisons of the load velocity and the mean maximum load.**

A comparison of the mean value of the maximum loads with the load velocities, see

table A.4, shows, however, a tendency that the max. load is increased with increased load velocity. This tendency is well known.

Number of Rows (4, 5, 6, or 8)
In series 10, 11, 12, and 13, the influence of the number of rows is tested when the plate is fastened. The tests are not affected by the edge distance. In figure A.8 it is seen that the load-displacement curves from tests with 4, 5, 6 and 8 rows coincide. The initial stiffness is the same for all tests, but at a load between 150 - 200N/nail, the tests with several rows lose stiffness compared to test specimens with 1 row only.
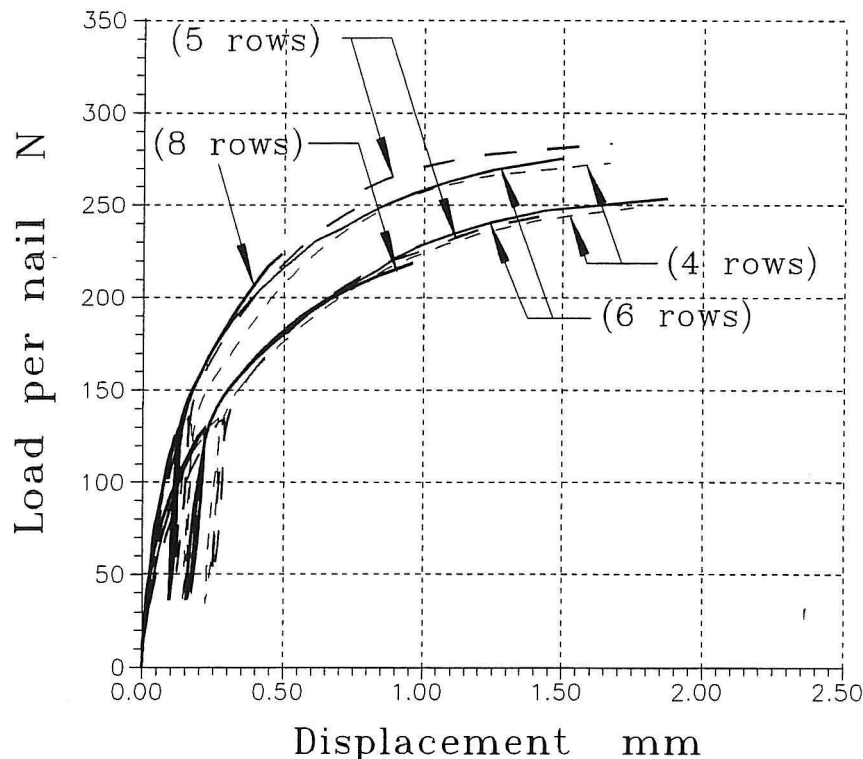
Figure A.8: Max. and min. load-displacement curves of series 10, 11, 12 and 13. All plates in the tests are fastened.

The difference can be caused by

- the load distribution over the nails, as it can be shown that the more uneven load distribution over the nails the smaller the stiffness and failure value of the joint,

- a sort of group effect. The wood in front of and between the nails is affected by several nails.

The failure value per nail of the tests with several rows and withdrawel of the nails is the same. However, the failure load in tests with 8 rows (S11) is smaller. This is caused by failure in the plate and is not a phenomenon of the "nail-to-wood" behaviour.

In figure A.9, the series 14 and 18 are compared. It is seen that the stiffness of the load-displacement curves from tests with 6 rows is higher than the stiffness of the load-
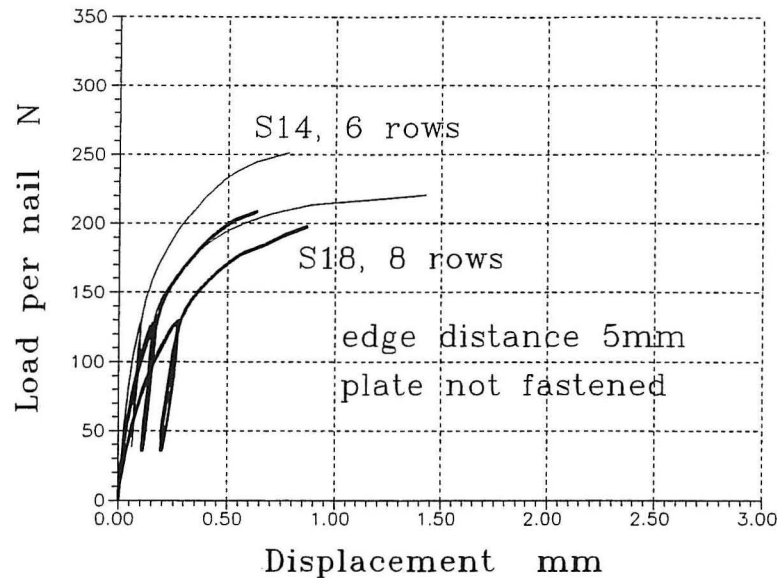
Figure A.9: Max. and min. load-displacement curves of series 14 and 18.

displacement curves from tests with 8 rows. In tests with 8 rows, failure occurs in the plate.

Distance to Timber Edge.
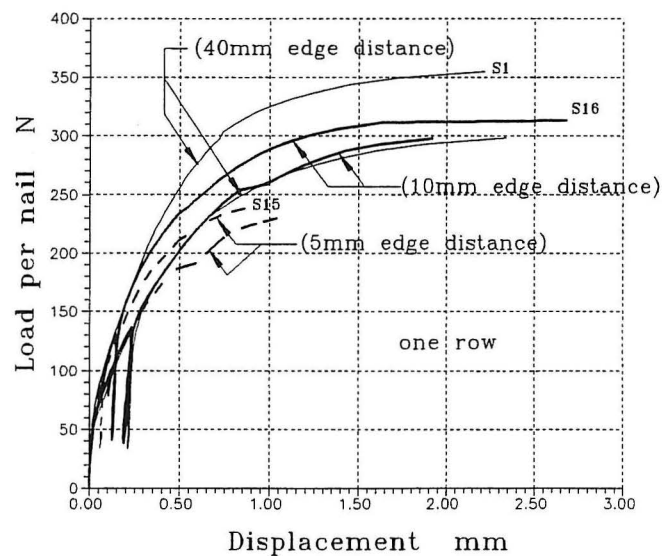In figure A.10 the load-displacement curves of series 1, 15 and 16 are shown.

Figure A.10: Max. and min. load-displacement curves of series 1, 15 and 16.

The influence of the distance from a nail row to the timber edge measured in the load direction is analysed. In figure A.10, it is seen that a test with a 10mm edge distance has obtained the full stiffness and load-carrying capacity compared to a test with 40mm edge distance (series 1). When the edge distance is 5mm, the initial stiffness is
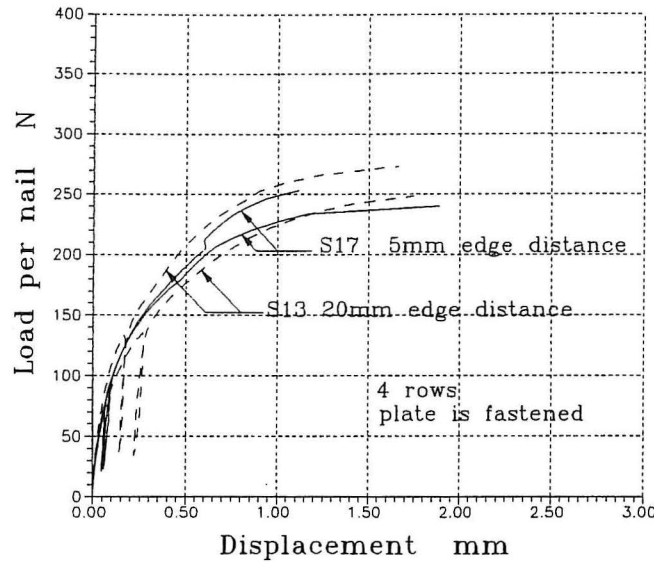
Figure A.11: Max. and min. load-displacement curves of series 13 and 17.

unaffected, but at the load 200N/nail the joint loses stiffness and fails at a much lower load. This is caused by failure in the wood in front of the nails closest to the timber edge. The wood in front of the nails is simply pressed away in small blocks.

In figure A.11, the edge distance effect is analysed in tests with 4 rows. It is seen that the stiffness is in general unaffected. The tests with 5mm edge distance have a lower failure value. The failure of the tests in series 17 is caused by wood failure in front of the nail row closest to the timber edge. In figure A.12 comparisons are made of
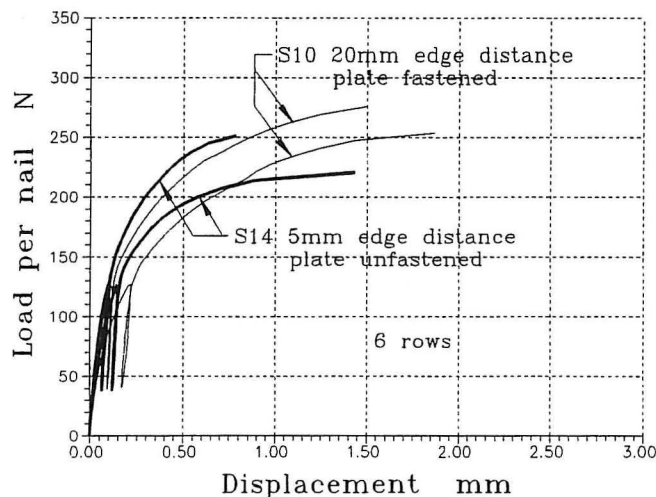
Figure A.12: Max. and min. load-displacement curves of series 10 and 14.

series 10 and 14 to test the edge distance effect for 6 nail rows. The difference between the series is small, the mean failure load of tests with 5mm edge distance is, however, smaller (234N < 266N).

Lau(1986) has made the same analysis on a similar plate, type GNA 20 (no-S) from

Gang-Nail Systems. The edge effect was found to have an influence on the failure load and stiffness within a distance of 15mm. No variation of the load-displacement curves is given, and the difference may lie in the properties of the timber.

A.6   Analysing Main Programme 3

In main programme 3, the influence of the orientation of grain, plate and load direction on the load-displacement curves is analysed. In figures A.14 and A.15, the mean load-displacement curves from each series are shown. The arrows indicate the load direction, and $(\alpha_p - \alpha_g)$ is the angular difference between the principal axes of the plate and the grain. All the tests are centrally loaded even though only a few nails are shown.
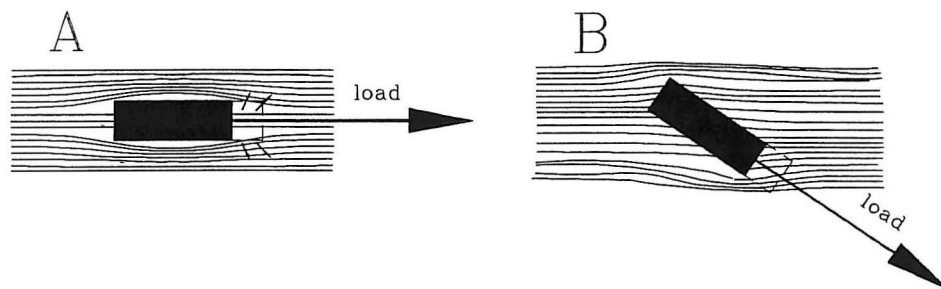
Figure A.13: Deformation of the timber in front of a nail. The thin lines show the grain and the black rectangle denotes a nail.

When the load is perpendicular to the grain, the load-displacement curves are not reliable. In tests with $\alpha_p - \alpha_g = 0°$ the initial stiffness is unaffected by the load direction, however, the initial stiffness is lower when the load direction is perpendicular to the grain. The failure load is getting smaller as the angle between load- and grain direction is increased. The failures in series 29 and 34 were caused by failure in the timber.

In tests with $\alpha_p - \alpha_g = 34°$, the stiffness is only slightly affected by the load direction, however, the stiffness in series 25 is increased a bit. In series 25 the load direction is nearly perpendicular to the principal axes of the plate, i.e. the bending stiffness of the nails is at a maximum. When the nail is loaded parallel to the grain, the nail will displace the wood in front of the nail - the wood is splitting, see figure A.13 A. The wood will easily split because of the low tensile strength perpendicular to grain. When the nail has a load direction, which forms a small angle with the grain, the splitting tendency will not occur easily, and the "nail to wood" behaviour will increase in stiffness, see figure A.13, B. This effect is obvious in series 26, see figure A.15.
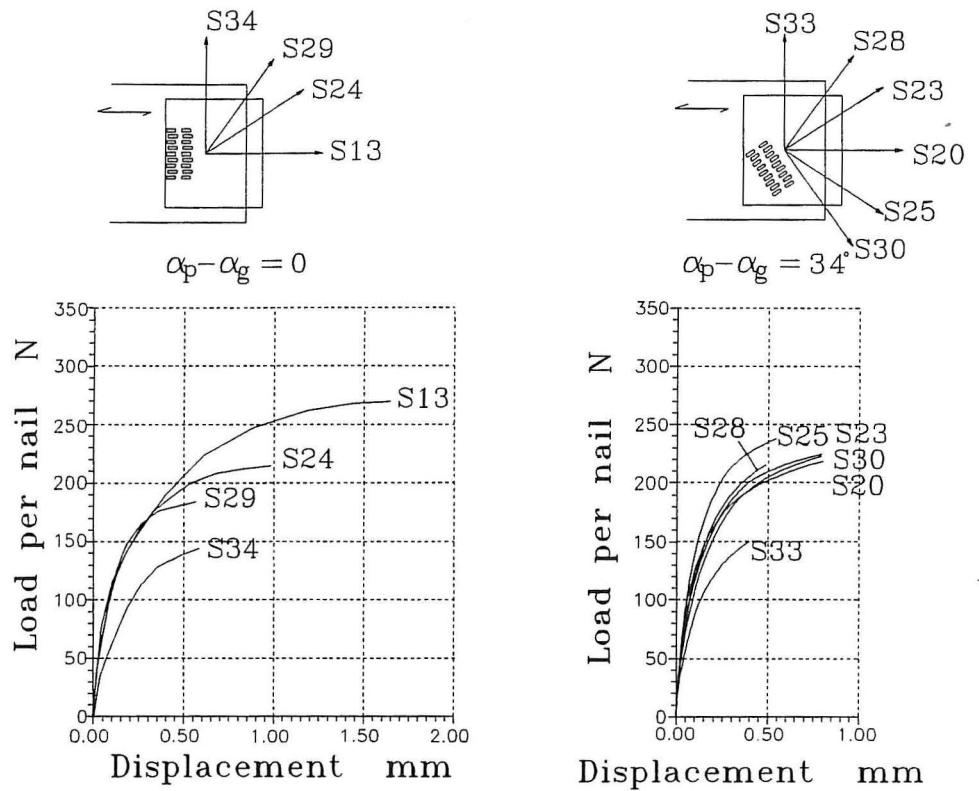
Figure A.14: Load-displacement curves from tests with an angular difference between plate and grain direction of 0° and 34°.
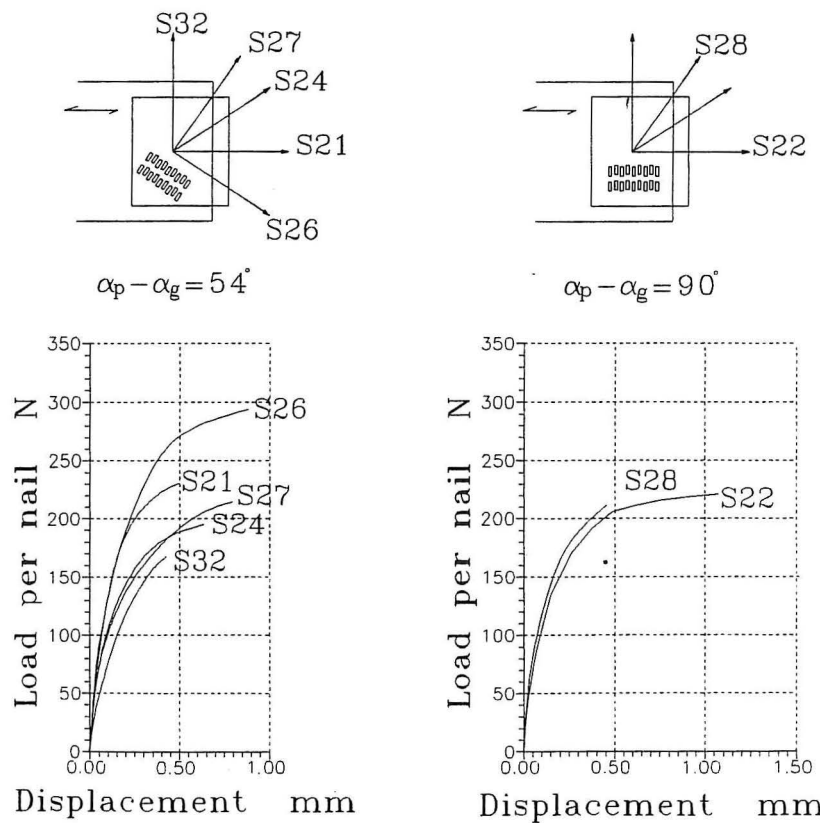

Figure A.15: Load-displacement curves from tests with an angular difference between plate and grain direction of 54° and 90°.

In figures A.14 and A.15 it is seen that the stiffness in several tests is only slightly affected by the orientation of the plate, grain and load. The failure load is, however, different.

A.7   Unloading

All the tests have been unloaded. Some tests have been unloaded once or twice to analyse the influence on the unloading curve. In figure A.16, the unloading part of the load-displacement curves from different tests is shown.
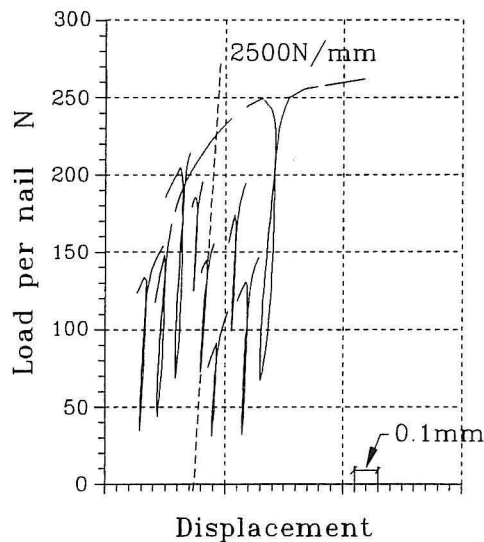
Figure A.16: Unloading curves from different tests.

There are unloading curves from tests in series 2, 4, 13, 15, 22, 26. To make the difference between unloading curves more distinct the curves have been moved horizontally. From figure A.16 is it seen that:

- the stiffness of the unloading curves is independent of the load level,

- the stiffness of the unloading curves is ~2500N/mm.

From figure A.16 and others it is seen that:

- the stiffness of the unloading curves is equal to the inital stiffness of the load displacement curves,

- the stiffness of the unloading curves is independent of the angles between grain, plate and load direction,

A.8 Conclusion

Laterally loaded nail plates have been analysed from measurings of about 200 tests distributed on 34 series.

The main results of the 3 main programmes are as follows:

- The tested load velocity $(18, 37, 57\mathrm{N/min})$ has no significant effect on the load-displacement curves.

- A group effect arises in tests with several nail rows. The stiffness and failure load per nail is smaller in tests with several nail rows than in tests with only one nail row.

- The full load and stiffness capacity is obtained with nails placed at a distance greater than or equal to 10mm from the timber edge.

- The stiffness is only slightly affected by the orientation of the plate, grain and load. The failure load is, however, different as the ultimate load gets smaller when the angular difference between the grain and load direction is increased.

- The unloading stiffness is independent of the load level, the orientation of the grain, plate and load direction. It has a value of about $\sim 2500\mathrm{N/mm}$.

For tests with the load perpendicular to the grain direction the load-displacement curves are not reliable, due to the small stiffness of timber. The deformations of the timber are large and they will disturb the displacement measurings.

Appendix B

Test on Nail-Plate

In this appendix, experimental tests on nail-plates are described. The aim is to analyse the stiffness and strength of the plate. The nail-plates are subjected to short-term tensile, compression and shear loads in order to determine the stiffness and strength parameters used in the programmes ABAQUS and AN-TRUSS.

B.1 Test Description

B.1.1 Tensile Tests

In figure B.1 a tensile test is shown. The load is supplied with a Mohr & Federhaff universal testing machine. The load velocity during the test is constant. The load is transmitted to the nail-plates by 2×2 jaw plates.
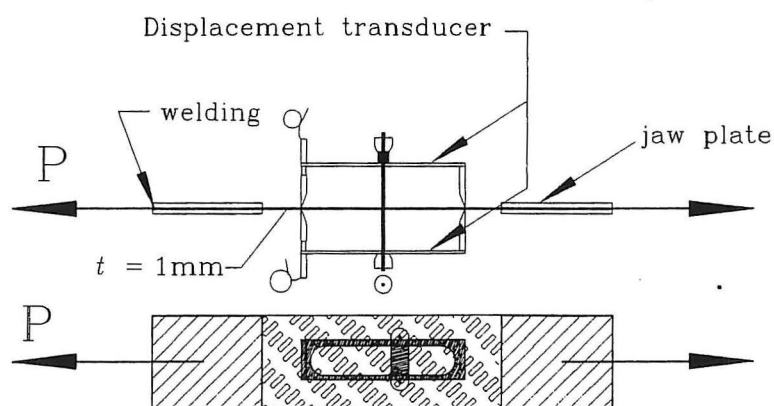
Figure B.1: Tensile test on plate. Teeth on nail-plate are not shown.

The displacements are measured with 2×2 displacement transduceres (HBMDD1) that are measuring the deformation over a length of 50mm or 100mm. The deformations

are measured parallel and perpendicular to the load direction. The masurings cannot be made at the same time, and then the test procedure is as follows:

- The test specimen is placed and centred in the tensile machine.
- Two 100mm displacement transduceres are placed parallel to the load direction (shown in figure B.1).
- A small tensile force is applied.
- The transduceres are reset.
- The loading is started.
- At a given load stage the test spicmen is unloaded until the initial position.
- Two 50mm displacement transduceres are placed perpendicular to the load direction.
- The transduceres are reset.
- The loading is started.
- At a given load state the test specimen is unloaded.

Three test series have been made where the angle, θ, between the load direction and principal axes of the plate is different. The test specimens are shown in figure B.2. To make a plane measuring area for the displacement transduceres, some teeth are cut off.
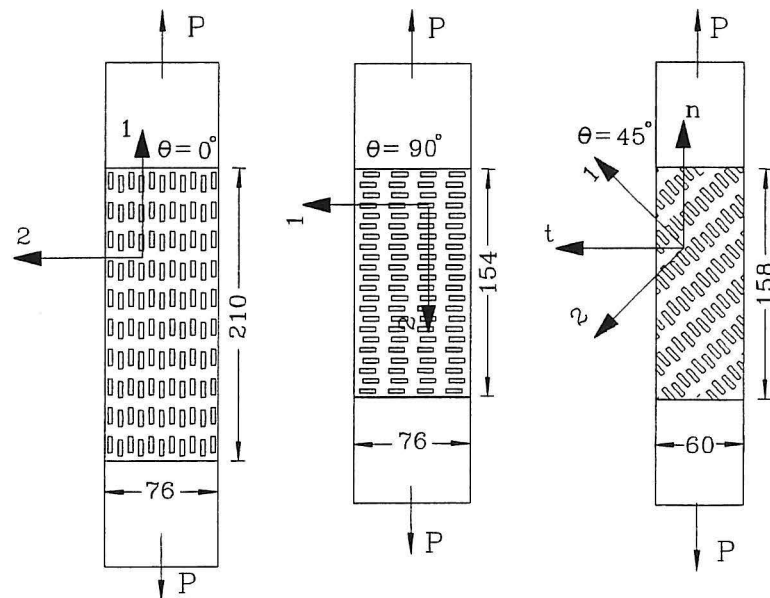
Figure B.2: Test specimens for tensile tests. Dimensions in mm.

The plate is assummed to be an orthotropic homogeneous linear elastic continuumm. The constitutive relation is given by (B.1). Plane stresses are assumed.

$$
\begin{bmatrix} \varepsilon_1 \\ \varepsilon_2 \\ \varphi_{12} \end{bmatrix} = \begin{bmatrix} \frac{1}{E_1} & \frac{-\nu_{12}}{E_2} & 0 \\ \frac{-\nu_{21}}{E_1} & \frac{1}{E_2} & 0 \\ 0 & 0 & \frac{1}{G_{12}} \end{bmatrix} \begin{bmatrix} \sigma_1 \\ \sigma_2 \\ \tau_{12} \end{bmatrix} \tag{B.1}
$$

The stiffness parameteres E_1, E_2, ν_{12}, ν_{21} and G_{12} are determined by tensile tests on the plate at 3 different angles $\theta = 0^o$, 90° and 45°.

Four tests with load in direction 1 ($\theta = 0^o$) are used to determine E_1 and ν_{21}, when ε_1 and ε_2 are measured. ($\sigma_1 = P/A$, $\sigma_2 = \tau_{12} = 0$,) A is the sectional area of the plate.

$$E_1 = \frac{\sigma_1}{\varepsilon_1} \qquad \nu_{21} = \frac{-\varepsilon_2 E_1}{\sigma_1} = \frac{E_1}{E_{1,90}} \tag{B.2}$$

The results are given in figure B.5 and table B.1 on page 133.

Four tests with load in direction 2 ($\theta = 90^o$) are used to determine E_2 and ν_{12} when ε_1 and ε_2 are measured. ($\sigma_2 = P/A$, $\sigma_1 = \tau_{12} = 0$)

$$E_2 = \frac{\sigma_2}{\varepsilon_2} \qquad \nu_{12} = \frac{-\varepsilon_1 E_2}{\sigma_2} = \frac{E_2}{E_{2,90}} \tag{B.3}$$

The results are given in figure B.6 and table B.2.

Three tests with $\theta = 45^o$ are used to determine G_{12} when ε_n and ε_t are measured, see figure B.2. Stresses and strains in $(1,2)$-system are ($\sigma_n = P/A$, $\sigma_t = \tau_{nt} = 0$)

$$\tau_{12} = -\frac{1}{2}(\sigma_n - \sigma_t)\sin(2\theta) + \tau_{nt}\cos(2\theta) = -\frac{1}{2}\sigma_n \tag{B.4}$$

$$\varphi_{12} = -2(\varepsilon_n - \varepsilon_t)\cos\theta\sin\theta + \varphi_{nt}\cos(2\theta) = -(\varepsilon_n - \varepsilon_t) \tag{B.5}$$

$$G_{12} = \frac{\tau_{12}}{\varphi_{12}} = \frac{\sigma_n}{2(\varepsilon_n - \varepsilon_t)} = \frac{1}{2(\frac{1}{E_{45}} - \frac{1}{E_{45,90}})} \tag{B.6}$$

The results are given in figure B.7 and table B.3 on page 135.

To determine the yield properties of the plate, two tensile tests are performed, where the tests are loaded parallel to the 1-axis until failure. The deformations are measured with one displacement transducer between the compression heads on the tensile machine. The result is shown in figure B.8 on page 136.

B.1.2   Compression Tests

2×3 tests have been made with plates in compression. The tests are subjected to contant load velocity until falilure. As the plate fails in buckling, two "column lengths" (35mm,15mm) are tested, see figure B.3. The teeth in the nail-plates are cut off.

The load-displacement curves are shown in figure B.9 on page 136. The deformation is measured with a displacement transducer between the compression heads on the tensile machine.
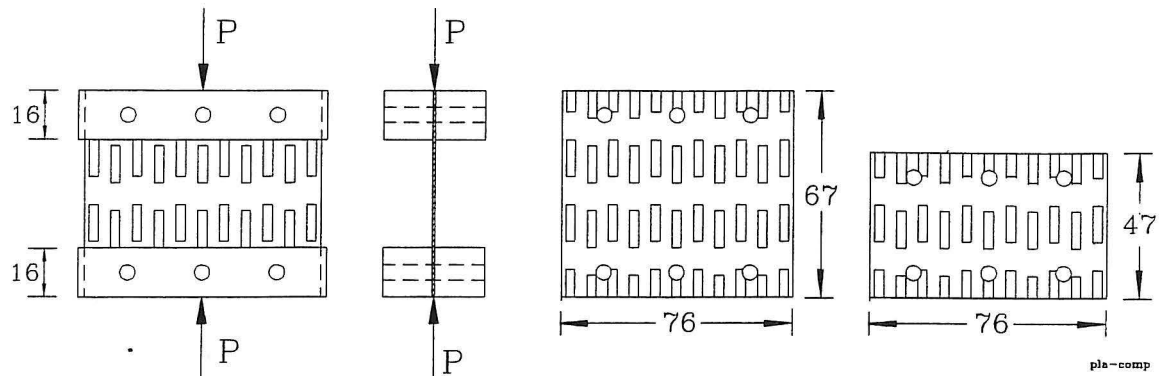
Figure B.3: Compression test of the plate. Dimensions in mm.

B.1.3   Shear Tests

Three shear tests have been made, see figure B.4. The load velocity is constant until failure and the plate is unloaded once during the test. The teeth in the nail-plates are cut off. The load is transmitted to the nail-plates by friction between the plate and 2×3 fixed steel bars. The bars are located at the end of the holes in the plate so that the tested shear length is about 13mm.
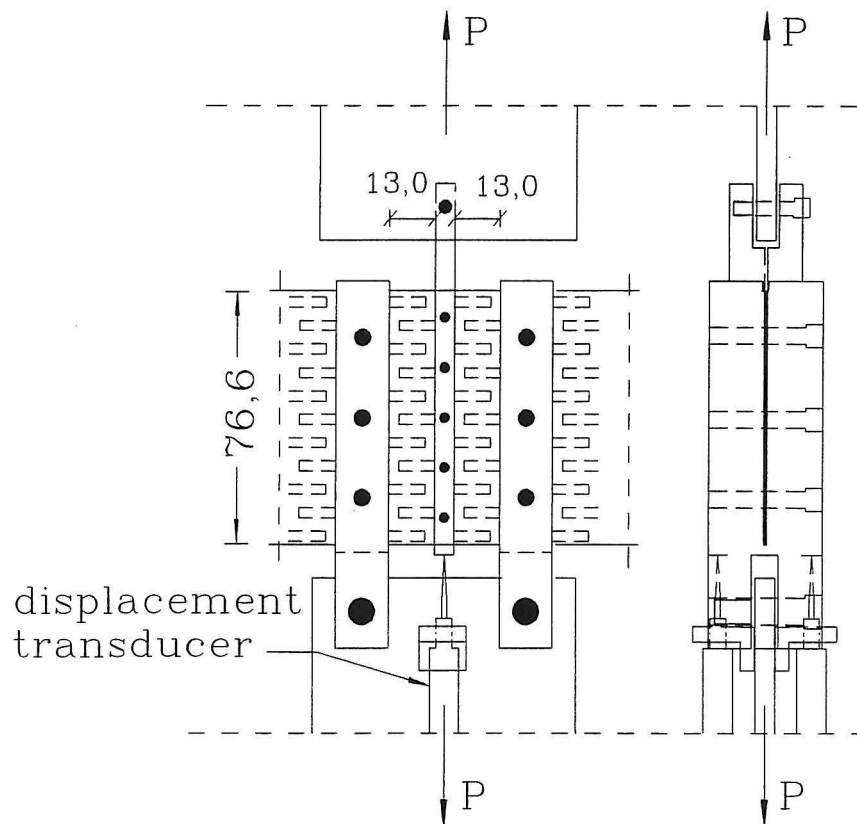

Figure B.4: Plate subjected to shear load. Dimensions in mm.

The displacements are measured with two displacements transduceres. Results are shown in figure B.10 on page 137.

B.2   Results

In the following the results for the tensile, compression and shear tests are shown. In tests with two displacement measurings, only the average curve is shown. In some figures the fitted straight line is shown too.
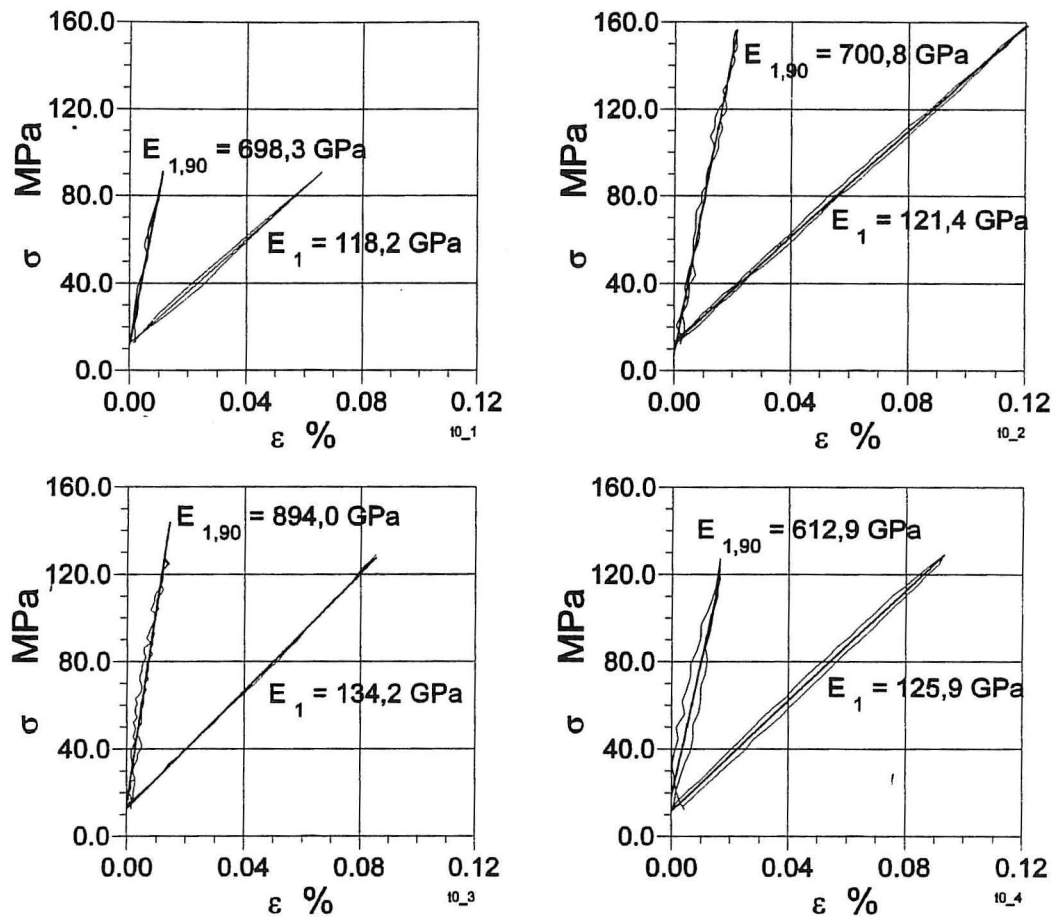
Figure B.5: Four tensile tests on nail-plates with load parallel to 1-axis.

		Test number				
	Unit	1	2	3	4	Average
E_1	GPa	118.2	121.4	134.2	125.9	125
$E_{1,90}$	GPa	698.3	700.8	894.0	612.9	
ν_{21}	-	0.17	0.17	0.15	0.21	0.17

Table B.1: Determination of E_1 and ν_{21}.
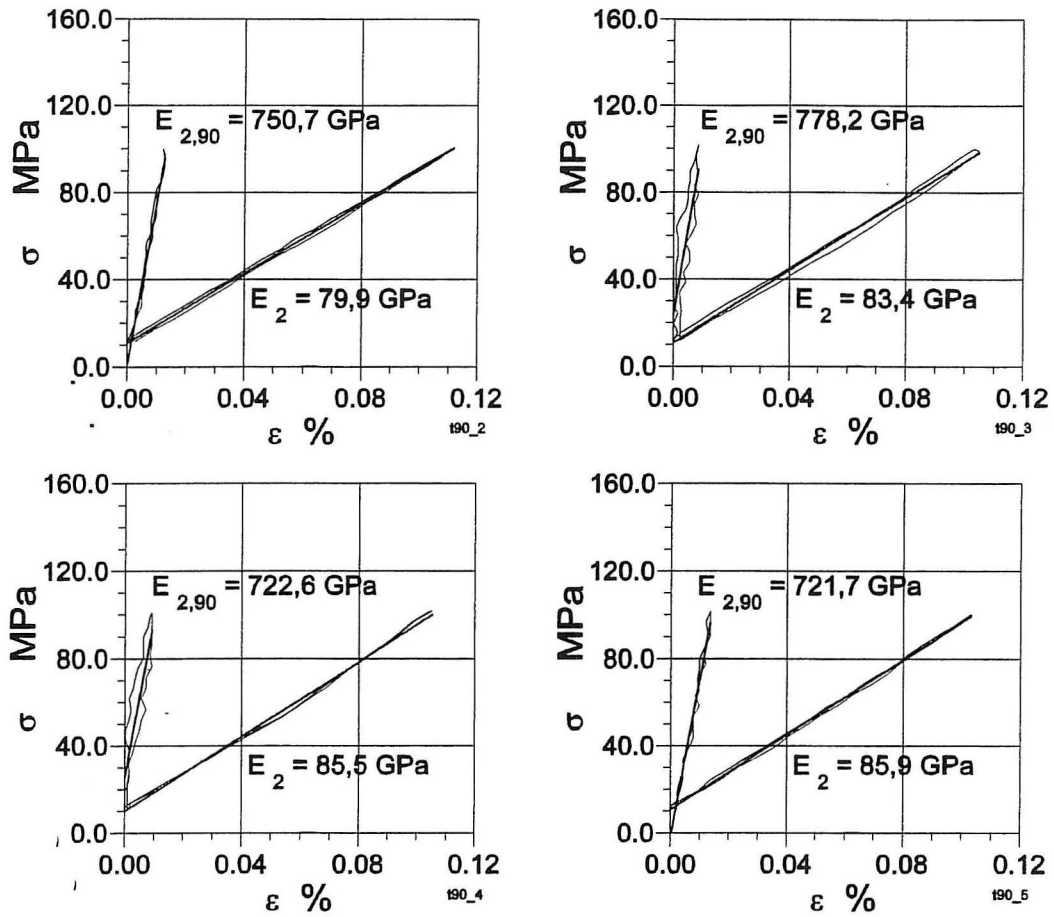
Figure B.6: Four tensile tests on nail-plates with load parallel to 2-axis.

		Test number				
	Unit	1	2	3	4	Average
E_2	GPa	79.9	83.4	85.5	85.9	83.6
$E_{2,90}$	GPa	750.7	778.2	722.6	721.7	
ν_{12}	-	0.11	0.11	0.12	0.12	0.11

Table B.2: Determination of E_2 and ν_{12}.
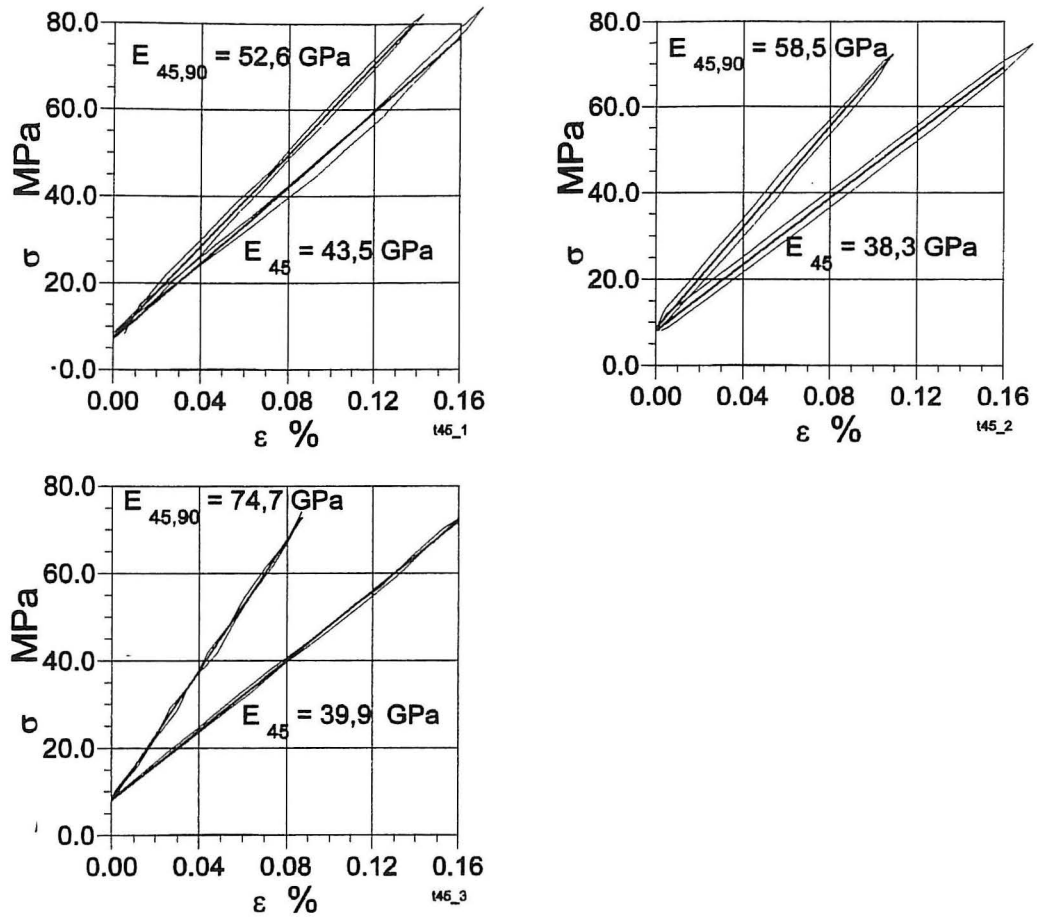
Figure B.7: Three tensile tests on nail-plates with $\theta=45°$.

		Test number			
	Unit	1	2	3	Average
E_{45}	GPa	45.5	38.3	39.9	
$E_{45,90}$	GPa	52.6	58.5	74.7	
G_{12}	GPa	125.7	55.4	42.8	74.6

Table B.3: Determination of G_{12}.
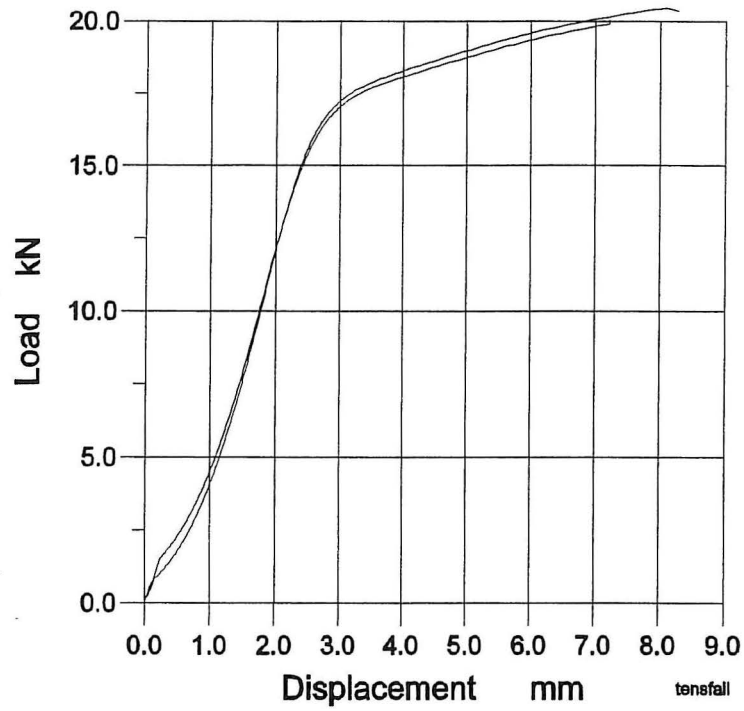
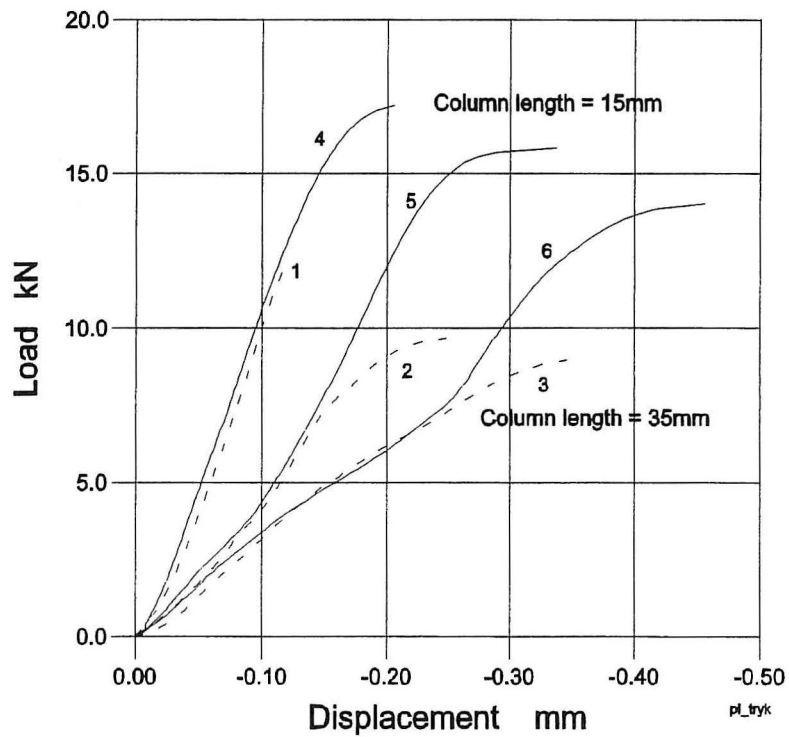Figure B.8: Two tensile tests until failure. Load in direction 1.

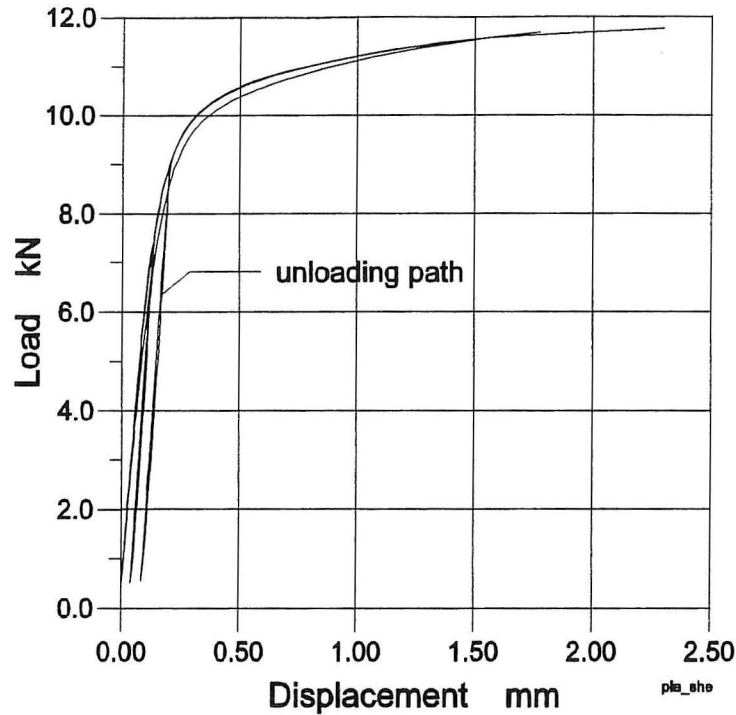Figure B.9: Load-displacement curves of six compression tests.

Figure B.10: Load-displacement curves of three shear tests.

B.3 Discussion

The variation of the strain data from the tensile tests is large. This is due to the measuring method of the deformation of the nail-plate. The stress and strain distributions in the nail-plate are very complicated due to the holes, and furthermore, nail stamping will give rise to prestresses to cause a stiffness difference on both sides of the plate. This can be observed by a small deflection of the plate in tension. A linearly material property is, however, observed.

In tensile tests with $\theta = 0^o$ and $\theta = 90^o$, the assumption of $\tau_{12} = 0$ is fairly good, but in tensile tests with $\theta = 45^o$, this assumption is wrong. The jaws on the tensile machine will prevent a deformation in the t direction, see figure B.11: Influence of end constraints is discussed in Pagano et al.(1968). The value of G_{12} is, however, used in the following. The constitutive matrix in (B.1) is assumed symmetric. This is only valid if (B.7) satisfied.

$$
\begin{aligned}
\nu_{12} E_1 &= \nu_{21} E_2 \\
0.11 \cdot 125 GPa &= 0.17 \cdot 84.6 GPa \\
13.8 GPa &= 14.4 GPa
\end{aligned}
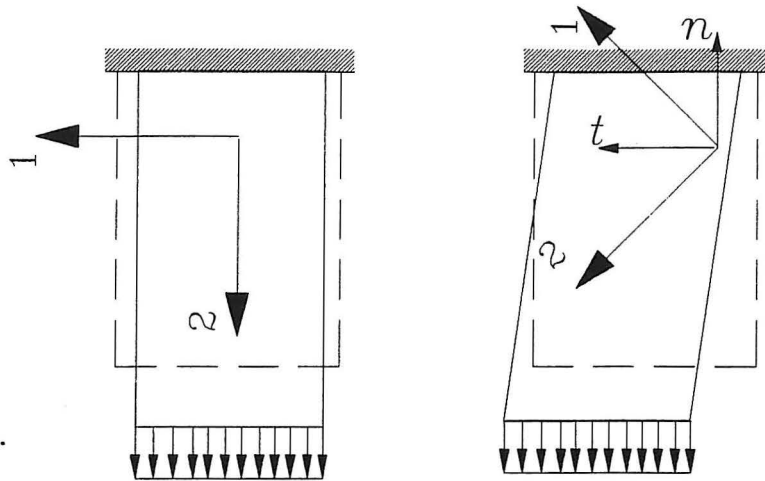\tag{B.7}
$$

In ABAQUS, the values in table B.4 will be used.

Figure B.11: Deformation of anisotropic bodies.

E_1	125000MPa
E_2	84000MPa
G_{12}	75000MPa
ν_{12}	0.11

Table B.4: Stiffness parameteres used in ABAQUS.

The variation of two tensile tests loaded until failure is small. E_1 determined by failure tests is much smaller than E_1 determined in table B.1. As the displacement at the failure tests is measured between the compression heads, the measuring will also contain some sliding between the jaws and the jaw plates. Therefore, the yield load is the only reliable value determined. It is found to be ~15.5kN, see figure B.8.

The variation of the compression tests is large. The failure loads in tests with 15mm column length are larger than the failure loads in tests with 35mm column length. The stiffness of the test specimens seem to fit in pairs (1,4), (2,5), (3,6), and furthermore, the stiffness and the failure load decrease in each test. (The numbers on the curves in figure B.9 denote the test order.) The reason for this can be sliding of the bars on the plate, see figure B.3. The bars transmit the load to the nail-plate by friction. prior to test 1 and test 4, the friction area on the bars is blasted with sand to make the friction high. After each test, this friction will decrease due to the compression load on the bars. The sliding effect will then increase during the test series. The tests results are unreliable and will not be used.

The variation of the shear tests is small and yielding occours at ~9-10kN. The tests fail at the ends of the columns caused by the high stress at the corner of the holes. On the test specimens it is seen that the plate at the ends of the oblong holes rotate a bit, and therefore the test shear length must be larger than 13.0mm. The tests are used to determine the plate stiffness for the programme AN-TRUSS, see section 6.1 on page 69.

Appendix C

Experimental Tensile Test

In this appendix the experimental tensile tests on splices are described. The aim of the work is to analyse the influence of the load procedure on the load-slip curve. Jensen et al.(1993) applied the load stepwise and the load on the tests described here is applied at constant load velocity. This is the only difference between the two test programmes. Load-slip curves from Jensen et al.(1993) are used to show the difference between the results.

C.1 Test Specimen

The tests specimens are from the same delivery of test specimens as the tests used in Jensen et al.(1993). The nail-plates are embedded in the wood at the truss factory. The tests specimens are conditioned at 65% RH and 21°C for about 20 months. The timber is Swedish spruce (Picea abies) of strength class K-24 according DS 413 [56]. The moisture content is about 13%. A test specimen is shown in figure C.1.
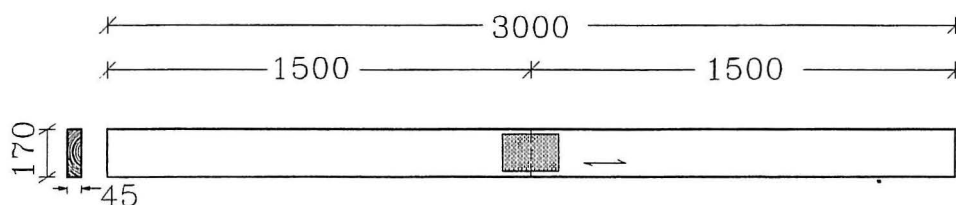

Figure C.1: Measurement of test specimens. Dimensions in mm.

18 tests specimens are divided into 5 series with different plate sizes, see table C.1.

In the series with plate size 130×218mm, the thickness of the timber is only 30mm, however, this will not affect the results compared to tests with 45mm thickness, see Jensen et al. (1993).

Plate size mm	Number of nails on a plate	Number of tests
76×159	11×16	3
103×159	15×16	3
130×159	19×16	4
130×218	19×22	4
130×317	19×32	4

Table C.1: Plate sizes in 5 series.

C.2 Test Equipment

The tensile machine is made at Aalborg University, see Andersen et al.(1977). The load is transmitted by 2×2 jaws by friction in the hatched area in figure C.2. The load velocity per nail is constant about 37N/min, which is the same load velocity as used in tests with few nails, see appendix A. Since the load is applied manually, the load-time curves flutter a bit, see e.g. the thin curves on figure C.4 on page 142.
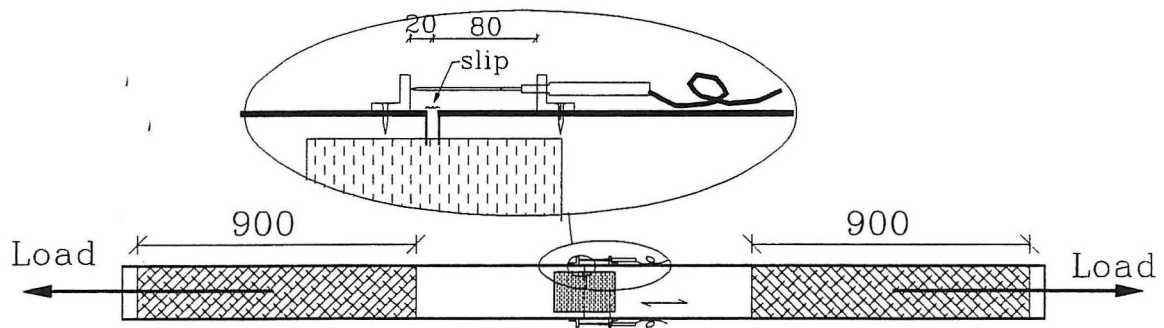
Figure C.2: Load of tensile splices and locations of displacement transducers. Dimensions in mm.

The slip is measured by two HBM displacement transducers of type W2TK. The transducers are mounted on angle fittings with screws. A storage programme from HBM, (UG6IEBE, 15/9-89), was used to store the data from the force and the two displacement measurings through an HBM data acquisition system (HMB UGR 60). The recording frequency is 0,2Hz. The data are saved on disk.

C.3 Results

In table C.2, the estimated failure load and the failure mode are compared to failure
load and failure mode determined from tests.

	Estimated		Tensile tests (1993) ⋆			Tensile tests (1994)		
Plate size	P_{max}	Failure	P_{max}	Stand.dev.	Failure	P_{max}	Stand. dev.	Failure
mm	kN	mode	kN	kN	mode	kN	kN	mode
76×159	32,6	W	32,9	4,0	W	38,6	4,6	W
103×159	44,2	W	40,3	3,0	W	48,0	3,8	W
130×159	55,8	W	60,6	5,0	W	70,6	1,8	W/P
130×218	69,7	P	68,2	1,5	P	68,4	0,6	P
130×317	69,7	P	65,1	1,2	P	66,1	1,1	P

⋆ Jensen et al. (1993). Failure mode: $W=$ Nail Withdrawal, $P=$ Plate Failure.

Table C.2: Failure load (P_{max}) and failure mode in tensile tests.

The estimated failure loads are characteristic short-term values (5 % fractile) according
to (Træ 31) [58] and (DS 413) [56].

In the following figures, the load-slip curves from the tensile tests are shown. Load-slip
curves from Jensen et al.(1993) are shown as dashed lines, and load-slip curves from
1994 are shown as solid lines. Also, load-time curves for the two tests programmes are
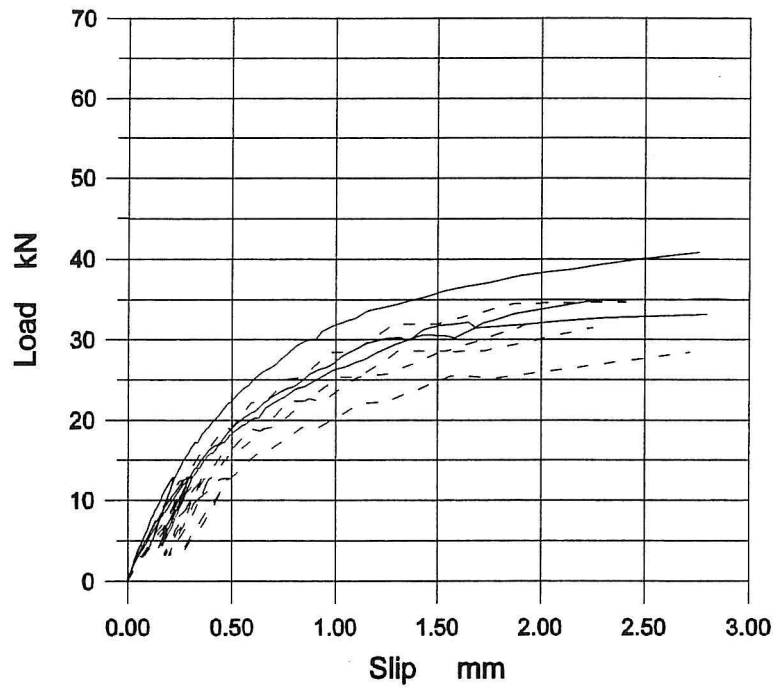shown. The stepwise load-time curves are from Jensen et al.(1993).

Figure C.3: Load-slip curves from experimental tests on tensile splices
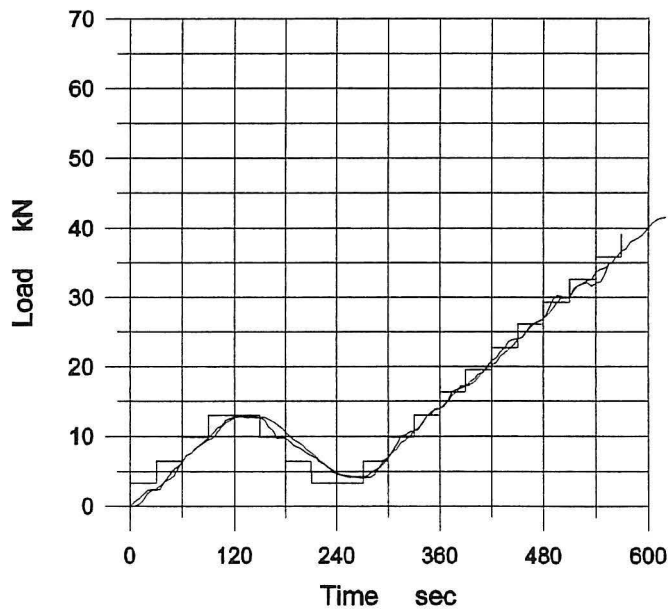with plate size 76X159mm.

Figure C.4: Load-time curves from experimental tests on tensile splices
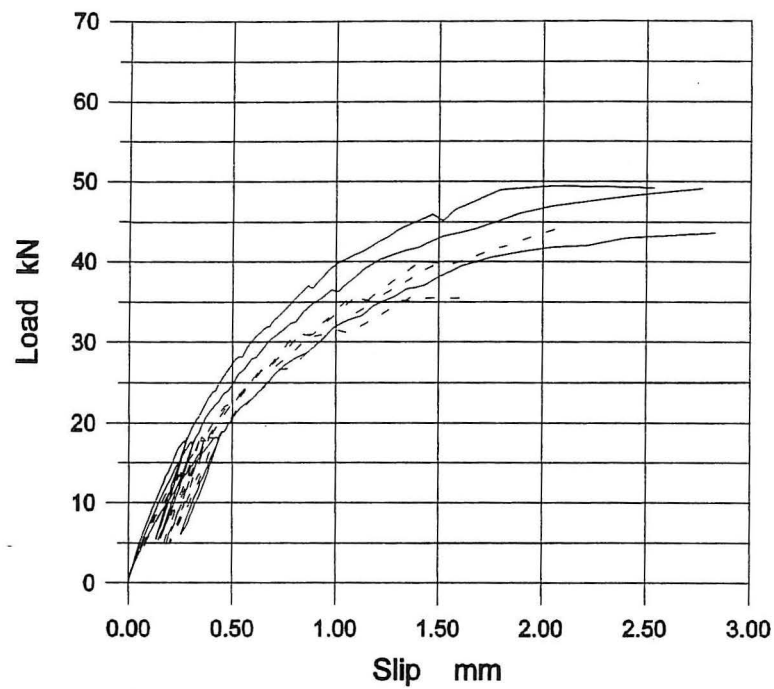with plate size 76X159mm.

Figure C.5: Load-slip curves from experimental tests on tensile splices
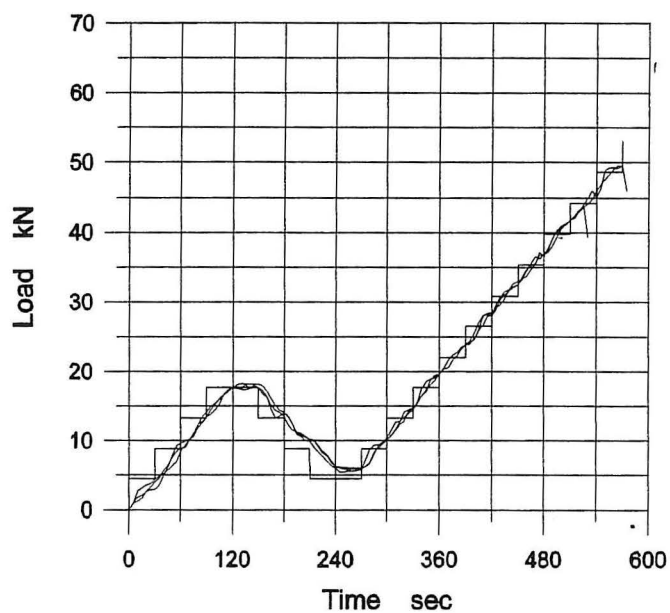with plate size 103x159mm.

Figure C.6: Load-time curves from experimental tests on tensile splices
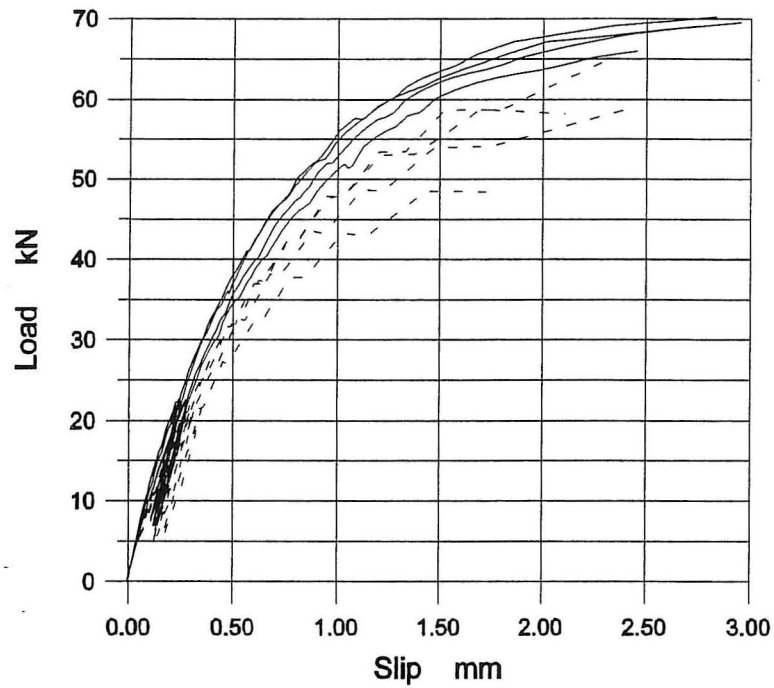with plate size 103x159mm.

Figure C.7: Load-slip curves from experimental tests on tensile splices
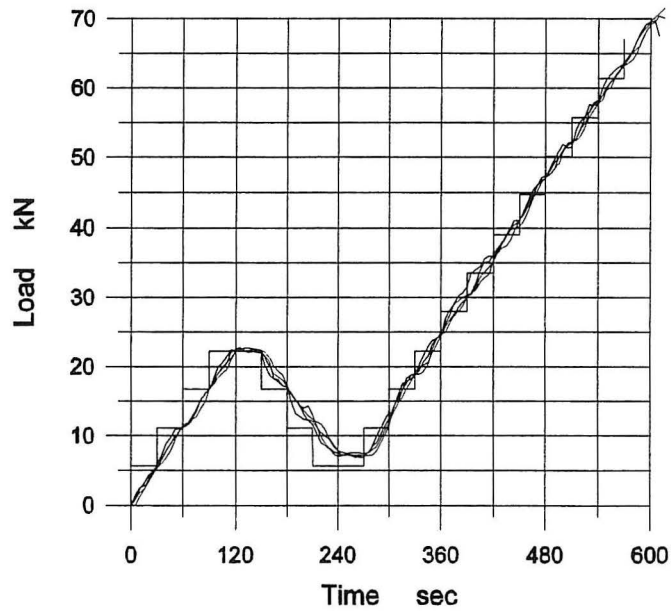with plate size 130x159mm.

Figure C.8: Load-time curves from experimental tests on tensile splices
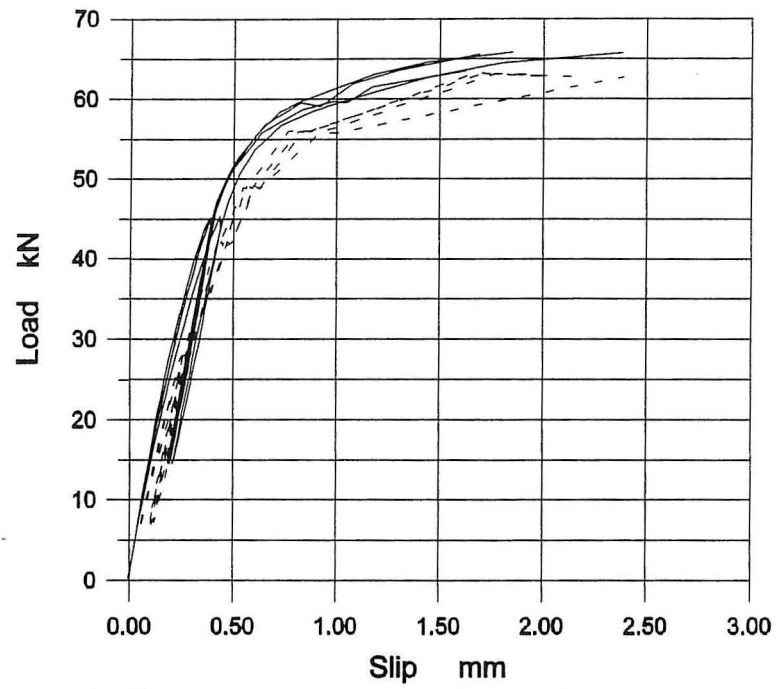with plate size 130x159mm.

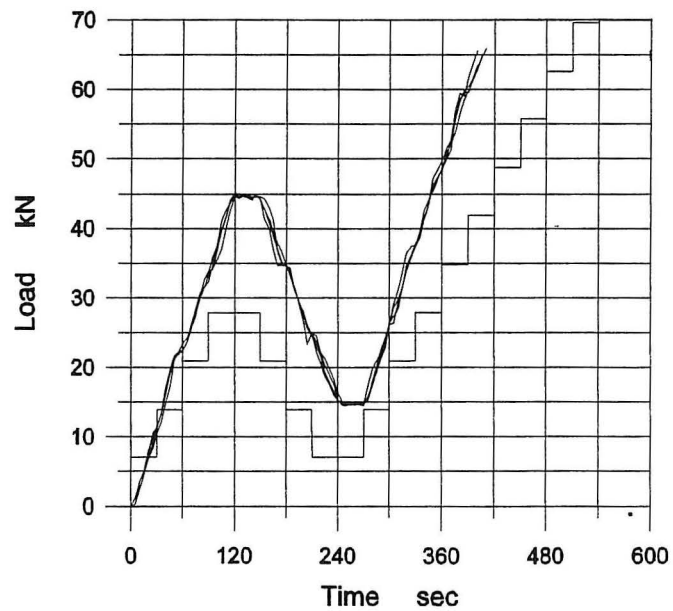Figure C.9: Load-slip curves from experimental tests on tensile splices with plate size 130x218mm.

Figure C.10: Load-time curves from experimental tests on tensile splices with plate size 130x218mm.
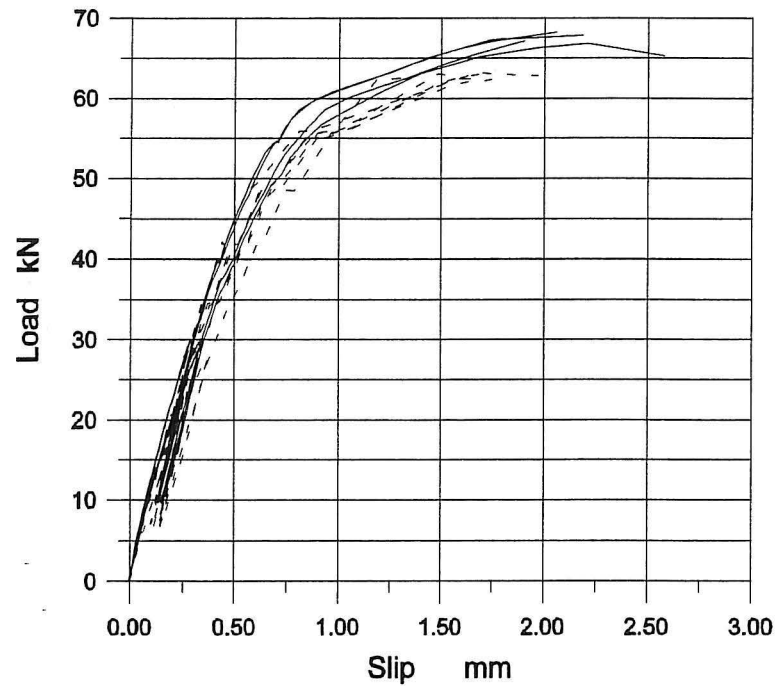
Figure C.11: Load-slip curves from experimental tests on tensile splices with plate size 130 x317mm. Thickness of the timber: 30mm.
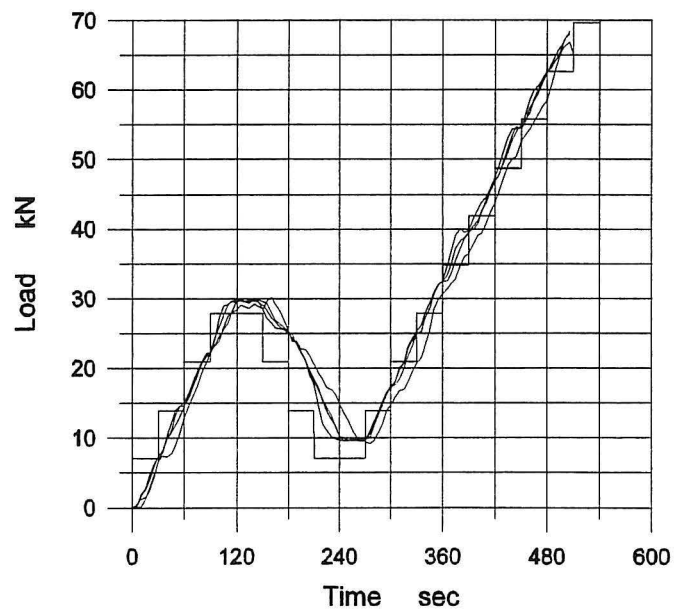

Figure C.12: Load-time curves from experimental tests on tensile splices with plate size 130x317mm.

C.4 Discussion

In table C.2 it is seen that the failure load has increased by almost 20% on tensile splices with constant load velocity (1994) and with nail withdrawal. In some tests with plate size 130×159mm, the failure mode has changed from nail withdrawal to failure in these plate. In tests with only plate failure, the failure load is almost unchanged. Comparison of the load-slip curves shows that also the stiffness has increased.

The estimated failure load and failure modes correspond to the test results. However, P_{max} for the plate sizes 130×218mm and 130×317mm seems to be overestimated a bit.

The moisture content in the timber of the two test programmes is the same (13%). The tests used in Jensen et al.(1993) were stored in the conditioning room for about 2-3 months. No changes in the plate surface have been observed.

The main reasons for an increased stiffness and failure load can be caused by:

- a difference in the load procedure,
- an increased stiffness of the timber caused by longer storage in the conditioning room (18 months).

It seems strange that a longer storage time can result in increased stiffness and failure load. After the plate has been impressed into the timber, the friction stresses from the timber on the nails will decrease with time caused by relaxation and it will demand less stiffness and strength of the joint. This effect is not observed.

When testing the joints, it is observed that test specimens have warped. Warping is normally generated by changes in moisture content, but the temperature and the humidity in the conditioning room were constant in the storage period.

It is concluded that the load procedure will affect the stiffness and the failure load of the joint. The tensile tests from 1994 are compared to numerical results in chapter 2.

Appendix D

Experimental Bending Test

In this appendix, the experimental bending tests are described. The aim of the work is to analyse the influence of plate size, plate location, and contact between the timber members on the stiffness and failure load of the joint.

D.1 Test Specimen

The tests specimens are conditioned at 65% RH and 21°C for about 2 months. The timber is Swedish spruce (Picea abies) of strength class K-24 according DS 413 [56]. The moisture content is about 13%. The test specimens have the same dimensions as the test specimens used for tensile tests, see figure D.1.
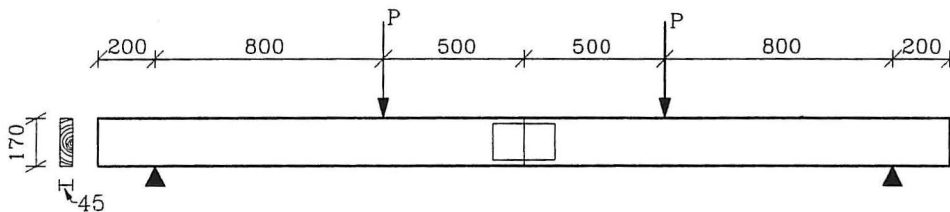

Figure D.1: Measurements of test specimen. Dimensions in mm.

40 tests specimens are divided into 9 series (5 specimens in each series - the specimens used in series BE0 and BE2 are the same) with different plate sizes, plate locations and gaps between the timber members, see table D.1.

The test specimens in series BE0 are beams without joints and, therefore, they are used to determine the stiffness properties of the timber. Series BE1, BE3 and BE6 are used to analyse the influence of the plate size, and BE1, BE4, BE5 and BE6 are used in pairs to analyse the influence of the plate location.

Series BE6, BE7 and BE8 are used to analyse the effect of the gap size. The gap size is difficult to determine. It can be measured manually, but the horizontal distance between the timber members is not the same all over the gap. Furthermore, the fibres

149

| Series | Plate size | Plate location | | Gap size |
no.	mm		★	mm
BE0	-	-	-	-
BE1	76×159	centre	(47mm)	∼ 0
BE2	76×159	eccentric	(10mm)	0
BE3	130×317	centre	(20mm)	∼ 0
BE4	76×159	eccentric	(10mm)	∼ 0
BE5	103×159	eccentric	(10mm)	∼ 0
BE6	103×159	centre	(34mm)	∼ 0
BE7	103×159	centre	(34mm)	∼ 0.5
BE8	103×159	centre	(34mm)	∼ 0.7

★ distance from plate to lower timber edge.

Table D.1: Plate size and location in the series.

in the compression zone will butt on each other. To analyse this effect, series BE2 and series BE4 will be compared. The test specimens in series BE2 are made from the beams used in series BE0 with sawkerfs perpendicular to the grain in the tensile zone of the beams, see figure D.2. In the compression zone the fibres have not been cut, and the "butt effect" is vanishing.
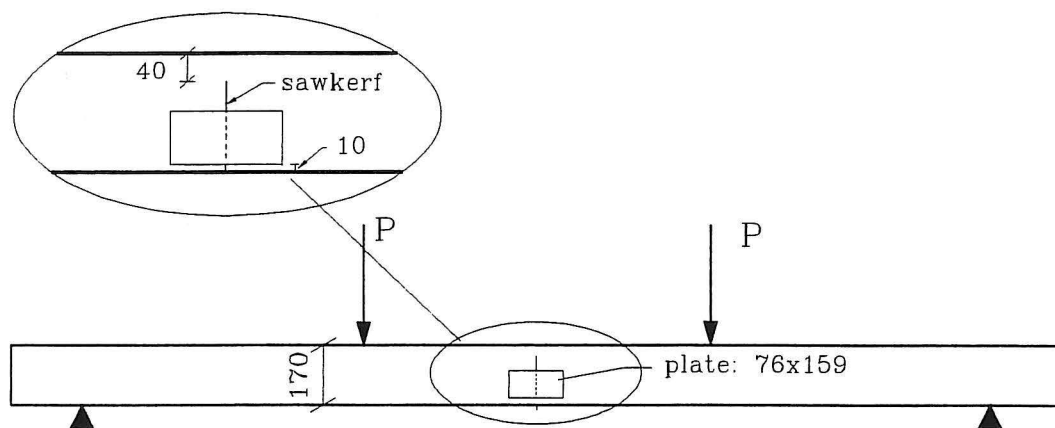

Figure D.2: Sawkerf in test specimens for series BE2. Dimension in mm.

The length of the cross section above the sawkerf is made the same as the extent of the compression zone known from an ABAQUS model of a joint in series BE4.

D.2   Test Equipment

The bending machine is shown in figure D.3. The load is made by a hydraulic jack and transmitted through a "stiff" steel beam to the two loading points.

Three force transduceres measure the force from the hydraulic jack and the two
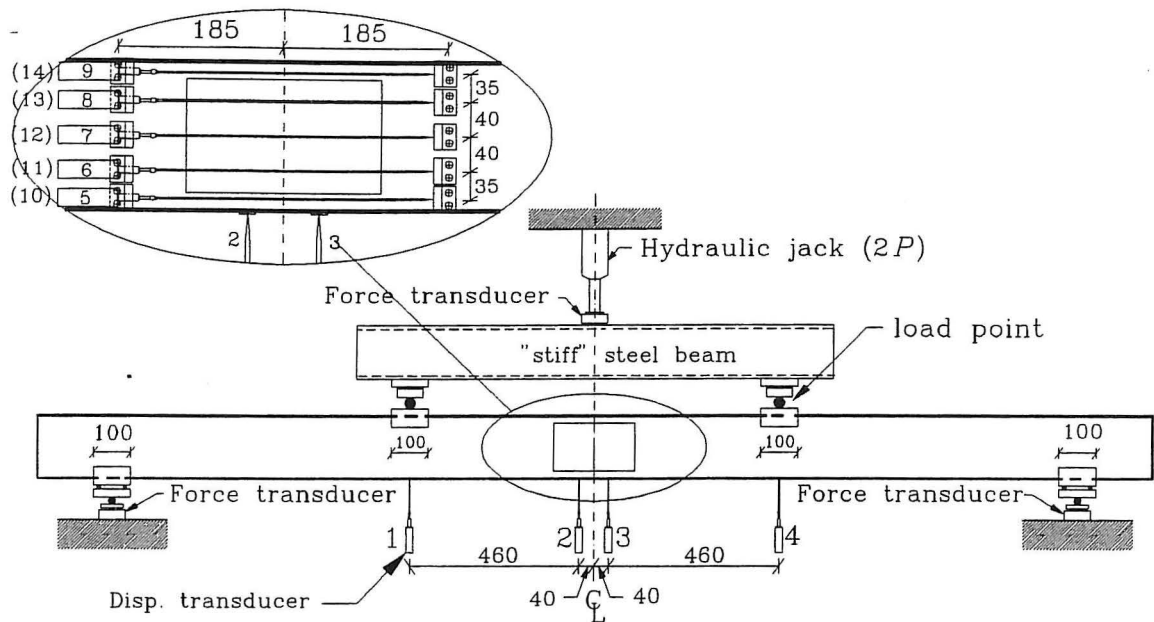
Figure D.3: **Load of bending splices and locations of displacement transduceres. Dimensions in mm.**

reaction forces. The net weight of the test specimen and the test equipment is not included in the forces. The two reaction forces at the end of the beam are used to indicate the load distribution. Load-time curves from test BE1-2 and BE8-3 are shown in figure D.4. It is seen that the curves from the two reaction forces and the load are very similar, (the signal from the load is divided by 2) and therefore the load is equally distributed and the friction effect in the test equipment is very small.
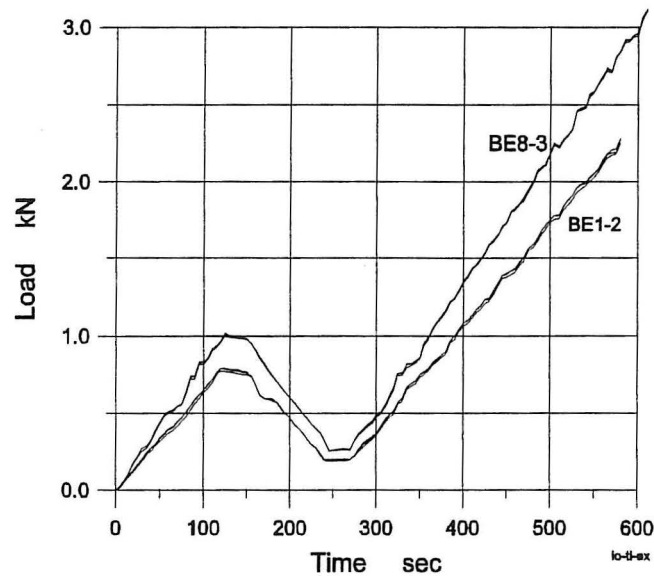

Figure D.4: **Load-time curves from test BE1-2 and BE8-3 to analyse the load distribution.**

As the load is applied manually, the load-time curves flutter a bit. The load procedures used in each test series are shown in figure D.5. All the test specimens are unloaded once during the test.

The vertical displacements are measured by four HBM displacement transducers of
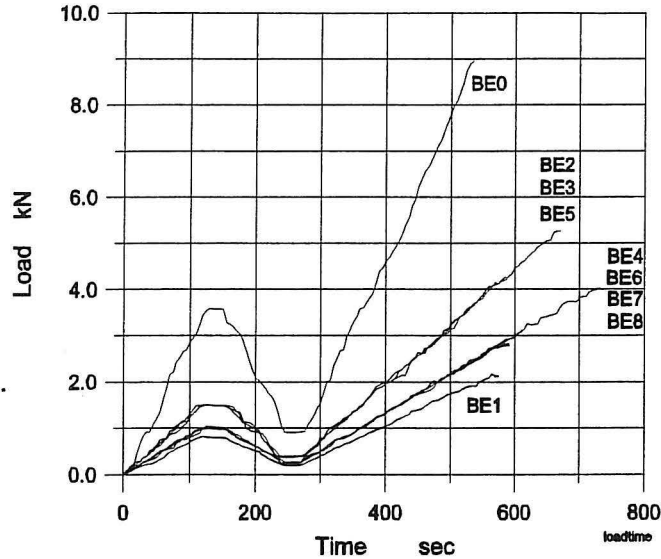
Figure D.5: Load-time curves for the test series.

the type W20TK(±20mm) and W50TK(±50mm). The two W20TK-transduceres (no. 1 and no. 4 in figure D.3) are located below the loading points, and two W50TK-transducers (no. 2, 3) are located at the centre of the beam. 2×5 displacement transduceres (no. 5 to 9 and no. 10 to 14) are located horizontally at the centre of the beam. The transducers are mounted on either side with angle fittings and screws. A storage programme from HBM, (UG6IEBE, 15/9-89), was used to store the data form the forces and the displacement measurings through an HBM data acquisition system (HMB UGR 60). The recording frequency is 0,2Hz. The data are saved on disk.

D.3   Results

In the following, load-displacement curves from the bending tests are shown. The load is given as the force P (half the load from the hydraulic jack) and the displacement is given as the average of the two vertical displacement measurings (no. 2 and 3 in figure D.3) at the middle of the beam (positive in the load direction).

In order to analyse the gap size, load-displacement curves are given as the average of the two horizontal measurings (no. 9 and no. 14 in figure D.3 at the top of the beam, negative in compression). During loading, contact appears in the compression zone at the top of the beam. Numbers on the curves denote the test number. In figure D.6 and figure D.7, fitted straight lines are shown too.

Figure D.6: Load-displacement curves of series BE0.

Figure D.7: Load-displacement curves of series BE0.

Figure D.8: Load-displacement curves of series BE1.

Figure D.9: Load-displacement curves of series BE1.

Figure D.10: Load-displacement curves of series BE2.

Figure D.11: Load-displacement curves of series BE2.

Figure D.12: Load-displacement curves of series BE3.

Figure D.13: Load-displacement curves of series BE3.

Figure D.14: Load-displacement curves of series BE4.

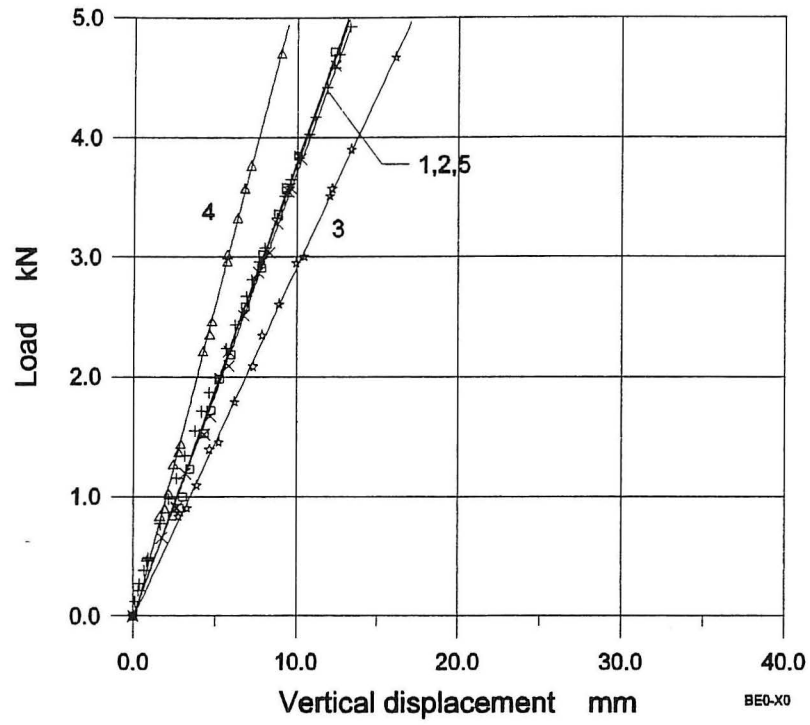Figure D.15: Load-displacement curves of series BE4.

Figure D.16: Load-displacement curves of series BE5.

Figure D.17: Load-displacement curves of series BE5.

Figure D.18: Load-displacement curves of series BE6.
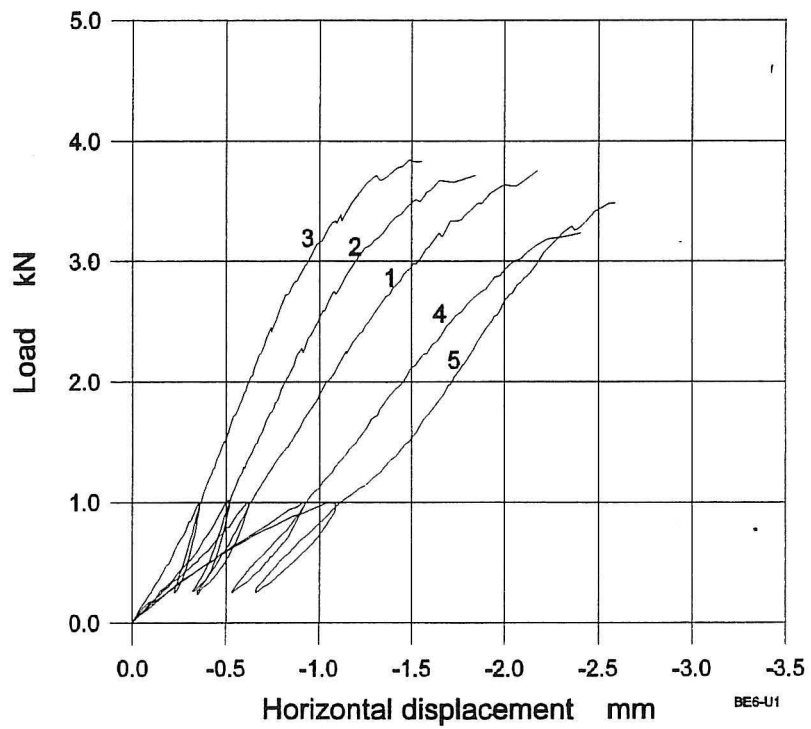
Figure D.19: Load-displacement curves of series BE6.
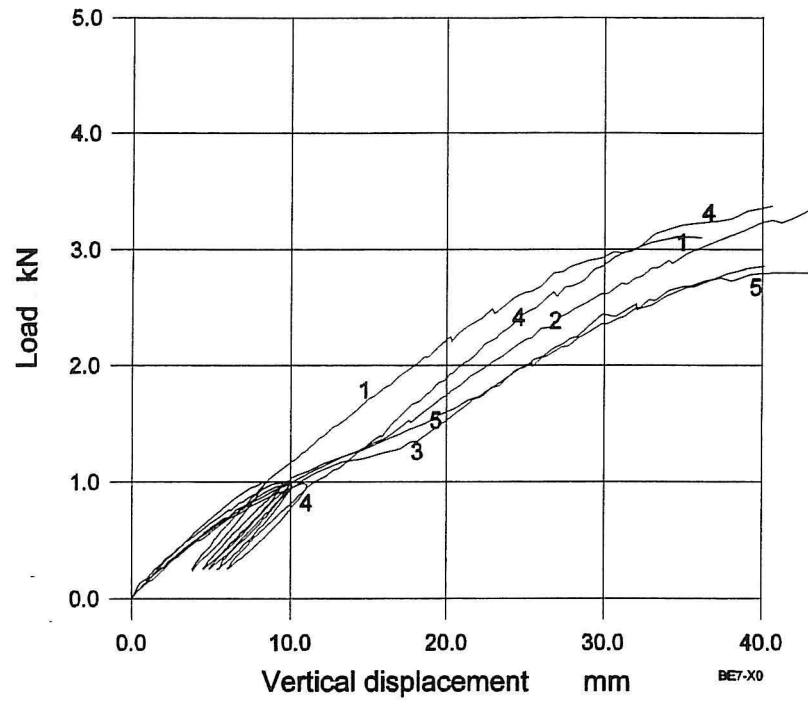
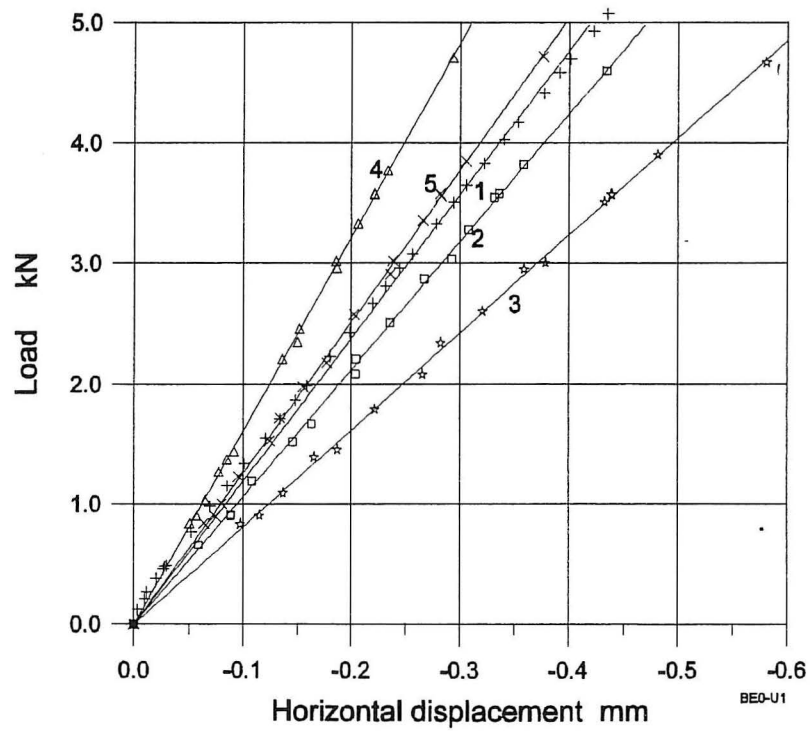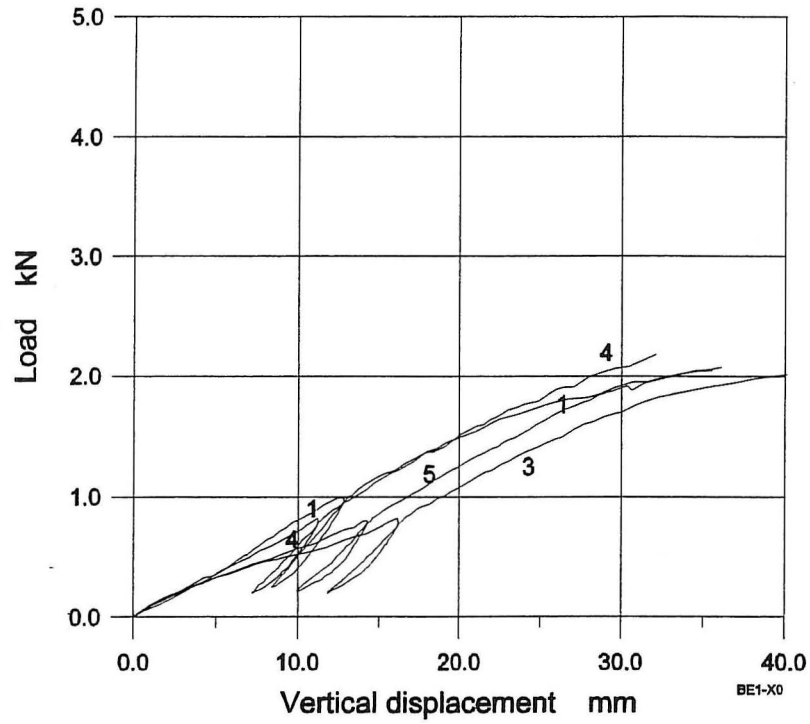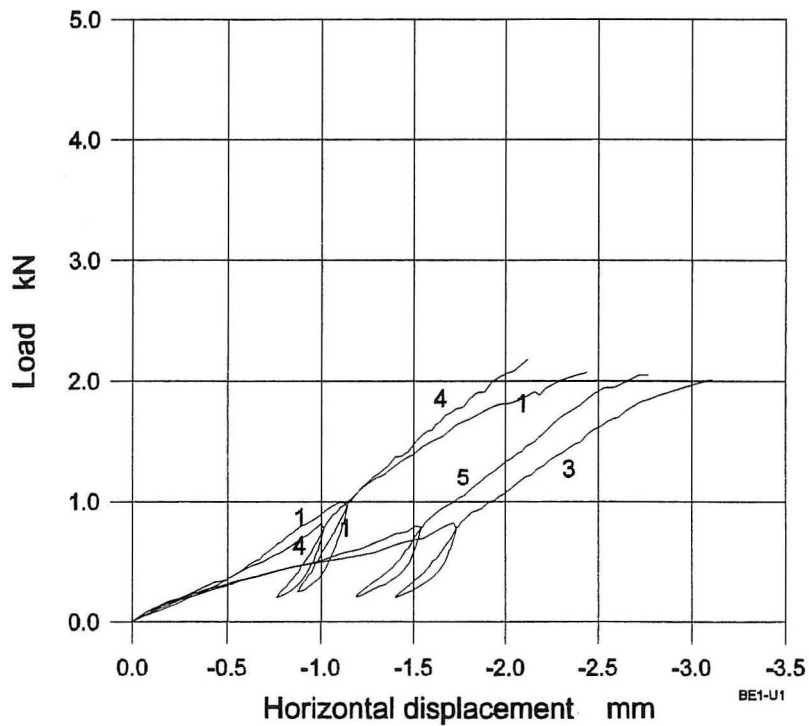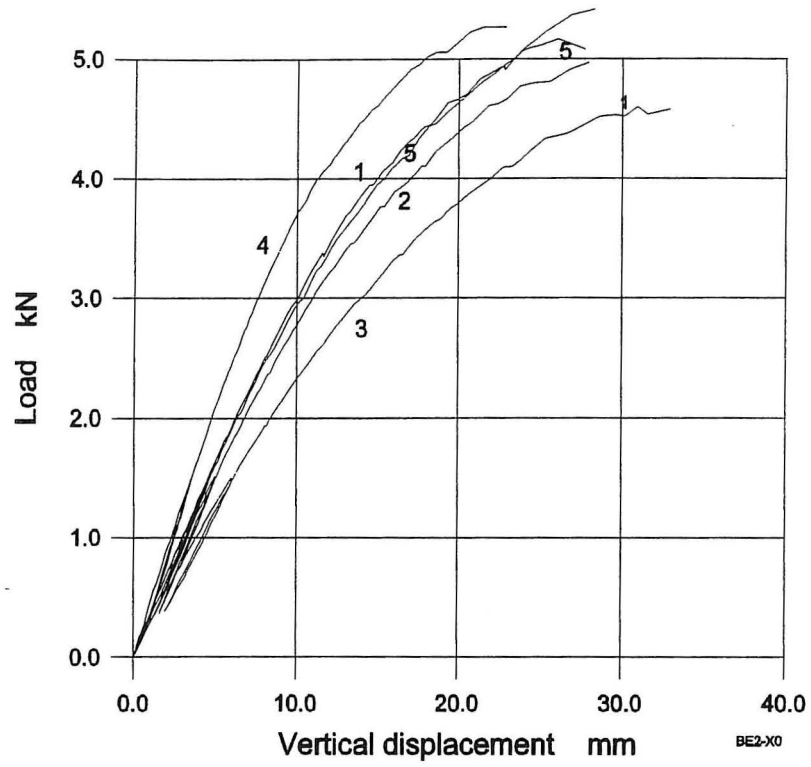Figure D.20: Load-displacement curves of series BE7.
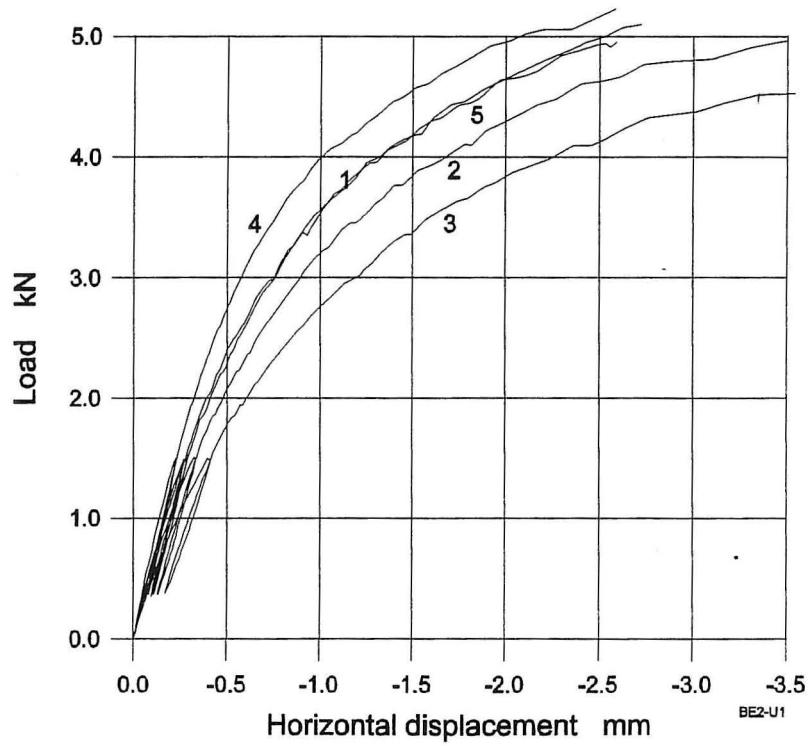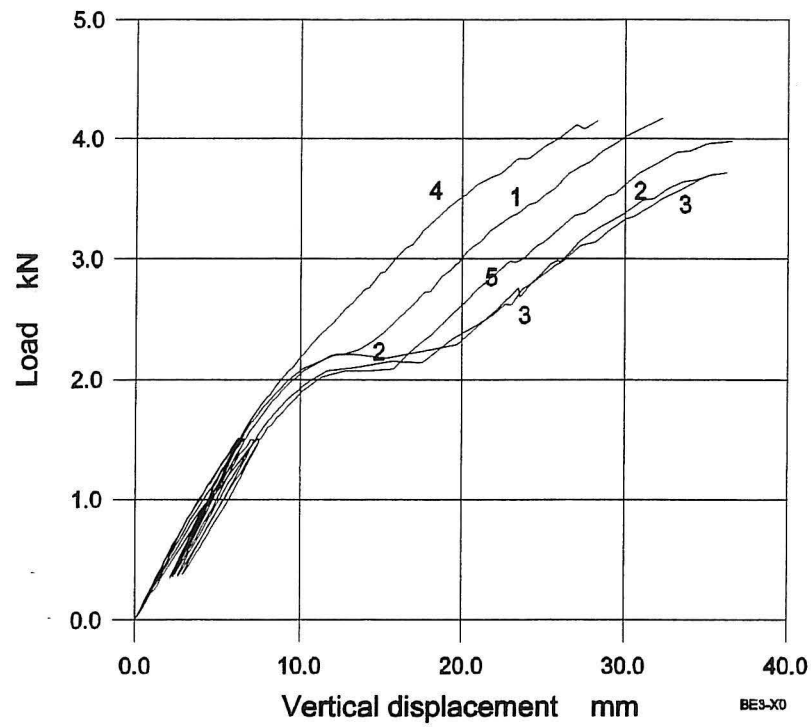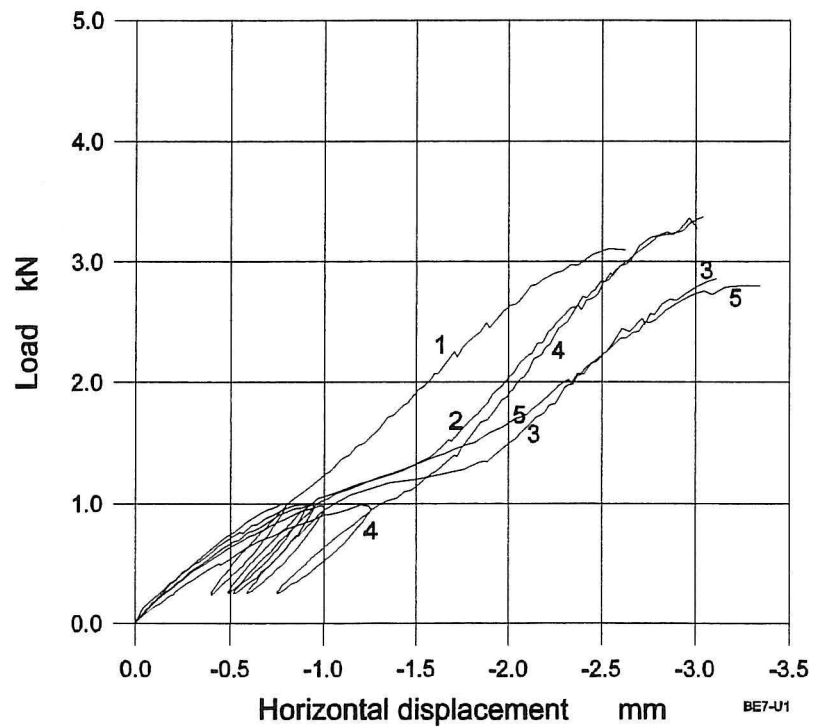

Figure D.21: Load-displacement curves of series BE7.
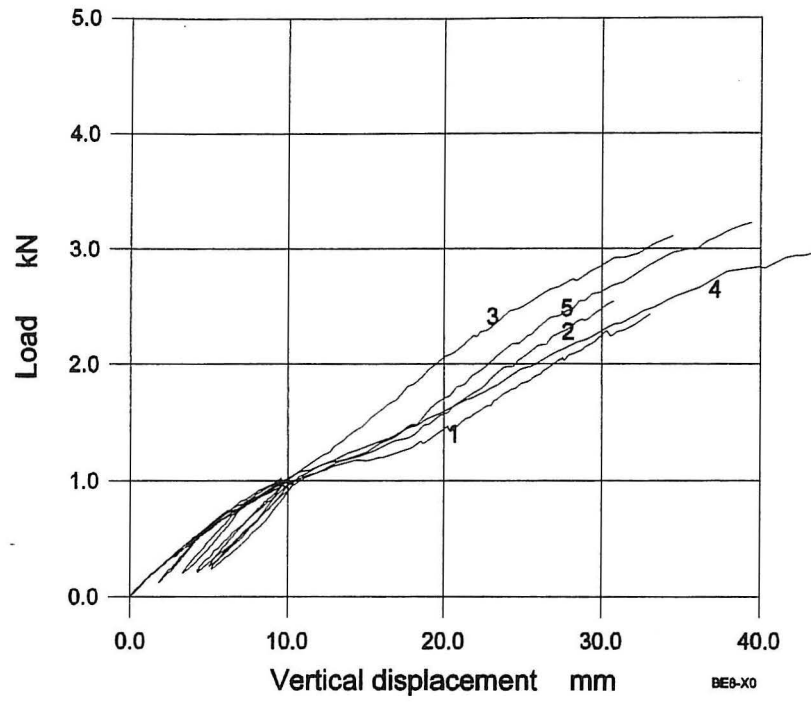
Figure D.22: Load-displacement curves of series BE8.
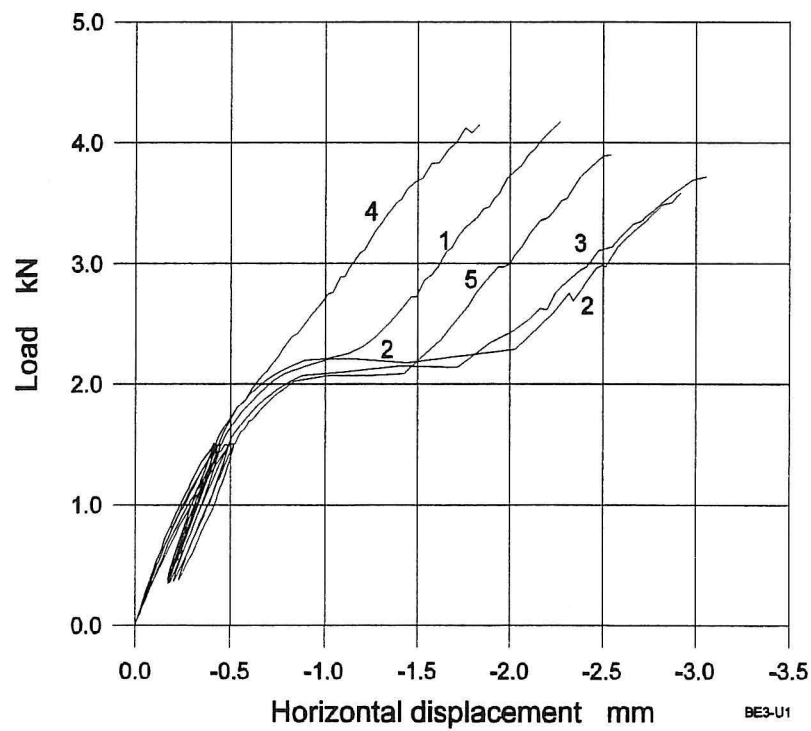

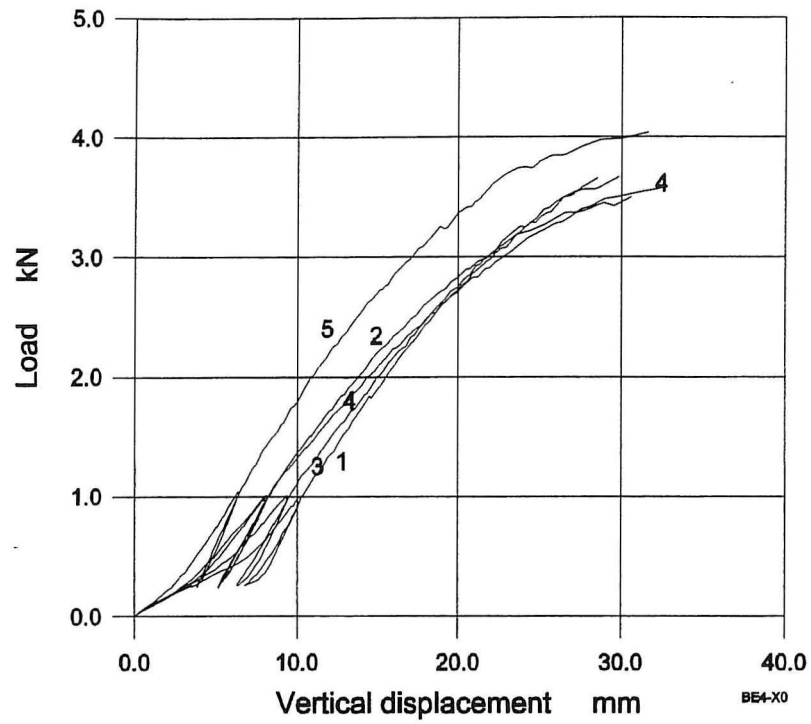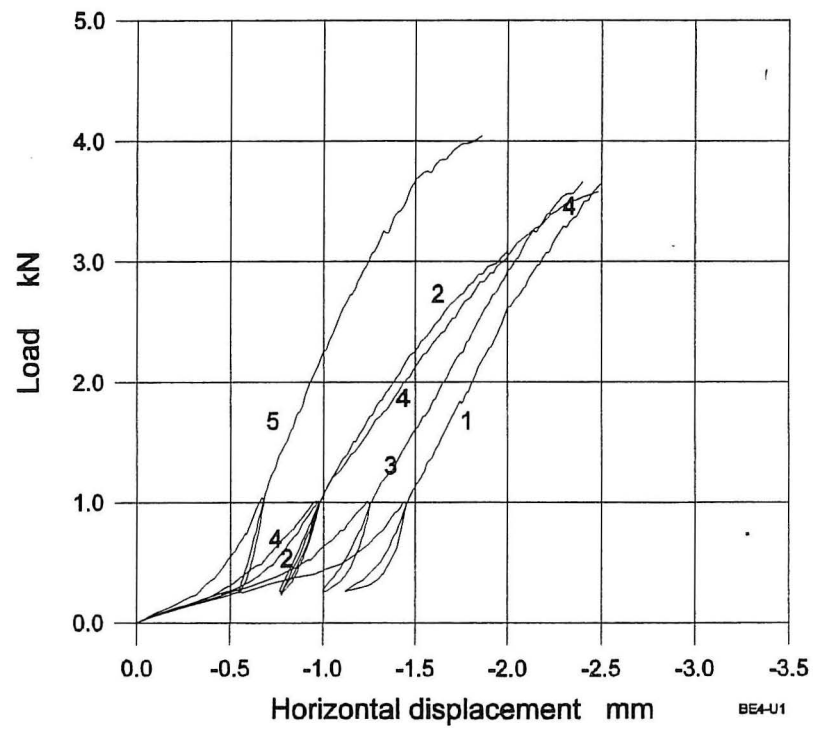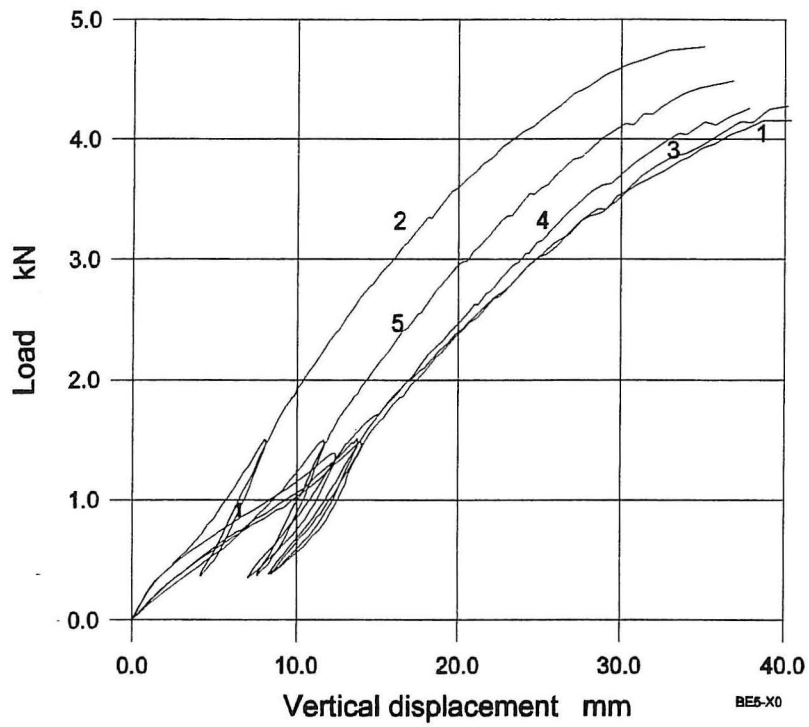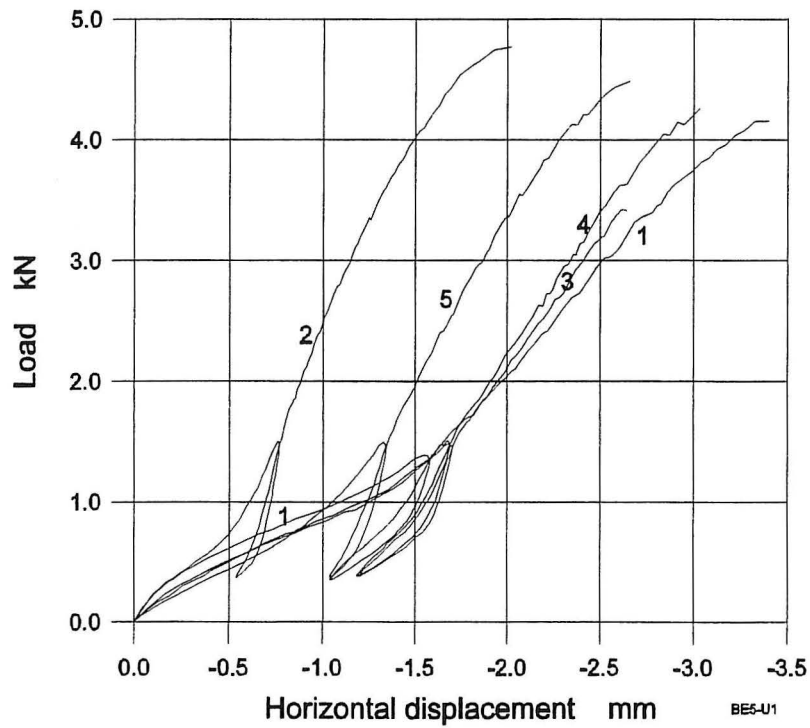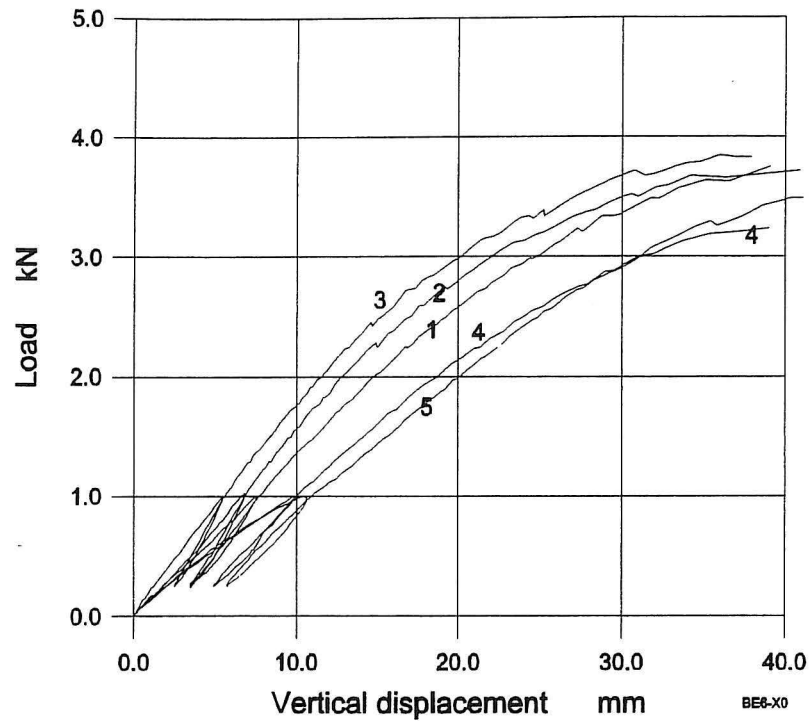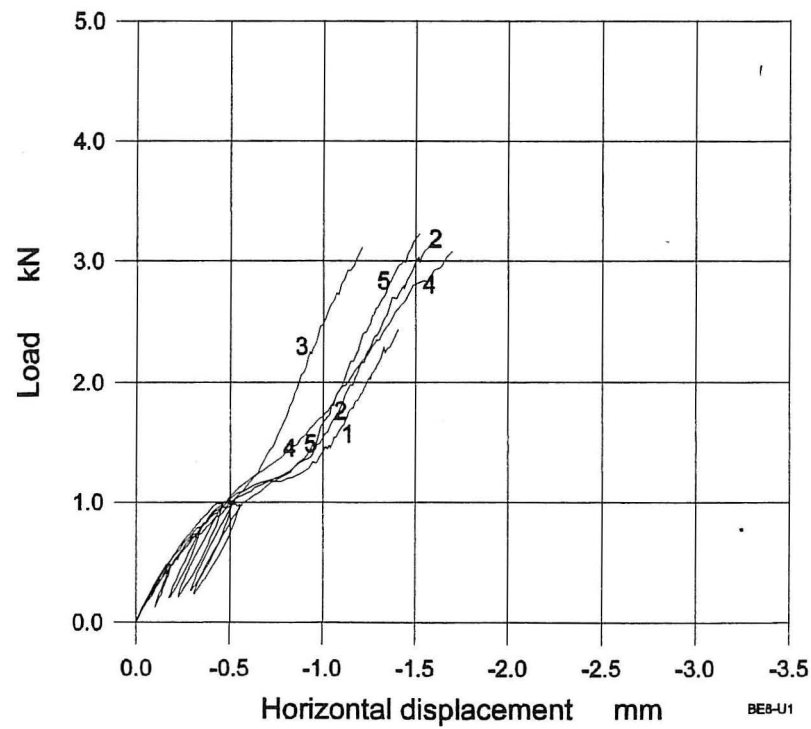Figure D.23: Load-displacement curves of series BE8.

In table D.2 to table D.9, the following test information is given:

- Gap (by test): The gap in the compression zone of the timber is measured before the start of the test. The sign "?" denotes that the gap was not measured.
- Gap (by curve): The gap is determined by the load-displacement curves. When the gap is closed, the joint stiffness will increase. Here the gap size is defined as the horizontal displacement, when the curve tends to increase.
- Weight: The total weight of the timber and the plate.
- Failure load: The failure load is defined as the maximum observed load $(2P)$. As the maximum load is recorded simultaneously it can differ a bit from the end of the load-displacement curves.
- Failure type: The failure types are denoted: plate failure PF, withdrawel of the nails W. If the plate buckles during the test, it is denoted by a B.

BE1		1	2	3	4	5
Gap (by test)	mm	~ 0	$\star$	?	0.25	?
Gap (by curve)	mm	0.4		1.3	0.4	0.9
Weight	kg	10.052	10.272	10.215	10.088	9.633
Failure load	kN	4.1	4.6	4.0	4.3	4.1
Failure type		B/PF	B/PF	B/PF	B/PF	B/PF

$\star$ In load procedure in test BE1-2 was unrealiable.

Table D.2: Test results for series BE1.

BE2		1	2	3	4	5
Gap (by test)	mm			There is no gap. $(=0)$		
Gap (by curve)	mm					
Weight	kg	10.624	9.963	9.133	12.815	11.007
Failure load	kN	10.5	10.0	9.3	10.6	10.9
Failure type		PF	W/PF	W	PF	PF

Table D.3: Test results for series BE2.

BE3		1	2	3	4	5
Gap (by test)	mm	0.8	1.0	1.0	0.1-0.3	1.0
Gap (by curve)	mm	1.0	2.0	1.7	0.6	1.4
Weight	kg	12.318	12.123	10.931	12.301	11.187
Failure load	kN	8.25	7.5	7.5	8.3	8.1
Failure type		B/PF	B/PF	B/PF	PF/B	PF/B

Table D.4: Test results for series BE3.

BE4		1	2	3	4	5
Gap (by test)	mm	0.95	0.8	0.55-1.0	0.15-0.75	0.1
Gap (by curve)	mm	1.1	0.6	0.9	0.5	0.3
Weight	kg	11.288	10.789	11.052	10.404	11.633
Failure load	kN	7.4	7.0	7.3	7.2	8.1
Failure type		PF	PF	PF	W/PF	PF

Table D.5: Test results for series BE4.

BE5		1	2	3	4	5
Gap (by test)	mm	0.9-1.2	0.25	1.0	1.0-1.1	0.35-1.0
Gap (by curve)	mm	1.6	0.5	1.6	1.6	0.8
Weight	kg	11.777	11.692	11.010	10.366	11.391
Failure load	kN	8.4	8.5	9.0	8.4	9.0
Failure type		PF	PF	PF	PF	PF

Table D.6: Test results for series BE5.

BE6		1	2	3	4	5
Gap (by test)	mm	0.6	0.1	~ 0	0.7	1.0-1.1
Gap (by curve)	mm	0.4	0.3	~ 0	1.0	1.2
Weight	kg	11.109	11.773	11.113	10.555	10.328
Failure load	kN	7.5	7.4	7.7	6.5	7.0
Failure type		PF	PF	PF	PF	PF

Table D.7: Test results for series BE6.

BE7		1	2	3	4	5
Gap (by test)	mm	0.55	1.2	1.25	1.0	0.85-1.0
Gap (by curve)	mm	0.8	1.6	1.8	1.4	1.8
Weight	kg	12.125	10.598	11.266	10.463	10.292
Failure load	kN	6.3	6.4	5.7	6.6	5.7
Failure type		PF	B/PF	B/PF	B/PF	B/PF

Table D.8: Test results for series BE7.

BE8		1	2	3	4	5
Gap (by test)	mm	1.4-1.6	?	~ 1	0.9-0.95	1.4-1.6
Gap (by curve)	mm	1.0	0.8	0.7	0.9	0.8
Weight	kg	9.862	10.431	11.525	9.982	10.516
Failure load	kN	5.7	6.8	6.2	6.2	6.5
Failure type		B/PF	W/PF	PF	B/PF	B/PF

Table D.9: Test results for series BE8.

According to the beam theory, the slope of the curves in figure D.6 is in direct proportion to Young's modulus. E, given by (D.1)

$$E = \frac{Pal^2}{u\,I\,6}\left(\frac{3}{4} - \left(\frac{a}{l}\right)^2\right)$$
(D.1)

where l is the distance between the reactions, a is the distance from the reactions to the load P. u is the vertical displacement at the middle of the beam, and I is the moment of inertia. Values of E is given in table D.10.

Test no.	$\frac{P}{u}$ $\frac{kN}{mm}$	E MPa	Weight kg
1	0.379668	12172	10.624
2	0.371061	11896	9.963
3	0.29131	9339	9.133
4	0.521161	16673	12.815
5	0.377661	12108	11.007

Table D.10: The slope, E, and the weight of the beams in series BE0.

The average value of E is found as 12.4GPa. In figure D.24, the dependence between the weight and Young's modulus E is shown.
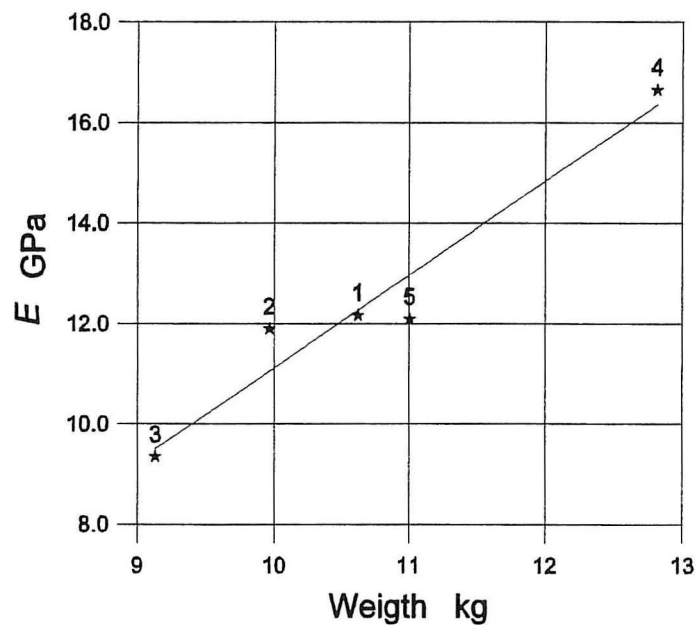
Figure D.24: Relation between E and weight of the beams.

The well-known effect of increasing stiffness for increasing density is observed.

D.4 Discussion

From figure D.8 to figure D.23 it is observed that there is a link between the load-displacement curves. The stiffness order of tests is the same whether the displacements are measured in horizontal or vertical direction.

Plate Size

In figure D.25, three typical load-displacement curves from tests with different plate sizes are shown. The plates are all located at the centre of the beam.
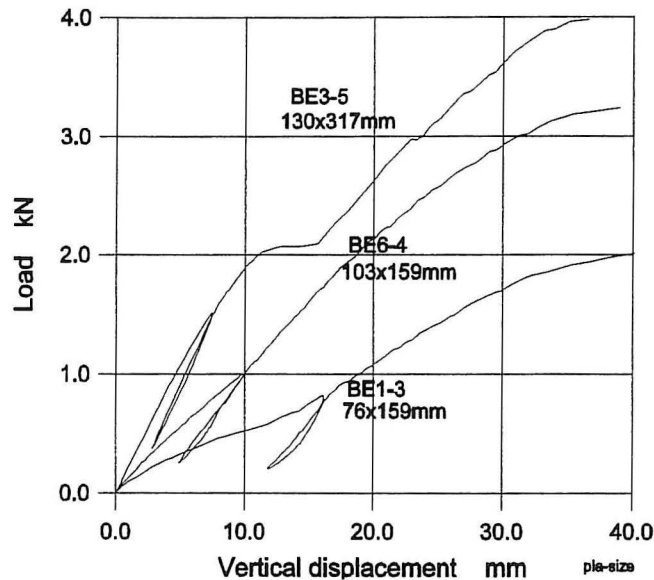
Figure D.25: **Load-displacement curves from tests with different plate sizes.**

In table D.11, the average failure load in series BE1, BE6 and BE3 is shown.

Series	Plate size	Failure load $(2P)$ [kN]		Failure type	Weight [kg]	
	mm×mm	mean	stand.dev.	mean s	Stand.dev.	
BE1	76×159	4.22	0.24	B/P	10.052	0.251
BE6	103×159	7.22	0.48	P	10.976	0.563
BE3	130×317	7.93	0.40	B/P	11.772	0.662

Table D.11: **Average failure loads in series with different plate size.**

From figure D.25 and table D.11 it is seen that the stiffness and the failure load are increasing with increasing plate size. The failure load is increased by 70% when the plate width is changed from 76mm to 103mm. The difference between the failure loads in series BE6 and BE3 is only 10%.

In tests from series BE1 buckling occurs in two or three of the nail-columns in the compression zone of the plate (not shown). The buckling effect has no observed effect on the load-displacement curves.

In series BE6, the buckling effect was not observed. This fact is caused by the small gap sizes in these series. In series BE7 and BE8 the gap sizes were larger and buckling occurred in several tests.

In series BE3 there is buckling in a larger area in the compression zone (two to eight nail-columns) and the buckling effect is observed as the horizontal part of the load-displacement curves, see figure D.25, figure D.12 and figure D.13. The buckling effect is dependent on the gap size.

Plate Location

In figure D.26 four typical load-displacement curves from tests with different plate sizes and locations are shown.
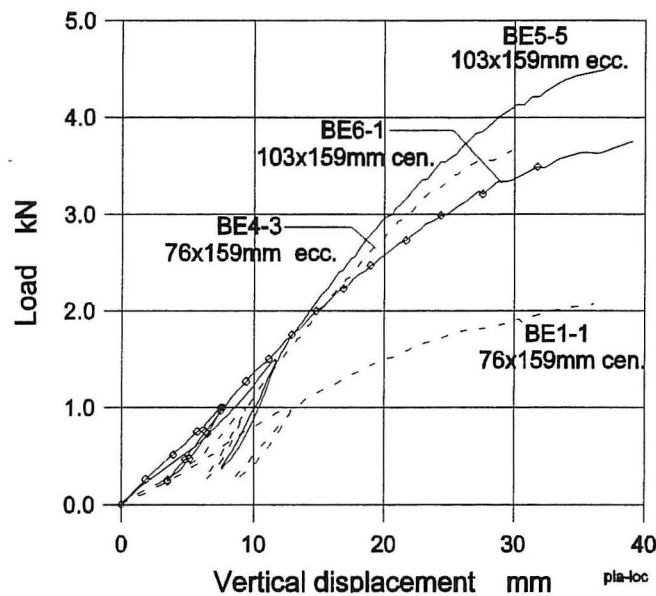
Figure D.26: **Typical load-displacement curves from tests with different location of the plate.**

In figure D.26 it is seen that when a 76×159mm plate is located eccentrically, the stiffness is increased to the stiffness achieved in tests with a 103×159mm plate. The stiffness change for an eccentrically located 103×159mm plate is rather small and it is only increased for joints in contact and large deformations.

Series	Plate size	Failure load ($2P$) [kN]		Failure type	Weight [kg]	
	mm×mm	mean	stand.dev. kN		mean	stand.dev.
BE1	76×159 cen.	4.22	0.24	B/P	10.052	0.251
BE4	76×159 ecc.	7.4	0.42	W, P	10.833	0.641
BE6	103×159 cen.	7.22	0.48	P	10.976	0.563
BE5	103×159 ecc.	8.66	0.31	P	11.247	0.577

Table D.12: **Average failure loads in series with different plate locations.**

The failure load is increased when the plate is located eccentrically. In tests with

76×159mm plate the failure load is increased by 75% and in tests with 103×159mm plate the failure load is increased by 20%.

Gap Size

In table D.7 to table D.9 it is seen that the gap size is different in each test. From the beginning it was planned that the gap size should be as stated in table D.1, but the timber beams have been cut with a rough saw and, therefore, the timber ends do not fit very well. This is the reason for the variation of the gap sizes. This problem has also been observed in other series. However, in all series it has been observed that the stiffness is increased when there is contact between the timber members.

In figure D.27 the gap size is plotted against the failure load for the series BE6, BE7 and BE8.
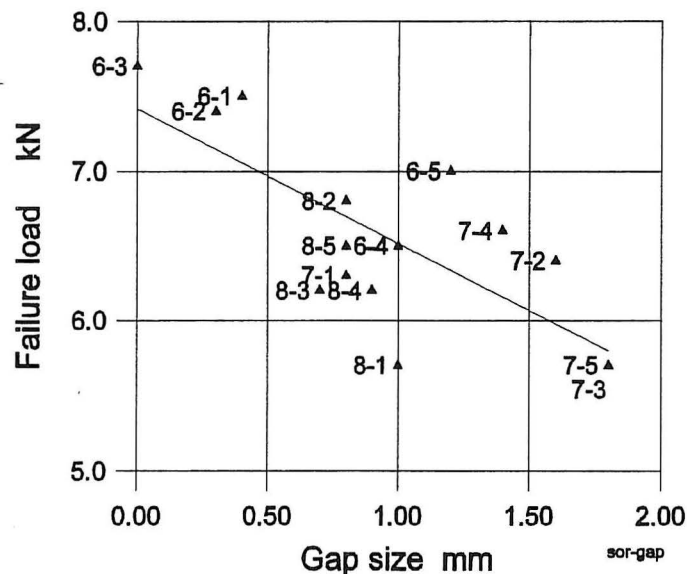
Figure D.27: Dependence between gap size and failure load.

In figure D.27, it is seen that the failure load is increased with decreasing gap size. The explanation for the location of test BE8-1 (8-1 in figure D.27) is a very low weight of the beam.

Butt Effect

The test specimens are (as well as the test numbers) the same for series BE0 and BE2. The reason for the variation of the load-displacement curves in series BE2 is the same as for series BE0 - it is mainly caused by a variation of the timber stiffness. The curves are located in the same order in the two series, see figure D.6 and figure D.10.

In figure D.28 three typical load-displacement curves form series BE2 (without the butt effect) and BE4 (with the butt effect) are shown.

It is seen that the tests without the but effect are much stiffer, than the test with the a gap.
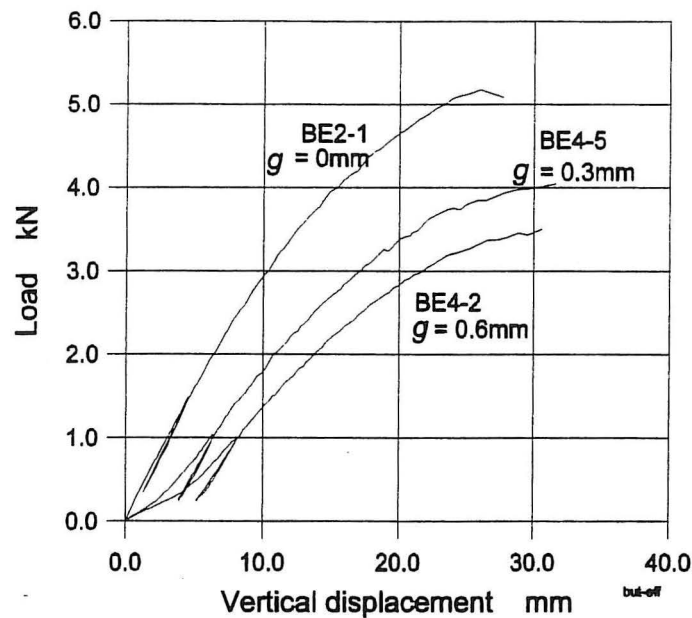
Figure D.28: **Load-displacement curves from series BE2(without the butt effect) and BE4.**

D.5   Conclusion

40 tests specimens have been divided into 9 series to test the influence of different plate sizes, plate locations and gaps between the timber members.

Almost all test specimens failed by the plate. In some tests the specimen failed by withdrawal of the nails. Also buckling in the compression zone of the plate occurs during loading, and the fenomenon is dependent on the size of the gap. In all tests, the timber members are in contact before failure.

The stiffness and the failure load are increased with increasing plate size.

The plate location is significant for the stiffness and the failure load. The stiffness of a splice with contact, where the plate is in the tensile zone, is larger than the stiffness of a splice with the same plate, but located at the centre. An eccentrically located 76×159mm plate has the same stiffness and failure load as a splice with a 103×159mm plate located at the centre of the beam. This is only valid if there is contact between the timber members. The effect is most obvious by the small plates.

The failure load is dependent on the gap size. A decreased gap size will increase the failure load (and the stiffness).

The test results will be used to evaluate the numerical results.

Appendix E

Drawings of Trusses.

In this appendix, the drawings of the trusses used in chapter 6 are given. The drawings are made by Gang Nail Systems.

Collar Tie Truss

A N V I S N I N G E R

SPÆRET ER BEREGNET MED PROGRAM
ECOTRUSS BASERET PÅ DANSK INGENIØR-
FORENINGS NORMER DS 409, DS 410 OG
DS 413. PLADER: MK 5.60/0925 OG
MK 5.60/1034.
TEGNINGEN MÅ IKKE REVIDERES UDEN
VOR TILLADELSE.
PLADSERINGSTOLERANCE PLADER: 5 MM
TANDPLADER AF FABRIKAT GANG-NAIL
TYPE GN-T150, GN-T150S OG GNA-20S
PLADERNES HOVEDRETNING: A=VÆNDRET
B=LODRET RESP. UDSTIKKENDE PLADER I
STØDSAMLING.
☒ AFSTIVNING AF GITTER
▨ PLADERNES HOVEDRETNING

BELASTNINGAR:

EGENLAST TAGDÆKNING	= 300.	N/M2
EGENLAST FOD	= 450.	N/M2
EGENLAST HANEBÅND	= 250.	N/M2
EGENLAST LOFT	= 200.	N/M2
EGENLAST SKILLEVÆGGE	= 500.	N/M2
NYTTELAST BJÆLKELAG	= 1500.	N/M2
NYTTELAST HANEBÅND	= 250.	N/M2
SNE kar. So	= 1.0	kN/M2
VINDLAST	= 700.	N/M2

MAX C/C-AFSTAND   = 1000. MM
MAX ÅSAFST. HOVED = 400. MM

MAXIMAL NEDBØJNING FOD
KND 7 - 8 : 2. MM

VEDERLAGSREAKTIONER:

KND NR	BRUD MIN kN	BRUD MAX kN	BRUDS MIN kN	BRUDS MAX kN	ERF. MAX	ERF. BREDD
7	4.9	5.9	2.1		3.8	30
9	5.1	5.1	2.8		4.9	39
1	4.9	5.9	2.1		3.8	30

TANDPLADER

KN. NR.	KN. TYP.	B. MM.	L. MM.	X. MM.	Y. MM.	PLADE TYPE
1	2	206.	350.	175.	0.	GNA 20S
2	20A	206.	350.	285.	7.	GNA 20S
3	2	152.	198.	99.	0.	GNA 20S
4	4B	130.	119.	197.	65.	GNA 20S
5	2	152.	198.	99.	0.	GNA 20S
6	20A	206.	350.	285.	7.	GNA 20S
7	2	206.	350.	175.	0.	GNA 20S
11	11A	130.	139.	0.	0.	GNA 20S
12	11A	130.	139.	0.	0.	GNA 20S

TRÆDIMENSIONER
TRÆTYKKELSE: 45. MM.

	DIM. (MM)	KVAL.
2 - 11	195.	K24
11 - 4	195.	K24
4 - 12	195.	K24
12 - 6	195.	K24
5 - 3	195.	K18
1 - 2	220.	K24
6 - 7	220.	K24

SOL - Consulting
Stenstrup Byvej 4
9510 Arden
TEL: 9855 4477   FAX: 9855 4433

ORDRE   JACOB2

TEGNING KONTROLLERET
Sv. O. Lisberg
Arden   06 09 1995

REV. ANT.   SIGN.   DATO

KODE TYPE POS   TEGNINGSNUMMER   REV.

SKALA 1: 40

Pitched W-Truss

ANVISNINGER

SPÆRET ER BEREGNET MED PROGRAM
ECOTRUSS BASERT PÅ DANSK INGENIØR-
FORENINGS NORMER DS 409, DS 410 OG
DS 413. PLADER: MK 5.60/0925 OG
MK 5.60/1034.
TEGNINGEN MÅ IKKE REVIDERES UDEN
VOR TILLADELSE.
PLADSERINGSTOLERANSE PLADER: 5 MM
TANDPLADER AF FABRIKAT GANG-NAIL
TYPE GN-T150, GN-T150S OG GNA-20S
PLADERNAS HOVEDRETNING: A-VÆNDRET
B-LODRET RESP. UDSTIKKENDE PLADER I
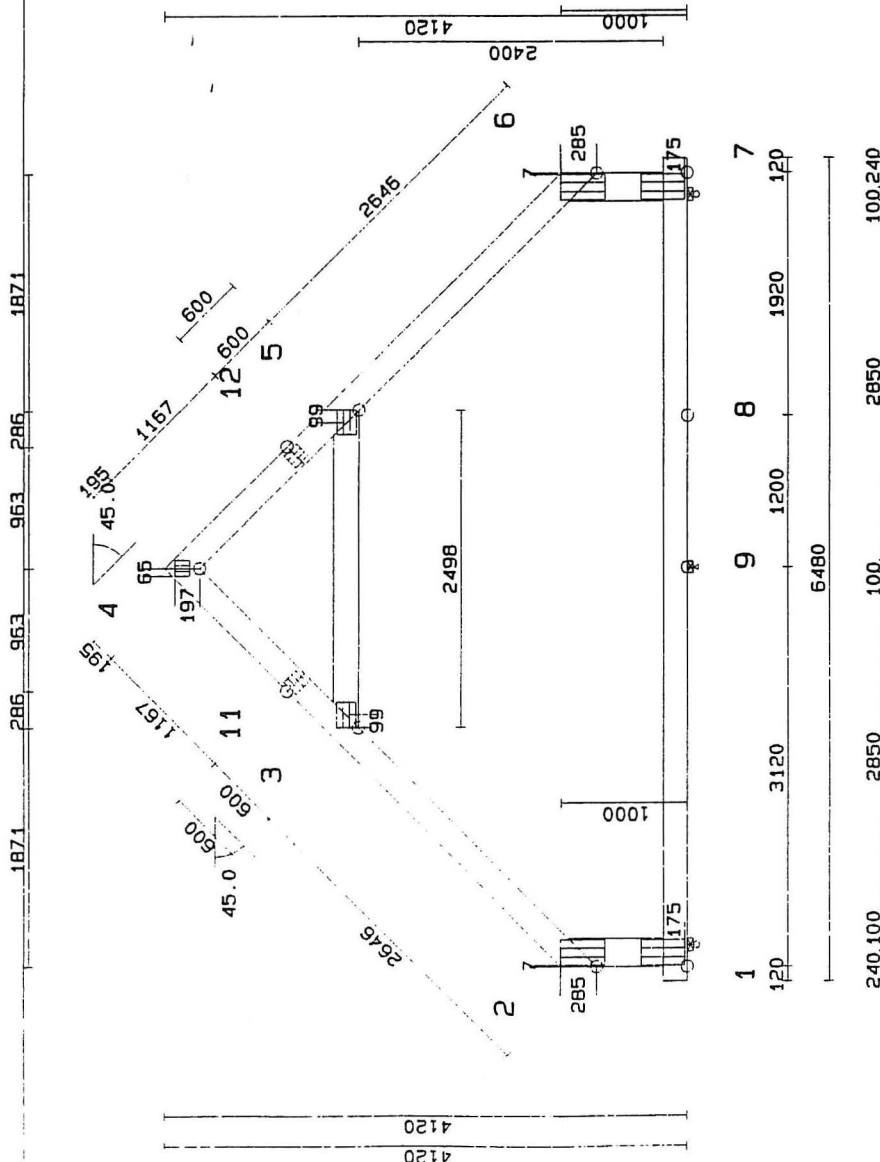STØDSAMLING.
⊠ AFSTIVNING AF GITTER
▢ PLADERNES
▨ HOVEDRETNING

BELASTNINGAR:

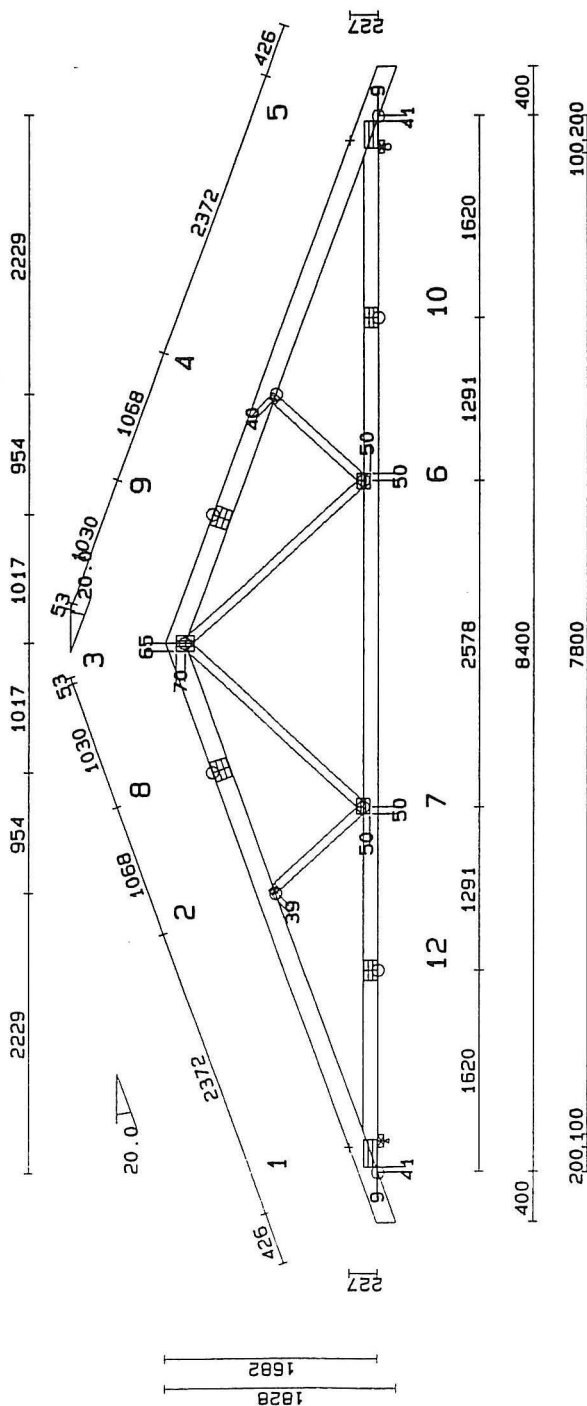|		
EGENLAST TAGDÆKNING	=	600. N/M2
EGENLAST FOD	=	300. N/M2
GANGBROLAST	=	500. N/M2
SNE kar. So	=	1.0 kN/M2
VINDLAST	=	700. N/M2

MAX C/C-AFSTAND = 1000. MM
MAX ÅSAFST.HOVED = 350. MM

MAXIMAL NEDBØJNING FOD

KND 61 - 62 : 11. MM

VEDERLAGSREAKTIONER:

	BRUD		BRUDS		ERF.
KND	MIN	MAX	MIN	MAX	BREDD
NR	kN	kN	kN	kN	MM
5	9.2	10.2	.3	4.3	62
1	9.2	10.2	.3	4.3	62

TANDPLADER

KN. NR.	KN. TYP.	B. MM.	L. MM.	X. MM.	Y. MM.	PLADE TYPE
1	20A	103.	218.	41.	9.	GNA 20S
2	2	55.	79.	39.	0.	GNA 20S
3	4B	130.	139.	70.	65.	GNA 20S
4	2	55.	79.	40.	0.	GNA 20S
5	20A	103.	218.	41.	9.	GNA 20S
6	7A.	103.	119.	50.	50.	GNA 20S
7	7A	103.	119.	50.	50.	GNA 20S
8	11A	130.	159.	0.	0.	GNA 20S
9	11A	130.	159.	0.	0.	GNA 20S
10	11A	103.	159.	0.	0.	GNA 20S
12	11A	103.	159.	0.	0.	GNA 20S

TRÆDIMENSIONER

TRÆTYKKELSE: 45. MM.

	DIM. (MM)	KVAL.
1 - 8	145.	K18
8 - 9	145.	K18
3 - 9	145.	K18
9 - 5	145.	K18
5 - 10	120.	K18
10 - 12	120.	K18
12 - 1	120.	K18
2 - 7	70.	K18
3 - 7	70.	K18
3 - 6	70.	K18
4 - 6	70.	K18

TEGNING KONTROLLERET	ORDRE JACOB1		SKALA 1:40
ØREBRO	03 08 1995		REV.
	KODE TYPE POS	TEGNINGSNUMMER	

REV. ANT.   SIGN.   DATO

Appendix F

Notation

Scalars

E	:	modulus of elasticity
G	:	shear modulus
A	:	section area
A_c	:	contact area
t	:	thickness
l	:	length of nail-plate
b	:	width of nail-plate
ν	:	Possion's ratio
f_y	:	yield stress
$\Im$	:	nail density
I	:	moment of inertia
U	:	disp. in x-dir.
V	:	disp. in y-dir.
α	:	rotation
L_b	:	length of beam element
L	:	length of elastic- plastic beam in plate
L_c	:	length of contact elem.
N	:	section normal force
Q	:	section shear force
M	:	section moment
φ	:	angel between glob. and local system
ϑ	:	angel between grain and $\mathbf{p}$
γ	:	angel between grain and $\boldsymbol{\Delta}$
n	:	no. of nails or no. of beams
^iW	:	internal work
^eW	:	external work
Δ	:	abs. disp. of a nail
p_0, k_1, k_2	:	stiffness par. of the nails
ε	:	strain
Φ	:	shear deformation parameter
p	:	nail force
P	:	external load

Vector and matrices

$\mathbf{f}$	:	external force vector
$\mathbf{f^u}$	:	force vector of uniformly distributed loads
$\mathbf{u}$	:	displacement vector
$\mathbf{g}$	:	gap vector
$\mathbf{p}$	:	nail force vector
$\boldsymbol{\Delta}$	:	nail displacement vector
$\mathbf{K}$	:	local stiffness matrix
$\mathbf{D}$	:	orthogonl matrix
$\mathbf{T}$	:	transformation matrix

Subscripts

x	:	direction x
y	:	direction y
1	:	direction, or local node no.
2	:	direction, or local node no.
p	:	plastic or plate
g	:	global
j	:	component no. of a vector
a,b	:	points a, b

Superscripts

T	:	transpose of a matrix
c	:	compression or contact
s	:	shear
t	:	tension

STRUCTURAL DESIGN PAPERS

PAPER NO. 1: J. Nielsen & A. Rathkjen: *Laterally Loaded Nail-Plates*. ISSN 0902-7513 R9406.

PAPER NO. 2: J. Nielsen: *Stiffness Analysis of Nail-Plate Joints subjected to Short-Term Loads*. Ph.D.-Thesis. ISSN 1395-7953 R9613.